THE RESONATING VALENCE BOND MODEL OF MOLECULES AND REACTIONS

Thesis by

Arthur F. Voter

In Partial Fulfillment of the Requirements

for the Degree of

Doctor of Philosophy

California Institute of Technology

Pasadena, California

1983

(Submitted January 11, 1983)

The scientist does not study nature because it is useful; he studies it because he delights in it and he delights in it because it is beautiful. Of course, I do not speak here of that beauty which strikes the senses, the beauty of qualities and appearances, not that I undervalue such beauty, far from it, but it has nothing to do with science; I mean that profounder beauty which comes from the harmonious order of the parts and which a pure intelligence can grasp.

Henri Poincaré

To Dad

ACKNOWLEGEMENTS

First, I thank my research advisor, Bill Goddard, for his guidance, encouragement, and constant scientific stimulation. The considerable freedom he allowed me gave me the opportunity to pursue a variety of exciting research projects, and contributed to my scientific and personal maturity.

Technical assistance from Adria McMillan and Henriette Wymar, who typed part of the thesis, and Valerie Purvis, who drew most of the figures, is gratefully acknowleged.

I am also grateful to Caltech, and various government agencies, for providing financial support during my graduate career.

I thank all the members of the Goddard group, present and recent past, for years of friendship and scientific interaction. In this regard, I particularly want to mention Bob Cave, Tony Rappé, Barry Olafson, Ray Bair, Tony Redondo, Tom Upton and Marv Goodgame. I am especially grateful to Eugene Knight, Mark McAdon, Bob Cave, Barry Olafson, Emily Carter, and Mark Brusich, who pitched in to help me get this thesis typed into the computer as the deadline approached. The thesis would not have been finished without their help.

I thank Jean for the love and patience that helped me survive candidacy. Little did we know how hard graduate school would be.

I thank Mary Nouri, Jes Sellers, Tom Gaffney, and Ken Arnold, whose friendship helped keep me going, probably more than they know.

Finally, I thank my family, especially Mom and Dad, for their endless support, encouragement, love, and understanding.

TABLE OF CONTENTS

ABSTRACT

This thesis presents an ab initio generalization of Pauling's theory of resonance, the generalized resonating valence bond (GRVB) method. In GRVB, we optimize a wavefunction of the form

$$\Psi_{TOT} = C_A\Psi_A + C_B\Psi_B \ ,$$

where Ψ_A and Ψ_B are multiconfigurational wavefunctions with arbitrary overlap. This type of wavefunction has been considered unfeasible for more than a few electrons due to the $n!$ computational dependence of evaluating the matrix element $\langle\Psi_A|H|\Psi_B\rangle$. We reduce this dependence to $\sim n^5$ by biorthogonalizing the orbitals in each determinant pair. GRVB is ideally suited to describing systems which require a resonance of more than one bonding structure, such as benzene, molecules with three-electron bonds, and reaction transition states. Besides yielding a conceptually simple wavefunction, we find that GRVB yields quantitative results for processes in which the dominant differential correlation is a resonance effect. For example, the GRVB barrier heights for the HCl + H and HF + H exchange reactions are each within one kcal of the basis set limit, in contrast to the orthogonal configuration interaction (CI) approaches which require hundreds or thousands of configurations to achieve the same accuracy. We also present application to the three-electron bonding in noble gas dimer ions, and various other examples.

Introduction to Thesis

For many molecules, the natural way to describe the electronic wavefunction is as a linear combination of bonding structures,

$$\Psi_{TOT} = c_A\Psi_A + c_B\Psi_B + \cdots \quad . \tag{1}$$

As an example, consider the classic resonating system, benzene, which chemists have for years described as a superposition of two structures with localized π bonding,

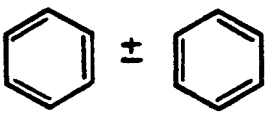

(2)

The "resonance energy" resulting from this superposition is accepted as the reason for the unusual stability of the benzene molecule,[1] and indeed, this resonance energy concept has been pervasive in organic chemistry ever since the early work of Pauling[2], Slater[3] and Hückel.[4] In addition, systems with coupled localized excitations, such as the n-π^* state in glyoxal,[5]

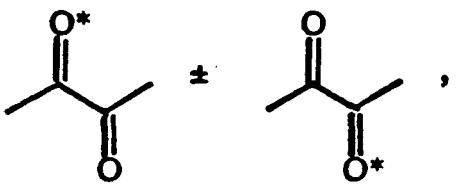

(3)

hypervalent compounds such as ClF_3,

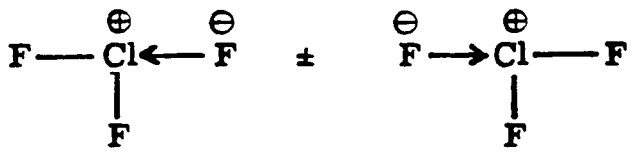

(4)

and even reaction transition states,

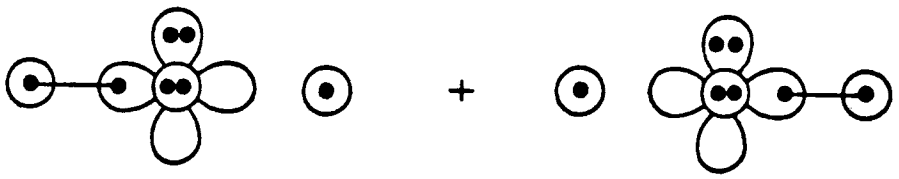

(5)

are best described as a resonance of more than one bonding structure. However, while an ab initio technique such as the generalized valence bond (GVB)[6] method is particularly suited to optimizing one of these localized bonding structures, allowing more than one localized structure to mix has been impractical due to the overlap of the orbitals in Ψ_A with those in Ψ_B.

The GVB method has been successful in obtaining quantitative results using a conceptually simple wavefunction,[7] and has been instrumental in reinforcing the concepts of the valence bond model of Pauling.[1] For systems such as (2)-(5), in which a single valence bond structure is inadequate, there has been no method[8] which could yield quantitative results from a compact wavefunction. The development of a method which could solve directly for a wavefunction such as (1) should lead to quantitative and conceptual progress in understanding such systems, and provide a rigorous test for the concept of resonance. In this thesis we describe such a method and demonstrate its utility on a variety of systems.

Chapter 1 gives an introduction to resonating wavefunctions, and an overview of their behavior. Chapter 2 reviews the previous work along

these lines. Chapter 3, Section II describes the *resonating* GVB (R-GVB) method, in which Ψ_A and Ψ_B are found using the conventional GVB method and then the resonance energy and energy of Ψ_{TOT} are evaluated, and Section III describes the generalized resonating valence bond (GRVB) method in which Ψ_A and Ψ_B are optimized in the presence of resonance; that is, Ψ_{TOT} is optimized directly. Later chapters present various applications of R-GVB and GRVB. These applications demonstrate that the R-GVB and GRVB methods do indeed provide a simple yet quantitative description of resonating molecular systems and verify that the concept of resonance is valid and useful. In particular we find that the GRVB method can be used to predict reaction barriers to kcal accuracy using only the two valence bond structures corresponding to reactants and products. Thus, the GRVB method may prove extremely useful in elucidating reaction transition states and pathways, a problem of current chemical interest.

References

1) L. Pauling, *The Nature of the Chemical Bond*, 3rd *ed.*, (Cornell University Press, Ithaca, New York, 1960)

2) L. Pauling, J. Am. Chem. Soc. **53,** 1367, 3225 (1931); **54,** 988, 3570 (1932); Proc. Nat. Acad. Sci. **18,** 293 (1932)

3) J.C. Slater, Phys. Rev. **37,** 481 (1931)

4) E. Hückel, Z. Physik **70,** 204 (1931); **72,** 310 (1931); **76,** 628 (1932); **83,** 632 (1933)

5) C.E. Dykstra, R.R. Lucchese and H.F. Schaeffer III, J. Chem. Phys. **67,** 2422 (1977)

6) F.W. Bobrowicz and W.A. Goddard III, in: *Modern Theoretical Chemistry, Vol. 3, Methods of Electronic Structure Theory*, edited by H.F. Schaeffer III (Plenum, New York 1977), Chap. 4

7) For example, see W.A. Goddard III and L.B. Harding, Ann. Rev. Phys. Chem. **29,** 363 (1978)

8) This is not strictly true; see Chapter 2 of this thesis.

CHAPTER 1

Resonating Wavefunctions - Introduction and Overview

I. Introduction

This chapter introduces many of the concepts which are important for understanding the results presented in later chapters, and gives an overview of the features of resonating wavefunctions. The first sections build up a description of the generalized valence bond (GVB) wavefunction, because it is the GVB form which is used to construct the resonating wavefunctions, while later sections discuss various results and examples. The reader who is uninterested in the details of how the resonating wavefunctions are optimized should find that this chapter provides the necessary background, while those familiar with wavefunctions and their optimization will still wish to read the latter sections of this chapter, as they introduce many concepts not contained in the "Description of the Method" chapter. The reader wishing more detail on the basics presented in the following sections should see Reference 1.

II. The MO and VB Wavefunctions - 2 Electrons

The valence bond (VB) wavefunction for the two electron system H_2 is written as

$$\Psi_{VB} = A[(lr+rl)]\,\alpha\,\beta] \tag{1}$$

where A is the antisymmetrizer and l and r are the atomic 1s orbitals on the left and right hydrogens, respectively,

(2)

In the VB wavefunction , when one electron is on the left-hand hydrogen the other electron is on the right-hand hydrogen, and vice-versa, stressing the atomic or covalent character of the bonding. The molecular orbital (MO) wavefunction for H_2 is

$$\Psi^{MO} = A[gg\,\alpha\beta] \tag{3}$$

where φ_g is the "MO" formed by adding l and r,

$$g = l + r \tag{4}$$

(we will not worry about normalization most of the time). The MO wavefunction emphasizes the "molecular" character of the bond, by putting two electrons in an orbital smeared over the molecule. The disadvantage of the MO wavefunction appears when we try to pull the molecule apart - the two electrons are still smeared over the whole molecule, leading to a higher energy state than two H atoms. This is easily demonstrated by expanding the Ψ^{MO} orbital in terms of l and r,

$$\Psi^{MO} = (l+r)(l+r)(\alpha\beta-\beta\alpha) = (ll+lr+rl+rr)(\alpha\beta-\beta\alpha) \tag{5}$$

While the lr and rl terms correspond to one electron on each H atom (covalent terms), the ll and rr terms correspond to an H^- ion and a H^+ (ionic terms), and the long R wavefunction is forced to include these terms because of the *form* of the MO wavefunction. Thus, while the MO wavefunction gives a good description of the electronic structure at small internuclear distances, it does not "dissociate" properly. The VB wavefunction, on the other hand, dissociates properly, leading to two ground state H atoms, as seen by inspection of equation (1).

III. The HF and GVB Wavefunctions - 2 Electrons

The Hartree-Fock (HF) wavefunction is the generalized version of the

MO wavefunction, in which the orbital g in equation (3) is allowed to have any shape which will give the lowest energy for the wavefunction. This gives a better description then MO in the bonding region, but still dissociates improperly, because no matter what shape φ_g takes, there will still be at least half "ionic" character at long R, due to the *form* of the wavefunction.

The generalized valence bond (GVB) wavefunction is the generalized form of the VB wavefunction, in which "l" and "r" are allowed to have any shape which will minimize the energy for the VB *form* of the wavefunction. The GVB wavefunction still dissociates properly, of course, and gives a better description of the electronic structure at short R than the VB wavefunction (and is equivalent to VB at long R). The result of allowing the orbital shapes to optimize in the GVB wavefunction is that the orbitals polarize to increase the favorable bonding overlap, shown schematically here:

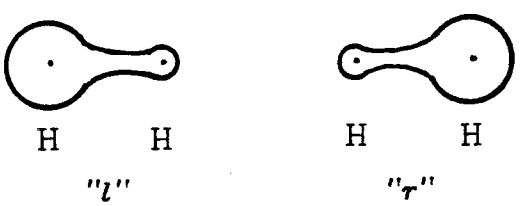

(6)

IV. The N.O. Representation of GVB

Because it is computationally more convenient to work with orthogonal orbitals, we actually solve for the GVB wavefunction using "Natural Orbitals" (NO), which are defined as

$$\varphi_{NO_1} = l + r \tag{7a}$$

$$\varphi_{NO_2} = l - r \tag{7b}$$

(again we are ignoring normalization). The GVB wavefunction can be rigorously written in terms of these NOs as

$$\Psi^{GVB} = A[(c_1(\varphi_{NO_1})^2+c_2(\varphi_{NO_2})^2)\alpha\beta] \tag{8}$$

where we must optimize the shapes of φ_{NO_1} and φ_{NO_2}, and also the values of C_1 and C_2 (with the constraint that $C_1^2 + C_2^2 = 1$). Once we have optimized the wavefunction, we can decompose φ_{NO_1} and φ_{NO_2} (using C_1 and C_2) to get back the orbitals "l" and "r", which look something like the drawings in (6), and which we call the "GVB orbitals". Inspecting equation (8), we can recognize the following important property of the GVB wavefunction. By choosing $C_2 = 0$, the GVB wavefunction becomes the Hartree-Fock wavefunction,

$$\Psi^{GVB}(c_2 = 0) = \Psi^{HF} = A[(\varphi_{NO_1})^2\alpha\beta]. \tag{9}$$

Since the orbital shapes and coefficients in the GVB wavefunction are optimized to give the lowest energy, the GVB energy will always be equal to or lower than the HF energy. Thus, the GVB wavefunction is able to describe both the MO-like character and the VB-like character in the bonding region. In general, at short R, we find that φ_{NO_1} looks very much like the optimum HF orbital, and C_1 is close to 1 while C_2 is small and negative. (At long R, $C_1 = -C_2 = \sqrt{2}$, which is pure VB.)

V. The HF and GVB Wavefunctions for Many Electrons

For many-electron systems, the HF wavefunction has many doubly occupied orbitals, and possibly some high-spin singly occupied orbitals,

$$\Psi^{HF} = A[\varphi_1^2\varphi_2^2 \cdots \varphi_m^2\,\alpha\beta\alpha\beta \cdots \alpha\beta\varphi_{m+1}\varphi_{m+2} \cdots \varphi_n\,\alpha\alpha \cdots \alpha] \ . \tag{10}$$

In the many-electron GVB wavefunction, we replace certain doubly occupied orbitals in the HF wavefunction with pairs of singlet-coupled GVB orbitals. Since the majority of electron pairs in a many-electron system are reasonably well described as two electrons in one orbital (e.g. the 1s

and 2s pairs in N atom), we usually perform this substitution only for a few pairs. We choose those pairs in which the extra correlation afforded by the GVB form will yield a more accurate description of the process of interest. For example, if we wish to describe the bond dissociation process in N_2, we apply this substitution to each of the three bond pairs, yielding

$$\Psi_{N_2}^{GVB} = A[\varphi_{1\sigma_g}^2 \varphi_{1\sigma_u}^2 \varphi_{2\sigma_g}^2 \varphi_{2\sigma_u} (\sigma_l \sigma_r + \sigma_r \sigma_l)(x_l x_r + x_r x_l)(y_l y_r + y_r y_l)\alpha\beta\alpha\beta \cdots \alpha\beta] \quad (11)$$

In the GVB terminology, we say that we have "correlated" three pairs, or that this wavefunction has three "GVB pairs". We call $\Psi_{N_2}^{GVB}$ a GVB(3/6) wavefunction, because we correlated three pairs using six natural orbitals (two per pair). In general, a GVB(n/m) wavefunction has n GVB pairs, correlated with m natural orbitals, and usually $m = 2n$. Sometimes, if we want to describe more of the correlation in a particular pair of electrons, we use more than two natural orbitals on that pair. The reader is referred elsewhere[2] for a discussion of the physical interpretation of using multiple NO's per GVB pair. Such a wavefunction is no longer a "single particle" wavefunction, a term we discuss in the next section.

VI. Definition of a Single Particle Wavefunction

Both the HF and GVB(n/$2n$) wavefunctions are "single particle" wavefunctions, which means that each electron can be assigned to a particular orbital. An example of a wavefunction which is *not* a simple particle wavefunction is a configuration interaction (CI) wavefunction,

$$\Psi^{CI} = c_1 \varphi_1^2 + c_2 \varphi_2^2 + c_3 \varphi_3^2 + \cdots \quad . \quad (12)$$

Because the electron pair is partly in φ_1 and partly in φ_2 and partly in φ_3, etc., we cannot assign a particular orbital to either electron. If the orbi-

tals in (12) are optimized simultaneously with the CI coefficients, we call this a multiconfigurational self consistent field (MCSCF) wavefunction. The GVB wavefunction as written in (8) is actually an MCSCF wavefunction, but due to its restricted form, it can be decomposed into one-electron orbitals (as in (1)), and thus it is still a single particle wavefunction. The advantage of a single particle wavefunction is that it retains a simple physical interpretation, since, for example, we can plot the orbitals and see where the electrons are. Thus, single particle wavefunctions enable us to extract principles which can be used to make predictions on other molecules and understand trends. The disadvantage of single particle wavefunctions is that they often do not contain enough of the important electron correlation to yield accurate results. For example, the GVB wavefunction predicts a bond energy of 94.9 kcal for H_2,[3] while a fancy MCSCF wavefunction is able to get 108.6 kcal,[4] much closer to the experimental value of 109.4 kcal.[5] The most highly correlated many-electron wavefunction which still retains a single particle interpretation is one which has one orbital for each electron, makes no restriction on the overlap of these orbitals with each other, and allows a totally general spin coupling of the electrons. We can write this wavefunction for n electrons as

$$\Psi^{OPT} = A[(\varphi_1\varphi_2\varphi_3 \cdots \varphi_n)\Theta] \ , \tag{13}$$

where Θ is the totally general spin function. We will refer to this wavefunction as spin-optimized GVB.[6,7] Solving for this wavefunction is unfeasible for more than a few electrons, so we usually try to make do with more restricted wavefunctions, such as HF and GVB.

VII. The R-GVB wavefunction

We wish to describe systems which require a resonance of more than one valence bond structure, such as benzene

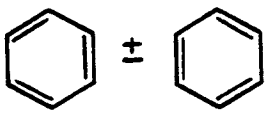

(14)

or the transition state in the HCl + H exchange reaction

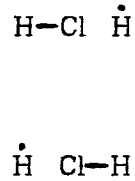

(15)

The GVB wavefunction is ideally suited for describing one of these localized structures, since it emphasizes the bonding character of a wavefunction. Taking benzene as our sample case, the first step is to solve for the GVB(3/6) wavefunction which correlates the three π bond pairs in one localized structure, and we denote this as Ψ_A,

Ψ_A = 

$$= A[(\sigma core)(\varphi_1\varphi_2+\varphi_2\varphi_1)(\varphi_3\varphi_4+\varphi_4\varphi_3)(\varphi_5\varphi_6+\varphi_6\varphi_5)\alpha\beta\alpha\beta\alpha\beta]. \tag{16}$$

The orbitals φ_1 through φ_6 are the GVB orbitals centered predominantly on carbon 1 through carbon 6, respectively

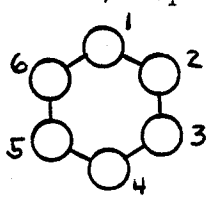

(17)

The orbitals φ_1 and φ_2 are plotted in Figure 1, and the localized bonding character is clearly evident. Due to the symmetry of the molecule, orbitals φ_3 and φ_4 are simply $\hat{C}_3$ rotated versions of φ_1 and φ_2, and φ_5 and φ_6 can be generated by rotating by $\hat{C}_3$ again.[8] The other resonance

structure, Ψ_B is also a GVB(3/6) wavefunction,

Ψ_B = 

$$= A[(\sigma core')(\varphi_1'\varphi_2'+\varphi_2'\varphi_1')(\varphi_3'\varphi_4'+\varphi_4'\varphi_3')(\varphi_5'\varphi_6'+\varphi_6'\varphi_5')\alpha\beta\alpha\beta\alpha\beta] \tag{18}$$

where we know by symmetry that a $\hat{C}_6$ rotation relates these two wavefunctions,

$$\Psi_B = \hat{C}_6(\Psi_A) \tag{19}$$

so that

$$\varphi_1' = \hat{C}_6(\varphi_1) \tag{20a}$$
$$\varphi_2' = \hat{C}_6(\varphi_2) \tag{20b}$$
$$\varphi_3' = \hat{C}_6(\varphi_3) \tag{20c}$$
$$\varphi_4' = \hat{C}_6(\varphi_4) \tag{20d}$$
$$\varphi_5' = \hat{C}_6(\varphi_5) \tag{20e}$$
$$\varphi_6' = \hat{C}_6(\varphi_6) \tag{20f}$$

We wish to mix Ψ_A with Ψ_B, leading to a total wavefunction of the form

$$\Psi_{TOT} = C_A\Psi_A + C_B\Psi_B \tag{21}$$

which has energy

$$E_{TOT} = \frac{<C_A\Phi_A+C_B\Phi_B\,|\,H\,|\,C_A\Phi_A+C_B\Phi_B>}{<C_A\Phi_A+C_B\Phi_B\,|\,C_A\Phi_A+C_B\Phi_B>}$$

$$= \frac{C_A^2H_{AA}+C_B^2H_{BB}+2C_AC_BH_{AB}}{C_A^2+C_B^2+2C_AC_BS_{AB}} \tag{22}$$

Because of the symmetry of this system, we know that

$$H_{AA} = H_{BB} \tag{23a}$$

$$C_A = \pm C_B \tag{23b}$$

and (22) thus reduces to

$$E_{TOT} = H_{AA} \pm \frac{H_{AB} - S_{AB} H_{AA}}{1 \pm S_{AB}} \tag{24}$$

where H_{AA} is the energy of Ψ_A ,

$$H_{AA} = \langle \Psi_A | H | \Psi_A \rangle \tag{25a}$$

H_{AB} is the Hamiltonian matrix element between

Ψ_A and Ψ_B,

$$H_{AB} = \langle \Psi_A | H | \Psi_B \rangle \tag{25b}$$

and S_{AB} is the overlap of Ψ_A with Ψ_B ,

$$S_{AB} = \langle \Psi_A | \Psi_B \rangle \tag{25c}$$

Ψ_{TOT} is a two-configuration CI wavefunction, but unlike most CI's, the configurations are not orthogonal. Ψ_A overlaps Ψ_B because we have made no restriction on the overlap of the orbitals in Ψ_A with those in Ψ_B. The advantage of this approach is that Ψ_A and Ψ_B are free to look like the chemically meaningful resonance structures shown in (14), so that mixing them corresponds to the "resonance" which chemists associate with the benzene molecule. The disadvantage of this wavefunction with overlapping configurations is that the H_{AB} and S_{AB} matrix elements are much harder to evaluate. Thus, with very few excepitions, chemists have used orthogonal CI wavefunctions, which sacrifice interpretability for affordability. The next chapter presents a method which vastly simplifies the computation of H_{AB}, making overlapping CI wavefunctions feasible (though still much more expensive than orthogonal CI's).

Using the method of the next chapter, we obtain[9]

$$H_{AB} = -5.713776$$
$$S_{AB} = \ \ 0.887276$$

which combined with

$$H_{AA} = E_A = -6.415199$$

enables us to compute the energy of the resonant and antiresonant states from (24) as

$$E_1 = E_A - 7.5 \text{ kcal} \quad (C_A = + C_B = 0.51)$$

$$E_2 = E_A + 128.4 \text{ kcal} \quad (C_A = - C_B = 2.11) \ .$$

Thus, mixing the two GVB(3/6) wavefunctions leads to a lowering of 7.5 kcal. We call this a *resonating* GVB or R-GVB wavefunction, (in this case an R-GVB(3/6)). The R-GVB wavefunction is not strictly a single-particle wavefunction, since each electron is partly in a Ψ_A orbital and partly in a Ψ_B orbital. However, the R-GVB wavefunction does retain a physically meaningful form, corresponding to the drawings in (14) for example, which chemists have felt comfortable with for years. Thus we say that the R-GVB wavefunction retains a "single particle plus resonance" interpretation.

The first thing we notice in our benzene case is that the antiresonant state goes up much more than the resonant state goes down. This can be understood by examining the second term in equation (24), which is responsible for the raising and lowering of the two states. If S_{AB} were zero, the two states would be displaced equally about E_A, with a splitting of $2H_{AB}$, but for nonzero S_{AB}, the denominator causes an imbalance in the displacement. Because S_{AB} is large in this case, the effect is dramatic. It is always the antiresonant state which is displaced further, even if S_{AB} is less than zero (in which case H_{AB} will be positive, and $C_A = - C_B$ will be the resonant state). This is not obvious from inspecton of (24), but we can understand it physically as follows: When the GVB wavefunctions are mixed, the resonant state is lowered because the combination of

wavefunctions samples a larger region of configuration space than either one alone. Any amount the wavefunctions overlap corresponds to a redundancy, and thus cannot help in lowering the energy. In the limit where $S_{AB} = 1$, the resonance lowering is zero, because there is no new space obtained by mixing Ψ_A and Ψ_B. The antiresonant state, however, is essentially the piece left over after mixing Ψ_A and Ψ_B , and the more that Ψ_A and Ψ_B overlap, the less that is left over to adequately describe the antiresonant state, thus raising its energy. In the limit where $S_{AB} = \pm 1$, the antiresonant state is undefined, since there is only one degree of freedom in the space, which is used up by the resonant state.

Another aspect we notice is that the "resonance energy" of 7.5 kcal is much smaller than the 36 kcal usually associated with the resonance in benzene, obtained by comparing the heat of hydrogenation of benzene to three times the heat of hydrogenation of cyclohexene.[10] There are at least three reasons for this difference. First, the experimental resonance energy is obtained by comparing systems with different steric interactions, and thus may not be the same as the purely electronic resonance energy at a fixed benzene geometry (though this is not the key issue here). Second, by comparing the R-GVB energy to the GVB energy, we imply that the GVB wavefunction is a "nonresonating" reference state. However, the GVB wavefunction does include some resonance as we discuss later. Third, the orbitals in the GVB wavefunction were optimized for the GVB form of the wavefunction, but the orbitals in the R-GVB wavefunction were not optimized for the R-GVB form; i.e. the orbitals were not reoptimized in the presence of resonance. The second and third flaws each cause the calculated resonance energy to be too low, so that 7.5 kcal is a lower bound on the resonance energy.

One way to allow the wavefunction to partially relax in the presence of resonance is reoptimizing the natural orbital coefficients in eqn (8). We call this a pairwise-relaxed R-GVB, or R-GVB(pr) wavefunction, because we relax the NO coefficients while maintaining the pairwise normalizations which ensures that each subwavefunction is still a single-particle GVB wavefunction. (We could lower the energy further by allowing totally general relaxation of the coefficients, but this would lose the simple interpretation, so that we might as well do a large CI using an orthogonal basis.) The R-GVB(pr) wavefunction for benzene leads to

$$E_{RES} = E_A - 8.7 \text{ kcal}$$

and

$$E_{ANTI} = E_A + 128.4 \text{ kcal}$$

where we have allowed a different set of coefficients for each state, so that both states are lowered from R-GVB.

VIII. The GRVB Wavefunction

If we allow the orbital shapes in Ψ_A and Ψ_B to reoptimize in the presence of resonance, we have a generalized resonating valence bond (GRVB) wavefunction, so called because it is the "generalized" (orbital-shape optimized) version of the resonating VB wavefunction. The form of the GRVB wavefunction is still exactly as in (16), (18) and (21) (so that each subwavefunction is still a GVB wavefunction), except that Ψ_{TOT} is optimized rather than Ψ_A. A GRVB(3/6) calculation on benzene leads to

$$E_{RES} = E_A - 13.5 \text{ kcal}$$

$$S_{AB} = 0.602618$$

for the resonant state, and the GVB orbitals from this wavefunction are plotted in Fig. 1, along with the GVB(3/6) orbitals for comparison. The GRVB orbitals are seen to be much more localized than the GVB orbitals. The GVB wavefunction includes some resonance by smearing out the orbitals of the one structure to contain some character of the other structure. At the GRVB level, the orbitals in each GVB subwavefunction are free to localize strongly, since the other resonance structure is explicitly included in the wavefunction. This is also evident from the drop in S_{AB} from 0.887 to 0.603 upon going to GRVB, an occurrence which is generally true of GRVB wavefunctions.

Optimizing the GRVB wavefunction for the antiresonant state leads to

$$S_{AB} = 0.716054$$

$$E_{ANTI} = E_A + 96.4 \text{ kcal},$$

an energy drop of 32.0 kcal from R-GVB. This large change is in accord with the idea that the GVB wavefunction is trying to describe both the localized VB structure *and* the resonance, so that GVB orbitals are more appropriate for the resonant state than the antiresonant state. The antiresonant GRVB orbitals are plotted in Figure 2.

IX. On the Definition of a Resonance Energy

Comparing the GVB(3/6) energy to the GRVB(3/6) energy leads to a resonance lowering of 13.5 kcal. However, we demonstrated in Section VIII that the GVB(3/6) wavefunction does include some resonance. To rigorously define a resonance energy, the energy of the pure, nonresonating state must be known, and this is not easily determined. Thus, the GRVB energy lowering (compared to GVB) does not correspond to the true electronic resonance energy. It *can*, however, be taken as a lower bound on the true resonance energy, since E(GVB) will always lie at or below the energy of the pure, nonresonating state.

X. Resonance Between Multiple or Nondegenerate Structures

If the two VB structures being resonated are not related by a symmetry operation, so that $E_A \neq E_B$, or if more than two structures are involved, then evaluating the energy of Ψ_{TOT} requires solving for the coefficients C_A, C_B, $\cdots$ in equation (21). This is accomplished by solving the secular equation, written here in matrix form

$$\mathbf{HC} = \mathbf{SCE} \tag{26}$$

where the elements of **H** are the hamiltonian matrix elements H_{AA}, H_{AB}, etc., **S** contains the overlap elements, **E** is the resulting diagonal matrix of energies, and **C** is the matrix of solution vectors, so that a column of **C** contains $C_A, C_B, \cdots$. The R-GVB and GRVB approaches are still well defined for wavefunctions of this type.[11]

For the case of two nondegenerate structures, the R-GVB approach requires that both GVB structures be optimized (rather than generating one from the other using a symmetry operation). Sometimes this is not

possible, if one structure (Ψ_B) is too much higher in energy. A GVB solution for Ψ_B is artificial, since if the orbitals were truly "optimum", the wavefunction would have the energy of the lower state. However, very often such wavefunctions can be "trapped", due to the localized nature of GVB, and do have a certain physical meaning, corresponding to a VB structure. If Ψ_B can not be trapped, the R-GVB is inapplicable, but the GRVB approach can still be used. An example of this is the H-H-F transition state of the H_2 + F reaction. The reaction has a very "early" transition state, with a short H-H bond and a very stretched H-F bond.[12] A GVB(1/2) calculation leads to a strongly localized H-H bond pair, with the unpaired electron on the F atom (Ψ_A), and the GVB(1/2) wavefunction with an H-F bond (Ψ_B) can not be trapped because it relaxes to Ψ_A. Using the GRVB approach, Ψ_B can be trapped, since Ψ_A is already included in the wavefunction, and the result is C_A = 0.9147, C_B = -0.2180, E_{RES} = E_A - 9.1 kcal. In general, in a nondegenerate resonance system, the lower (resonant) state will be predominantly Ψ_A. The amount of resonance lowering usually will be smaller than similar systems with degenerate VB structures, and will decrease as the energy separation is made larger. For example, in the cyclobutadiene system,

$\Psi = C_A$  $+ C_B$ 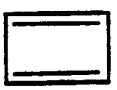 (27)

the resonance energy is 22 kcal at a square geometry where $E_A = E_B$, but reduces to 4.3 kcal at the optimum rectangular geometry where $E_B = E_A$ + 66.2 kcal.

The GRVB approach must be applied judiciously in cases where E_B is far above E_A, since the Ψ_B orbitals may converge to something other than the VB structure. For example, in the reaction

(28)

the transition state is well described by

$$\Psi_{TOT} = C_A(\ \dot{N}{=}N{-}H\ ) + C_B(\ N{\equiv}N\ \dot{H}\ )\ . \qquad (29)$$

(Ψ_A) (Ψ_B)

However, solving for the GRVB wavefunction at a geometry near the HNN limit results in a Ψ_B which does not look like that in (29), but rather is describing the correlation of one of the N_2 electron pairs which was not correlated in Ψ_A. This happens because mixing in the highly unfavorable Ψ_B structure leads to a smaller resonance energy than the energy lowering obtained by correlating another electron pair. When this occurs, the GRVB energy is no longer appropriate for interpretation within the resonating VB model, though it is a lower bound on the "correct" GRVB energy.

In the case where there are multiple degenerate resonance structures, each of which have the same interaction matrix elements (H_{AB},S_{AB}) with every other structure (this will not always be the case), the total resonance lowering is increased less with each new structure which is mixed in (assuming R-GVB level, so that H_{AB} and S_{AB} don't change). For example, in the positive ion of VCl_4, which has one bond which is predominantly metal 4s to chlorine 3p, while the other three are metal 3d to chlorine 3p,

$\Psi_A =$ 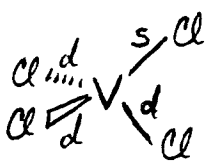 (30)

there are four possible resonance structures. Mixing two, three or four of

these together leads to

$$E(1) = E_A \tag{31a}$$

$$E(2) = E_A - 12.2 \text{ kcal} \tag{31b}$$

$$E(3) = E_A - 16.9 \text{ kcal} \tag{31c}$$

$$E(4) = E_A - 19.5 \text{ kcal} \tag{31d}$$

and using the same matrix elements (H_{AA} = -142.9183, H_{AB} = -114.257655, S_{AB} = 0.799216) to predict the lowering of the hypothetical wavefunctions with more than four resonance structures gives

$$E(8) = E_A - 23.3 \text{ kcal} \tag{31e}$$

$$E(16) = E_A - 25.4 \text{ kcal} \tag{31f}$$

$$E(32) = E_A - 26.5 \text{ kcal} \tag{31g}$$

$$E(64) = E_A - 27.0 \text{ kcal} \tag{31h}$$

If, instead of converging, the resonance energy kept increasing, systems such as graphite (which has a nearly infinite number of resonance structures) would be extraordinarily stable.

XI. Other Features of Resonating Systems

The effects of resonance in the benzene example are fairly representative of the behavior of many resonating molecules we have studied. Table 1 shows the R-GVB and GRVB results for a variety of systems, and in this section we point out some of the trends and the reasons for the exceptions to these trends.

While we know that if all else is equal, a high overlap, S_{AB}, will yield

less resonance lowering than a low overlap because low overlap means more of configuration space is sampled, examination of Table 1 shows no clear correlation between S_{AB} and the R-GVB resonance lowering. This is because there are two ways that the overlap can be small, as demonstrated with the one-electron wavefunctions φ_1, φ_2, and φ_3:

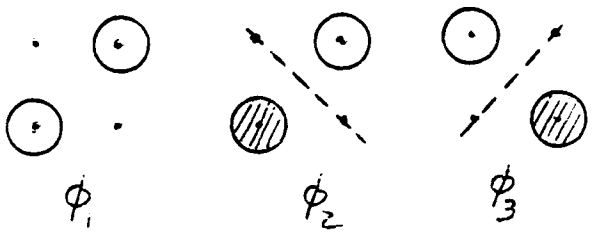

(32)

The overlap between φ_1 and φ_2 is zero because of a cancelation of regions of positive and negative overlap, while the overlap $\langle\varphi_1|\varphi_3\rangle$ is zero because there is no region of overlap. We can say that φ_1 and φ_2 have a large "absolute overlap", meaning that the overlap between $|\varphi_1|$ and $|\varphi_2|$ would be large, while φ_1 and φ_3 have a small absolute overlap. If the overlap between two wavefunctions is low because of low absolute overlap, then the resonance interaction will likewise be small. This is observed in the N_2^+ and CO_2^+ core ionized states, which have low absolute overlap due to the high degree of localization in the 1s core holes. The R-GVB resonance lowering is seen to be only 1 kcal (S_{AB}<0.01). In contrast, the R-GVB mixing of the two forms of neutral CO_2

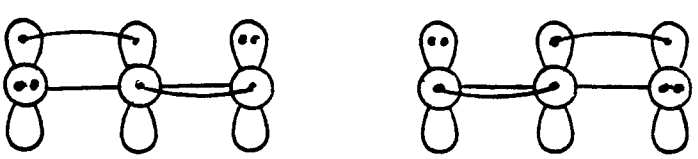

(33)

leads to a resonance lowering of 12.4 kcal, even though the overlap is 0.945.

The relation between overlap and resonance lowering does hold when comparing R-GVB and GRVB wavefunctions for the same molecule. For every system we have studied, S_{AB} is smaller (in magnitude) for the GRVB wavefunction than the R-GVB wavefunction, in accord with the concept that there is less delocalization of Ψ_A to include Ψ_B character once the resonance is included explicitly in the wavefunction. Since a large S_{AB} between the GVB wavefunctions is indicative of a large amount of "delocalization resonance", we expect a large S_{AB} to signal a large GRVB resonance lowering compared to R-GVB. This is because the delocalization tendency will be strongest when the molecule has the most to gain from the resonance, and if it is strongly delocalized, it will gain more additional resonance lowering in a GRVB optimization than a wavefunction which is already fairly localized at the GVB level. In some of the systems listed in Table 1, the delocalization tendency is so strong that the wavefunction overlap is unity (e.g. triplet cyclobutadiene, H_3, He_2^+), and the additional GRVB lowering is more than 10 eV in each of these cases (HHF is excluded, since $E_A \neq E_B$).

Another trend is that related systems often have similar resonance lowerings. For example, the square H_4 system (the saddle point in the rectangle-square-rectangle $H_2 + D_2 \rightarrow 2HD$ pathway has an R-GVB resonance of 23.1 kcal, while the isomorphic system, square cyclobutadiene has an R-GVB resonance of 21.8 kcal. These systems have the special property that the GVB wavefunction is almost resonance-free, due to the principles of forbidden reactions (see Chapter 5 Section V), and thus the R-GVB resonance lowering is very close to being the true electronic resonance energy. This property makes the comparison of H_4 and C_4H_4 especially clean. This 22-23 kcal resonance is for each species in its optimum

square geometry. The relationship also appears to hold for other geometries as well; distorting H_4 by the same amount as the rectangular geometry of C_4H_4 leads to an R-GVB resonance of 4.3 kcal for C_4H_4, and 5.7 kcal for H_4. If the square geometry is retained, but the side length is stretched to infinity, the resonance in both C_4H_4 and H_4 vanishes.

Similar resonance effects are also exhibited in the reaction transition state species HFH and HClH. For both cases the R-GVB lowering is small (due to delocalization), 3.1 kcal and 5.2 kcal, respectively, and increases to 21.8 and 23.8, respectively, for GRVB. The H_3 transition state shows slightly different behavior. At the GVB level, the delocalization tendency is so strong that $S_{AB} = 1$, so that $E_{RES}^{R-GVB} = 0$, and the GRVB resonance lowering is 13.7 kcal (actually GRHF[13]). The 13.7 kcal GRVB lowering cannot be directly compared to the 22-24 kcal lowering in HFH and HClH, since the GVB reference state contains an undetermined amount of extra lowering, due to delocalization resonance, not present in HFH and HClH. Removing this extra lowering from the H_3 reference state would raise the effective GRVB lowering, making it closer to the HClH and HFH values.

XII. Conclusions

The reader should now have a feeling for the nature of resonating VB wavefunctions. More in depth examples are given in the following chapters. To summarize, the GVB wavefunction is the basic unit of the R-GVB and GRVB methods, because it allows the appropriate VB character in the localized bonding structures. The R-GVB approach simply mixes two GVB wavefunctions, which is sufficient if the two wavefunctions are already highly localized. The GRVB method allows the orbitals to reoptimize in the presence of resonance, an effect that is important if the

GVB wavefunction is strongly delocalized. The difference between the GVB energy and the GRVB energy is a lower bound to the true fixed-geometry electronic resonance energy. Both the R-GVB and GRVB wavefunctions retain a "single-particle plus resonance" interpretation, so that orbitals may be plotted and chemical concepts may be developed.

References

1) (a) W.A. Goddard III, Course Notes for Chem. 120, Caltech (1981); (b) L. Pauling, *The Nature of the Chemical Bond*, 3rd *ed.* (Cornell University Press, Ithaca, New York, 1960); (c) H.F. Schaeffer III, *The Electronic Structure of Atoms and Molecules. A Survey of Rigorous Quantum Mechanical Results* (Addison-Wesley, London, 1972); (d) I.N. Levine, *Quantum Chemistry*, 2nd *ed.* (Allyn and Bacon, Boston, Mass., 1976); (e) M.A. Morrison, T.L. Estle and N.F. Lane, *Quantum States of Atoms, Molecules and Solids*, (Prentice Hall, Englewood Cliffs, N.J., 1976)

2) F.W. Bobrowicz and W.A. Goddard III, in: *Modern Theoretical Chemistry, Vol. 3, Methods of Electronic Structure Theory*, edited by H.F. Schaeffer III (Plenum, New York 1977), Chap. 4

3) See Chapter 5, Table 9 of this thesis.

4) S. Hagstrom and H. Schull, Rev. Mod. Phys. %35, 624 (1963)

5) K.P. Huber and G. Herzberg, *Molecular Spectra and Molecular Structure, Vol. 4, Constants of Diatomic Molecules*, (Van Nostrand Reinhold Co., New York 1979)

6) R.C. Ladner and W.A. Goddard III, J. Chem. Phys. **51,** 1073 (1969)

7) Spin-optimized GVB is not the same as "SOGVB", which stands for "strong-orthogonal" GVB; see W.J. Hunt, T.H. Dunning Jr. and W.A. Goddard III, Chem. Phys. Lett. **3,** 606 (1969); W.J. Hunt, P.J. Hay and W.A. Goddard III, J. Chem. Phys. **57,** 738 (1972)

8) $\hat{C}_n$ refers to the $\frac{2\pi}{n}$ radian rotation about the principle molecular axis.

9) The energies are small because we have eliminated the σ core electrons from the calculation. The GVB(3/6) total energy of benzene is -230.68504 h.

10) p. 193 of Ref. 1b.

11) The GRVB program is currently limited to two subwavefunctions.

12) C.F. Bender, P.K. Pearson, S.V. O'Neil and H.F. Schaeffer III, J. Chem. Phys. **56,** 4626 (1972)

13) GRHF is defined as generalized resonating Hartree-Fock.

Table 1. Some representative resonating systems. The energies are in kcal with respect tot he single structure GVB energy. A ± B means A + B is resonant and A - B is antiresonant (using a reasonable choice for the wavefunction phases). A ± λB means A is the dominant resonant structure and B is the dominant antiresonant structure.

System	Wavefunction Level	S_{AB}	R-GVB E_{res}	R-GVB E_{anti}	GRVB E_{res}	GRVB E_{anti}	GRVB S_{AB}^{res}	GRVB S_{AB}^{anti}
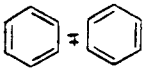	GVB(3/6)	0.8705	-7.5	128.4	-13.5	96.4	0.6026	0.7186
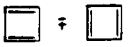	GVB(2/4)	-0.2483	-20.6	34.1	-21.8	33.4	-0.2140	-0.2781
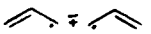	GVB(1/2)	-0.754	-9.8	69.9	-17.7	57.5	0.00029	-0.5441
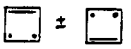	GVB(1/2)	1.0	0	--	-16.1	59.4	0.0826	0.00032
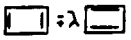	GVB(2/4)	-0.2532	-4.3	++18.9				
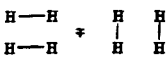	GVB(2/4)	-0.2254	-23.1	36.5				
H—H Ḣ ∓ Ḣ H—H	HF	1.0	0	--	-13.7			
H—F Ḣ ± Ḣ F—H	GVB(1/2)	0.9437	-3.1	107.6	-21.8	67.0	0.4539	-0.0686
	GVB(1/5)		-2.0		-22.3			
H—Cl Ḣ ± Ḣ Cl—H	GVB(1/2)	0.9443	-5.2	81.6	-23.8		0.55	
	GVB(1/5)	0.9371	-6.5	198.6				
H—H Ḟ + λ Ḣ H—F	GVB(1/2)	1.0	0	--	-9.1		0.2904	
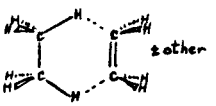	GVB(3/6)	0.9758	-4.1	331.8				
	GVB(5/10)	0.0023	-1.1	1.1				
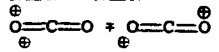	GVB(2/4)	0.00036	-1.4	1.4				
NeNe ∓ NeNe	HF	-0.7062	-13.0	75.8	-42.6			
HeHe ∓ HeHe	GRHF	1.0	0	--	-19.4			
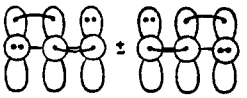 (CO_a)	GVB(2/4)	0.9448	-12.4	436.7				
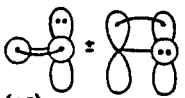 (CO)	GVB(1/2)	0.9752	-7.5	597.4	-18.2		0.6504	
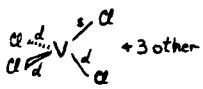 + 3 other	GVB(3/6)	0.7992	-16.9	109.6				
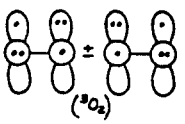 ($^3O_2$)	GVB(1/2)	1.0	0	--	-26.4	94.3	0.3798	0.0575
$Fe^{II}(H_2O)_n Fe^{III}(H_2O)_n$ + other	HF	<0.04	<0.3					
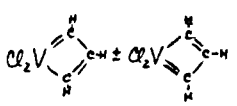	GVB(2/4)	0.626	-9.5	40.7				

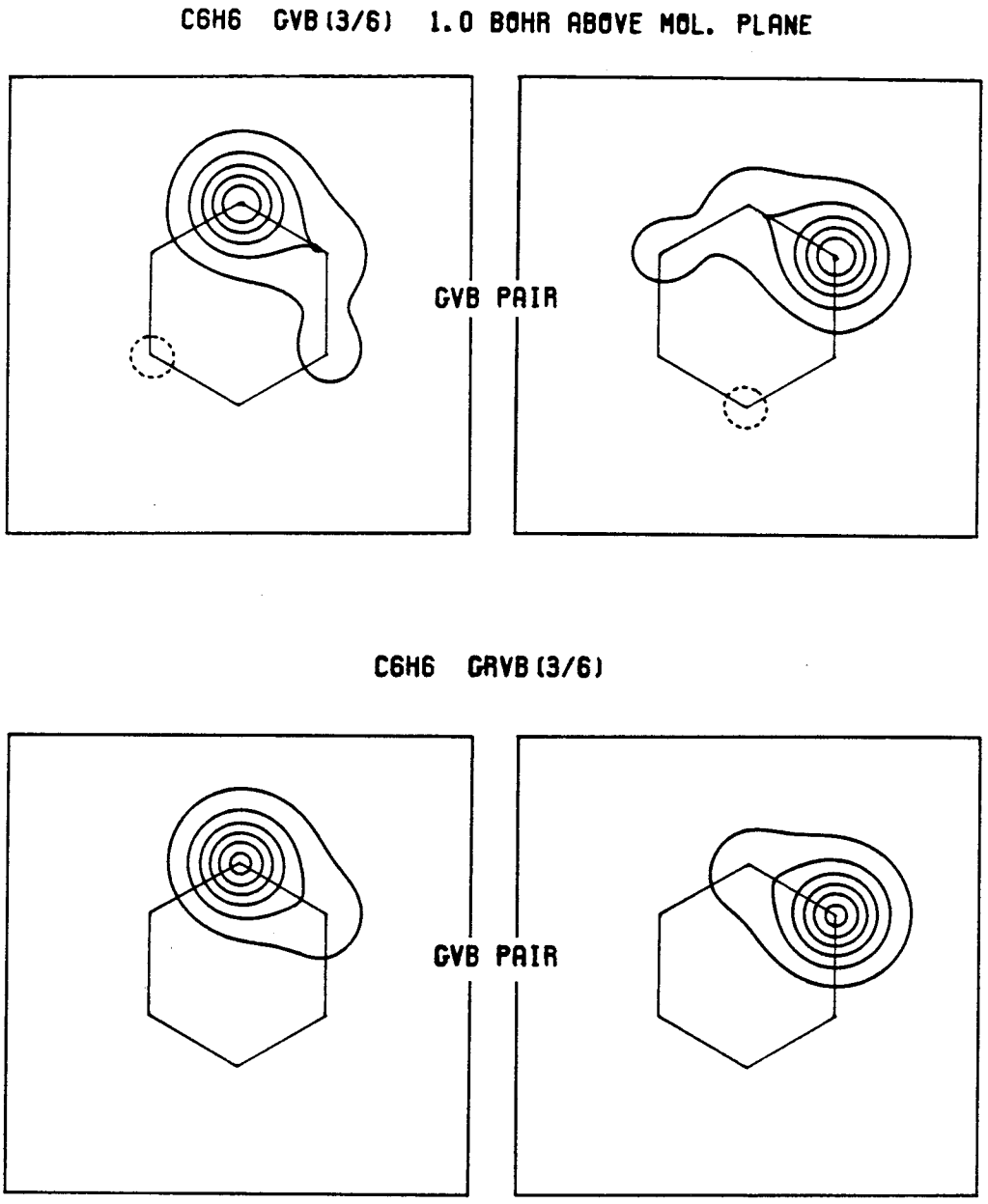

Figure 1. The GVB orbitals (top) and GRVB orbitals (bottom) for one bond pair in benzene. The plotting plane is 1.0 bohr above the molecular plane, with the projected position of the carbon framework indicated for clarity.

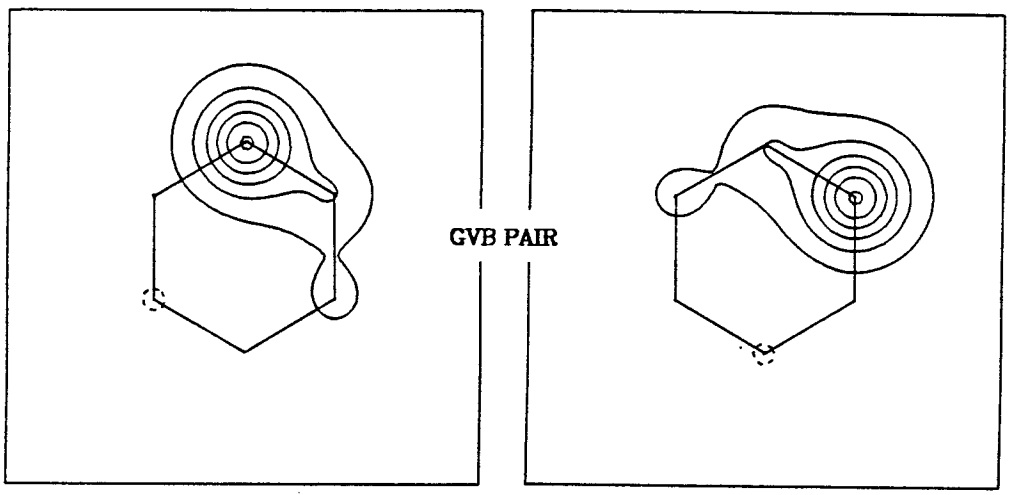

Figure 2. The GRVB orbitals for the antiresonant state of benzene, plotted as in Figure 1.

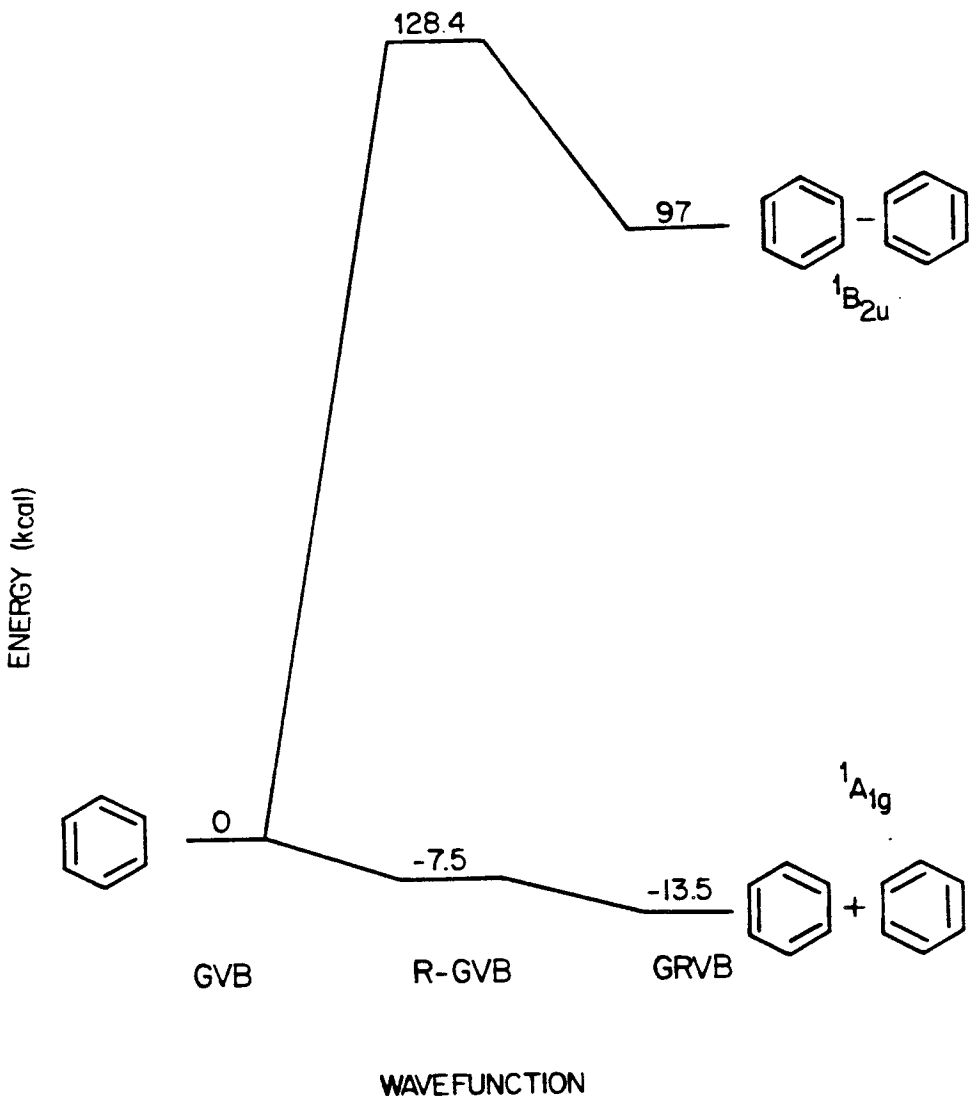

Figure 3. Energy diagram for various levels of resonance in benzene, GVB(3/6), R-GVB(3/6) and GRVB(3/6).

CHAPTER 2

Motivation and Previous Work

I. Introduction

In the last chapter we appealed to the principles of valence bond (VB) theory to recognize molecular systems which would be best described as a resonance of localized bonding structures. In this chapter we show that the problem of mixing nonorthogonal wavefunctions is of general interest, both to VB and molecular orbital (MO) theorists, and discuss the previous efforts to solve this problem.

It has been known for many years that certain systems require a localized wavefunction.[1-24,44-48] A dramatic example is the 1s core ionization of O_2.[6] Solving for the Hartree-Fock (HF) wavefunction with a 1s core hole localized on one oxygen yields an energy more than 10 eV lower than if the wavefunction is forced to retain the full molecular symmetry, with the singly-occupied core orbital delocalized onto both oxygens. This phenomenon, in which the wavefunction can achieve a better energy by relaxing to a lower symmetry than that of the molecular geometry, is known as "symmetry breaking". Other cases which have been observed include allyl radical[25,26] and allyl-like compounds,[2] the ground state of NO_2,[10] trimethylene methane,[27] the $n\pi^*$ states and lone pair ionized states of compounds with multiple carbonyl groups such as glyoxal,[17] parabenzoquinone[16,20,23] and PMDA (pyromellitic acid dianhydride),[22] nitrogen $n\pi^*$ and n ion states of pyrazine,[13,20] core-ionized states of various first-row compounds,[5,6,9,14,15,21,24,28] and the valence-ionized states of small copper clusters.[3,4,11] In mathematical terms, this effect can be viewed as an instability in the solution to the HF equations, and some

research has been directed towards determining when such instabilities should occur.[26,29] Such a viewpoint is natural within the context of MO theory, since molecular orbitals are expected to be delocalized over the molecule, each belonging to some irreducible representation of the molecular point group. In VB theory, on the other hand, broken symmetry (b.s.) solutions can be viewed as a tendency for the wavefunction to achieve the chemically intuitive localized structure (e.g., the b.s. solution in the π space of allyl radical corresponds to a localized π bond--the natural VB structure). From either viewpoint, however, the broken symmetry wavefunction causes problems for the following reasons. The true electronic wavefunction should possess the full symmetry of the nuclear geometry, and the broken symmetry solution does not. If the molecular symmetry is imposed on it (while optimizing), the resulting solution will give faulty energetics (e.g., for O_2, this approach would predict a 1s ionization potential 10 eV too high). However, using the b.s. solution to determine energetics is also inappropriate, since it is a mixture of two (or more) states with the full molecular symmetry, and the splitting between these states is thus unknown. Further, if a geometry optimization is being performed, using the b.s. solution can lead to an incorrect, distorted geometry (e.g., inequivalent bond lengths in allyl radical), while using the symmetry restricted solution will cause a discontinuity in the energy surface when the geometry passes from symmetric to asymmetric.

Clearly, the best approach to this problem is to resonate the b.s. solutions. This would yield the states of the proper symmetry, while retaining the important electron correlation which caused the break in symmetry. However, such a calculation is not trivial, as is shown in the

following paragraph.

Taking the total wavefunction as a linear combination of two broken symmetry solutions ψ_A and ψ_B,

$$\Psi_{TOT} = c_A\psi_A + c_B\psi_B \ , \tag{1}$$

we obtain an energy expression,

$$E = \frac{c_A^2 H_{AA} + c_B^2 H_{BB} + 2\, c_A c_B H_{AB}}{c_A^2 + c_B^2 + 2\, c_A c_B S_{AB}} \ , \tag{2}$$

where H_{AA} and H_{BB} are the energies of ψ_A and ψ_B, respectively,

$$H_{AB} = \langle\psi_A|\mathbf{H}|\psi_B\rangle \tag{3}$$

and

$$S_{AB} = \langle\psi_A|\psi_B\rangle \ , \tag{4}$$

where **H** is the usual Hamiltonian operator. Expressing ψ_A and ψ_B as an antisymmetrized product of spin orbitals,

$$\psi_A = A[\varphi_1^A\varphi_2^A\cdots\varphi_n^A] \tag{5a}$$
$$\psi_B = A[\varphi_1^B\varphi_2^B\cdots\varphi_n^B] \ , \tag{5b}$$

where A is the antisymmetrizer, and each φ_i is a spatial orbital times a spin function, we can write the overlap term as

$$\begin{aligned} S_{AB} &= \langle A[\varphi_1^A\varphi_2^A\cdots\varphi_n^A]\,|\,A[\varphi_1^B\varphi_2^B\cdots\varphi_n^B]\rangle \\ &= \langle\varphi_1^A\varphi_2^A\cdots\varphi_n^A\,|\,A[\varphi_1^B\varphi_2^B\cdots\varphi_n^B]\rangle \ . \end{aligned} \tag{6}$$

Because there is no restriction on the overlap between the orbitals in ψ_A with the orbitals in ψ_B,

$$\langle \varphi_i^A | \varphi_j^B \rangle = ? \quad , \tag{7}$$

all $n!$ permutations of the φ_B orbitals generated by the antisymmetrizer yield terms which may be nonzero (many of these terms will be zero by spin overlap). Similarly, H_{AB} is composed of $n!$ terms which need to be calculated. In a normal configuration interaction (CI) wavefunction, in which every configuration is constructed from the same set of orthonormal orbitals, at most n^2 terms survive in any Hamiltonian matrix element between two configurations. This is because any permutation of higher order than a simple transposition lines up three or more orthogonal spin orbitals, and the Hamiltonian contains only one- and two-electron operators, leaving at least one zero orbital overlap multiplying the term.

Hence, while a conventional CI involving 20 or 30 electrons and thousands of configurations is easily solved, an overlapping CI with $n!$ dependence is computationally unfeasible for more than a few electrons.

II. Orthogonal CI Approaches

The usual approach to this problem has been to use standard CI wavefunctions to simulate the nonorthogonal CI. This can be accomplished in two ways:

(1) The symmetry-restricted SCF orbitals are used as the CI basis, and the CI is designed to restore the localized character to the total wavefunction, while retaining the full symmetry.

(2) The symmetry-broken SCF orbitals are used as the CI basis, and the CI is designed to restore the full molecular symmetry to the wavefunction.

Procedure (1) has the advantage of using a symmetrical CI basis which is computationally more efficient than an asymmetric basis [as in

procedure (2)]. The disadvantage of procedure (1) is that the CI must include very high-order excitations to actually restore the localized character to the wavefunction. This approach was used by Butscher *et al.*[28] in describing the 1s ionized state of N_2. Using a multi-reference singles and doubles CI (MRDCI) approach, they were able to reduce the IP from the SCF value of 419.77 eV to 410.51 eV (experiment = 409.92[30]). This required a 31,694 configuration CI (though a selection procedure reduced the actual computational work to 2118 configurations). Their similar treatment of the core-ionized shakeup states required 200,000 to 300,000 configurations, a calculation which is well beyond the capabilities of most CI programs. On a similar system, O_2^+, Ågren *et al.*[5] used a multiconfigurational SCF (MCSCF) procedure called complete active space SCF (CASSCF),[31,32] but were not able to do as well as the broken symmetry ΔSCF results in describing either the IP or the splittings between the shakeup states. Very recently, Bénard[4] has proposed a systematic procedure for designing compact CI expansions to describe localized hole states. The procedure defines as a subset of the occupied orbitals those n orbitals which would be recombined to give the localized hole orbital (e.g., this subset would be $\varphi_{1\sigma_g}$ and $\varphi_{1\sigma_u}$ for the 1s core hole state of N_2^+). Within this subset, all single excitations are performed (i.e., the hole is moved into each of the other n-1 orbitals), and from this list of n-1 configurations (the original reference configuration is excluded), all single excitations are performed. Bénard tested this approach on the d_{σ_u} hole state of Cu_2^+ by generating this CI expansion for both the symmetry-restricted orbitals (37 configurations) and the symmetry-relaxed orbitals (71 configurations). In contrast to previous (slightly more extensive) CI's he had performed, the special expansion led to a lower energy for the

symmetry-restricted basis than for the symmetry-relaxed basis. From this he concluded that all the localization correlation errors had been recovered in the symmetry-restricted CI wavefunction. Bénard's approach is appealing since it is generalizable to any localized hole system, and requires only a very short CI list. However, it is the feeling of this author that the method would not work for a case involving more extensive valence electron reorganization, such as core-ionized O_2.

One other point can be made about MCSCF and CI methods using procedure (1). Such an approach cannot be used if a geometry optimization is being performed along the asymmetric coordinate corresponding to the symmetry of the broken symmetry wavefunction. This is because there will be a discontinuity at the point where the geometry passes from slightly asymmetric (with an asymmetric wavefunction) to symmetric (where the wavefunction is symmetry-constrained), unless a sufficiently large CI is being used (in general, this would need to be a full CI). For such a geometry search, the type (2) procedure must be used, and we discuss it next.

The advantage of procedure (2) is that the localization correlation is automatically included in the wavefunction. The disadvantage is that a very large CI may be required to include the character of the other broken symmetry solution. Whether the CI is accomplishing this can be tested by checking whether the full symmetry is restored to the wavefunction when the calculation is performed at a symmetric geometry. Davidson and co-workers[10,27,33] have investigated the potential surfaces of various molecules using a CI from a broken symmetry solution. They obtained satisfactory results for the excited states of trimethylene methane[27] by performing a full π CI in an STO-3G minimum

basis. For the two lowest states of NO_2,[10] they found that even an all singles and doubles CI was insufficient to restore the dual character from one set of SCF orbitals, and the results of truncated CI lists were strongly dependent on the choice of molecular orbitals for the CI basis. For glyoxal they concluded that the CI required to investigate the distorted geometries of the $n\pi^*$ states was computationally unfeasible.[33]

Another approach, which incorporates the localized character from *both* broken symmetry solutions directly into the CI basis, is that used by Wadt and Goddard[1] in describing the $n\pi^*$ and n ion states of pyrazine. They took linear combinations of each occupied with the corresponding occupied from the opposite b.s. solution, thus forming a doubled set of symmetry orbitals to use as the CI basis. This approach is appealing since the CI basis contains both the localized character and (at symmetric geometries) the fully symmetry of the molecule. In addition, this method may be used as the geometry becomes asymmetric with no loss of continuity, assuming that both b.s. solutions may still be found (one will be higher energy and may relax to the lower-energy solution, though often the higher-energy wavefunction can be successfully trapped). Hence, this approach would be suitable for geometry searches. However, though Wadt and Goddard obtained reasonable results for the state splittings in the pyrazine case, there is no general prescription for generating the CI in this basis which corresponds to a simple resonating wavefunction, making it difficult to describe different states with consistent levels of correlation.

III. Nonorthogonal CI Approaches

The above discussion represents a fairly complete survey of the methods

which have been investigated for describing resonance of localized structures using a single orthogonal orbital set. A few researchers[10,34-38,44] have used nonorthogonal CI approaches to directly resonate the two localized wavefunctions, in a fashion related to the method described in this thesis; we discuss these below.

In his study of the $n\pi^*$ and n ion states of pyrazine and benzoquinone, Martin[20] computed the direct resonance of two HF wavefunctions using a biorthogonalization approach[35] like we describe in the next chapter. This 2 x 2 nonorthogonal CI corresponds to what we call *resonating* HF, or R-HF. Newton has also used the biorthogonalization approach to compute the matrix element between two HF wavefunctions,

$$\langle Fe^{II}(H_2O)_6\, Fe^{III}(H_2O)_6 | Fe^{III}(H_2O)_6 Fe^{II}(H_2O)_6 \rangle ,$$

to use in calculating electron transfer rates.[37] Jackals and Davidson used an R-HF wavefunction for the geometry search on NO_2,[10] finding this description superior to the best CI they could design. In each of these cases the resonance involved a pair of single-determinant SCF wavefunctions. The R-GVB method we present in the next chapter allows the resonance of any number of multiconfigurational wavefunctions.

Lastly, we note two methods which actually allow optimization of the orbitals in the resonating wavefunction. The spatially-projected spin-optimized valence bond (PSOGI) method described by Huestis[38] optimizes a wavefunction of the form

$$\psi^{PSOGI} = A\{[(\varphi_1\varphi_2\cdots\varphi_n) \pm (\bar{\varphi}_1\bar{\varphi}_2\cdots\bar{\varphi}_n)]\Theta\}$$

where Θ is a totally general spin function, φ_1 through φ_n are one-electron orbitals with completely general shape and no overlap restriction, and

each $\bar{\varphi}_i$ corresponds to φ_i by

$$\bar{\varphi}_i = \hat{R}\,\varphi_i \ ,$$

where $\hat{R}$ is a symmetry operator which interconverts the two localized orbital sets. This method is very elegant as it incorporates resonance into the most general possible single-particle* wavefunction, leading to a "single-particle plus resonance" picture. This method has been applied to the excited states of H_2 (Huestis and Goddard[39]), the excited states of He_2 (Guberman and Goddard[40,41]), and to the π space of allyl radical[34] and cyclobutadiene[42] (Levin and Goddard). The PSOGI wavefunction is more general than the GRVB wavefunction presented in this thesis, since in PSOGI there is no restriction on the overlap between orbitals *within* a given determinant (i.e., φ_1 and φ_2 may overlap), while the GRVB method usually employs the perfect-pairing (PP) approximation, requiring that each determinant be expressed in terms of orthonormal natural orbitals. (The PP restriction on full GVB has become quite common among practitioners of the GVB method, resulting in great computational savings with only a slight loss in generality.[43]) While the GRVB program has the capability of handling any general spin coupling of the orthogonal orbitals, thus allowing relaxation of the PP restriction, the majority of cases presented in this thesis retain the PP restriction. The GRVB method represents an improvement over the PSOGI method in two ways:

(1) The PSOGI method required specific programming for each number of electrons, and this programming was especialy cumbersome for more than four electrons, while the GRVB program is applicable for

* By "single-particle" we mean that each electron can be assigned to a single orbital, so that a simple physical picture is retained. This concept is discussed in more depth in Chapter 1.

any number of electrons (given enough computer time).

(2) The PSOGI method can only be used on cases in which a symmetry operator relates ψ_A and ψ_B, while GRVB can optimize any two (or more) resonating wavefunctions, so that the molecule need not be at a symmetric geometry.

The other method which optimizes the orbitals in a nonorthogonal CI is the "VB SCF" approach presented by van Lenthe and Balint-Kurti.[36] They applied this method to the potential curve of OH, allowing the $O(^3P)H(^2S)$, $O(^1D)H(^2S)$, $O^+(^2D^0)H^-(^1S)$, $O^+(^2P^0)H^-(^1S)$, and $O^-(^2P^0)H^+$ valence bond configurations to mix. However, their approach appears to retain the $n!$ computational dependence, so that more than a few electrons would be unmanageable. They were able to simplify the computation for the OH study by restricting each orbital to mix only with those basis functions on the same atomic center.

References

1) W.R. Wadt and W.A. Goddard III, J. Amer. Chem. Soc. **97,** 2034 (1974)

2) E.R. Davidson, Int. J. Quantum Chem. **15,** 65 (1981)

3) P.A. Cox, M. Benard and A. Veillard, Chem. Phys. Lett. **87** 159 (1982)

4) M. Benard, Theor. Chim. Acta **61,** 379 (1982)

5) H. Ågren, P.S. Bagus and B.O. Roos, Chem. Phys. Lett. **82,** 505 (1981)

6) P.S. Bagus and H.F. Schaefer III, J. Chem. Phys. **56,** 224 (1972)

7) D.T. Clark, B.J. Cromarty and A. Sgamellotti, J. Elect. Spectrosc. **14,** 49 (1978)

8) L.S. Cederbaum and W. Domcke, J. Chem. Phys. **66,** 5084 (1977)

9) W. Domcke and L.S. Cederbaum, Chem. Phys. **25,** 189 (1977)

10) C.F. Jackels and E.R. Davidson, J. Chem. Phys. **64,** 2908 (1976)

11) D. Guenzburger, Chem. Phys. Lett. **86,** 316 (1982)

12) J. Müller, E. Poulain, O. Goscinski and L. Karlsson, J. Chem. Phys. **72,** 2587 (1980)

13) S. Canuto, O. Goscinski and M. Zerner, Chem. Phys. Lett. **68,** 232 (1979)

14) R.L. Lozes, O. Goscinski and U.I. Wahlgren, Chem. Phys. Lett. **63,** 77 (1979)

15) L.S. Cederbaum, W. Domcke, J. Schirmer, W. Von Niessen, G.H.F. Diercksen and W.P. Kraemer, J. Chem. Phys. **69,** 1591 (1978)

16) J. Goodman and L.E. Brus, J. Chem. Phys. **69,** 1604 (1978)

17) L.E.Nitzsche and E.R. Davidson, Chem. Phys. Lett. **58,** 171 (1978)

18) D. Pose and E.J. Baerends, Chem. Phys. Lett. **86,** 176 (1982)

19) L. S. Snyder, J. Chem. Phys. **55,** 95 (1971)

20) R.L. Martin, J. Chem. Phys. **74,** 1852 (1981)

21) H. Ågren, L. Selander, J. Nordgren, C. Nordling, K. Siegbahn and J. Müller, Chem. Phys. **37,** 161 (1979)

22) C.P. Keijzers, P.S. Bagus and J.P. Worth, J. Chem. Phys. **69,** 4032 (1978)

23) H.T. Jonkman, thesis, University of Groningen (1975), The Netherlands, unpublished; H.T. Jonkman, G.A. van der Velde and W.C. Nieuwpoort, "Quantum Chemistry, The State of the Art", Proceedings

of the S.C.R. Atlas Symposium, Vol. 4 (1974) p 245

24) J. Müller, H. Ågren, O. Goscinski, Chem. Phys. **38,** 349 (1979)

25) J. Mc Kelvey and W.J. Hehre, Mol. Phys. **25,** 983 (1973)

26) J. Pablus and A. Veillard, Mol. Phys. **35,** 445 (1978)

27) E.R. Davidson and W.T. Borden, J. Amer. Chem. Soc. **99,** 2053 (1977)

28) W. Butscher, R.J. Buenker and S.D. Peyerimhoff, Chem. Phys. Lett. **52,** 449 (1977)

29) J. Cizek and J. Paldus, J. Chem. Phys. **53,** 821 (1970)

30) K. Siegbahn, C. Nordling, G. Johansson, J. Hedman, P.F. Heden, K. Hamrin, U. Gelius, T. Bergmark, L.O. Werme, R. Manne and Y. Baer, eds., *ESCA Applied to Free Molecules*, (North-Holland, Amsterdam, 1969)

31) B.O. Roos, P.R. Taylor and P.E.M. Siegbahn, Chem. Phys. **48,** 157 (1980)

32) P.E.M. Siegbahn, J. Almlöf, A. Heiberg and B.O. Roos, J. Chem. Phys. **74,** 2384 (1981)

33) E.R. Davidson, private communication, 3rd Annual West Coast Theoretical Conference, NASA-Ames, Moffett Field, CA, April 1981.

34) G. Levin and W.A. Goddard III, Theor. Chim. Acta **37,** 253 (1975)

35) A.T. Amos and G.G. Hall, Proc Roy. Soc. London Ser. A **263,** 483 (1961)

36) J.H. van Lenthe and G.G. Balint-Kurti, Chem. Phys. Lett. **76,** 138 (1980)

37) M.D. Newton, Int. J. Quant. Chem. Symp. **14,** 363 (1980)

38) D. Heustis, Ph.D. Thesis, Caltech 1973

39) D.L. Heustis and W.A. Goddard III, Chem. Phys. Lett. **16,** 157 (1972)

40) S.L. Guberman and W.A. Goddard III, Chem. Phys. Lett. **14,** 460 (1972)

41 S.L. Guberman and W.A. Goddard III, Phys. Rev. A **12,** 1203 (1975)

42 G. Levin, Ph.D. Thesis, Caltech 1974

43 F.W. Bobrowicz and W.A. Goddard III, in: *Modern Theoretical Chemistry, Vol. 3, Methods of Electronic Structure Theory*, edited by H.F. Schaeffer III (Plenum, New York 1977), Chap. 4

44 P.-O. Löwdin, Rev. Mod. Phys. **35,** 496 (1963)

45 N.C. Baird, R.R. Gupta and K. F. Taylor, J. Amer. Chem. Soc. **101,** 4531 (1979)

46 T.M. Rescigno and A. E. Orel, J. Chem. Phys. **70,** 3390 (1979)

47 A.F. Voter and W.A. Goddard III, J. Chem. Phys. **75,** 3638 (1981)

48 A.F. Voter and W.A. Goddard III, Chem. Phys. **57,** 253 (1981)

CHAPTER 3

Description of the Method

I. Introduction

We have recently developed a new ab initio method which allows the optimization of a wavefunction in which the orbitals in different configurations need not be orthogonal. This generalized resonating valence bond (GRVB) approach is useful for treating molecules which are best described as a resonance of more than one localized bonding structure. In addition to applications involving classical resonating systems such as allyl radical or benzene, the approach is especially suited to describing the transition states for reactions. For example, in the HF + D → H + FD and HCl + D → H + ClD exchange reactions, the GRVB wavefunction using just the two GVB configurations corresponding to the product and reactant wavefunctions (a total of four determinants) yields quantitative accuracy (~1 kcal/mol) for the reaction barriers[1]. This chapter will describe the GRVB method in more detail.

In GRVB the problem is to minimize the energy of a wavefunction having the form

$$\Psi_{TOT} = C_A\Psi_A + C_B\Psi_B + \cdots , \qquad (1)$$

where each subwavefunction (Ψ_A or Ψ_B) is a correlated multiconfigurational wavefunction (e.g. GVB). The determinants within one of these subwavefunctions are expressed in terms of a single orthonormal set of orbitals, but there is no overlap constraint between the orbitals of different subwavefunctions. There is also no constraint on the overlap of subwavefunctions, $\langle\Psi_A|\Psi_B\rangle$. Because of the complexity of this

wavefunction, rather than using Fock operators we optimize the wavefunction by numerically evaluating the energy derivatives for each possible orbital rotation, using optimal searching procedures to minimize the number of iterations required to obtain the optimum wavefunction.

In Section II we describe how the energy of a wavefunction such as (1) is evaluated, and in Section III how the energy derivatives are obtained and used to optimize the wavefunction.

II. Evaluating the Energy - R-GVB

For simplicity we discuss the case with only two subwavefunctions, Ψ_A and Ψ_B; the generalization to multiple terms is trivial. Our wavefunction is thus

$$\Psi_{TOT} = C_A\Psi_A + C_B\Psi_B \ , \tag{4}$$

where Ψ_A and Ψ_B are each multideterminant wavefunctions,

$$\Psi_A = \sum_i^{N_A} C_i^A \psi_i^A \ ; \ \ \Psi_B = \sum_i^{N_B} C_i^B \psi^B \ . \tag{5a}$$

The energy of this wavefunction is

$$E_{TOT} = \frac{C_A^2 E_A + C_B^2 E_B + 2C_A C_B H_{AB}}{C_A^2 + C_B^2 + 2C_A C_B S_{AB}} \tag{6}$$

(assuming Ψ_A and Ψ_B are normalized), where E_A and E_B are the energies of Ψ_A and Ψ_B,

$$H_{AB} = \langle\Psi_A|\hat{H}|\Psi_B\rangle = \sum_{i,j} C_i^A C_j^B \langle\psi_i^A|\hat{H}|\psi_j^B\rangle \ . \tag{7}$$

and

$$S_{AB} = \sum_{i,j} C_i^A C_j^B \langle\psi_i^A|\hat{H}|\psi_j^B\rangle \ . \tag{8}$$

Since the essence of the method lies in evaluating terms such as $\langle\psi_i^A|\hat{H}|\psi_j^B\rangle$ and $\langle\psi_i^A|\psi_j^B\rangle$, we temporarily restrict our discussion to one determinant pair ψ_i^A, ψ_j^B, and drop the i and j subscripts to simplify notation. Consider first the case where ψ^A and ψ^B are both closed shell determinants,

$$\psi^A = A\{(\varphi_1^A)^2(\varphi_2^A)^2 \cdots (\varphi_n^A)^2 \alpha\beta\alpha\beta \cdots \alpha\beta\} \tag{9a}$$

$$\psi^B = A\{(\varphi_1^B)^2(\varphi_2^B)^2 \cdots (\varphi_n^B)^2 \alpha\beta\alpha\beta \cdots \alpha\beta\} \ . \tag{9b}$$

Because of the nonorthogonality of the ψ^A orbitals $\{\varphi_i^A\}$ with the ψ^B orbitals $\{\varphi_i^B\}$, the evaluation of $\langle\psi^A|\hat{H}|\psi^B\rangle$ or $\langle\psi^A|\psi^B\rangle$ would normally

involve the tedious computation of numerous minors and subminors of the determinant of the overlaps between the two orbital sets, leading to computational work which scales as $n!$. Using the invariance (to within a phase) of any determinental wavefunction under a unitary transformation of spinorbitals, one can find[2,3] a pair of transformations U^A and U^B that biorthogonalize the two orbital sets. Thus, the new orbital sets $\{\bar{\varphi}_i^A\}$ and $\{\bar{\varphi}_i^B\}$ found by

$$\bar{\varphi}_i^A = \sum_j \varphi_j^A U^A{}_{ji} \tag{10a}$$

and

$$\bar{\varphi}_i^B = \sum_j \varphi_j^B U^B{}_{ji} \tag{10b}$$

meet the biorthogonality condition

$$\langle \bar{\varphi}_i^A | \bar{\varphi}_j^B \rangle = \lambda_i \delta_{ij} \quad . \tag{11}$$

This greatly simplifies the evalutation of H_{AB} and S_{AB}. The appropriate transformations U^A and U^B may be found using the procedure described in Appendix A.

Using the biorthogonalized orbital sets, the overlap matrix element is reduced to a single term,

$$\langle \psi^A | \psi^B \rangle = \lambda_1^2 \lambda_2^2 \lambda_3^2 \cdots \lambda_n^2 \quad . \tag{12}$$

because any orbital transposition generated by the antisymmetrizer yields a term including an off-diagonal orbital overlap which is zero by equation (11).

The Hamiltonian matrix element becomes

$$\langle \psi^A | \hat{H} | \psi^B \rangle = 2\sum_i \eta_i \langle \bar{\varphi}_i^A | h | \bar{\varphi}_i^B \rangle + \sum_{i,j} \eta_{ij} \left[2J_{ij}^{AB} - K_{ij}^{AB} \right] \quad . \tag{13}$$

where

$$\eta_i = \langle \psi^A | \psi^B \rangle / \lambda_i \tag{14}$$

and

$$\eta_{ij} = \langle \psi^A | \psi^B \rangle / \lambda_i \lambda_j \quad . \tag{15}$$

Here the simplifying notation

$$J_{ij}^{AB} = \langle \bar{\varphi}_i^A \bar{\varphi}_j^A | \frac{1}{r_{12}} | \bar{\varphi}_i^B \bar{\varphi}_j^B \rangle \tag{16}$$

$$K_{ij}^{AB} = \langle \bar{\varphi}_i^A \bar{\varphi}_j^A | \frac{1}{r_{12}} | \bar{\varphi}_j^B \bar{\varphi}_i^B \rangle \tag{17}$$

has been introduced, utilizing the similarity of these terms to standard coulomb and exchange integrals. Equation (13) looks like an energy expression for a closed shell wavefunction except that two orbital sets are involved and the factors η_i and η_{ij} are included. Thus, evaluation of $\langle \psi^A | \hat{H} | \psi^B \rangle$ for two closed shell determinants requires roughly the same work as evaluating the energy of ψ^A, plus the work required to find the biorthogonalized orbital sets. Since each orbital is expanded in a P dimensional basis set,

$$\varphi_i = \sum_{\mu}^{P} C_{\mu i} \chi_\mu \quad . \tag{18}$$

the work involved in evaluating $\langle \psi^A | \hat{H} | \psi^B \rangle$ scales as nP^4[4], and is always much greater than the work required to obtain the biorthogonalized orbitals [5].

If ψ^A and ψ^B are open shell determinants, the determinants are rewritten with the orbitals grouped by spin

$$\psi^A = A\{\varphi_{1a}^A \varphi_{2a}^A \cdots \varphi_{na}^A(\alpha\alpha\cdots\alpha)\varphi_{1b}^A \varphi_{2b}^A \cdots \varphi_{mb}^A(\beta\beta\cdots\beta)\} \tag{19a}$$

$$\psi^B = A\{\varphi_{1a}^B \varphi_{2a}^B \cdots \varphi_{na}^B(\alpha\alpha\cdots\alpha)\varphi_{1b}^B \varphi_{2b}^B \cdots \varphi_{mb}^B(\beta\beta\cdots\beta)\} \quad , \tag{19b}$$

and then two pairs of transformations are found, one to biorthogonalize the n orbitals with α spin, and the other to biorthogonalize the m orbitals with β spin. The biorthogonalization condition is thus[6]

$$\langle \bar{\varphi}^A_{ia} | \bar{\varphi}^B_{ja} \rangle = \lambda_{ia} \delta_{ij} \tag{20a}$$

and

$$\langle \bar{\varphi}^A_{ib} | \bar{\varphi}^B_{jb} \rangle = \lambda_{ib} \delta_{ij} \quad , \tag{20b}$$

where a and b subscripts represent α and β spin, respectively. The overlap term for this case is

$$\langle \psi^A | \psi^B \rangle = \lambda_{1a} \lambda_{2a} \cdots \lambda_{na} \lambda_{1b} \lambda_{2b} \cdots \lambda_{mb} \quad , \tag{21}$$

and $\langle \psi^A | \hat{H} | \psi^B \rangle$ becomes

$$\begin{aligned} \langle \psi^A | \hat{H} | \psi^B \rangle = & \sum_{ia}^{n} \eta_{ia} \langle \bar{\varphi}^A_{ia} | h | \bar{\varphi}^B_{ia} \rangle + \sum_{ib}^{m} \langle \bar{\varphi}^A_{ib} | h | \bar{\varphi}^B_{ib} \rangle \\ & + \sum_{ia>ja}^{n} \eta_{ia,ja} \left[J^{AB}_{ia,ja} - K^{AB}_{ia,ja} \right] \\ & + \sum_{ib>jb}^{m} \eta_{ib,jb} \left[J^{AB}_{ib,jb} - K^{AB}_{ib,jb} \right] \\ & + \sum_{ia>jb}^{n,m} \eta_{ia,jb} \left[J^{AB}_{ia,jb} \right] \quad , \end{aligned} \tag{22}$$

where the definitions for the η's are the same as before. For open shell wavefunctions it is important that the biorthogonalization not change the phase of either wavefunction. This can be ensured by requiring that the determinant of each transformation matrix U be positive.

To obtain the full S_{AB} and H_{AB} matrix elements, the primitive matrix elements for each determinant pair are contracted according to equations (7) and (8). Since the appropriate biorthogonalization matrices depend on the orbitals in both Ψ_A and Ψ_B, a different biorthogonalization must be performed for each determinant pair. Hence the work required to evaluate H_{AB} between two multiconfigurational wavefunctions scales as $N_A N_B n p^4$, where N_A and N_B are the the number of determinants in ψ^A and ψ^B.

To find the energy of the super wavefunction Ψ_{TOT} we take the matrix elements found by (7) and (8) and the self terms H_{AA} and H_{BB}, and solve

the two by two secular equation,

$$\begin{bmatrix} H_{AA} & H_{AB} \\ H_{AB} & H_{BB} \end{bmatrix} \begin{bmatrix} C_A \\ C_B \end{bmatrix} = E \begin{bmatrix} 1 & S_{AB} \\ S_{AB} & 1 \end{bmatrix} \begin{bmatrix} C_A \\ C_B \end{bmatrix} , \tag{23}$$

to obtain C_A, C_B and E. If Ψ_A and Ψ_B are generalized valence bond (GVB)[7] wavefunctions, we call Ψ_{TOT} a *resonating* GVB or R-GVB wavefunction[8]. While the R-GVB wavefunction is not strictly a single particle wavefunction, it maintains chemical interpretability as the resonance of two single particle wavefunctions, and for many systems this is the lowest level which yields an adequate description.

In general, the determinant coefficients C_i^A and C_i^B (equation (5)) which have been optimized for the individual wavefunctions Ψ_A and Ψ_B are not optimal for the super wavefunction Ψ_{TOT}. If desired, these coefficients may be reoptimized (with unchanged orbital shapes) by solving the N_A+N_B dimensional secular equation using the matrix elements from each determinant pair between Ψ_A and Ψ_B (e.g. $<\psi_i^A|\hat{H}|\psi_j^B>$) in addition to the matrix elements within each subwavefunction (e.g. $<\psi_i^B|\hat{H}|\psi_j^B>$). This has the effect of allowing the coefficients to relax in the presence of resonance, and the magnitude of this readjustment is useful as an indicator for the expected readjustment upon orbital relaxation. In a GVB wavefunction[7],

$$\Psi^{GVB} = A\{[core](g_{1a}\varphi_{1a}^2+g_{1b}\varphi_{1b}^2)(g_{2a}\varphi_{2a}^2+g_{2b}\varphi_{2b}^2)\cdots(g_{qa}\varphi_{qa}^2+g_{qb}\varphi_{qb}^2)\} , \tag{24}$$

the single particle interpretation is maintained by requiring that

$$g_{ia}^2 + g_{ib}^2 = 1 \tag{25}$$

for all q GVB pairs (the a and b subscripts here do not refer to α and β spin, but rather to the 1^{st} and 2^{nd} natural orbitals within a GVB pair). This allows (24) to be rewritten as

$$\Psi^{GVB} = A\{[core](\varphi_{1l}\varphi_{1r}+\varphi_{1r}\varphi_{1l})(\varphi_{2l}\varphi_{2r}+\varphi_{2r}\varphi_{2l})\cdots(\varphi_{ql}\varphi_{qr}+\varphi_{qr}\varphi_{ql})\} \quad , \quad (26)$$

in which φ_{il} and φ_{ir} are the overlapping GVB orbitals making up the i^{th} valence bond pair. Although general coefficient relaxation while resonating would destroy the GVB interpretation, a modified relaxation procedure which maintains the pairwise normalization leads to subwavefunctions which are still rigorously GVB wavefunctions. This procedure is described in Appendix B. We call this a pairwise relaxed R-GVB wavefunction or R-GVB(pr). This same procedure can be used for the more general case of more than two natural orbitals per GVB pair.

III. Orbital Optimization - GRVB

While the R-GVB wavefunction leads to a very good description for many systems, it is often desirable to allow the orbital shapes to relax in the presence of resonance. Optimizing the orbital shapes and coefficients for a wavefunction such as (1) leads to a variational resonating wavefunction which we call the GRVB wavefunction.

Given some trial wavefunction Ψ_{TOT}, (e.g. an R-GVB wavefunction), we form the perturbed wavefunction Ψ^{ij}_{TOT} in which orbitals φ_i^A and φ_j^A are mixed by a small amount λ, so that

$$(\varphi_i^A)' = \varphi_i^A \cos(\lambda) + \varphi_j^A \sin(\lambda) \tag{27a}$$

$$(\varphi_j^A)' = -\varphi_i^A \sin(\lambda) + \varphi_j^A \cos(\lambda) \ , \tag{27b}$$

and evaluate the R-GVB(pr) energy of this perturbed wavefunction using the procedure in Section II. The energy derivative for this rotation δ_{ij}^A is then found by

$$\frac{\partial E}{\partial \delta_{ij}} = \frac{E(\Psi^{ij}_{TOT}) - E(\Psi_{TOT})}{\lambda_{ij}} \ , \tag{28}$$

assuming $\lambda_{ij} \ll 2\pi$. To optimize the wavefunction, we are interested in accumulating the gradient for all orbital rotations which can lead to a change in the energy. Since all the determinants in a given subwavefunction use a common orthonormal set of orbitals, the number of necessary orbital rotations does not depend explicitly on the number of determinants. The number of rotations required within subwavefunction Ψ_A is

$$N^A_{ROT} = N^A_c N^A_{CVB} + \tfrac{1}{2} N^A_{CVB}(N^A_{CVB} - 1) + N^A_o N^A_c + N^A_o N^A_{CVB} + N^A_v N^A_o \ , \tag{31}$$

where

N^A_c = number of closed shell orbitals in Ψ_A
(doubly occupied in every determinant),

N^A_{GVB} = number of orbitals involved in GVB pairs in Ψ_A
(occupation varies with determinant),

N^A_o = number of high spin orbitals in Ψ_A
(singly occupied in every determinant),

N^A_v = number of virtual orbitals in Ψ_A
(zero occupation in every determinant),

and

$$N^A_o = N^A_{core} + N^A_{GVB} + N^A_{open} \quad .$$

The total dimensionality of the gradient is

$$N_{ROT} = N^A_{ROT} + N^B_{ROT} \quad . \tag{32}$$

Since rotations with all virtual orbitals are allowed within each subwavefunction, there is no need to perform rotations between orbitals in Ψ_A and orbitals in Ψ_B. Thus all rotations are within one orthogonal orbital set. If Ψ_A and Ψ_B are related by symmetry, as in allyl radical for example, then only the rotations among Ψ_A orbitals need be considered ($N_{ROT} = N^A_{ROT}$), since Ψ^{ij}_B is generated from Ψ^{ij}_A for each rotation. That is

$$\begin{aligned} \Psi^{ij}_{TOT} &= \Psi^{ij}_A + \Psi^{ij}_B \\ &= \Psi^{ij}_A + \hat{R}\Psi^{ij}_A \quad , \end{aligned} \tag{33}$$

where $\hat{R}$ is the symmetry operation which converts Ψ_A to Ψ_B.

In addition to calculating the N_{ROT} dimensional gradient vector **g**, by performing pairs of incremental rotations, we can calculate the elements in the curvature matrix **B** by

$$\mathbf{B}_{ijkl} = \frac{\partial^2 E}{\partial \delta_{ij}\, \partial \delta_{kl}} = \frac{E(\Psi^{ij,kl}_{TOT}) - E(\Psi^{kl}_{TOT}) - E(\Psi^{ij}_{TOT}) + E(\Psi_{TOT})}{\lambda_{ij}\lambda_{kl}} \tag{34}$$

Using **B** and **g** we can solve for an improved set of orbitals using the Newton Raphson method[9]

$$\mathbf{B}\Delta = -\mathbf{g} \ , \tag{35}$$

where Δ is the solution vector of orbital rotations. Such an approach leads to quadratic convergence, but requires roughly $(N_{ROT})^2$ energy evaluations in constructing the curvature matrix. We find satisfactory convergence can be obtained with considerably less work by evaluating only the diagonal curvature matrix elements and utilizing the principles of conjugate gradient techniques[10]. Since the most important correction to a solution vector in the steepest descent method (in which only the gradient is used), is usually along the (orthogonal) direction of the previous solution, such methods often converge slowly because they oscillate in a two dimensional subspace. The conjugate gradient method, which also uses only a gradient vector, circumvents this problem by including a component of the previous solution in the current solution vector. In our approach the gradient plus diagonal curvatures are used to find an initial solution vector with components

$$\Delta_i^{(1)} = -g_i / B_{ii} \ , \tag{36}$$

and then a fully quadratic search is performed in the two dimensional subspace defined by $\Delta^{(1)}$ and the solution vector from the previous iteration. This solution is then further improved by performing a similar search in the two dimensional subspace defined by the current solution vector and the gradient vector. It is important to note that each energy evaluation allows a relaxation of all determinant coefficients (pairwise relaxed to retain GVB interpretation), and the C_A, C_B subwavefunction coefficients, so that coefficient optimization and orbital optimization are fully coupled. This leads to rapid convergence, and if the full curvature matrix is evaluated, rigorous quadratic convergence is achieved.

To retain orbital orthonormalization during rotations involving more

than one orbital pair, the matrix exponentiation method described by Yaffe[11] is employed. In this approach the orbital transformation **T** (N_{TOT} by N_{TOT}, where $N_{TOT} = N_{occ} + N_{virt}$) is obtained as

$$\mathbf{T} = exp\,[\mathbf{A}] \quad , \tag{36}$$

where **A** is the antisymmetric N_{TOT} by N_{TOT} matrix of rotations so that

$$\mathbf{A}_{ij} = -\mathbf{A}_{ji} = \lambda_{ij} \quad . \tag{37}$$

The new orbitals for Ψ_A (the first N_{occ} of which are occupied) are found by

$$\begin{aligned} \varphi_i^{A'} &= \sum_j \varphi_j^A \mathbf{T}_{ji} \\ &= \sum_j \chi_\mu C_{\mu j}^A \mathbf{T}_{ji} \quad , \end{aligned} \tag{38}$$

or in matrix notation,

$$\mathbf{C}^{A'} = \mathbf{C}^A \mathbf{T} \quad . \tag{39}$$

Appendix A. Biorthogonalization

We present here the method of biorthogonalization used in the GRVB program. The proof that such a transformation exists for the general case has been given by Amos and Hall[3]. We consider here only the case in which each orbital set contains an equal number of real orbitals.

Given two sets of n orbitals, $\{\varphi_i^A\}$ and $\{\varphi_i^B\}$, we wish to find a suitable pair of orthogonal transformations to yield new orbital sets $\{\bar{\varphi}_i^A\}$ and $\{\bar{\varphi}_i^B\}$ in which each orbital in set A overlaps only one orbital in set B. We define the n by n orbital overlap matrix $\mathbf{S_{AB}}$ by

$$(\mathbf{S_{AB}})_{ij} = \langle \varphi_i^A | \varphi_j^B \rangle \ , \tag{A-1}$$

or in matrix notation

$$\mathbf{S_{AB}} = \mathbf{T_A^t S T_B} \ , \tag{A-2}$$

where $\mathbf{S}$ is the basis set overlap matrix, and $\mathbf{T_A}$ and $\mathbf{T_B}$ are the matrices whose columns represent the orbitals in this basis for orbital sets A and B respectively. We seek orthogonal transformations $\mathbf{U^A}$ and $\mathbf{U^B}$ which when applied to $\mathbf{T_A}$ and $\mathbf{T_B}$ yield new orbital sets $\bar{\mathbf{T}}_\mathbf{A}$ and $\bar{\mathbf{T}}_\mathbf{B}$

$$\bar{\mathbf{T}}_\mathbf{A} = \mathbf{T_A U^A} \tag{A-3a}$$

$$\bar{\mathbf{T}}_\mathbf{B} = \mathbf{T_B U^B} \ , \tag{A-3b}$$

which meet the biorthogonality condition

$$\bar{\mathbf{T}}_{\mathbf{A}}^{\dagger}\,\mathbf{S}\bar{\mathbf{T}}_{\mathbf{B}} = \Lambda \ , \tag{A-4}$$

where Λ is the diagonal matrix of overlaps. Combining (A-2), (A-3) and (A-4) we see that this is equivalent to finding $\mathbf{U}^{\mathbf{A}}$ and $\mathbf{U}^{\mathbf{B}}$ such that

$$\mathbf{U}^{\mathbf{A}t}\mathbf{S}_{\mathbf{AB}}\mathbf{U}^{\mathbf{B}} = \Lambda \ . \tag{A-5}$$

Right multiplying $\mathbf{S}_{\mathbf{AB}}$ by its transpose ($\mathbf{S}_{\mathbf{AB}}{}^{t} = \mathbf{S}_{\mathbf{BA}}$) yields a positive definite Hermitian matrix which we can diagonalize with the orthogonal matrix $\mathbf{V}^{\mathbf{A}}$

$$\mathbf{V}^{\mathbf{A}t}(\mathbf{S}_{\mathbf{AB}}\mathbf{S}_{\mathbf{BA}})\,\mathbf{V}^{\mathbf{A}} = \mathbf{D}^{\mathbf{A}} \ , \tag{A-6}$$

Rewriting (A-6) as

$$(\mathbf{S}_{\mathbf{BA}}\mathbf{V}^{\mathbf{A}})^{t}(\mathbf{S}_{\mathbf{BA}}\mathbf{V}^{\mathbf{A}}) = \mathbf{D}^{\mathbf{A}} \tag{A-6}$$

shows that $\mathbf{S}_{\mathbf{BA}}\mathbf{V}^{\mathbf{A}}$ is itself a matrix with orthogonal (Aut not normalized) columns. Hence $\mathbf{S}_{\mathbf{BA}}\mathbf{V}^{\mathbf{A}}$ may be written as an orthogonal matrix ($\mathbf{V}^{\mathbf{B}}$) times a diagonal matrix which appropriately "denormalizes" the columns,

$$\mathbf{S}_{\mathbf{BA}}\mathbf{V}^{\mathbf{A}} = \mathbf{V}^{\mathbf{B}}(\mathbf{D}^{\mathbf{A}})^{1/2} \ . \tag{A-7}$$

Left multiplying (A-7) by $\mathbf{V}^{\mathbf{B}t}$ and taking the transpose of each side yields

$$\mathbf{V}^{\mathbf{A}t}\mathbf{S}_{\mathbf{AB}}\mathbf{V}^{\mathbf{B}} = (\mathbf{D}^{\mathbf{A}})^{1/2} \ , \tag{A-8}$$

and comparison to (A-5) shows we have found the desired biorthogonalization transformations $\mathbf{U}^{\mathbf{A}} = \mathbf{V}^{\mathbf{A}}$ and $\mathbf{U}^{\mathbf{B}} = \mathbf{V}^{\mathbf{B}}$, with $\Lambda = (\mathbf{D}^{\mathbf{A}})^{1/2}$.

The computational procedure is as follows:

a) Given $\mathbf{T_A}$, $\mathbf{T_B}$, and $\mathbf{S}$, form the overlap matrix $\mathbf{S_{AB}} = \mathbf{T_A^\dagger S T_B}$.

b) Right multiply $\mathbf{S_{AB}}$ by $\mathbf{S_{AB}^t}$ and diagonalize; this yields $\mathbf{U^A}$ and $\mathbf{D^A}$.

c) Find the *A* biorthogonalized orbitals by $\bar{\mathbf{T}}_\mathbf{A} = \mathbf{T_A U^A}$

d) Find the $\mathbf{U^B}$ transformation by $\mathbf{U^B} = \mathbf{S_{AB}^t U^A (D^A)^{-½}}$. Inverting $\mathbf{D^A}$ is trivial since it is diagonal. (The case where $(\mathbf{D^A})^{-½}$ is undefined due to zero diagonal elements is discussed below.)

e) Find the *B* biorthogonalized orbitals by $\bar{\mathbf{T}}_\mathbf{B} = \mathbf{T_B U^B}$.

We now consider the case in which some diagonal element d_k of the eigenvalue matrix $\mathbf{D^A}$ is zero, causing $(\mathbf{D^A})^{-½}$ in step d to be undefined. Since the procedure for finding $\bar{\mathbf{T}}_\mathbf{A}$ is still well defined, we are only faced with finding $\bar{\mathbf{T}}_\mathbf{B}$. From (A-4) we know that $(\mathbf{D^A})^{½}$ is the matrix of overlaps of the biorthogonalized orbital sets, so that

$$\langle \bar{\varphi}_i^A | \bar{\varphi}_j^B \rangle = \delta_{ij} d_{ij}^{½} \quad . \tag{A-9}$$

Hence, a zero element d_k indicates that $\bar{\varphi}_k^A$ does not overlap any orbital in the set B, and we may choose any linear combination of orbitals from set B in constructing $\bar{\varphi}_k^B$ without violating the condition (A-9) for $i = k$. The biorthogonalization procedure can thus be effected by replacing step d above with the following:

> d) Reorder $\mathbf{D^A}$ so that any zero elements appear last (let m equal the number of zero elements), and correspondingly reorder the columns of $\bar{\mathbf{T}}_\mathbf{A}$. Perform the matrix multiplication $\mathbf{U^B} = \mathbf{S_{AB}^t U^A (D^A)^{-½}}$ only for the first $n-m$ columns of $\mathbf{U^B}$. Find the last m columns of

$\mathbf{U^B}$ by Schmidt orthogonalization (pick as trial vectors those m orbitals least used in the first $n-m$ columns of $\mathbf{U^B}$).

Appendix B. Pairwise Coefficient Optimization

The GVB wavefunction with q pairs can be written as

$$\Psi^{GVB} = A\{[core](g_{1a}\varphi_{1a}^2+g_{1b}\varphi_{1b}^2)(g_{2a}\varphi_{2a}^2+g_{2b}\varphi_{2b}^2)\cdots(g_{qa}\varphi_{qa}^2+g_{qb}\varphi_{qb}^2)\} \quad \text{(B-1)}$$

We are interested in optimizing the GVB coefficients (g_{ia}, g_{ib}) in two such wavefunctions which are resonating,

$$\Psi_{TOT} = C_A\Psi_A^{GVB} + C_B\Psi_B^{GVB}, \quad \text{(B-2)}$$

(hereafter we drop the *GVB* superscript; Ψ_A and Ψ_B are assumed to be GVB wavefunctions), while maintaining the pairwise normalization,

$$g_{ia}^2 + g_{ib}^2 = 1, \quad \text{(B-3)}$$

for each GVB pair. We have available the matrix elements between any determinant from Ψ_A or Ψ_B and any other determinant. Hence we wish to solve the secular equation,

$$\mathbf{HC} = \mathbf{SCE}, \quad \text{(B-4)}$$

using the determinants from Ψ_A plus the determinants from Ψ_B as the basis states, but with the constraint (B-3).

We can reexpress Ψ_A as

$$\Psi_A = g_{ia}\Psi_{ia}^A + g_{ib}\Psi_{ib}^A, \quad \text{(B-5)}$$

where

$$\Psi_{ia}^{A} = A\{[core](g_{1a}\varphi_{1a}^{2}+g_{1b}\varphi_{1b}^{2})\cdots(\varphi_{ia}^{2})\cdots(g_{qa}\varphi_{qa}^{2}+g_{qb}\varphi_{qb}^{2})\} \qquad \text{(B-6a)}$$

and

$$\Psi_{ib}^{A} = A[core](g_{1a}\varphi_{1a}^{2}+g_{1b}\varphi_{1b}^{2})\cdots(\varphi_{ib}^{2})\cdots(g_{qa}\varphi_{qa}^{2}+g_{qb}\varphi_{qb}^{2}) \qquad \text{(B-6b)}$$

so that the coefficients for GVB pair i premultiply the Ψ_A subwavefunctions Ψ_{ia}^{A} and Ψ_{ib}^{A}. If we do the same for GVB pair j of Ψ_B, we have

$$\Psi_{TOT} = C_A(g_{ia}^{A}\Psi_{ia}^{A} + g_{ib}^{A}\Psi_{ib}^{A}) + C_B(g_{j}^{B}\Psi_{ja}^{B} + g_{jb}^{B}\Psi_{jb}^{B}), \qquad \text{(B-7)}$$

where superscripts have been added to the GVB coefficients to distinguish Ψ_A coefficients from Ψ_B coefficients. By using Ψ_{ia}^{A}, Ψ_{ib}^{A}, Ψ_{ja}^{B}, and Ψ_{jb}^{B} as the basis states for a four by four secular determinant, we solve for a coefficient vector **C** in which

$$C(1) = C_A g_{ia}^{A} \qquad \text{(B-8a)}$$
$$C(2) = C_A g_{ib}^{A} \qquad \text{(B-8b)}$$
$$C(3) = C_B g_{ja}^{B} \qquad \text{(B-8c)}$$
$$C(4) = C_B g_{jb}^{B}. \qquad \text{(B-8d)}$$

Combining these four equations with the two constraints given by (B-3) yields all six coefficients uniquely, and by cycling through all GVB pairs i and j the solution will converge to self consistency. Matrix elements such as $\langle\Psi_{ia}^{A}|\hat{H}|\Psi_{jb}^{B}\rangle$ are computed by contracting the primitive determinant pair matrix elements using the same algorithm as for $\langle\psi^{A}|\hat{H}|\psi^{B}\rangle$ except that all determinants in Ψ_A involving φ_{ib}^{A} and all determinants in Ψ_B involving φ_{ja}^{B} are excluded.

Appendix C. Computational Procedure for GRVB Program

Input Routine

a) Read in a starting guess for Ψ_A and Ψ_B.

b) Orthonormalize the orbitals within Ψ_A and within Ψ_B.

c) Find the number of determinant pairs (NDET), etc.

d) Read one and two electron integrals over atomic basis functions into memory if there is room.

e) Call routine SEARCH.

SEARCH Routine - Performs search to optimize Ψ_{TOT}

a) Call ENERGY (which returns the energy of Ψ_{TOT}) with starting guess orbitals. The first call to ENERGY also returns the number of orbital rotations N_{ROT}.

b) Call ENERGY with each possible incremental orbital rotation. This enables calculation of the gradient vector (g), and combining pairs of rotations allows evaluation of the curvature matrix ($\mathbf{B}$). (Usually only make calls required for diagonal $\mathbf{B}$ matrix elements.)

C) Solve the Newton Raphson equation,

$$\mathbf{B}\Delta = -\mathbf{g} \ .$$

in the N_{ROT} dimensional space. This yields the solution vector Δ.

d) Rotate the orbitals by 0.6Δ.

e) Perform a two-dimensional search in the space made up of Δ and **g**. This yields the solution Δ'.

f) Perform a two-dimensional search in the space made up of Δ' and the final solution from iteration $n-1$. This yields Δ''.

g) The final solution vector Δ_n'' equals the vector corresponding to the best energy found (the lowest energy ever returned from ENERGY), minus the position at the beginning of this iteration.

h) If Ψ_{TOT} is not converged (e.g. if the magnitude of Δ_n'' is above a threshold value), go to step b.

ENERGY Routine - Evaluates Energy of Ψ_{TOT}

a) Form the rotation matrix from the vector (containing N_{ROT} components) passed by SEARCH.

b) Exponentiate this rotation matrix to get the transformation to apply to the Ψ_A orbitals.

c) If Ψ_B is related to Ψ_A by a symmetry operation, "reflect" Ψ_A to get Ψ_B. If not, some of the N_{ROT} rotations are used to transform Ψ_B (Ψ_A and Ψ_B are optimized simultaneously).

d) Make the following calls to routine RES:

call RES(Ψ_A, Ψ_A) (RES returns the matrices $\mathbf{H_{AA}}$ and $\mathbf{S_{AA}}$)

call RES(Ψ_B, Ψ_A) (RES returns the matrices $\mathbf{H_{BA}}$ and $\mathbf{S_{BA}}$)

call RES(Ψ_B, Ψ_B) (RES returns the matrices $\mathbf{H_{BB}}$ and $\mathbf{S_{BB}}$) where

$$(\mathbf{H_{AB}})_{ij} = \langle \psi_i^A | H | \psi_j^B \rangle$$

and

$$(\mathbf{S_{AB}})_{ij} = \langle \psi_i^A | \psi_j^B \rangle.$$

e) Merge the three matrices $\mathbf{H_{AA}}$, $\mathbf{H_{BA}}$, and $\mathbf{H_{BB}}$ from step d into a super matrix **H** over all determinants in Ψ_{TOT}, and likewise form **S**.

f) Solve the secular equation **HC=SCE** in a pairwise fashion (see Appendix A) to obtain the GVB coefficients, the wavefunction coefficients C_A and C_B, and the total energy $E(\Psi_{TOT})$.

e) Return $E(\Psi_{TOT})$ to the calling routine (SEARCH).

RES Routine

RES evaluates H and S matrix elements for all determinant pairs in a given pair of subwavefunctions, Ψ_A and Ψ_B (where Ψ_A may be the same as Ψ_B). RES returns these matrix elements as the matrices $\mathbf{H_{AB}}$ and $\mathbf{S_{AB}}$, which are defined in step d above.

a) By comparing the orbitals in Ψ_A and Ψ_B to those at the beginning of the iteration, determine which (if any) determinants in Ψ_A and in Ψ_B have not changed.

b) Pick the next determinant pair ij; that is, ψ_i^A and ψ_j^B.

c) If ψ_i^A and ψ_j^B are both unchanged from original, go to step b. (Skip this determinant pair, since $(\mathbf{H_{AB}})_{ij}$ and $(\mathbf{S_{AB}})_{ij}$ are already known.)

d) Biorthogonalization: (trivial if $\Psi_A = \Psi_B$)

Closed Shell

biorthogonalize $\{\varphi^A\}$ with $\{\varphi^B\}$ to get $\{\bar{\varphi}^A\}$ and $\{\bar{\varphi}^B\}$, where $\langle \bar{\varphi}_i^A | \bar{\varphi}_j^B \rangle = \lambda_i \delta_{ij}$

Open Shell

separate α and β orbitals

biorthogonalize α sets

biorthogonalize β sets

put the new β orbitals after the new α orbitals for both determinants

e) Call OFFDAG($\{\bar{\varphi}^A\}$, $\{\bar{\varphi}^B\}$) (OFFDAG evaluates $\langle\psi_i^A|H|\psi_j^B\rangle$ and $\langle\psi_i^A|\psi_j^B\rangle$)

f) Go to step b unless there are no more determinant pairs

g) Return $\mathbf{H_{AB}}$ and $\mathbf{S_{AB}}$ to calling routine (ENERGY).

OFFDAG Routine

Evaluates $H_{AB} = \langle\psi_i^A|H|\psi_j^B\rangle$ and $S_{AB} = \langle\psi_i^A|\psi_j^B\rangle$

a) Evaluate S_{AB}

Closed Shell (f=2): $S_{AB} = \prod_i^n \lambda_i^2$

Open Shell (f=1): $S_{AB} = \prod_i^{nel} \lambda_i$, $nel = n_\alpha + n_\beta$

b) Set up η_i and η_{ij} , $i,j = 1,\text{norb}$

$$\eta_i = \frac{S_{AB}}{\lambda_i} \quad \eta_{ij} = \frac{S_{AB}}{\lambda_i \lambda_j}$$

(These are actually calculated by taking the product of all λ's except the i^{th} one (or the i^{th} and j^{th}), to prevent a divide by zero when $\lambda_i = 0$.)

c) Evaluate the one-electron part of H_{AB} ($H_{AB} = H_{AB}^{(1)} + H_{AB}^{(2)}$)

$$H_{AB}^{(1)} = f\sum_i \eta_i \langle\bar{\varphi}_i^A|h|\bar{\varphi}_i^B\rangle$$
$$= f\sum_i \eta_i \sum_{\mu\nu} \bar{c}_{\mu i}^A \bar{c}_{\nu i}^B h_{\mu\nu}$$

d) Evaluate the two-electron part of H_{AB}

closed shell:

$$H_{AB}^{(2)} = \sum_{i,j} \eta_{ij} (2J_{ij}^{AB} - K_{ij}^{AB})$$

open shell:

$$H_{AB}^{(2)} = \sum_{i,j} \eta_{ij} (1 - \frac{1}{2}\delta)(J_{ij}^{AB} - \delta K_{ij}^{AB})$$

where $\delta \equiv \delta_{spin(i),spin(j)}$,

$$J_{ij}^{AB} = \langle \bar{\varphi}_i^A \bar{\varphi}_j^A | \frac{1}{r_{12}} | \bar{\varphi}_i^B \bar{\varphi}_j^B \rangle$$

$$= \sum_{\mu\nu\sigma\rho} \bar{c}_{\mu i}^A \bar{c}_{\nu i}^B \bar{c}_{\sigma j}^A \bar{c}_{\rho j}^B (\mu\nu|\sigma\rho) \ ,$$

$$K_{ij}^{AB} = \langle \bar{\varphi}_i^A \bar{\varphi}_j^A | \frac{1}{r_{12}} | \bar{\varphi}_j^B \bar{\varphi}_i^B \rangle$$

$$= \sum_{\mu\nu\sigma\rho} \bar{c}_{\mu i}^A \bar{c}_{\nu i}^B \bar{c}_{\sigma j}^A \bar{c}_{\rho j}^B (\mu\rho|\sigma\nu)$$

While this appears to require $(NBF)^4(NORB)^2$ work, it can be accomplished with $(NBF)^4(NORB)$ work, by performing two half-transformations.

e) Return to calling routine (RES).

References

1) A.F. Voter and W.A. Goddard III, J. Chem. Phys. **75,** 3638 (1981)

2) P.O. Löwdin, Phys. Rev. **97,** 1474 (1955)

3) A.T. Amos and G.G. Hall, Proc. Roy. Soc. A **263,** 483 (1961)

4) This appears to require $n^2 P^4$ work, but by first performing two half-transformations the work is reduced to $n P^4$.

5) The Biorthogonalization step requires diagonalization of an n by n matrix - see App. A.

6) We need not worry about the overlap between Φ_{ia}^{A} and Φ_{jb}^{B}, because any such terms will vanish due to the spin overlap $< \alpha | \beta >$.

7) F.W. Bobrowicz and W.A. Goddard III, in: *Modern Theoretical Chemistry, Vol. 3, Methods of Electronic Structure Theory*, edited by H.F. Schaeffer III (Plenum, New York 1977), Chap. 4

8) A.F. Voter and W.A. Goddard III, Chem. Phys. **57,** 253 (1981)

9) J.E. Dennis, Jr., Proc. Symp. Appl. Math. **22,** 19 (1978)

10) I. Vandoni and E. Gianinetti, Chem. Phys. Lett. **82,** 105 (1981)

11) L.G. Yaffe and W.A. Goddard III, Phys. Rev. A **13,** 1682 (1976)

CHAPTER 4

The Resonating Valence Bond Description of Cyclobutadiene

I. Introduction

Cyclobutadiene (CBD), the simplest cyclic four-electron π system, has generated interest for many years. In agreement with simple Hückel theory arguments, the molecule is highly unstable, though it has been isolated in low temperature matrix studies,[1] and observed as a short-lived intermediate in solution.[2,3] Two features of CBD are particularly intriguing. First, the most stable geometry is found both experimentally[1-3] and theoretically[4-7] to be rectangular, with the square geometry 6-12 kcal higher, representing a saddle point for interconversion of the two rectangular structures.[8] Second, the lowest state at the square geometry is found to be a singlet, in contradiction to the molecular orbital (MO) theory prediction of a triplet ground state.

Because the resonating valence bond (VB) model offers a different view of these (and other) features than MO theory, the cyclobutadiene molecule makes a good vehicle for contrasting these two theories. In the following we discuss the electronic structure of square cyclobutadiene at a qualitative level from both points of view. Then, using self-consistent field (SCF) calculations to represent the MO wavefunctions, and generalized resonating valence bond (GRVB) calculations to represent the resonating VB wavefunctions, we compare these results to each other and to accurate configuration interaction (CI) calculations. We then consider distortions from the square geometry to give the observed rectangular geometry.

II. Molecular Orbital (MO) Approach - Square Geometry

In the MO approach, we combine the four atomic $p\pi$ functions of CBD into four symmetry-adapted MOs,

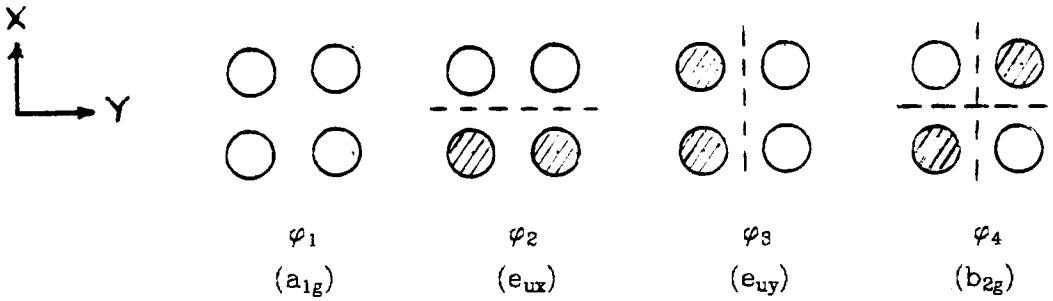

which have the energy ordering shown here:

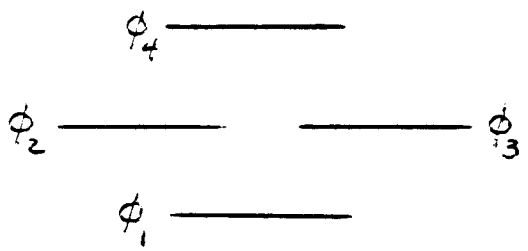

Occupying these MOs with four electrons leads to various states, the lowest of which is the ${}^3A_{2g}$ state,

$$\Psi^{MO}({}^3A_{2g}) = A[(\sigma \text{ core})\varphi_1^2\varphi_2\varphi_3\alpha\beta\alpha\alpha] \ . \tag{1}$$

This state is the lowest because φ_2 and φ_3 are degenerate. Considering all possible states which can arise from keeping φ_1 filled and φ_4 empty, we can write (leaving off the redundant filled orbitals and ignoring normalization)

$$\Psi^{MO}({}^3A_{2g}) = (\varphi_2\varphi_3 - \varphi_3\varphi_2)(\alpha\beta + \beta\alpha) \tag{2a}$$

$$\Psi^{MO}(^1B_{2g}) = (\varphi_2\varphi_3 + \varphi_3\varphi_2)(\alpha\beta - \beta\alpha) \tag{2b}$$

$$\Psi^{MO}(^1B_{1g}) = (\varphi_2^2 - \varphi_3^2)(\alpha\beta - \beta\alpha) \tag{2c}$$

$$\Psi^{MO}(^1A_{1g}) = (\varphi_2^2 + \varphi_3^2)(\alpha\beta - \beta\alpha) \tag{2d}$$

Factoring away the spin function, and replacing φ_2 by "X" and φ_3 by "Y" (since this is the symmetry they have), we have

$$^3A_{2g} = XY - YX \tag{3a}$$

$$^1B_{2g} = XY + YX \tag{3b}$$

$$^1B_{1g} = XX - YY \tag{3c}$$

$$^1A_{1g} = XX + YY \tag{3d}$$

Taking the orbital shapes to be the same for each state, the energies are

$$E(XY - YX) = E_0 + J_{XY} - K_{XY} \tag{4a}$$

$$E(XY + YX) = E_0 + J_{XY} + K_{XY} \tag{4b}$$

$$E(XX - YY) = E_0 + J_{XX} - K_{XY} \tag{4c}$$

$$E(XX + YY) = E_0 + J_{XX} + K_{XY} \tag{4d}$$

where J and K are the usual two-electron coulomb and exchange integrals,

$$J_{XY} = \langle X(1)Y(2) | \frac{1}{r_{12}} | X(1)Y(2) \rangle \tag{5a}$$

$$K_{XY} = \langle X(1)Y(2) | \frac{1}{r_{12}} | Y(1)X(2) \rangle \tag{5b}$$

We see immediately that $E(XY - YX)$ lies below $E(XY + YX)$, because the J and K integrals are always positive, and similarly $E(XX - YY)$ lies below

$E(XX+YY)$. We also know that J_{XX} is greater than J_{XY}, so that $E(XY-YX)$ is below $E(XX-YY)$, and $E(XY+YX)$ is below $E(XX+YY)$. Thus, the ${}^3A_{2g}(XY-YX)$ state lies lowest, and the ${}^3A_{2g}(XY+YX)$ state lies highest, but we have not yet placed the ${}^1B_{1g}(XX-YY)$ states. To compare these, we make use of the fact that

$$XX-YY = (X+Y)(X-Y) + (X-Y)(X+Y) \ , \tag{6}$$

i.e. the $XX-YY$ wavefunction is equivalent to singlet-coupling one electron in an $X+Y$ orbital with one electron in an $X-Y$ orbital. Thus $E(XX-YY)$ becomes

$$E(XX-YY) = E_0 + J_{X+Y,X-Y} + K_{X+Y,X-Y} \ , \tag{7}$$

and by inspection of the shapes of the $X+Y$ and $X-Y$ orbitals,

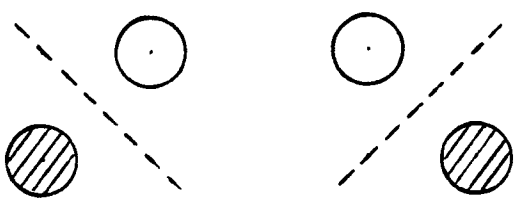

$X+Y$ $\qquad$ $X-Y$ (8)

we expect $J_{X+Y,X-Y}$ and $K_{X+Y,X-Y}$ to be smaller than J_{XY} and K_{XY}, respectively, because the node in the $X+Y$ orbital passes through the maximum density region of the $X-Y$ orbital, and vice versa. This is not true for the X and Y orbitals. Thus, ${}^1B_{1g}(XX-YY)$ lies below ${}^1B_{2g}(XY+YX)$. This state ordering is shown in Figure 1, along with the relative energies from self-consistent field (SCF) calculations on each state. Even though the SCF allows slightly different orbital shapes for each state, the ordering is exactly as predicted.

The ${}^1B_{1g}(XX-YY)$ state is seen to be only 4.4 kcal above the

$^3A_{2g}(XY-YX)$ state. As we noted above, the $^1B_{1g}(XX-YY)$ wavefunction can be rigorously rewritten as the singlet coupling of two electrons in $X+Y$ and $X-Y$ orbitals. Because any determinant is invariant to mixing orbitals of the same spin, we can reexpress the $^3A_{2g}(XY-YX)$ state as a triplet coupling of $X+Y$ and $X-Y$ orbitals, so that

$$E(^3A_{2g}) = E_0 + J_{X+Y,X-Y} - K_{X+Y,X-Y} \tag{9a}$$

$$E(^1B_{1g}) = E_0 + J_{X+Y,X-Y} + K_{X+Y,X-Y} \ , \tag{9b}$$

which means that

$$K_{X+Y,X-Y} \approx 2.2 \text{ kcal} \ . \tag{10}$$

In contrast, comparing the $^1B_{2g}(XY+YX)$ state with the $^3A_{2g}(XY-YX)$ state yields

$$K_{XY} = 28.2 \text{ kcal} \ , \tag{11}$$

so that K_{XY} is much larger than $K_{X+Y,X-Y}$, as we claimed above. Thus, in MO theory, the lowest two states of this system can be thought of as arising from the singlet and triplet couplings of the two weakly interacting orthogonal orbitals shown in (8).

We have also included in Figure 1 the first excited triplet state,

$$\Psi(^3E_u) = A[\varphi_1^2\varphi_2\varphi_3\alpha\beta\alpha\alpha] \tag{12}$$

which is seen to be far above the three singlets.

III. Resonating Valence Bond Approach - Square Geometry

In the valence bond (VB) formalism, the natural description of cyclobutadiene has two π bonds,

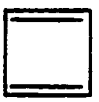

(13)

Denoting the atomic orbitals as a, b, c, and d,

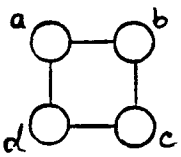

(14)

we can write this wavefunction as

$$\Psi(\square) = A[(\sigma\ \text{core})(ab+ba)(cd+dc)\alpha\beta\alpha\beta] \quad . \tag{15}$$

However, we could just as easily write

$$\Psi(\square) = A[(\sigma\ \text{core})(ad+da)(bc+cb)\alpha\beta\alpha\beta] \quad . \tag{16}$$

so that the appropriate description of the ground state is a resonance of these two structures,

$$\Psi^{R-VB}(^1B_{1g}) = \square - \square$$

$$= A\{(\sigma\text{core})[(ab+ba)(cd+dc)\alpha\beta\alpha\beta - (ad+da)(bc+cb)\alpha\beta\alpha\beta]\} \quad . \tag{17}$$

The other linear combination leads to an antiresonant state,

$$\Psi(^1a_{1g}) = \square + \square \quad . \tag{18}$$

To construct a triplet state, we must break one of these two π bonds, leading to four equivalent structures,

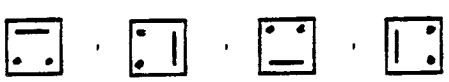

which we can write as

$$\Psi^{VB}(\quad) = A[(\sigma\ \text{core})abcd(\alpha\beta - \beta\alpha)\alpha\alpha] \tag{19a}$$

$$\Psi^{VB}(\quad) = A[(\sigma\ \text{core})bcda(\alpha\beta - \beta\alpha)\alpha\alpha] \tag{19b}$$

$$\Psi^{VB}(\quad) = A[(\sigma\ \text{core})cdab(\alpha\beta - \beta\alpha)\alpha\alpha] \tag{19c}$$

$$\Psi^{VB}(\quad) = A[(\sigma\ \text{core})dabc(\alpha\beta - \beta\alpha)\alpha\alpha] \tag{19d}$$

Combining these triplets into symmetry adapted wavefunctions leads to a resonant $^3A_{2g}$ state,

$$\Psi^{R-VB}(^3A_{2g}) = \quad + \quad + \quad + \quad , \tag{20}$$

and a degenerate pair of antiresonant states,

$$\Psi^{R-VB}(^3E_u) = \quad - \quad , \quad - \quad . \tag{21}$$

(There are only three linearly independent triplets for four electrons in four orbitals,[9] so we lose the fourth linear combination.) So far we have predicted four states, a resonant and antiresonant pair of singlets, and a resonant and antiresonant pair of triplets. Unless the resonance energy is much greater for the triplet state, we expect a ground state singlet, and a low lying triplet. The other singlet state predicted by MO theory, the $^1B_{2g}$ (XY+YX) state, arises in VB theory from an ionic wavefunction,

$$\Psi(\quad) = A[(\sigma\ \text{core})aacc\ \alpha\beta\alpha\beta] \tag{22}$$

which is combined with its rotated form to give

$$\Psi^{R-VB}(^1B_{2g}) = \quad - \quad \tag{23a}$$

and

$$\Psi^{R-VB}(2^1A_{1g}) = \quad + \quad . \tag{23b}$$

In Figure 2 we show the splitting of the VB singlet and triplet wavefunctions into resonant and antiresonant states. The energies

assigned to each state are the results of GVB and GRVB calculations, which find the best orbital shapes for the particular VB or resonating VB form of the wavefunction. These resonating wavefunctions are not exactly as written in (17), since the orbitals are allowed to have a different shape in each resonance structure. Thus

$$\Psi^{GRVB}({}^1B_{1g}) = A[(ab+ba)(cd+dc)\alpha\beta\alpha\beta - (a'd'+d'a')(b'c'+c'b')\alpha\beta\alpha\beta] \quad (24)$$

and the result is that each orbital polarizes to achieve higher overlap with its bonding partner. We know that $\Psi($  $)$ should be the 90 degree rotation of $\Psi($  $)$,

 $= \hat{R}($  $)$, (25)

and thus the primed set of orbitals are simply related to the unprimed set by

$$a = \hat{R}(b') \quad (26a)$$

$$b = \hat{R}(c') \quad (26b)$$

$$c = \hat{R}(d') \quad (26c)$$

$$d = \hat{R}(a') \quad (26d)$$

We discuss the GRVB wavefunctions in depth in the following sections, and conclude this section with a brief summary of the resonating VB description of CBD.

In cyclobutadiene, the lowest lying VB structure is a singlet, with a triplet at higher energy. Each of these structures can resonate with energetically equivalent VB structures to give a lower energy (resonant) state and a higher energy (antiresonant) state. Because the resonance lowering is comparable, these states interleave to give a singlet, triplet,

singlet, triplet state ordering. There is also an ionic state at some higher energy (see equation (23)), but we cannot say *a priori* whether it lies above or below the antiresonant states.

IV. Calculational Details

All calculations employed Dunning's valence double zeta contraction of Huzinaga's 9s5p carbon basis[11] and 4s hydrogen basis (scaled by 1.2). The square geometry was that optimized by Borden, *et al.*[5] (R_{CC} = 1.453, R_{CH} = 1.10). The rectangular calculation was performed at R_1 = 1.54 Å, R_2 = 1.38 Å, R_{CH} = 1.10 Å, very near the geometry optimized by Walkup, Ho, and Goddard[12] for the singlet state using a full π CI wavefunction in the same basis as ours. The SCF wavefunctions used to describe the MO states were performed using the Caltech GVB2P5 program.[13] The triplet states were simple Hartree-Fock wavefunctions, while the singlet states were two configuration wavefunctions, as given by equations (2b), (2c), and (2d). The VB wavefunctions were also optimized using GVB2P5, using a GVB(2/4) wavefunction for the VB singlet, and a GVB(1/2) wavefunction for the triplet. The resonating VB wavefunctions were optimized using the GRVB program described elsewhere in this thesis, while the R-GVB energies were evaluated using the RESGVB program (also described in this thesis). All GRVB and full π CI calculations were performed using a frozen symmetric sigma core taken from the $^1B_{2g}$ state for the square geometry, and from the GVB(2/4) singlet for the rectangular geometry. With the sigma core removed, the GRVB and CI calculations were optimized in a space of eight basis functions. The effect of allowing the sigma space to relax was found to be only 1.2 kcal for the GVB(2/4) singlet state, and we feel that the effect on the relative state energies is negligible. Both the full CI and the GRVB calculations are unfeasible if

the sigma space is included in the calculation.

The form of the GRVB(2/4) singlet wavefunction which was optimized is given in equations (24), (25), and (26), and a separate calculation was performed for the resonant and antiresonant states, leading to slightly different orbital shapes. The effect on the energy of allowing the orbitals to relax from GVB to GRVB is discussed in section VI. The GRVB program actually works in terms of natural orbitals, rather than overlapping GVB orbitals, but the number of orbitals which need to be optimized is still four. The other resonance structure is completely defined by these four orbitals, and the 90 degree rotation operator $\hat{R}$. It is interesting to note that for the GRVB(2/4) singlet, the number of unique orbitals can be reduced to one by taking advantage of the various symmetry operations in D_{4h}. For example,

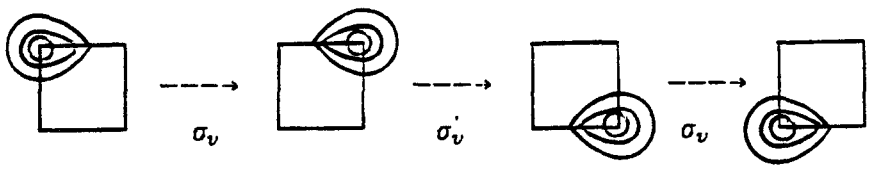

(28)

Since there are eight basis functions total, optimizing the shape of this one orbital would require optimizing only seven orbital rotations. However, this approach would be messy, since in general, a rotation of φ_a with one of the seven virtual orbitals would introduce an overlap between φ_a with φ_c and φ_d,* which is unallowed in the perfect pairing GVB wavefunction. Thus, after each orbital rotation, a symmetric orthogonalization would be necessary, to maintain both the required orthogonality and the symmetry relation between the orbitals. We instead optimize all four

* φ_a is allowed to overlap φ_b, of course, since they are singlet paired.

orbitals, in terms of the natural orbitals

$$\varphi_1 = \varphi_a + \varphi_b \quad (28a)$$

$$\varphi_2 = \varphi_a - \varphi_b \quad (28b)$$

$$\varphi_3 = \varphi_c + \varphi_d \quad (28c)$$

$$\varphi_4 = \varphi_c - \varphi_d \quad (28d)$$

and take advantage of the symmetry with respect to the σ_v reflection plane. Thus there are two symmetric occupieds (φ_1 and φ_3) which can mix with each other and with two symmetric virtual orbitals, and two antisymmetric occupieds (φ_2 and φ_4) which can mix with each other and two virtuals, leading to a total of ten orbital rotations.[23]

The GRVB(1/2) triplet wavefunction was optimized using only two of the four resonance structures shown in (20) ((19a) and (19c)), and then these orbitals were used to construct the full four structure resonating wavefunction using the RESGVB program. The effect of including the two extra resonance structures is seen from Figure 2 to be 6.9 kcal, but the effect of *optimizing* the orbitals with four structures rather than two is expected to be negligible. This is because the dominant effect in going from GVB to GRVB is the localization of the orbitals, and examination of Figure 5 shows that the localization appears to be complete. It is interesting to note that if the orbital shapes a, b, c, and d, are restricted to be the same for each resonance structure, as written in the VB wavefunctions (19a) - (19d), then the two-structure form of the triplet is equivalent to the four-structure form, since

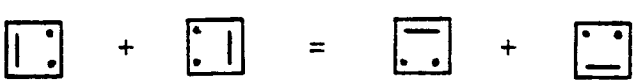

(29)

The 6.9 kcal lowering we observe by including the third and fourth structures indicates the importance of allowing the orbitals to polarize for

optimum bonding overlap. Simultaneously optimizing four symmetry-related structures would require roughly twice the computational work as for two resonance structures, since there are two unique off-diagonal matrix elements to be evaluated,

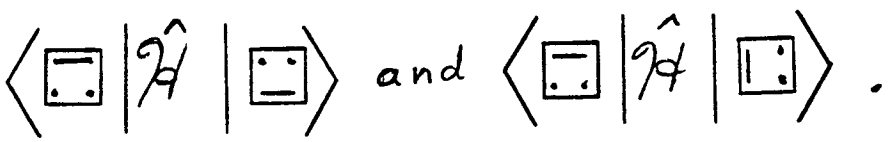

While this is easily feasible, the current version of the GRVB program is restricted to two subwavefunctions. As with the singlet, the shapes of φ_a, φ_b, φ_c and φ_d are transferred between subwavefunctions by a symmetry operation, in this case a $\hat{C}_2$ rotation. This leads to two unique orbitals, φ_a and φ_c in (19a), just as there was one unique orbital for the GRVB singlet, but as above, we optimize four orbitals, the two GVB natural orbitals

$$\varphi_1 = \varphi_a + \varphi_b \tag{30a}$$

$$\varphi_2 = \varphi_a - \varphi_b \tag{30b}$$

and the two high spin orbitals φ_c and φ_d. By combining the high spin orbitals as

$$\varphi_3 = \varphi_c + \varphi_d \tag{30c}$$

$$\varphi_4 = \varphi_c - \varphi_d \tag{30d}$$

we can impose symmetry constraints on the orbitals, so that φ_1 and φ_3 are symmetric under vertical reflection plane, while φ_2 and φ_4 are antisymmetric. Thus, as with the singlet there are ten orbital rotations. For the antiresonant GRVB(1/2) triplet state, using two resonance structures to optimize the orbitals is not a restriction, as the third and fourth structures cannot interact with the first two, because they represent the

other degenerate component of the ^3E_u state.

All orbitals are plotted in a plane which is 0.5Å above, and parallel to, the plane of the molecule. The projected positions of the atoms are included on the plots for clarity, and the contour range from −1.0 a.u. to 1.0 a.u. by increments of 0.05, with negative contours represented by dotted lines.

V. Results and Discussion - Square Geometry

In Figure 3 we show the energy levels (relative to the $^1B_{1g}$ state) resulting from a full π CI calculation, along with the SCF and GRVB results. The full π CI is the fully correlated limit of this basis set (which excludes the sigma space), and thus represents the "correct" set of energy levels to which we can compare SCF and GRVB. The disadvantage of the full CI wavefunction is that we cannot extract simple physical ideas from the multitude of configurations (in this case, 266), as we can from the SCF and GRVB wavefunctions.

With the exception of the $^1B_{2g}$ state, which was not optimized, the GRVB results are seen to be in very good agreement with the CI. The ground state is correctly predicted to be $^1B_{2g}$ state, the first triplet is about 10 kcal up (CI: 10.2, GRVB: 13.0) and the $^1A_{1g}$ and ^3E_u antiresonant states are within 5.2 kcal and 1.7 kcal, respectively, of the CI. Thus, the key features of the valence state spectrum are produced by the resonating VB model.

The SCF results are seen to be in poorer agreement with the CI. The ground state is incorrectly predicted to be a triplet (a relative error of 14.6 kcal), the $^1B_{2g}$ state is 31.0 kcal too low, the ^3E_u state is 31.3 kcal too high, and the $^1A_{1g}$ and $^1B_{2g}$ states are interchanged.

That MO theory predicts the incorrect ground state is significant, as this is considered to represent a violation of Hund's rule.[7] Kollmar and Staemmler have proposed a mechanism they call "dynamic spin polarization" [14] by which the singlet state in a biradical species is expected to be lowered by CI more than the triplet. They have used this mechanism to justify the Hund's rule violation in H_4, twisted ethylene, and planar methane, as well as in cyclobutadiene. The effect is expected to cause a

state crossing when the singlet and triplet states are nearly degenerate, as occurs when the exchange integral between the two singly-occupied orthogonal orbitals is small. As discussed in section II, the exchange integral in this case is

$$K_{X+Y,\,X-Y} = 2.2 \text{ kcal} \quad . \tag{10}$$

The spin polarization theory is a formalized version of a qualitative explanation put forth earlier by Borden[15] to explain the cyclobutadiene violation. Without going into the details of the dynamic spin polarization theory, we simply point out that the CI terms which are purported to cause this "spin polarization" are similar to those required to convert the SCF wavefunction into a resonating VB wavefunction. Thus the same effect can be accounted for with a much simpler model than those authors proposed. Using the resonating valence bond model also leads to the correct ground state of square H_4, which is isomorphic to the π space of cyclobutadiene. (The singlet-triplet inversion in twisted ethylene can also be explained using a single-particle wavefunction (spin-optimized GVB), rather than resorting to dynamic spin polarization.[16])

In Figure 4 we show the bond pair from the GVB(2/4) singlet wavefunction (equation (15)). The orbitals are seen to be strongly localized, and polarized to achieve favorable bonding overlaps. The GRVB(2/4) orbitals from the resonant ($^1B_{1g}$) and antiresonant ($^1A_{1g}$) states are also displayed, and are virtually indistinguishable from the GVB orbitals. Unlike in benzene, for example, the orbitals are completely localized even before resonance is included. This is discussed in the next section. Figure 5 shows the orbitals from the GVB(1/2) triplet and the GRVB(1/2) resonant and antiresonant triplet states. In contrast to the singlet state, the triplet orbitals are completely delocalized in the GVB wavefunction, and become

very localized in the GRVB wavefunctions. This is because the orbitals try to include the effect of resonance at the GVB level by smearing out over the molecule. This tendency is so strong that the GVB "bond pair" is distorted into a bond between the diagonal carbons. When the resonance is explicitly included in the GRVB wavefunction by allowing two structures, the orbitals are free to localize, taking on shapes expected from VB theory. This occurs in most systems to which we have applied GRVB, and the next section discusses why the CBD singlet is an exception. Another noticeable feature of the GRVB triplet orbitals is that the antiresonant state orbitals are more localized than those of the resonant state. This "tightening up" of each orbital reduces the interaction between the two resonance structures, thereby reducing the amount that the antiresonant state is driven up in energy from the energy of a single resonance structure. It is important to understand that reducing this "interaction" does not necessarily mean reducing the wavefunction overlap. The whole term

$$E_{ANTI} = H_{AA} - \frac{H_{AB} - S_{AB} H_{AA}}{1 - S_{AB}}$$

must be reduced, though in fact, the wavefunction overlap does decrease from 0.0826 for the resonant state to 0.003227 for the antiresonant state.

It is interesting that the ionic $^1B_{2g}$ state is actually below the antiresonant triplet state. Perhaps a better description of this state is as a resonance of two structures, each of which has four one-electron bonds. By appropriately singlet-coupling pairs of these one-electron bonds, we can get the desired $^1B_{2g}$ symmetry:

$\Psi^{R-VB}(^1B_{2g}) =$ 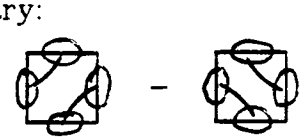 . (32)

Since the carbon-carbon two-electron π bond is more than twice as

strong as the one-electron π bond, the four one-electron bonds will not be competitive with two two-electron bonds. However, it seems reasonable that such a structure might be more stable than the structure with two negatively charged carbons. The antiresonant combination of these "ionic" structures leads to a state with A_{1g} symmetry (see equation (23b)), and thus the $^1A_{1g}$ state at 50.0 kcal may contain a small amount of this character. This would explain why the GRVB description of the $^1A_{1g}$ state is 5.2 kcal too high, since the GRVB wavefunction does not include this "ionic character".

Finally, we note that the GRVB value for the $^1B_{1g}$ to $^3A_{2g}$ excitation is 2.8 kcal above the CI value. Since the correlation error in the two bond pairs is expected to be greater than the correlation error in one bond pair plus a triplet coupled pair, this result is opposite to expectation. One possible implication is that the triplet resonance is not completely described, a result of using only two resonance structures to optimize the orbitals. As discussed in Section IV, we believe this error is negligible. Another possibility is that there is a contribution from the one-electron bond structures

$\Psi(^3A_{2g}) =$ 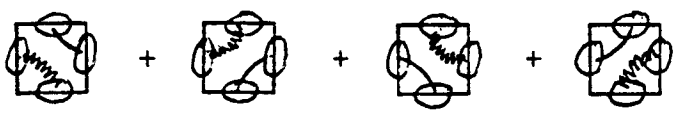 (33)

(where the wiggly line represents triplet coupling), which is included in the CI, but not in the GRVB wavefunction.

VI. The VB Singlet State - A "Forbidden Reaction"

In the last section we saw that the GRVB(1/2) singlet oribitals differed only slightly from the GVB(2/4) orbitals. In contrast, the triplet state orbitals behave much more like those of most systems we have studied, going from very delocalized in the GVB wavefunctions (because they are trying to include resonance), to very localized at the GRVB level (because the resonance is included explicitly). The reason for this anomolous behavior of the single can be understood by appealing to the orbital phase continuity principle (OPCP)[17], which is used to predict whether a reaction is "allowed" or "forbidden". the OPCP approach makes identical predictions as the Woodward-Hoffmann rules[18] for systems with symmetry, but OPCP does not require symmetry to work. For example, using OPCP, the $H_2 + D_2 \rightarrow 2HD$ reaction is predicted to be forbidden for any approach geometry, based on what necessarily happens to the *phases* of the orbitals as they convert from the reactant bonding structure to product bonding structure. Because the relative phases of the two orbitals in one of the bond pairs must change sign, the transition state corresponds to breaking a bond. We do not give a derivation of OPCP here, but simply state the consequence that bears on the problem at hand. *If the interconversion of two bonding structures is "allowed" by OPCP, then an SCF which describes one of these bonding structures may delocalize to contain some character from the other bonding structure. If the interconversion of the two bonding structures is OPCP- "forbidden", then an SCF will not delocalize to include character from the other bonding structure.* Since the π space of the cyclobutadiene singlet is isomorphic with a "forbidden" 2+2 reaction, the two VB structures cannot interconvert by OPCP. Thus, the "smearing out", which allows some resonance at

the GVB level, is forbidden by OPCP for the CBD singlet. Whatever extent the wavefunction tries to include resonance by smearing out, it picks up character of a broken bond, which is energetically unfavorable. However, this inability to interconvert bonding structures has no bearing on the ability to gain a lowering in energy upon resonating the two structures, and indeed the resonance is a 22 kcal effect. The CBD triplet, and most of the other resonating systems we have studied, are isomorphic with "allowed" reactions, and thus show considerable delocalization at the SCF level.

An important ramification of this property of the CBD singlet is that the GRVB wavefunction is only slightly different than the R-GVB wavefunction, as shown in Figure 6. The resonance lowering for the R-GVB wavefunction is 20.6 kcal, only 1.2 kcal less than GRVB. Similarly, the antiresonant state only drops by 0.7 kcal in going from R-GVB to GRVB. Thus for single CBD, and any other resonating system that is isomorphic with a forbidden reaction, the much less expensive R-GVB wavefunction can be used to get near-GRVB results.

Another consequence of this result is that cyclobutadiene is one of the few systems in which the electronic resonance energy can be estimated to high accuracy, because the GVB wavefunction corresponds very closely to the non-resonating reference state. Assuming that the resonance lowering would not change significantly upon increasing the basis set,[19] we can state that the electronic resonance energy in square cyclobutadiene is between 21.8 kcal (E(GVB)-E(GRVB)) and 23.1 kcal ($E(\Psi_A^{GRVB}) - E$ (GRVB)).

VII. Rectangular Distortion

We now consider distorting square CBD to a rectangular geometry. In resonating VB theory, this leads to two VB structures which are inequivalent,

$\Psi_{TOT} = C_A$  $+ C_B$ 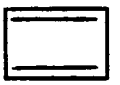 . (34)

The good structure (Ψ_A) goes down in energy because it attains bond lengths closer to the ideal values for single and double bonds. The bad structure (Ψ_B) goes up in energy, leading to a decrease in the resonance energy. Thus, the molecule will distort if the good structure drops in energy faster than the resonance energy declines. Figure 7 shows the potential curves before and after resonance. The resonance is not strong enough to prevent the distortion, and the rectangular geometry is 4.8 kcal below square. This is in excellent agreement with the π CI result of 5.1 kcal at the same geometry. The MO theory analysis of the distortion relies on a perturbation theory argument known as the second-order Jahn-Teller effect.[20] This theory is discussed by Pearson,[21] and we state only the result here. If a low-lying electronic state (Ψ_e) has the symmetry such that the integral $\langle\Psi_0|\partial H/\partial Q|\Psi_e\rangle$ is nonzero, then a distortion *might* occur along coordinate Q. The integral is nonzero if the direct product of the symmetry representations of Q and Ψ_e contains the symmetry representation of Ψ_0. For CBD, the rectangular distortion is of b_{1g} symmetry, the first excited singlet is $^1A_{1g}$ (a_{1g} symmetry), and the ground state is b_{1g} symmetry, so that a second-order Jahn-Teller distortion is plausible. As in resonationg VB theory, we cannot make an *a priori* prediction that the distortion will occur, only that is reasonable. The SCF results are also displayed in Figure 7, and the SCF is seen to correctly

predict the ground state of the molecule to be a rectangular singlet, with the 7.5 kcal lower than the square singlet.

Other theoretical estimates have placed this energy difference at 4.2 kcal (STO-3G basis [5]) and 6 kcal (6-31G* basis [6]), using full π CI calculations, and the barrier roughly doubles if σ correlation is included. Probably the best estimate so far is 12 kcal made by Jafri and Newton[6] using $\sigma\pi$ CI in a 6-31G* basis set. Whitman and Carpenter have recently placed an experimental lower bound on this barrier to interconversion of the rectangles, by comparing the rate of interconversion to the rate of Diels-Alder trapping[3]. The CBD was isotopically labeled in a way that yielded different trapping products for the two rectangular forms, and the activation energy for automerization was determined to be 1.6 kcal higher than the activation for trapping. Since the trapping reaction should not have a negative activation energy, 1.6 kcal is a lower bound on the CBD automerization barrier.

VIII. Conclusions

We have applied MO theory and resonating VB theory to understand the low lying states of cyclobutadiene in its square geometry. The MO description of CBD is as a diradical with a triplet ground state and a corresponding open shell singlet slightly higher. VB theory describes ground state CBD as a resonance of two structures, each with two π bonds, and the triplet state is higher because it has one broken bond. Through the use of SCF and GRVB techniques, the orbital-optimized versions of the MO and resonating VB wavefunctions can be found, and the resulting state energies are consistent with the model predictions. Comparison to the results of a full π CI indicates that the VB model more accurately portrays the features of the CBD system, giving the correct

ground state and reasonable excitation energies. While in MO theory CBD is often described as "antiaromatic", and attributed with a negative resonance energy,[22] we find a positive resonance energy of 22 kcal with respect to a single VB structure. This apparent discrepancy results from a difference in the conventions for the reference energy.

In VB theory, the distortion to a rectangular geometry is favored by a relaxation of strained bonds, and disfavored by a loss of resonance energy. In MO theory the distortion is possible due to a second-order Jahn-Teller coupling with the $^1A_{1g}$ state. Neither theory predicts qualitatively whether the distortion will actually occur, but the SCF and GRVB calculations both find a rectangular singlet ground state, as does the full π CI.

References

1) S. Masamune, F.A. Aouto-Bachiller, T. Machiguchi, and J.E. Bertie, J. Am. Chem. Soc. **100,** 4889 (1978)

2) D.W. Whitman, B.K. Carpenter, J. Am. Chem. Soc. **102,** 4272 (1980)

3) D.W. Whitman, B.K. Carpenter, J. Am. Chem. Soc. **104,** 4272 (1980)

4) H. Kollmar and V. Staemmler, J. Am. Chem. Soc. **100,** 4304 (1978)

5) W.T. Borden, E.R. Davidson, and P. Hart, J. Am. Chem. Soc. **100,** 388 (1978)

6) J.A. Jafri and M.D. Newton, J. Am. Chem. Soc. **100,** 5012 (1978)

7) W.T. Borden and E.R. Davidson, Acc. Chem. Res. **14,** 69 (1981)

8) This was a subject of controversy for a long time, since experimental evidence previously indicated a square geometry. See reference 3 and references therein.

9) F.W. Bobrowicz, Ph.D. Thesis, California Institute of Technology (1974)

10) T.H. Dunning, Jr. and P.J. Hay, in: *Modern Theoretical Chemistry, Vol. 3, Methods of Electronic Structure Theory*, edited by H.F. Schaeffer III (Plenum, New York 1977), Chap. 1

11) S. Huzinaga, J. Chem. Phys. **42,** 1293 (1965)

12) R.E. Walkup, W. Ho and W.A. Goddard III, unpublished results.

13) F.W. Bobrowicz and W.A. Goddard III, in: *Modern Theoretical Chemistry, Vol. 3, Methods of Electronic Structure Theory*, edited by H.F. Schaeffer III (Plenum, New York 1977), Chap. 4

14) H. Kollmar and V. Staemmler, Theor. Chim. Acta (Berl.) **48,** 223 (1978)

15) W.T. Borden, J. Am. Chem. Soc. **97,** 5968 (1975)

16) A.F. Voter, M.M. Goodgame and W.A. Goddard III, submitted for publication.

17) W.A. Goddard III, J. Am. Chem. Soc. **94,** 793 (1972)

18) R. Hoffmann and R.B. Woodward, J. Am. Chem. Soc. **87,** 2046, 4388, 4389 (1965); R.B. Woodward and R. Hoffmann, *ibid*

87, 395, 2511 (1965); R.B. Woodward and R. Hoffmann, Angew. Chem., Int. Ed. Engl., **8,** 781 (1969).

19) The R-GVB(pr) resonance lowering does decrease from 28.5 kcal with a STO3G basis to 21.7 kcal with a VDZ basis.

20) U. Öpik and M.H.L. Pryce, Proc. Roy. Soc. (London) **A238,** 425 (1957)

21) R.G. Pearson, J. Am. Chem. Soc. **91,** 4947 (1969)

22) H. Kollmar, J. Am. Chem. Soc. **101,** 4832 (1979)

23) This is because the orbital space consists of four symmetric and four antisymmetric orbitals (with respect to the σ_v plane).

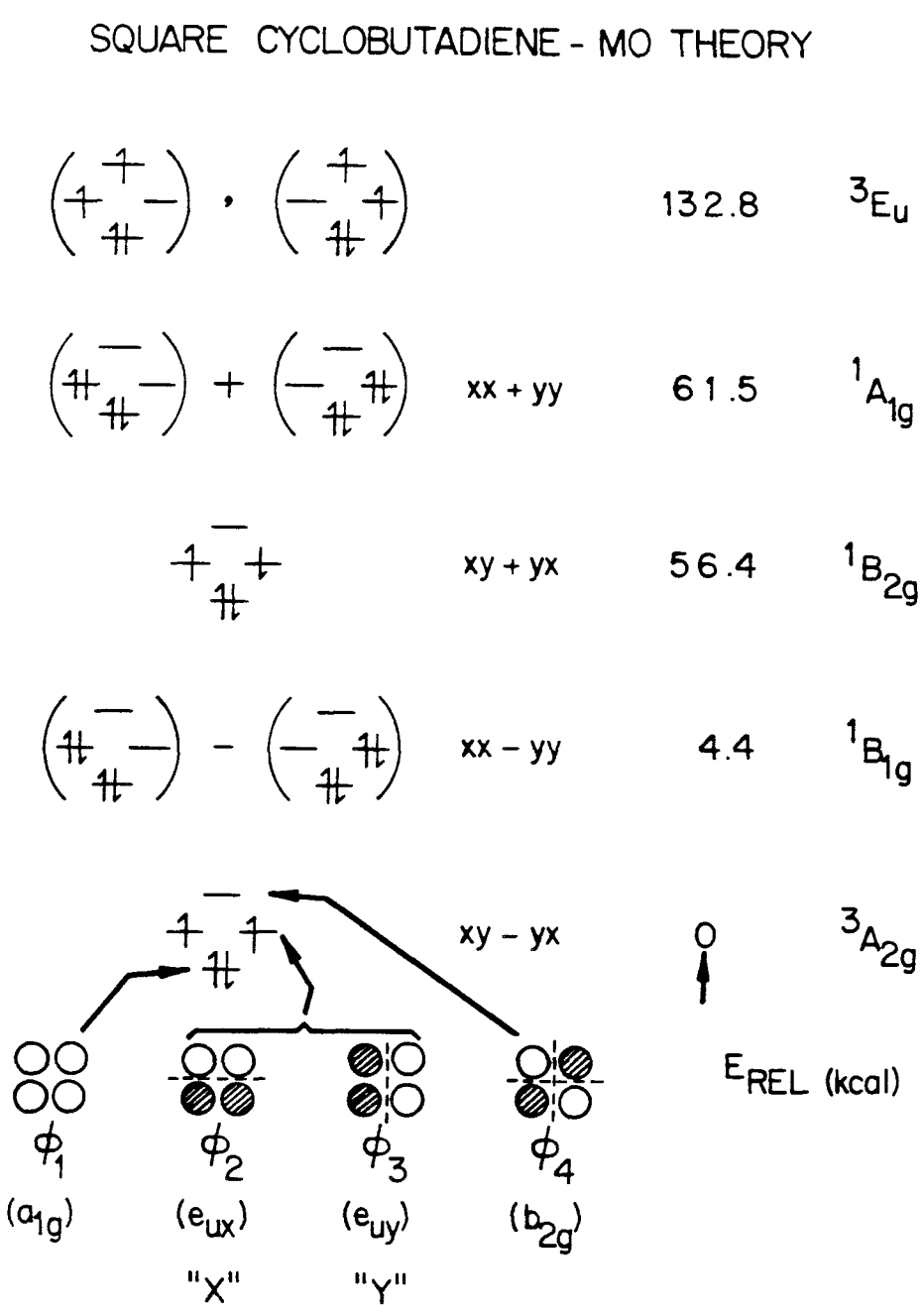

Figure 1. MO theory description of the low lying states of square cyclobutadiene. The energies are from an SCF calculation on each state.

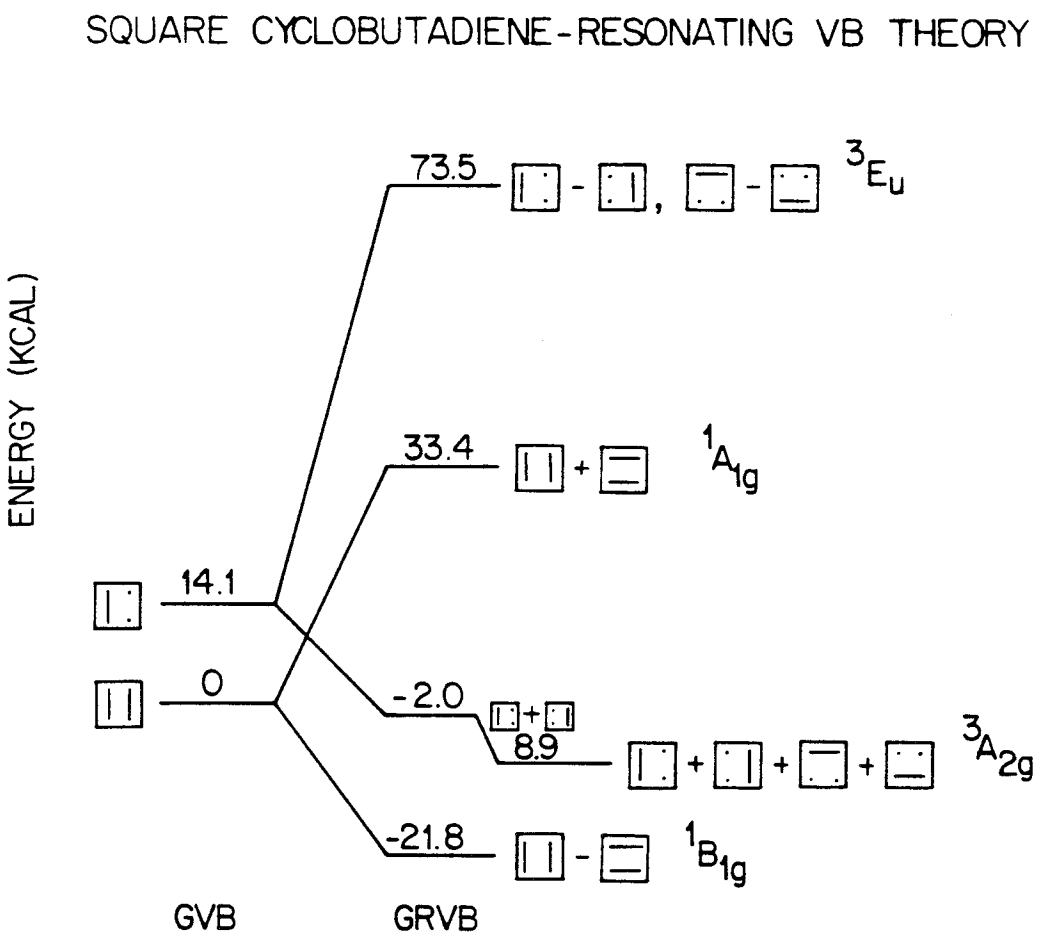

Figure 2. Resonating VB theory description of the low lying states of square cyclobutadiene.

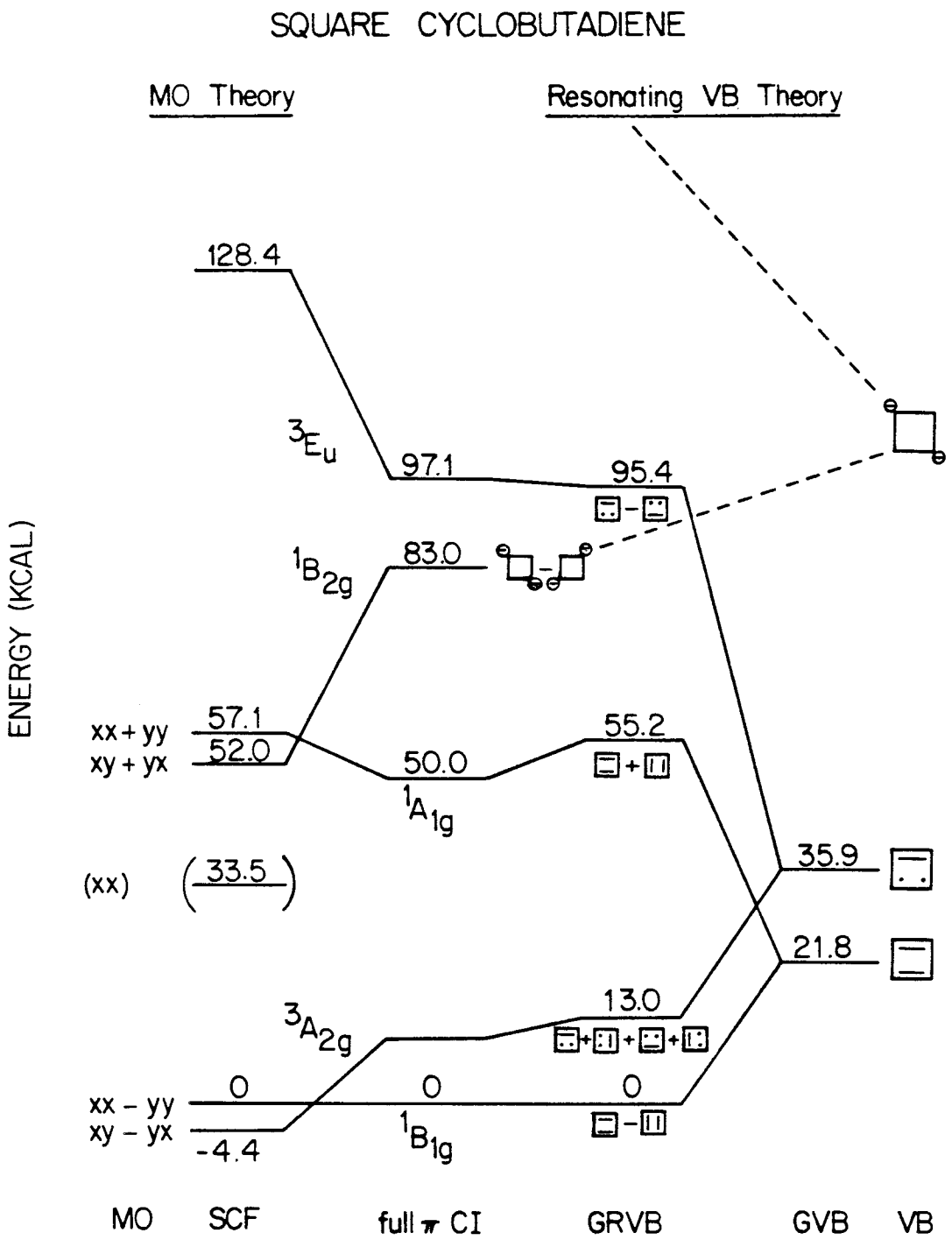

Figure 3. Quantitative comparison of MO theory and resonating VB theory. The total energies for the $^1B_{1g}$ state are: SCF: -153.58584, GRVB: -153.76295, and full π CI: -153.657826. The GRVB and π CI wavefunctions use the same frozen σ core, while the SCF wavefunctions are completely relaxed.

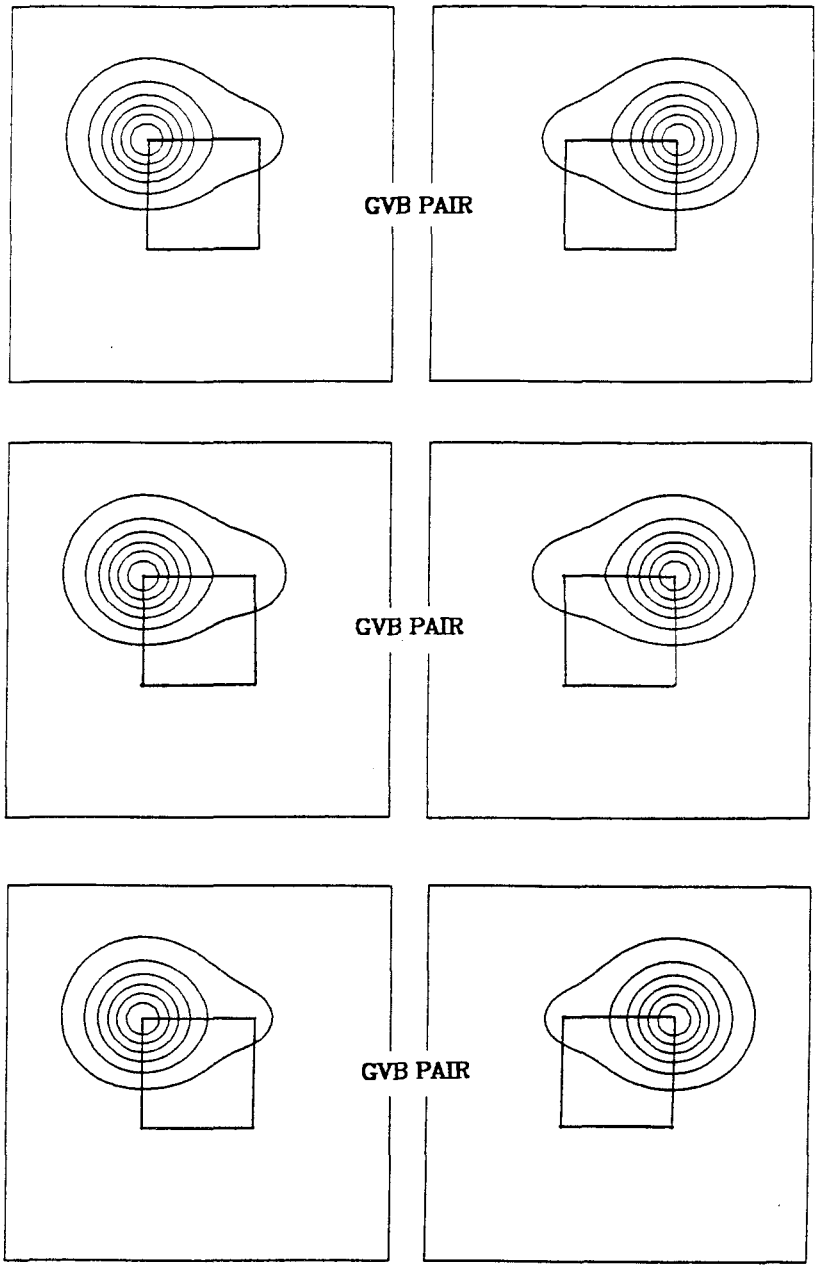

Figure 4. The GVB and GRVB orbitals for singlet cyclobutadiene. Top: GVB(2/4); Middle: GRVB(2/4), $^1B_{2g}$ (resonant) state; Bottom: GRVB(2/4), $^1A_{1g}$ (antiresonant) state. Only one of the two (equivalent) bond pairs is shown in each case. The plotting plane is 0.5 Å above the molecular plane, and the projected positions of the carbon atoms are indicated.

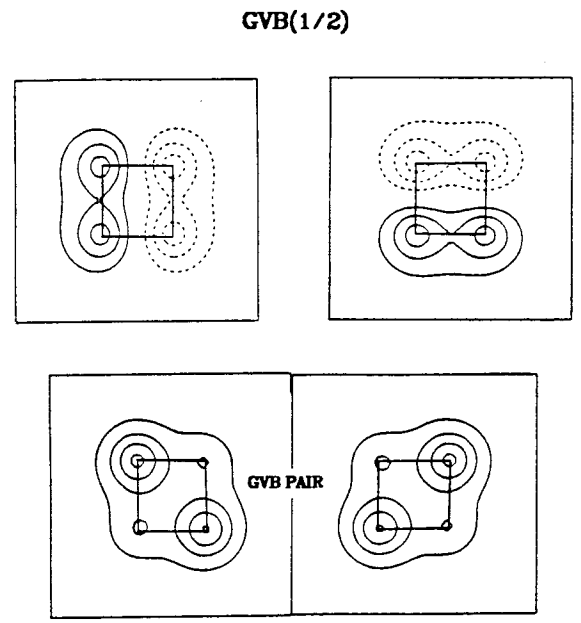

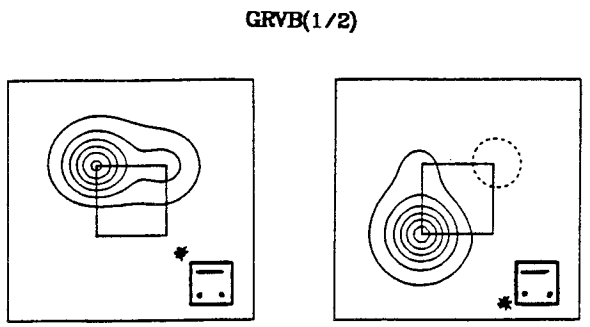

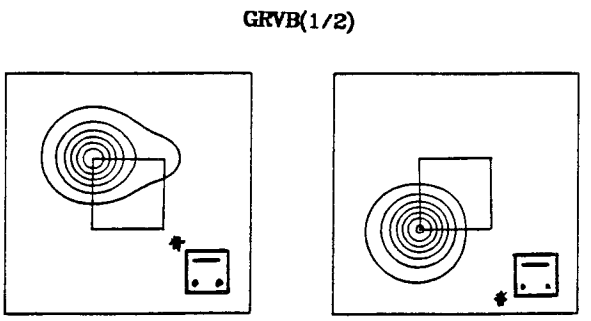

Figure 5. The GVB and GRVB orbitals for triplet cyclobutadiene. Top: GVB(1/2) (delocalizes); Middle: GRVB(1/2), $^3A_{2g}$ (resonant) state; Bottom: GRVB(1/2), ^3E_u (antiresonant) state.

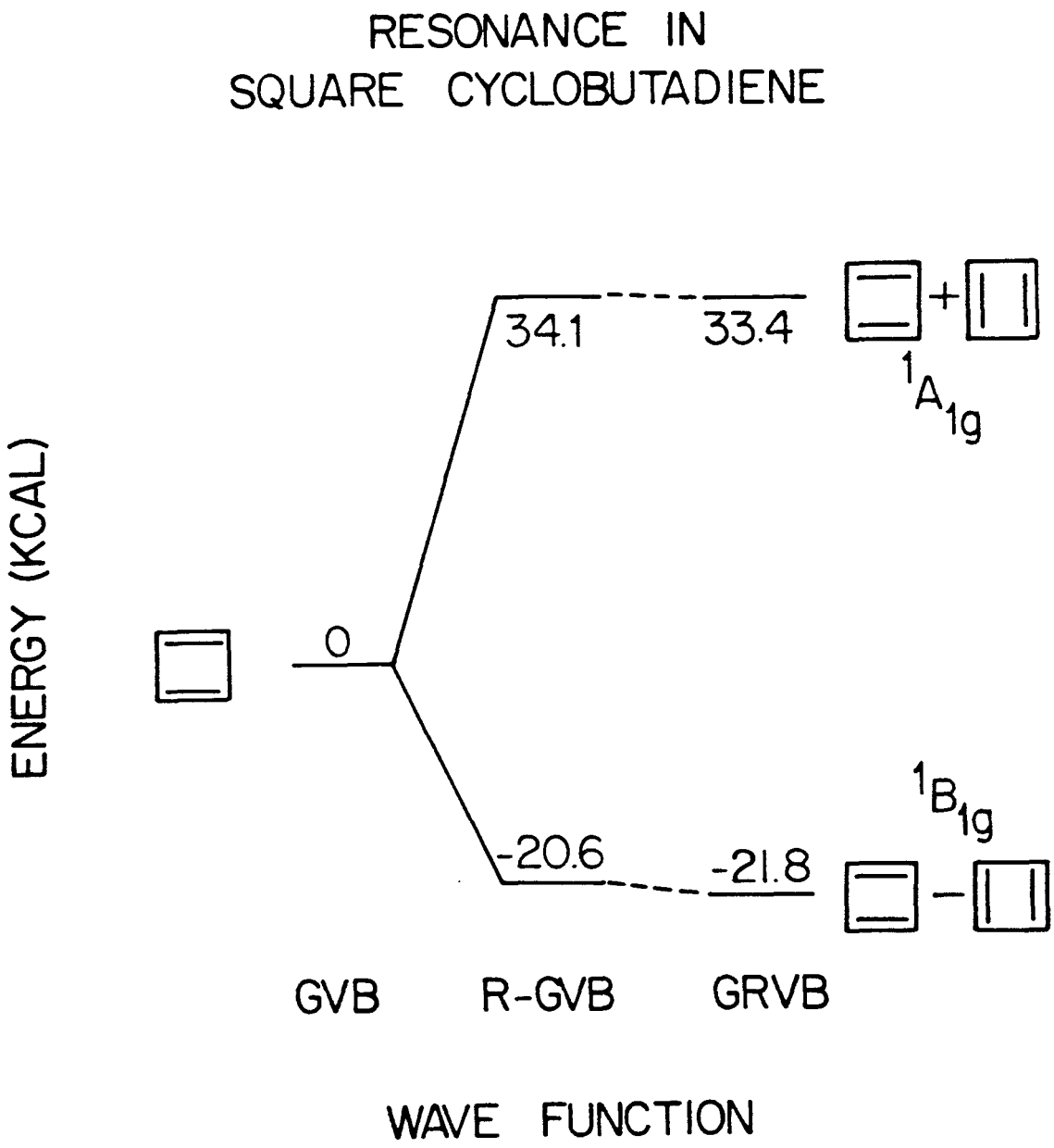

Figure 6. Various levels of resonance in cyclobutadiene; GVB(2/4), R-GVB(2/4) and GRVB(2/4). All calculations used the same sigma space.

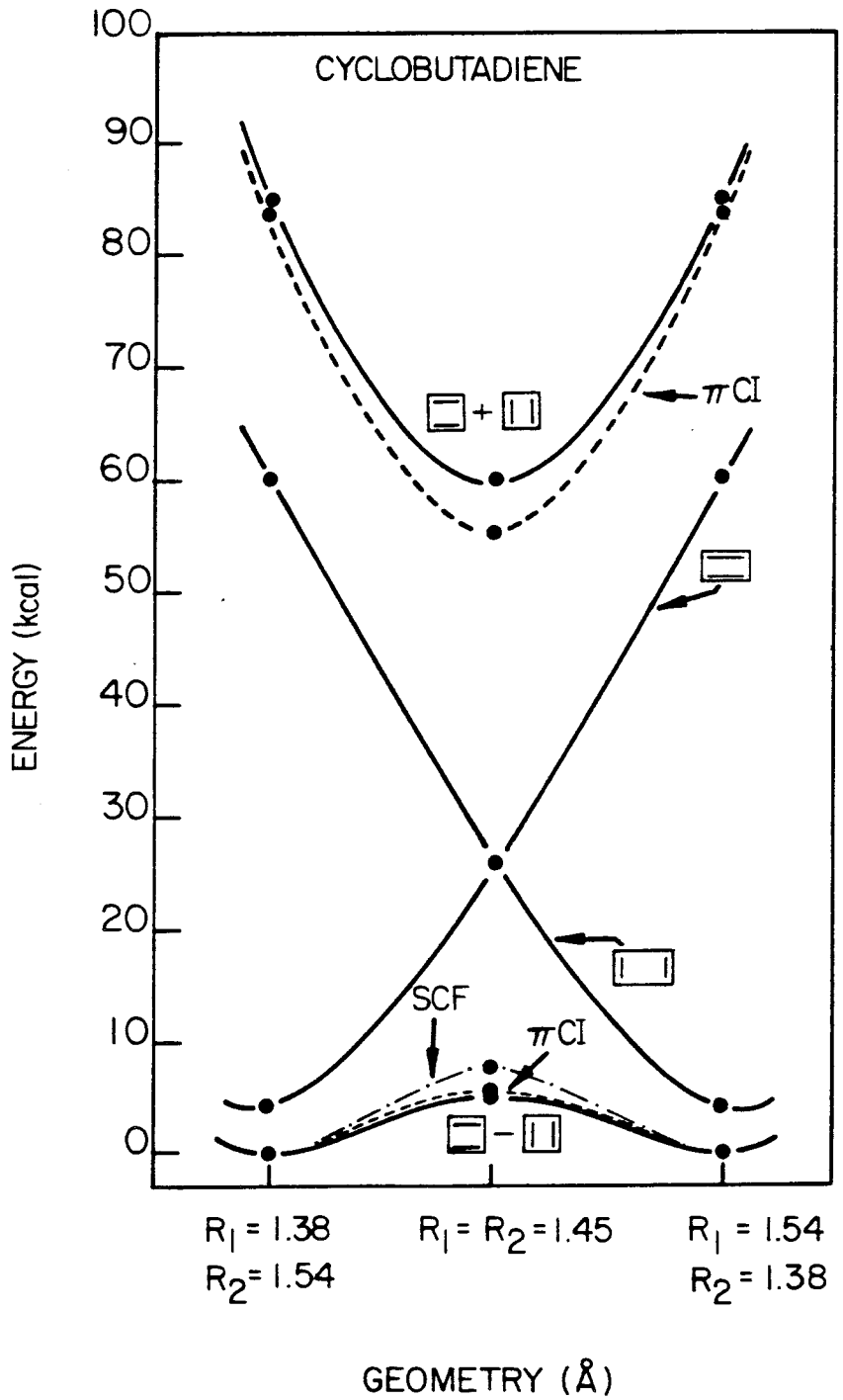

Figure 7. Resonating VB model of the rectangular distortion at square cyclobutadiene. The solid lines are R-GVB results, while the full π CI is indicated by a dashed line. Energies are with respect to the rectangular ground state.

CHAPTER 5

The Resonating Valence Bond Description of Chemical Reactions

I. Introduction

Most chemical reactions are ideally suited to a resonating valence bond model, since in the process of a reaction a bonding structure corresponding to reactants is converted to a bonding structure corresponding to products. Thus, the wavefunction along the reaction pathway can be represented as a continuously varying linear combination of reactant structure and product structure.

For example, in the HCl + D exchange reaction,

$$\underset{\text{reactants}}{\text{H--Cl + D}} \longrightarrow \underset{\text{products}}{\text{H + Cl--D}} \qquad (1)$$

the "reactant structure" (Ψ_A) has a bond between the H and Cl with an unpaired electron on D, while the "product structure" (Ψ_B) has a bond between Cl and D, and we can write the total wavefunction as

$$\Psi_{TOT} = C_A\Psi_A + C_B\Psi_B \ , \qquad (2)$$

where C_A and C_B depend on nuclear geometry. Even without explicitly defining the form of Ψ_A (so long as Ψ_A is reactant-like and Ψ_B is product-like), we can see that (2) yields a very neat conceptual picture of the reaction process, as shown in Figure 1. The diabatic states Ψ_A and Ψ_B are completely appropriate for the reactant and product limits,* while C_A, C_B, and the energy of Ψ_{TOT} at any other point along the reaction coordinate

* There may be a small contribution to E_{TOT} from the other structure at the reaction limits, but the corresponding energy lowering will be negligible.

can be found by solving the two-dimensional secular equation using Ψ_A and Ψ_B as the basis states. The resonance energy, defined as

$$E_{RES} = E_{lower} - E_{TOT} \ , \tag{3}$$

where E_{lower} is the lower of E_A or E_B, is seen to be larger when E_A and E_B are closer. For a symmetric reaction such as (1)*, we can state that the transition state will occur at a point where E_A and E_B cross, that this will be a maximum in E_{RES} along the reaction coordinate q, and that at this point

$$|C_A| = |C_B| \ .$$

For a nonsymmetric reaction such as

$$H + Cl_2 \longrightarrow HCl + Cl \ , \tag{4}$$

the transition state may not occur at the crossing of E_A and E_B, but the resonance energy will reach a maximum near this crossing point, and the transition state will also be nearby, unless the slopes of E_A and E_B are very different at the crossing. If E_A and E_B are fairly smooth in this region, the transition state will be shifted towards the state with the more shallow slope, as shown in Figure 2. If E_{RES} could be expressed as a function of $E_A - E_B$, a simple expression for the magnitude of this shift could be obtained in terms of the slopes of E_A and E_B. However, E_{RES} results from a delicate interplay of the matrix element $\langle\Psi_A|H|\Psi_B\rangle$, and the overlap $\langle\Psi_A|\Psi_B\rangle$, and a simple expression could thus be misleading.

The R-GVB and GRVB methods presented in Chapter 3 allow us to

* Within the Born Oppenheimer approximation, the HCl + D reaction has a symmetric potential energy surface.

solve for the wavefunctions Ψ_A and Ψ_B and mix them to obtain C_A, C_B, E_{RES}, and E_{TOT}. These wavefunctions and energies can be interpreted directly within the framework of the simple model just discussed, and thus provide a test of the validity of the resonating valence bond model of chemical reactions. The results of various test cases are presented in the following sections.

II. The HF + D Exchange Reaction

A. Introduction

The reactions of HF with a hydrogen atom,

$$HF + D \text{ ----- } H + FD, \tag{5}$$

and

$$D + HF \text{ ----- } DH + F, \tag{6}$$

have received considerable experimental[1-3] and theoretical[4-7] attention in recent years, primarily due to the influence of such reactions on the performance of the HF chemical laser. In the following we compare various theoretical methods in describing the activation barrier of the thermoneutral exchange reaction (5). Calculations by Wadt and Winter[4] have shown that the activation barrier is 1-2 kcal lower for a nonlinear transition state geometry. We consider this bent state in Section II.F, but the majority of our calculations were performed at a collinear geometry. The collinear transition state has been the subject of all other previous work, and is thus well suited to a comparison of calculations. In particular, we compare the results from simple wavefunctions in which one-electron orbitals can be plotted with the results from complex, highly correlated wavefunctions. We find that the GRVB wavefunction yields a barrier height in excellent agreement with the accurate wavefunctions (49 kcal),

while all other simple approaches give a barrier more than 9 kcal too high (in most cases, 15-20 kcal high). Further, the GRVB orbitals supply strong evidence for the validity of the resonating valence bond model at the transition state.

B. Calculational Details

All collinear calculations employed the flexible contracted gaussian basis set listed in Table 1. The fluorine basis is Huzinaga's (9s,5p) basis[9] as contracted to (3s,2p) by Dunning,[10] augmented by a single d polarization function (α = 1.34), and the hydrogen basis is a triple zeta contraction of Huzinaga's 6s basis plus a single p polarization function (α = 1.45). This basis is comparable to the double zeta polarization basis employed by Dunning,[8] and the less flexible of the two basis sets used by Wadt and Winter.[4] The more flexible basis they used contained diffuse s and p Rydberg functions on the fluorine, which were necessary for accurate description of the bent geometries but only had a slight effect (~2 kcal) on the collinear transition state. The Caltech Program GVB2P5[11] was used for all Hartree-Fock and GVB calculations, Caltech GVB3 program[12] was used for the full-valence multiconfigurational SCF's (MCSCF), and the Caltech CI2P5 program was used for the configuration interaction (CI) wavefunctions. All CI, MCSCF, and GRVB wavefunctions maintained a frozen 1s orbital on the fluorine, taken from the Hartree-Fock calculations which used full symmetry. A number of wavefunctions allowed optimization of orbitals in the sigma space only, and for these the doubly-occupied $2p_x$ and $2p_y$ orbitals were taken from Hartree-Fock wavefunctions with full symmetry. The relaxation of these pπ orbitals to an asymmetric shape in the GRVB wavefunction lowered the total energy

by only 0.7 kcal. In this sigma-space basis, the GRVB wavefunction had four occupied orbitals (a closed-shell 2*s*, a GVB pair for the bond, and an open shell) and 9 virtual orbitals, leading to 42 orbital rotations to be optimized. For the symmetric geometries, Ψ_B was defined by the reflection of Ψ_A, so that only the Ψ_A orbitals were explicitly optimized. At the asymmetric geometries, the Ψ_B orbitals and Ψ_A orbitals were each optimized, requiring 42 rotations for each subwavefunction. Using the procedure described in Chapter 3, all 84 rotations were optimized in a single GRVB run. The desired orthonormality of occupied and virtual orbitals within a subwavefunction was maintained by using a different set of virtual orbitals for Ψ_A and Ψ_B.

Typical CPU times on a DEC VAX 11/780 computer were 12,000 seconds for the σ-GRVB at symmetric geometries, 14,400 seconds at asymmetric geometries (20 iterations using a new basis each iteration), 115 seconds to perform the GVB(1/2) calculations, 2,776 seconds for the σ-full CI at symmetric geometries, 11,835 seconds at asymmetric geometries, and 192 seconds to compute the atomic integrals (assymetric geometry).

Unless otherwise noted, calculations were performed at the $R_1 = R_2 =$ 1.17 Å collinear geometry of HFH as optimized by Wadt and Winter,[4] and the experimental geometry of R = 0.9176 Å for HF.[13] The geometry used for the bent transition state study was that optimized by Wadt and Winter ($R_1 = R_2 =$ 1.08 Å, $\Theta = 106°$), and some of our calculations employed their large (4s,3p,1d/2s,1p) basis.

All orbital contour plots use the same scale (the horizontal width of the box is always 7 Å), and are plotted in a plane containing the molecule. Contours from 1.0 a.u. to -1.0 a.u. are displayed in steps of 0.05, with

negative contours represented by dashed lines.

C. Results from High Level Wavefunctions

In Table 2 we list the activation barrier for collinear HF + H as calculated from highly correlated wavefunctions by various workers. These values represent the most accurate theoretical estimates currently available and are seen to be in reasonable agreement with each other. They are probably an upper bound on the barrier which would result from a full CI in an infinite basis, since barriers in other systems have invariably dropped when more correlation or a larger basis was employed.[14] However, there is no reason to believe that the barrier would drop more than another 5 kcal. Thus, these results are in agreement with the only experimental estimate,[3] which brackets the barrier between 42 and 53 kcal. The various abbreviations are defined here:

A GVB(*n*/2*n*) wavefunction is GVB perfect-pairing[11] in which n orbitals are correlated with two natural orbitals each (the Wadt and Winter GVB(3/6) calculations correlated the H-F bond, the F 3*s* pair and one of the *pπ* orbitals).

A GVB-CI is a full CI within the GVB active space, which consists of the 2n GVB natural orbitals plus any open-shell orbitals.

An SD-CI is all single and double excitations from some configuration or configurations. Thus, Wadt and Winter's GVB + SD-CI is a GVB-CI plus (not times) an SD-CI from the GVB dominant configuration, and their POL(3)CI is a GVB-CI plus an all triples CI from the GVB dominant, restricted to have only one electron in the virtual space.

SOGVB refers to "strongly orthogonal" GVB in which the spin coupling of the GVB electrons is optimized (while maintaining orthogonal GVB natural orbitals), in contrast to GVB perfect-pairing (which we call simply GVB), which only allows the singlet coupling within each GVB pair.

PNO-CEPA refers to the pseudo-natural orbital correlated electron pair approximation.[15]

The σ-full CI wavefunction is a full CI in the sigma space only, as defined in Section II-B. Some of the wavefunctions we will describe in the following sections (σ-GRVB, σ-SOGI, σ-full valence) are optimized in this same sigma space, and the barriers thus obtained should be compared with the σ-full CI barrier of 48.6 kcal, the fully correlated limit of this basis.

D. Results and Discussion of Conceptually Simple Wavefunctions

In Table 3 we list the barrier heights obtained from various wavefunctions, which retain a "single particle" (or "single particle plus resonance") interpretation, i.e., each electron in in the system can be assigned to one orbital. (This is not possible for most CI and MCSCF wavefunctions.) The simplest of these is the Hartree-Fock wavefunction, which gives a barrier ~20 kcal too high (67.8). Using a GVB(1/2) wavefunction in which the bond pair is described by two singlet-coupled one-electron orbitals*, the barrier is calculated by comparing the GVB(1/2) energy of HF (and Hartree-Fock H atom) with the GVB(1/2) energy of HFH. Interestingly, this leads to an even higher barrier than Hartree-Fock (69.5 kcal versus

*GVB(n/2n) refers to n electron pairs correlated with two orbitals each, while GVB(n/m) means that n electron pairs are correlated with a total of m natural orbitals. The reader who is unfamiliar with GVB is referred to Chapter 1.

67.8 kcal). This can be understood by examination of Figure 3, in which we have plotted the Hartree-Fock and GVB(1/2) orbitals. The GVB pair is seen to be only *slightly* localized, and is essentially an "in-out" correlation on the F 2*p* orbital, rather than "left-right" bond pair correlation. This occurs because the GVB wavefunction is trying to incorporate resonance, and having only one bond structure available, accomplishes this to a degree by simply smearing this bonding over the whole molecule. This also occurs in the Hartree-Fock wavefunction, where the delocalization tendency is so strong that forcing symmetry on the wavefunction does not change the energy (i.e., the Hartree-Fock wavefunction does not "break symmetry"). Thus the GVB barrier height is even higher than Hartree-Fock because while the HF energy is lowered by the sigma bond correlation (14.6 kcal), the HFH energy is not, because the wavefunction refused to scarifice the energy gained by delocalization. The GRVB(1/5) wavefunction, which correlates the bond pair with five natural orbitals, gives an even higher barrier, for the same reasons. The most sophisticated single-particle wavefunction we can optimize that does not include resonance* is the "SOGI(3)" wavefunction,[16] in which each electron in the active space (in this case, three electrons) has its own orbital and the spin coupling among these electrons is completely optimized with no restrictions on the overlap between the orbitals. The SOGI wavefunction on HFH is consistent with a GVB(1/2) wavefunction on HF [since SOGI(2) for the bond pair is equivalent to GVB(1/2)], yielding a barrier of 57.7 kcal. The σ-SOGI(3) wavefunction listed in Table 3 was optimized with a frozen π space, so the appropriate comparison is to the σ-full CI barrier of 48.6

* We refer to the smearing out tendency exhibited by the Hartree-Fock and GVB wavefunctions as "delocalization" and reserve the term "resonance" for wavefunctions that explicitly include multiple resonating subwavefunctions, such as R-GVB or GRVB.

kcal.

The SOGI(3) barrier is 9 kcal high because even though the spin coupling corresponding to each bond structure is included in the wavefunction, the *shapes of the orbitals are not able to optimize for each resonance configuration*. We now consider wavefunctions that include resonance explicitly.

The R-GVB(1/2) wavefunction in which a GVB(1/2) wavefunction is resonated with its reflection* gives a barrier 66.5 kcal, corresponding to E_{res} = 3.0 kcal. This resonance energy is small because the GVB(1/2) wavefunction is only very slightly localized, as evidenced by the high overlap of 0.94 (if it were completely delocalized, E_{res} would be zero). The same problem occurs for the GVB(1/5) wavefunction (E_{res} = 2.0 kcal), and allowing the GVB coefficients to relax in the resonating wavefunction [see the R-GVB(pr) entries] has only a negligible effect. Thus the R-GVB approach gives only marginal improvement over GVB in describing the barrier height.

The strong delocalization tendency of the GVB wavefunctions is an indicator of the importance of resonance in this system. A GRVB(1/2) wavefunction in which each GVB(1/2)-like subwavefunction is optimized in the presence of resonance [this dissociates to a GVB(1/2) wavefunction on HF and a Hartree-Fock H atom] yields a barrier height of 47.7 kcal, in much closer agreement with the high quality wavefunctions. The most meaningful comparison is between the σ-GRVB(1/2), optimized in the sigma space only, and the σ-full CI, which includes all possible correlations in this space. While the σ-full CI energy for HFH is 14.4 kcal lower

* "Reflection" refers to the symmetry operation that interchanges the two H atoms.

than σ-GRVB(1/2), the barrier heights differ by only 0.2 kcal. Thus it appears that the differential correlation in the activation process is completely included by resonating two localized structures. The orbitals from one of the two GRVB(1/2) subwavefunctions [e.g., Ψ_A in Eq. (2)] are plotted in Figure 4, along with the corresponding orbitals from the HF molecule and H atom. It can be seen that the GRVB subwavefunction looks very much like an HF molecule next to an H atom, with the H atom staying orthogonal to the HF orbitals. Note that the GRVB wavefunction was not forced to look like this. With only the restriction that Ψ_B be the reflection of Ψ_A, the best possible Ψ_A was optimized. The resulting orbitals and the highly accurate calculated barrier are strong evidence for the validity of the simple resonating valence bond model of the transition state species:

The Pauli-induced orthogonality of the hydrogen electron raises the energy of the wavefunction, and the fluorine 2*s* pair is the main contributor to this condition, since it pooches away from the H-F bond and towards the hydrogen. Thus we can understand why the barrier height in this "allowed" reaction is ~ 50 kcal, while H + H_2, for example, has a barrier of only 9.8 kcal.[17] The difference between the σ-GRVB(1/2) wavefunction and the GRVB(1/2) wavefunction is in the relaxation of the F $2p_x$ and $2p_y$ electron pairs in response to the localized bonding. This relaxation lowers the energy by only 0.7 kcal, and Figure 5 shows that the $2p$ π orbi-

tals

become only slightly asymmetric. We also find that the GRVB(1/5) wavefunction leads to a barrier within 0.6 kcal of GRVB(1/2). Thus the important differential effects appear to be contained in the sigma space.

The optimized resonance of two Hartree-Fock wavefunctions, termed GRHF, leads to a barrier of 52.5 kcal, 4 kcal above the σ-full CI result. We conclude from this that a proper description of the bond pair correlation is not nearly as important as explicit inclusion of resonance. It is reasonable that the GRHF barrier is higher than the GRVB barrier, as Hartree-Fock does not dissociate properly,[18] leading to an artificially high energy for the elongated HF bond at the saddle point geometry.

Another wavefunction tested was the full-valence MCSCF, in which orbitals are optimized for a full CI within the active valence space. Using a three-orbital, three-electron active space, and optimizing with the same restrictions as the σ-full CI, the full valence wavefunction led to a barrier of 57.7 kcal, 9 kcal high. This is noteworthy, as some researchers use the full valence approach to compute reaction barriers.[19] The deficiency in the full valence wavefunction results from the fact that it does not allow shape readjustments necessary for the two different resonance structures. The 3*s* orbital is optimized, but has only one shape for both spin couplings of the other three electrons. A full valence wavefunction that allowed two orbitals per valence electron, including the 3*s* pair, would be expected to give much more accurate results.

We also tested the GRVB approach in describing the position and shape of the minimum along the symmmetric stretch mode in the saddle point region. The results are in Table 4, and the σ-GRVB(1/2) minimum is seen to be in excellent agreement with the σ-full CI, differing by only

0.002 Å. The force constant is farther off, predicting a curvature that is too shallow by ~ 7%.

E. The Resonating Valence Bond Model Along the Reaction Coordinate

As discussed in the Introduction, the resonating VB model offers a compact representation of the wavefunction for all points along the reaction coordinate. This is shown diagrammatically in Figure 1 for a symmetric reaction such as HF + D. The reaction coordinate displayed is idealized, but the important features are present. Starting at the Ψ_A limit, where $C_A = 1$ and $C_B = 0$, and moving towards the transition state, the energy E_{TOT} is dominated at first by E_A, and smoothly increases. For this region, the reaction coordinate is roughly half symmetric H-F-stretch, and half asymmetric stretch, corresponding to the motion of a rigid HF molecule towards a D atom. As the saddle point is approached, the HF bond length increases, increasing the amount of asymmetric stretch in the reaction coordinate. The unfavorable structure, Ψ_B, which looks like a very long F-D bond with a hydrogen crowded next to the fluorine, begins to drop in energy due to the decrease in Pauli repulsion that accompanies the H-F stretch. The magnitude of C_B smoothly increases, as does the resonance lowering of E_{TOT}. At the transition state geometry, the reaction coordinate is purely asymmetric stretch, and the resonance energy is at a maximum. If there were no resonance of Ψ_A and Ψ_B, the wavefunction would be purely Ψ_A until the transition state, at which point it would switch to pure Ψ_B, leading to a cusp in the energy. Thus, resonance has the effect of flattening out the energy in the transition state region, and smoothing the conversion from Ψ_A to Ψ_B.

To explore the capability of GRVB in describing this process, we per-

formed calculations at various points along an approximate reaction coordinate. The true reaction coordinate is defined as the path of steepest descent leading away from the saddle point geometry, and finding this path would require a search of the two-dimensional hypersurface. The approximate coordinate we used, sufficient for our purposes, consisted of fixing one bond distance at 1.17 Å (the transition state bond length) and varying the other bond distance. This coordinate goes through the correct saddle point at 48.4 kcal, though it does not coincide with the asymmetric stretch mode at the saddle point. The results are displayed in Figure 6, and the agreement between the σ-full CI and σ-GRVB is excellent at both the saddle point and the reaction "limits". In our discussion, we will implicitly refer to the left side of Figure 6, where E_A is below E_B.

We do not show results from an R-GVB wavefunction because at asymmetric geometries, the "bad-bond" GVB(1/2) wavefunction (Ψ_B) is unstable and collapses to the lower-energy "good-bond" structure (Ψ_A). In the GRVB description, Ψ_B can be "trapped" because Ψ_A is already included in the wavefunction, so that Ψ_B contributes to the total energy via the resonance energy. If the energy of Ψ_B is high enough that the resonance energy is smaller than the energy of some other pair correlation in the system, then the bad-bond GRVB (1/2) subwavefunction may collapse to a good-bond structure, but with a different shape for some orbital. For example, the wavefunction may choose to describe the in-out correlation of the fluorine 2*s* pair, which is worth 2.4 kcal for the isolated HF molecule.[60] If the GRVB wavefunction collapses in this way, it is no longer appropriate for calculating an energy along the reaction coordinate, since it is describing a correlation that is not present in the reactant (or

product) fragments. This collapse should not occur when the geometry is still close enough to the saddle point that the resonance energy is large. Figure 6 shows that this collapse occurs for geometries farther than 0.1 Å from the saddle point, as evidenced by the erratic behavior of the diabatic subwavefunction energies, and the drop off in the GRVB energy compared with the σ-full CI. The orbital plots of the Ψ_B subwavefunction in this region (not shown) are also consistent with this collapse.

In the region where the GRVB wavefunction is well-behaved, the agreement with the σ-full CI is excellent (also see Table 5), and the qualitative trends discussed above are observed. The diabatic state energies, defined as the energies of the subwavefunctions Ψ_A and Ψ_B in Ψ_{TOT}, are changing rapidly as they cross, but the resonance effect yields a relatively flat E_{TOT} curve. We must be careful in assigning too much physical meaning to the diabatic energies defined in this way, since, for example, a different pair of curves would result by using E_A and E_B from the excited state wavefunction. The behavior of E_A and E_B does appear reasonable, approaching the GVB(1/2) energy as the distance from the saddle point is increased. E_A is always above the GVB energy, since the GVB wavefunction contains some resonance (from "smearing out"), while the diabatic energy contains no resonance. This is also required by the variational principle, since Ψ_A and Ψ_{GVB} have the same form, but Ψ_{GVB} is optimized to minimize its own total energy, while Ψ_A is varied to minimize the energy of a wavefunction of which Ψ_A is only a piece. That the GVB wavefunction does not contain the full resonance is evident from the cusped shape of E(GVB) at the saddle point.

Another feature of the resonating VB model is the antiresonant excited state curve, which should have its minimum at the saddle point

(hence, in this excited state, HFH is a bound species), and approach the diabatic curves at more asymmetric geometries. We solved for this state at the symmetric saddle point geometry, and the agreement between the σ-GRVB energy and the σ-full CI is very good (136.3 and 133.3, respectively). Using the resonant state GRVB orbitals to compute the energy of this antiresonant state leads to an energy of 223.8 kcal, indicating the importance of allowing the orbitals to readjust in the presence of the antiresonant interaction.

F. The Bent Transition State

In their study of the HF + H reaction, Wadt and Winter[4] considered bent transition state geometries and found the following interesting results:

1) At the POL(2) CI level (in their large basis set), the lowest collinear barrier height is 47.6 kcal (R_{HF} = 1.17 Å), while the global saddle point is at 106° (R_{HF} = 1.08Å) with a barrier of 47.2 kcal. Thus, the potential surface is very flat, with less than 1 kcal separating linear HFH from HFH bent 106°.

2) Adding diffuse fluorine functions to the basis set was found to have a small effect for collinear geometries (lowering the barrier from 48.7 kcal to 47.6 kcal), but had a very dramatic effect for bent geometries, lowering the barrier from 59.6 kcal to 47.2 kcal.

3) In either basis set, first optimizing the collinear transition state and then bending with a fixed HF distance predicts a collinear transition state. This is because the HF bond shortens as the angle decreases from 180°. Wadt and Winter interpreted these results as indicating that at bent geometries there is a contribution from the F(2*p* --> 3*s*)

Rydberg state, which can make two HF bonds, as shown here,

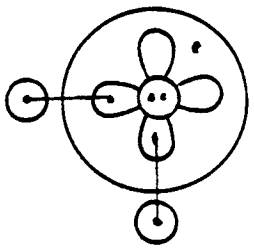

The energy of such a state can be estimated by subtracting an HF bond energy (6.1 eV) from the 2*p* --> 3*s* excitation energy in fluorine atom (12.8 eV[20]) to yield 6.7 eV, which is ~4.6 eV above the transition state energy. To invoke a similar state at the collinear geometry requires a 2*s* --> 3*s* Rydberg excitation, so that two *sp* hybrid lobe H-F bonds are formed,

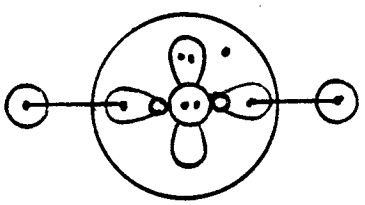

Ignoring the difference in bond strength between a p bond and a lobe bond, this state is expected to be ~20.5 eV higher than for the bent case (the energy of a 2*s* --> 2*p* excitation in F^{+}[20]), so that even if such a state is important for the bent geometry, it should make an insignificant contribution to the collinear energy. It is interesting to notice that the saddle point geometry has a bond angle very similar to H_2O, which is isoelectronic with H_2F^{+}, and the H-F bond lengths are shorter at the bent T.S. geometry than at the linear geometry, indicating more bonding character. Thus the Rydberg-like transition

state is a reasonable hypothesis.

We were interested in what a GRVB treatment would yield. Using the bent geometry optimized at the POL(2)CI level by Wadt and Winter, we performed two σ-GRVB(1/2) calculations,* one using our basis set and the other using the large basis of Wadt and Winter (WW). The results of these calculations are in Table 6. The σ-GRVB(1/2) barrier using the large WW basis is in excellent agreement with both the POL(2)CI and the POL(3)CI. Thus, whatever the character of the bent transition state is, the resonance of two mirror image wavefunctions contains the essential features. In addition, it is seen that our basis, which differs from the small WW basis only by having triple zeta hydrogens instead of double zeta, yields a σ-GRVB(1/2) barrier nearly as low as the large WW basis. From this we conclude that most of the energy lowering obtained with fluorine Rydberg functions can be recovered by using instead a more flexible hydrogen basis. Is the transition state Rydberg-like? The orbitals from one GRVB subwavefunction are plotted in Figure 7. As at the collinear geometry (Figure 4), the orbitals look very much like an HF molecule with a hydrogen nearby that must stay orthogonal, though in this case the dominant repulsive interaction is with a fluorine $2p$ orbital rather than a $2s$. The hydrogen open-shell orbital is clearly more diffuse than for the collinear case, and has built in more character on the fluorine. It appears that the open-shell orbital is a mixture of a hydrogen $1s$ and a fluorine Rydberg sp hybrid pointing towards the hydrogen. Thus we agree with the assessment of WW that the bent transition state contains some Rydberg character, and are encouraged to find that not only does GRVB describe the

* The sigma space at the bent geometry includes a $2p$ orbital that is of π symmetry at the linear geometry.

state adequately, it even helps us confirm the presence of Rydberg character.

At this point it is reasonable to ask whether we are being fooled by this simple model; perhaps the bent transition state is almost completely Rydberg in character. If it is, we might still conclude that the dominant feature is the resonance of two non-Rydberg structures with only one H-F bond, because that is the nature of the wavefunction we optimized. We can counter such an argument in three ways:

1) While the bond lengths in the bent transition state are shorter than at the linear saddle point (1.08 Å versus 1.17 Å), they are still considerably longer than in H_2F^+ (0.95 Å)[21] or H_2O (0.959 Å).[22]

2) The GVB(3/6) wavefunction, which would be expected to emphasize the Rydberg character (since it has two bond pairs correlated identically), predicts bond lengths 0.05 Å shorter than the POL(2)CI, which (we hope) contains the correct amount of Rydberg character. Furthermore, the drop in barrier height upon adding Rydberg functions is 18.4 kcal for the GVB(3/6) wavefunction, but only 12.4 kcal for the POL(2)CI (though these are at different geometries).

3) We have solved for a GVB(2/4) wavefunction with equivalently correlated bond pairs and a delocalized open shell, as in the Rydberg model, but this wavefunction is unstable by 0.9 kcal[23] with respect to an asymmetric GVB(2/4) wavefunction that has one H-F bond correlated with the open shell fairly localized on the other hydrogen, and the second GVB pair describing an in-out correlation of the other $p\ \sigma$ orbital.

While the transition state is not predominantly Rydberg-like, there does seem to be significant Rydberg character. Also, the POL(2)

surface WW published[4] shows a significant softening of the bond distance force constant in the region around 105°-115°, indicating the true Rydberg species, with short bond lengths, may not be too much higher in energy (though it is not a local minimum). This seems inconsistent with the estimate that the Rydberg species is 4.6 eV (106 kcal) above the saddle point. We can obtain a more accurate estimate in the following way. The energy of the HFH 3s Rydberg electron should be comparable to that of the 3s electron in the lowest Rydberg state of H_2O. The stabilization due to the partially deshielded protons is important,[24] and was missing from the earlier estimate. We use the average ionization potential (IP) of the $^1B_1$ (3s) and $^3B_1$ (3s) Rydberg states of H_2O,[25] and combine this with the proton affinity of HF (111 kcal at 0°K)[26] and the IP of hydrogen as shown diagrammatically in Figure 8. The H_2F Rydberg species is estmated to be 72 kcal above H + HF, or 25 kcal above the calculated saddle point energy, and it is thus reasonable that such a structure could mix into the transition state wavefunction. If the POL(2)CI without diffuse fluorine functions can be taken as an estimate of the saddle point energy in the absence of Rydberg character, then the Rydberg species is seen to be only 12.4 kcal (72 - 59.6) above the saddle point before mixing.

Finally, we note that one could solve for a GRVB wavefunction that allowed the resonance of three bonding structures, the two valence states, and the Rydberg state,

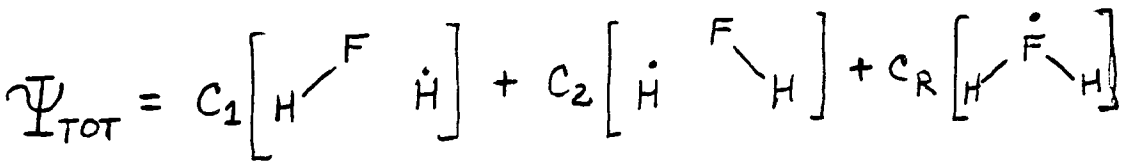

We would expect the two valence states to exhibit tighter open-shell orbitals than in the two-state GRVB wavefunction, since the Rydberg state is now explicitly included in a separate subwavefunction. Similarly, the Rydberg state would be expected to be more diffuse than in the two-state GRVB, and would be smeared symmetrically over the molecule. The coefficients C_1, C_2, and C_R would be expected to change dramatically as the bond length is varied, since the short-R wavefunction should be almost purely Rydberg, and the long-R wavefunction is dominated by the resonating valence states. One must be careful, however, in using such a wavefunction to calculate the activation barrier, since the transition state may be over-described compared with the H + HF limit. In designing GRVB wavefunctions, it is important to maintain a balanced, consistent description. If the two-state GRVB wavefunction can adequately describe the Rydberg character, the three-state GRVB wavefunction might use the extra degrees of freedom to include some additional correlation that is extraneous to the process of interest.

III. The HCl + H Exchange Reaction

A. Introduction

The H + HCl abstraction reaction,

$$H + HCl \longrightarrow H_2 + Cl, \qquad (7a)$$

and exchange reaction,

$$H + ClD \longrightarrow HCl + D, \qquad (7b)$$

have long been of interest due to their role in the hydrogen-chlorine chain reaction, the HCl chemical laser, and the photochemistry of the stratosphere, and have been the subject of numerous experimental studies.[27-40] For a long time there has been a controversy over the height of the barrier in the exchange reaction[27,28] (7b). Some experiments[37-39] imply that it is lower than the barrier to abstraction (3.1 kcal[30-32]), while others are consistent with a higher barrier[28,32,33,40] ranging from 8 kcal to over 20 kcal. Recent experiments by Miller and Gordon,[28,32] which measured the forward rate of the abstraction reaction, placed a lower bound of 7.2 kcal on the exchange barrier, and indicated that previous photochemical determinations were plagued by surface effects.

The use of semi-empirical potential surfaces has added to the confusion, since applying the LEPS surface on the abstraction reaction to the exchange reaction predicts a very low activation barrier including a well in the transition state region.[27] Ab initio calculations[41-44] have consistently predicted barriers between 20 and 25 kcal, though Botschwina and Meyer[43] estimate that accounting for the effects of missing correlation and a truncated basis could lead to a barrier of 10-15 kcal (they

actually calculate 22.1 kcal).

We present here a comparison of the accuracy of various ab initio wavefunctions in describing the barrier height for the exchange reaction (7a). We observe the same trends as in the analogous HF + H exchange reaction. The GRVB(1/2) wavefunction is in excellent agreement with the basis set limit, while all other single-particle wavefunctions lead to barriers 15-20 kcal high. The GRVB result (25.1 kcal) is also in good agreement with the best previous calculations, and we find no evidence in this basis set for a barrier below 20 kcal, assuming a collinear transition state.

B. Calculational Details

Our calculations employed a contracted gaussian basis set of valence double zeta plus polarization quality, as listed in Table 7. The chlorine basis was contracted to 4s,3p from Huzinaga's 12s,8p basis,[9] reoptimizing the exponents of three gaussians which were used twice in the contraction. The hydrogen basis was the standard Dunning double zeta contraction[10] of the Huzinaga four-gaussian basis,[9] scaled by 1.2 and augmented with a set of p functions (α = 1.0). Some of the calculations were repeated using the same valence basis but with the $1s$,$2s$, and $2p$ core functions replaced by an effective potential.[45] This was found to have an effect of less than 1 kcal on the calculated barrier height in all cases tested. All HClH calculations were performed at the collinear saddle point geometry optimized by Botschwina and Meyer[43] ($R_1 = R_2 = 1.502$), while the experimental geometry was used for HCl (R = 1.27455[13]). The programs used in optimizing the wavefunctions are described in the HF + H section. The σ-GRVB(1/2) and σ-full CI wavefunctions employed a frozen $1s$, $2s$, $2p$, and $3p$ π space, and the GRVB(1/2) used a frozen $1s$, $2s$,

and $2p$ space, taken from the Hartree-Fock wavefunction in each case. All orbital contour plots are in a plane containing the molecule, with the same scale and conventions as for the HFH plots.

C. Results and Discussion

Table 8 lists the results of various calculations on the barrier height. The highest level of calculation we performed is the σ-full CI, and the barrier of 25.5 kcal is seen to agree well with the results of other workers. The Hartree-Fock, GVB, and R-GVB wavefunctions give barriers 18 to 25 kcal higher than this, and orbital plots from these wavefunctions are shown in Figures 9 to 11. Just as for HF + H, the Hartree-Fock wavefunction is totally delocalized, and the GVB wavefunction shows only slight localization of the bonding pair, and hence has very high overlap with its reflection. All these effects are discussed in depth in the HF + H section. The GRVB(1/2) wavefunction yields a much more reasonable barrier (25.1 kcal), and the σ-GRVB(1/2) wavefunction, optimized in the same space as the σ-full CI gives a barrier of 25.3 kcal. Thus, as with HFH, the σ-GRVB(1/2) wavefunction gives a barrier within 1 kcal of the sigma basis set limit. We could not test the GRVB wavefunction against the full basis limit since a full CI is unfeasible. Relaxing the π space is seen to have a negligible effect on both the orbital shapes (Figure 11) and the total energy ($< \frac{1}{2}$ kcal), though these effects might increase slightly if the π polarization basis were made more flexible.

Examination of the orbital plots for one GRVB subwavefunction (Figure 10) shows that as for collinear HFH, the saddle point in this reaction is very aptly described as the resonance of two mirror image bonding structures, each of which looks like a stretched HCl molecule with an H atom nearby, which must stay orthogonal. However, Pauli-induced

orthogonalization is seen to be much less severe for HClH than for HFH, causing a much smaller perturbation of the hydrogen 1*s* orbital. This is probably because in chlorine the effective size of the 3p orbital is significantly larger than the 3*s* orbital, while in fluorine the 2*s* and 2*p* are comparable in size. (This results from the fact that the 2*s*, 3*d*, and 2*p* orbitals must stay orthogonal to filled orbitals of the same symmetry with lower principal quantum number, while the 2*p* does not.) Thus, as a hydrogen atom aproaches close enough to make a strong bond with the p orbital, it "bumps into" an s orbital much more severely for fluorine than chlorine. In HFH this effect is large enough that the H atom can approach the side of the HF molecule, bumping into a 2*p* orbital, with roughly the same barrier as the collinear case (with some help from the 3*s* Rydberg state). We did not test bent geometries for HClH, but we predict that they would be higher in energy than the collinear saddle point, both because of the reduced repulsion for the linear approach in HClH, and because the 2*p* --> 3*s* Rydberg state, which helped stabilize the bent transition state in HFH, is predicted to be at 64 kcal for HClH,* 39 kcal above the observed saddle point. This estimate was calculated in the same manner as for HFH (see Figure 8), using the proton affinity of HCL (139 kcal[46]), and the IP of the lowest Rydberg state of H_2S (110 kcal[47]).

The full valence and SOGI levels were not tested for HClH, but we expect they would lead to barriers at least 9 kcal too high, as for HFH.

* This is a lower bound; the actual value may be higher if the lowest Rydberg state at H_2S is not the 3*s* state. See reference 47.

IV. The H + HF Abstraction Reaction

A. Introduction

The H + HF abstraction reaction

$$H + HF \longrightarrow H_2 + F \qquad (8a)$$

has been well characterized experimentally[48,49] and studied theoretically.[7,8] The exothermic reverse reaction,

$$H_2 + F \longrightarrow H + HF \qquad (8b)$$

has the same features, of course, and we will use this form in our discussions. The H_2 + F reaction is characterized by a large exothermicity of 31.2 kcal[49] and a very low activation energy of 1.7 kcal,[48] as shown in Figure 12. The experimental activation energy is not identical to the barrier height on the adiabatic surface,[50] but is probably within 1 kcal (Muckerman estimates that the true barrier height is about 1 kcal[51]); we will not worry about this distinction. Ab initio potential surfaces that have been computed for this reaction indicate a collinear transition state. As is typical of computer reaction surfaces, the reactant and product fragments are better described than the transition state, so that insufficient electron correlation leads to barriers that are too high, and increasing the level of the calculation gives barriers that approach the true barrier from above. The best calculations to date on H_2 + F give a barrier in excellent agreement with experiment, and in accord with the Hammond Postulate,[52] the saddle point is found to be very reactant-like, with an H_2 bond stretched only 0.095 Å from equilibrium, and an H-F distance 0.26 Å longer than equilibrium HF. Thus the H_2 + F reaction is an example of the asymmetric reaction shown in Figure 2, with a saddle point that does not

occur at the crossing of the diabatic states, and makes a suitable test case for the ability of the GRVB method to describe reactions of this type. In the following we present results of preliminary calculations at a fixed transition state geometry. At this geometry, the σ-full CI predicts a barrier of 11.0 kcal, which is 9 kcal above experiment. As with the HF + H and HCl + H exchange reactions, we are more concerned with how well the GRVB method compares with the fully correlated limit of the basis than with experiment, and we find excellent agreement--the σ-GRVB(1/2) barrier is 10.7 kcal.

B. Calculational Details

The basis set is exactly as described for the HF and H exchange reaction (Section II-B), being valence double zeta plus polarization on the fluorine and triple zeta plus polarization on the hydrogen. The geometry used was that optimized by Dunning[8] at the GVB+SDCI level (R_{HH} = 0.790Å, R_{HF} = 1.413Å, Θ_{HHF} = 180°), with a double zeta plus polarization basis comparable in flexibility to ours. The σ-full CI and σ-GRVB(1/2) wavefunctions employed a frozen π space from the GVB(1/2) wavefunction. The barrier height (E_{a1}) for each level of wavefunction was calculated with respect to the minimum energy geometry of H_2 for that wavefunction. The optimum H_2 geometries are 0.734Å, 0.756Å, 0.741Å, 0.750Å, and 0.741Å, for Hartree-Fock, GVB(1/2), GVB(1/5), full σ CI, and full CI, respectively. If the experimental H_2 geometry (0.741Å)[13] is used, the change in the calculated bond dissociation energies (and in the barrier heights) is less than 0.1 kcal in each case. The experimental geometry (0.9176Å)[13] was used for HF. All contour plots use the same

scale and conventions as the HFH and HClH plots.

C. Results and Discussion

The results of various levels of calculation are listed in Table 9, and as anticipated, this system exhibits a number of features not present in symmetric exchange reactions. As in the exchange reactions, the Hartree-Fock and GVB(1/2) wavefunctions predict barriers (E_{a_1}) which are higher by 6.7 kcal and 8.8 kcal, respectively, than the σ-full CI barrier of 11.0 kcal. The discrepancy is not as large as for HFH, in which the GVB barrier was ~20 kcal too high, and this can be understood by examining Figure 2. While resonance is important in the saddle point region, the saddle point does not occur at the crossing of the diabatic states, where the resonance is largest, but is instead shifted toward reactants (H_2+F). This is borne out by the shapes of the GVB orbitals, shown in Figure 13, which are clearly describing a reactant-like state with a bond between the hydrogens. The fluorine 2p orbital, which must stay orthogonal to the H_2 bond pair, is seen to be only slightly perturbed, because the H-F distance is so large at this "early" transition state.

The R-GVB approach cannot be used on this system, because the GVB(1/2) wavefunction with a bond between the hydrogen and fluorine is unstable, collapsing to the H-H bonded form. Thus, to include resonance, we must use a GRVB wavefunction. In the GRVB wavefunction, one GVB(1/2) subwavefunction (Ψ_A) looks very much like the GVB(1/2) wavefunction described above (with an H-H bond), while the other subwavefunction (Ψ_B) describes the H-F bonded form. It does not collapse to the H-H form because that character is already explicitly included in Ψ_A. Instead, Ψ_B contributes to the total energy of Ψ_{TOT} through the reso-

nance energy, even though the diagonal energy (E_B) is many kcal above E_a. If the geometry is such that this E_B is too far above E_A, so that the resonance energy is very small, then Ψ_B might readjust to some different form which can contribute more to the total energy. This effect was observed for some asymmetric geometries in the HF+H exchange reaction, as discussed in Section II-E, but does not appear to be a problem here. The orbitals from the σ-GRVB(1/2) wavefunction are plotted in Figure 14. The Ψ_A orbitals look almost exactly like the GVB(1/2) orbitals, while the Ψ_B orbitals look like an H atom next to an HF molecule. (A peculiar feature of Ψ_B is that the open shell orbital is nodeless, while the doubly-occupied orbitals build in nodes to maintain orthogonality. This is contrary to the behavior of usual SCF wavefunctions, since the total energy is raised less when a singly occupied orbital incorporates a node than when a doubly occupied orbital does. This same phenomenon occurs in the GRVB wavefunction for the three-electron bond in He_2^+ and Ne_2^+). The resonance lowering compared to the GVB(1/2) energy is 9.1 kcal, leading to a GRVB(1/2) barrier height of 10.7 kcal. If the Ψ_A subwavefunction is constrained to be exactly the GVB(1/2) wavefunction, the σ-GRVB(1/2) energy is raised by only 0.8 kcal, and the resulting Ψ_B orbitals are virtually indistinguishable from the Ψ_B orbitals in the unconstrained σ-GRVB wavefunction. As in HF+H and HCl+H, a full CI wavefunction is unfeasible, so the best comparison we can make is between the σ-GRVB barrier and the σ-full CI barrier, since the σ-full CI represents the basis set limit for the space in which the σ-GRVB wavefunction was optimized. The agreement between σ-GRVB and σ-full CI is excellent for the forward direction barrier height (E_{a1}).

If we compare the σ-GRVB barrier height to the experimental activa-

tion barrier, we find that it is 8.3 kcal too high for the forward direction, but 6.3 kcal too *low* for the reverse direction (E_{a2}). This is because the GVB(1/2) wavefunction which is used to describe the reaction limits gives a better description of the H_2 bond than the HF bond, resulting in a heat of reaction different from experiment. Thus, another issue peculiar to asymmetric reactions emerges: can an accurate barrier height be obtained from a wavefunction which does not predict the correct ΔH, and if so, which activation barrier is the "correct" one - E_{a1} or E_{a2}? This question is not important if a large enough CI wavefunction is used, since presumably the CI will describe both E_a and ΔH accurately. However, wavefunctions which retain a conceptually simple form, such as GVB, will often lead to errors in the computed ΔH. Moreover, for most systems, the CI large enough to obtain an accurate ΔH is beyond current computational feasiblity. This can be seen from the ΔH values tabulated in Table 9. Even in this fairly small HHF system, the large CI wavefunction used by Bender *et al* gives a ΔH 3.6 kcal too large in magnitude, an error twice the size of the computed barrier height. Thus, the above question is important for assessing the accuracy of both the state-of-the-art CI calculations, and the GRVB method. In the following paragraph, we explore this question using a very simple model, and conclude that the error in the calculated barrier height should be less than half the error in ΔH, and for very early transition states (such as in H_2 and F), the error could be even smaller yet. We also show that the barrier is more reliable when calculated from the higher-energy side.

Take the energies of the diabatic states along the reaction coordinate to be simple parabolas, whose minima are displaced relative to each other by x_0 along the abcissa, and ΔH along the ordinate, as is sketched in

Figure 15. In this model, the barrier to reaction will be taken as the crossing point of the two parabolas, so that we are ignoring resonance effects. As a further simplification, we will take the force constant, k, of each diabatic state to be equal, and the states are thus represented by

$$E_A = \frac{k}{2}x^2 , \tag{9}$$

and

$$E_B = \frac{k}{2}(x - x_0)^2 + \Delta H. \tag{10}$$

Solving for $E_A = E_B$ yields the forward barrier height,

$$E_a = \frac{\alpha}{8} + \frac{\Delta H}{2} + \frac{(\Delta H)^2}{2\alpha} \tag{11}$$

where we have defined the parameter α as

$$\alpha = kx_0^2 \quad (\textit{energy units}). \tag{12}$$

We now make the assumption that an error in ΔH simply raises one parabola with respect to the other, without affecting either the force constant or x_0. Calling this error λ, we can compute the resulting change in E_a from (11) as

$$\Delta E_a = E_a(\Delta H + \lambda) - E_a(\Delta H) \tag{13a}$$

$$= \frac{\lambda}{2} + \frac{1}{2\alpha}(2\lambda\Delta H + \lambda^2). \tag{13b}$$

Using (11) we can re-express α as

$$\alpha = 4E_a - 2\Delta H + 4\sqrt{E_a^2 - E_a\Delta H} \tag{14}$$

so that by picking values for E_a and ΔH, we can compute the dependence of ΔE_a on λ. In Table 10, we have tabulated the values of ΔE_a for various choices of ΔH, E_a, and λ. It can be seen that ΔE_a is less than $\frac{\lambda}{2}$ in all cases,

and is significantly less than $\frac{\lambda}{2}$ for cases with very early transition states (low E_a, large, negative ΔH). This can be understood by examining the diagram in Figure 15b; when the E_B parabola is shifted vertically, the very steep slope of E_B compared to E_A causes only a slight change in E_a. It is also clear from this analysis that evaluating E_a from the high energy side (E_{a1}) yields a more accurate barrier than using the low energy side (E_{a2}), since E_{a2} picks up most of the error in ΔH. This model is admittedly crude, and pushing it too far would be a mistake, but we make one further point regarding the early transition state case. The parabolic assumption is probably valid for the reactant state E_A, which is near its minimum, but the product curve, E_B, is far from its minimum in the crossing region. In terms of the H_2+F reaction, this means the H-F distance is highly stretched at the saddle point. In this region, two effects contribute to the slope of E_B being non-parabolic. One is the anharmonicity of the H-F stretching mode, which acts to decrease the slope from parabolic. The other effect is a large Pauli repulsion between the two hydrogens, because the H-H distance is roughly that of an H_2 bond, and is highly unfavorable for a hydrogen staying orthogonal to an HF molecule. This acts to increase the slope of E_B, and the magnitude of this effect should increase rapidly as the transition state is made "earlier," due to the exponential nature of Pauli repulsions. (This will be mitigated by the fact that the reaction coordinate at the saddle point is dominated by H-F stretch for an early transition state, while the Pauli repulsion only acts on the H-H stretch component). If this latter effect dominates, the dependence of ΔE_a on λ will be even further reduced.

Thus it is possible that the GRVB(1/2) wavefunction could yield an accurate barrier height for the H_2+F reaction, and other reactions of this

type. The excellent agreement with the full σ-full CI at this one geometry is encouraging, but a two dimensional (R_{HF}, R_{HH}) search to find the true saddle point must be performed before the barrier height can be predicted for either the σ-full CI or GRVB wavefunction. In the symmetric exchange case, in which only one dimension (e.g. the symmetric H-F-H stretch) needs to be searched for the saddle point, a barrier calculated at any symmetric geometry gives an upper bound to the barrier obtained using the true saddle point geometry. In contrast, for an asymmetric reaction the error caused by an incorrect transition state geometry may be either positive or negative, since one coordinate, the reaction coordinate, has negative curvature, and the other has positive curvature. Thus, we cannot say whether the true σ-GRVB(1/2) barrier is above or below the 10.7 kcal calculated here. We do, however, expect that inclusion of the π space in the GRVB calculation should have a larger effect than in the HF+H symmetric exchange reaction (<1 kcal). This is because the fluorine π orbitals need a more diffuse radial form to describe the H H-F diabatic state than the H-H F diabatic state, due to the partial ionic character in the H-F bond. In the σ-GRVB(1/2) wavefunction, the π orbitals were taken from the GVB(1/2) wavefunction, thus destabilizing the H H-F species. In spite of our arguments in the last paragraph, the final GRVB(1/2) barrier may still be too high, simply because of the large discrepancy in the calculated ΔH. If this is the case, the GRVB description of the saddle point could be improved by resonating two wavefunctions which dissociate to limits with a more accurate ΔH. The error in ΔH at the GVB(1/2) level arises because the GVB(1/2) wavefunction gives a bond energy within 14.5 kcal of experiment for H_2 but is 30.2 kcal off for HF. The extra correlation error in HF is largely due to the need for both ionic

and covalent components,

$$\Psi_{HF} = C_{cov}(H{-}F) + C_{ionic}(H^{+}F^{-}), \qquad (15)$$

and while the GVB(1/2) wavefunction can incorporate partial ionic character in the bond, the shapes of the rest of the orbitals ($2p_x$, $2p_y$, 2s) are a compromise between the optimum F^- shapes and the optimum F shapes. Thus, a GRVB wavefunction of the form in (15) might lower the energy of HF to give better agreement with H_2, and hence a more reasonable ΔH. The corresponding GRVB description of the transition state would then contain three subwavefunctions, the GVB(1/2) wavefunction with an HH bond, the GVB(1/2) wavefunction with an HF covalent bond, and the Hartree-Fock wavefunction with an ionic HF bond.

V. Forbidden Reactions

A. Introduction

The HF+D, H+HF, HCl+D and H_2+D reactions presented above are classed as "allowed" reactions by the Woodward-Hoffmann rules(WHR)[53] or the Orbital Phase Continuity Principle(OPCP).[54] The resonating VB model can also be applied to "forbidden" reactions, and some important differences arise in the implementation of R-GVB and GRVB. In this section we demonstrate the resonating VB model for forbidden reactions using the $H_2 + D_2 \rightarrow 2HD$ reaction as an example. We begin with a brief review of the definition of a forbidden reaction.

B. Definition of a Forbidden Reaction

A forbidden reaction is defined by WHR or OPCP as one in which the orbitals and spin coupling of the reactant wavefunction cannot be converted smoothly into the orbitals and spin coupling of the product wavefunction.

WHR theory is a molecular orbital(MO) approach, in which a correlation diagram is constructed which maps each reactant MO onto a particular product MO based on the symmetries of the MOs. If an occupied MO in the reactants correlates with an unoccupied MO in the products, the reaction is forbidden, because the ground state of the reactants becomes an excited state of the products. This is shown in Figure 16 for the rectangular-square-reactangular reaction coordinate of the $H_2 + D_2 \rightarrow 2HD$ reaction. The barrier to reaction corresponds to the crossing of the $\varphi_1^2\varphi_2^2$ and $\varphi_1^2\varphi_3^2$ states.

In the OPCP method of analysis, a forbidden reaction is one in which the reactant VB structure cannot be converted to the product VB struc-

ture without breaking a bond, as shown in Figure 17. The barrier thus corresponds to the energy required to break this bond. OPCP predicts exactly the same classes of reactions to be forbidden as WHR, and the analysis does not require that symmetry be preserved throughout the reaction. Thus, the $H_2 + D_2$ reaction is predicted to have a high barrier for any approach geometry. Indeed, theoretical studies of tetrahedral, T-shaped, linear, rhombohedral, square and trapezoidal transition states for $H_2 + D_2$ have failed to find a barrier lower than the energy of H_2 and two H atoms.[55]

C. Consequences for Resonating VB theory

While a forbidden reaction is topologically different than an allowed reaction, the resonating VB model applies in the same way. The total wavefunction is expressed as a continuously varying linear combination of reactant wavefunction (Ψ_A) and product wavefunction (Ψ_B), with a resonance mixing that is strongest where E_A and E_B cross, though this crossing will occur at a much higher energy than in an allowed reaction. In applying R-GVB and GRVB to describe these reactions, an important difference arises, due to the following principle.

The same topological features of a forbidden reaction which prevent the smooth interconversion of reactant and products also prevent Ψ_A *from delocalizing to include some character of* Ψ_B *at the SCF level.* Thus the "smearing out" (to include resonance) observed in the GVB wavefunction for the HF+H and HCl+H transition states does not occur for a forbidden reaction. The ramification of this is that the GVB wavefunction will be almost as localized as the GRVB wavefunction, so that R-GVB can be used to obtain results nearly as accurate as the more expensive GRVB. We have demonstrated this property on the π space of cyclobutadiene (see

Chapter 4), which is topologically equivalent to a forbidden reaction. The GRVB energy was found to be only one kcal below R-GVB.

D. $H_2 + D_2$ **- Calculational Details**

Calculations on $H_2 + D_2$ employed a triple zeta plus polarization contracted gaussian basis. The three s functions were the same as described for the HF+H calculations, but the p exponent was different (α=1.0). The purpose of the calculations was to demonstrate the resonating VB model along a reaction coordinate, and a rectangle-square-rectangle pathway was chosen for simplicity. Transition states other than square have been shown to give a lower energy,[55] though none are lower than E(H_2+2H). The reaction coordinate was defined by first optimizing the square geometry at the R-GVB(2/4) level, leading to R_{HH}=1.28Å, and then considering rectangular distortions which maintained a constant perimeter. This definition for the reaction coordinate coincides with the exact rectangle-square-rectangle reaction coordinate at the square saddle point, and is a good approximation at nearby geometries. Making this assumption alleviated the need for a two - dimensional search of the rectangular energy hypersurface to find the true reaction coordinate. The R-GVB(2/4) wavefunction was defined as the resonance mixing of the "good" structure,

Ψ_A = (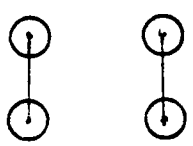) = $A[(ab+ba)(cd+dc)\alpha\beta\alpha\beta]$ (16a)

and the "bad" structure,

Ψ_B = (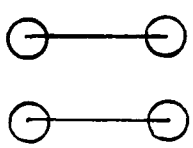) = $A[(a'b'+b'a')(c'd'+d'c')\alpha\beta\alpha\beta]$ (16b)

optimized in separate GVB(2/4) calculations. The "bad" structure does not have the same orbital shapes as the good structure, distinguishing these calculations from the SOGI calculations of Wilson and Goddard.[56] All R-GVB calculations are referenced to twice the energy of a GVB(1/2) calculation on H_2 at its experimental geometry 0.741 Å.[13] At geometries too far from the saddle point, trapping the GVB(2/4) wavefunction for Ψ_B became difficult, as it had a tendency to collapse to Ψ_A. We were able to trap Ψ_B for energies as much as 133 kcal above Ψ_A, where the resonance energy was less than 2 kcal. A reaction coordinate without the symmetry afforded by the rectangle would make this trapping more difficult. If we had optimized a GRVB wavefunction, Ψ_B would have been more stable with respect to collapse.

The effect of relaxing the GVB coefficients in the presence of resonance (i.e. GVB(2/4)(pr)) was 1.1 kcal at the square geometry, and 0.4 kcal at $\Delta R=0.16$ (see Figure 18 for the definition of ΔR).

E. $H_2 + D_2$ - Results and Discussion

Figure 18 shows the diabatic energy curves (GVB(2/4)) and the resulting resonant and antiresonant states (R-GVB(2/4)) for the rectangle-square-rectangle reaction pathway. Because we are using an R-GVB wavefunction, the same diabatic curves are appropriate for both the resonant and antiresonant states. As predicted above, the diabatic curves show no signs of delocalization resonance, crossing sharply at the square geometry, in contrast to the behavior of the GVB wavefunction in the HF+H exchange reaction (see Figure 6). As expected, the resonance lowering rapidly increases as the saddle point is approached, leading to a smoothing of the cusp present in the diabatic state crossing. The resonance lowering at the saddle point is 23.1 kcal, and drops to less than 2 kcal at $\Delta R=0.16$. The antiresonant state is raised by 36.5 kcal at the saddle point, and is still 16.6 kcal above the bad diabatic state at $\Delta R=0.16$.

The 143.0 kcal barrier calculated using R-GVB is in very good agreement with the σ-full CI value of 141.6 kcal and the 1.4 kcal error is comparable to the lowering expected if the orbitals were reoptimized using GRVB.[57] The antiresonant state is predicted by R-GVB to be at 202.5 kcal, compared to the σ-full CI value of 191.9 kcal. This discrepancy may be due to ionic character not included in the R-GVB wavefunction.[58] At $\Delta R=0.08$, the agreement is similar, R-GVB obtaining 128.4 kcal and 219.7 kcal, while the σ-full CI yields 126.0 kcal and 209.4 kcal. Figure 19 shows the behavior of C_A, C_B and S_{AB} along the reaction coordinate. C_A and C_B act as expected, with Ψ_{TOT} becoming almost purely diabatic by $\Delta R=0.16$Å. S_{AB} is seen to be almost constant for this portion of the reaction coordinate (-0.225 - -0.226).

It is interesting that the maximum resonance energy (23.1 kcal) is

almost identical to the isomorphic cyclobutadiene π system (22-23 kcal). Though the resonance energy is harder to define for the case of an allowed reaction, we did observe a similarity between the resonance lowering in the HFH and HClH systems. This strengthens the concept of a transferrable resonance energy.

Figure 20 shows the behavior of the energy quantities as the bond length of square H_4 is varied. While the GVB(2/4) wavefunction yields a minimum at R=1.31 Å, the R-GVB(2/4) minimum is at R=1.28Å. This is because the resonance energy is stronger at shorter R, it peaks and begins to decline at R shorter than 1.1Å. At infinite R, corresponding to four H atoms, E_{res} is zero, and S_{AB} is -0.5. This nonzero value for S_{AB} is easily obtained by expanding $\langle\Psi_A|\Psi_B\rangle$ with orthogonal orbitals. Since the atoms are infinitely separated, and cannot interact, the primed set of orbitals in equation 16b will be the same as the unprimed set. Thus,

$$\begin{aligned} S_{AB} &= \langle\Psi_A|\Psi_B\rangle \\ &= \frac{1}{4}\langle abcd(\alpha\beta-\beta\alpha)(\alpha\beta-\beta\alpha)|A[bcad(\alpha\beta-\beta\alpha)(\alpha\beta-\beta\alpha)]\rangle \end{aligned}$$

and only one term survives,

$$\begin{aligned} S_{AB} &= \frac{1}{4}\langle abcd|abcd\rangle\langle\alpha\beta\alpha\beta-\alpha\beta\beta\alpha-\beta\alpha\alpha\beta+\beta\alpha\beta\alpha|\alpha\alpha\beta\beta-\beta\alpha\beta\alpha-\alpha\beta\alpha\beta+\beta\beta\alpha\alpha\rangle \\ &= -0.5 \end{aligned}$$

However, though these wavefunctions overlap, the matrix element between them reduces to

$$H_{AB} = -\frac{1}{2}[\langle a|\hat{h}|a\rangle + \langle b|\hat{h}|b\rangle + \langle c|\hat{h}|c\rangle + \langle d|\hat{h}|d\rangle]$$

where $\hat{h}$ is the one-electron operator. The off diagonal one-electron terms (e.g. $\langle a|\hat{h}|b\rangle$), and the two electron terms (e.g. $\langle ab|\frac{1}{r_{12}}|ab\rangle$) all vanish

due to the infinite separation of the orbitals. The same terms vanish in the energy, H_{AA}, leaving the simple relation

$$H_{AB} = S_{AB}H_{AA},$$

and thus the resonance energy is zero, because the only interaction between the two wavefunctions arises from the pieces they have in common. At smaller R, S_{AB} decreases in magnitude, a result of the nodes which are built into the orbitals. At the smallest value of R we examined (R=0.9) S_{AB} was still decreasing (see Table 11). Thus, it is erroneous to think of an increase in interaction between two wavefunctions as necessarily causing an increase in the wavefunction overlap.

F. Conclusions

The resonating VB model applies well to forbidden reactions, and in fact results in a simplification in the implementation of R-GVB and GRVB. Because the reactant and product wavefunctions cannot delocalize into each other, the diabatic states are well defined and the less expensive R-GVB is sufficient to obtain GRVB-quality results. The concept of a "resonance energy" is also more well defined, and is ~23 kcal for the case of square H_4 at its equilibrium geometry.

It is interesting to note that both WHR and OPCP ignore the effect of resonance on the reaction barrier. The goal of WHR and OPCP is to predict whether a reaction will proceed at a reasonable rate (under reasonable conditions) in a concerted fashion, which classifies it as "allowed", or whether a concerted process is no better than a stepwise process with bond cleavage, in which case the reaction is "forbidden". Clearly, the rectangular H_2+D_2 reaction is "forbidden", whether or not the 23 kcal of resonance energy is included, since the barrier is still 35 kcal

greater than an H-H bond energy. However, it is possible that in some reaction, the inclusion of resonance could actually convert a "forbidden" reaction into an "allowed" reaction. We know of no such case, but in the WHR formalism, this anomaly could occur if the resonance energy were comparable in magnitude to the energy required to reach the crossing of the $\varphi_1^2\varphi_2^2$ and $\varphi_1^2\varphi_3^2$ states. In OPCP, the requisite condition would be that the resonance energy be comparable to the energy of a bond which is active in the reaction process.

VI. Conclusions

We have demonstrated that the GRVB wavefunction can yield accurate activation energies for symmetric exchange reactions, and the results look promising for asymetric reactions as well. Further, the orbitals from the GRVB subwavefunctions are strikingly similar to the orbitals of the corresponding reactant or product fragments, reinforcing the conceptual nature of the resonating VB model. The most general single particle wavefunction leads to an incorrect barrier height for the HF + H reaction, indicating the need for the "single-particle plus resonance" description provided by GRVB.

Because of the conceptual simplicity of the wavefunction, the effect of the Pauli-induced orthogonalization (which makes the HF + H barrier ~ 25 kcal higher than in HCl + H) could actually be seen in the orbital plots. The Rydberg character in the bent HFH species was also clearly visible.

The location of reaction transition states and the calculation of accurate barrier heights is a topic of current interest among ab initio theorists,[59] and the ramifications of the work presented here are three-fold. First, the GRVB approach appears to be as reliable as the currently used CI approaches for generating accurate transition state properties. The present GRVB program is very CPU intensive, because it optimizes the wavefunction numerically. If an analytical optimization procedure for GRVB were to be developed, GRVB would scale better than the CI approaches, and could become the method of choice for generating reaction potential surfaces. Proposition 4 demonstrates that an analytical optimization with first-order convergence can be programmed, representing a first step towards this goal.

Second, even if GRVB is never competitive with the state-of-the-art CI techniques, the principles which emerge from our GRVB study can be valuable in designing CI wavefunctions which will yield accurate results. For example, Feller, Schmidt and Ruedenberg[19] recently computed the barrier for the concerted exchange of hydrogen between ethane and ethylene,

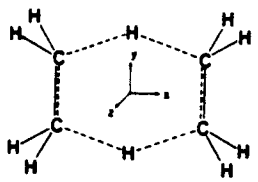

using the FORS approach. FORS (full optimized reaction space) is essentially a full-valence MCSCF wavefunction, which in this case would have a six-orbital active space, because six electrons are involved in the reaction process. They obtained a barrier height of 74.5 kcal using an SCF wavefunction and 69.3 kcal using FORS in the same double-zeta basis. We know from the HFH study that even a full CI in a space which has only one orbital per electron yields a barrier that is too high (> 5 kcal for HFH). Thus, the appropriate CI for ethane-ethylene exchange should contain twelve active orbitals, a doubled set. (This system is too large for GRVB presently, but an R-GVB study yielded 4.1 kcal of resonance lowering, with a very high overlap (S_{AB} = 0.9758), indicative of a potentially large GRVB lowering.)

Third, for forbidden reactions, the R-GVB approach may already be competitive with the state-of-the-art CI methods in both accuracy and computational speed, though forbidden reactions are usually less interesting chemically.

References

1) J.F. Bott and R.F. Heidner III, J. Chem. Phys. **68,** 1708 (1978)

2) J.F. Bott and R.F. Heidner III, J. Chem. Phys. **66,** 2878 (1977)

3) F.E. Bartoszek, D.M. Manos and J.C. Polanyi, J. Chem. Phys. **69,** 933 (1978)

4) W.R. Wadt and N.W. Winter, J. Chem. Phys. **67,** 3068 (1977)

5) C.F. Bender, B.J. Garrison and H.F. Schaeffer III, J. Chem. Phys. **62,** 1188 (1975)

6) P. Botschwina and W. Meyer, Chem. Phys. **20,** 43 (1977)

7) (a) C.F. Bender, P.K. Pearson, S.V. O'Neil and H.F. Schaeffer III, J. Chem. Phys. **56,** 4626 (1972)

(b) C.F. Bender, S.V. O'Neil, P.K. Pearson and H.F. Schaeffer III, Science **176,** 1412 (1972)

8) T.H. Dunning, private communication

9) S. Huzinaga, J. Chem. Phys. **42,** 1293 (1965)

10) T.H. Dunning, Jr. and P.J. Hay, in: *Modern Theoretical Chemistry, Vol. 3, Methods of Electronic Structure Theory*, edited by H.F. Schaeffer III (Plenum, New York 1977), Chap. 1

11) F.W. Bobrowicz and W.A. Goddard III, in: *Modern Theoretical Chemistry, Vol. 3, Methods of Electronic Structure Theory*, edited by H.F. Schaeffer III (Plenum, New York 1977), Chap. 4

12) L.G. Yaffe and W.A. Goddard III, Phys. Rev. A **13,** 1682 (1976)

13) K.P. Huber and G. Herzberg, *Molecular Spectra and Molecular Structure, Vol. 4, Constants of Diatomic Molecules*, (Van Nostrand Reinhold Co., New York 1979)

14) See, for example, R. Krishnan, M.J. Frish, J.A. Pople and P. Von R. Schleyer, Chem. Phys. Lett. **79,** 408 (1981)

15) W. Meyer, J. Chem. Phys. **58,** 1017 (1973); W. Meyer, in: *Modern Theoretical Chemistry, Vol. 3, Methods of Electronic Structure Theory*, edited by H.F. Schaeffer III (Plenum, New York 1977), Chap. 11; W. Kutzelnigg, in: *Modern Theoretical Chemistry, Vol. 3, Methods of Electronic Structure Theory*, edited by H.F. Schaeffer III (Plenum, New York 1977), Chap. 5

16) R.C. Ladner and W.A. Goddard III, J. Chem. Phys. **51,** 1073 (1969)

17) P. Siegbahn and B. Liu, J. Chem. Phys. **68,** 2457 (1978)

18) See Chapter 1 of this thesis

19) D.F. Feller, M.W. Schmidt and K. Ruedenberg, J. Am. Chem. Soc. **104,** 960 (1982)

20) C.E. Moore, *Atomic Energy Levels* (Nat. Stand. Ref. Data Ser., Nat. Bur. Stand. (U.S.), 1971)

21) C.E. Rechsteiner, R.P. Buck and L. Pederson, J. Chem. Phys. **65,** 1659 (1976)

22) R.L. Cook, F. DeLucia and P. Helminger, J. Mol. Spect. **53,** 62 (1974)

23) Symmetric GVB(2/4) = -100.4679 h, asymmetric = -100.4694 h

24) W.A. Goddard and W.J. Hunt, Chem. Phys. Lett. **24,** 464 (1974)

25) D.W. Turner, C. Baker, A.D. Baker and C.R. Brundle, *Molecular Photoelectron Spectroscopy*, (Wiley, New York 1970)

26) M.S. Foster and J.L. Beauchamp, Inorg. Chem. **14,** 1229 (1975), corrected to 0° K, but not corrected for zero point.

27) R.E. Weston, Jr., J. Phys. Chem. **83,** 61 (1979) and references therein

28) J.C. Miller and R.J. Gordon, J. Chem. Phys. **76,** 5167 (1982)

29) R.F. Heidner III and J.F. Bott, J. Chem. Phys. **64,** 2267 (1976)

30) A. Persky and F.S. Klein, J. Chem. Phys. **44,** 3617 (1966)

31) Y. Bar Yaakov, A. Persky and F.S. Klein, J. Chem. Phys. **59,** 2415 (1973)

32) J.C. Miller and R.J. Gordon, J. Chem. Phys. **75,** 5305 (1981)

33) J.D. McDonald and D.R. Herschbach, J. Chem. Phys. **62,** 4740 (1975)

34) A.A. Westenberg and N. de Haas, J. Chem. Phys. **48,** 4405 (1968)

35) M.A.A. Clyne and D.H. Stedman, Trans. Faraday Soc. **62,** 2164 (1966)

36) P.F. Ambidige, J.N. Bradley and D.A. Whytock, J. Chem. Soc. Faraday Trans. 1 **72,** 2143 (1976)

37) A.E. DeVries and F.S. Klein, J. Chem. Phys. **41,** 3428 (1964)

38) F.S. Klein and I. Veltman, J. Chem. Soc. Faraday Trans. 2 **74,** 17 (1978)

39) G.O. Wood, J. Chem. Phys. **56,** 1723 (1972)

40) H. Endo and G.P. Glass, Chem. Phys. Lett. **44,** 180 (1976)

41) A.F. Voter and W.A. Goddard, J. Chem. Phys. **75,** 3638 (1981)

42) T.H. Dunning, Jr., J. Chem. Phys. **66,** 2752 (1977)

43) P. Botschwina and W. Meyer, Chem. Phys. **20,** 43 (1977)

44) C.F. Bender, B.F. Garrison and H.F. Schaeffer III, J. Chem. Phys. **62,** 1188 (1975)

45) A.K. Rappé, T.A. Smedley and W.A. Goddard III, J. Phys. Chem. **85,** 1662 (1981)

46) M.A. Haney and J.L. Franklin, J. Phys. Chem. **73,** 4328 (1969)

47) G.L. Bendazzoli, G. Gottorelli and P. Palmeri, J. Am. Chem. Soc. **96,** 11 (1974); K. Watanabe and A.S. Jursa, J. Chem. Phys. **41,** 1650 (1964)

48) G.C. Fettis, J.H. Knox and A.F. Trotman-Dickenson, J. Chem. Soc. **1960,** 1064 (1960)

49) J. Berkowitz, W.A. Chupka, P.M. Guyon, J.H. Holloway and R. Spohr, J. Chem. Phys. **54,** 5165 (1971)

50) I. Shavitt, J. Chem. Phys. **49,** 4048 (1968)

51) J.T. Muckerman, J. Chem. Phys. **54,** 1155 (1971)

52) G.S. Hammond, J. Am. Chem. Soc. **77,** 334 (1955)

53) R. Hoffmann and R.B. Woodward, J. Am. Chem. Soc. **87,** 2046, 4388, 4389 (1965); R.B. Woodward and R. Hoffmann, *ibid* **87,** 395, 2511 (1965); R.B. Woodward and R. Hoffmann, Angew. Chem., Int. Ed. Engl., **8,** 781 (1969).

54) W.A. Goddard III, J. Am. Chem. Soc. **94,** 793 (1972)

55) D.M. Silver and R.M. Stevens, J. Chem. Phys. **59,** 3378 (1973)

56) C.W. Wilson and W.A. Goddard III, J. Chem. Phys. **51,** 716 (1969); C.W. Wilson and W.A. Goddard III, J. Chem. Phys. **56,** 5913 (1972);

57) Based on the R-GVB to GRVB lowering in the isomorphic cyclobutadiene system

58) See the discussion on this point for cyclobutadiene, Chapter 4, Section V of this thesis

59) See for example; D.J. Pasto and D.M. Chipman, J. Am. Chem. Soc. **101,** 2290 (1979); R.Jaquet and V. Staemmler, Chem. Phys. **68,** 479 (1982); see also reference 19

60) Energy of a GVB(1/2) wavefunction minus energy of a GVB(2/4) wavefunction.

Table 1. Contracted Gaussian Basis Used for HF + H Calculations.

Hydrogen Basis (6s, 1p/3s1p) "TZ + pol"

Function	Type	Exponent	Coefficient
1	S	68.1600000	0.0025500
1	S	10.2465000	0.0193800
1	S	2.3464800	0.0928000
1	S	0.6733200	0.2943000
2	S	0.2246600	1.0000000
3	S	0.0822170	1.0000000
4	P	1.45	1.0

Hartree-Fock Total Energy = -0.499940

MQM Basis Name: HU3Z6 and HU2PF

Fluorine Basis (9s, 5p, 1d/3s, 2p, 1d) "VDZ + pol"

Function	Type	Exponent	Coefficient
1	S	9995.0000000	0.0011660
1	S	1506.0000000	0.0088700
1	S	350.3000000	0.0432800
1	S	104.1000000	0.1429290
1	S	34.8400000	0.3553720
1	S	12.2200000	0.4620850
1	S	4.3690000	0.1408480
2	S	12.2200000	-0.1484520
2	S	1.2080000	1.0552700
3	S	0.3634000	1.0000000
4	P	44.3600000	0.0208760
4	P	10.0800000	0.1301070
4	P	2.9960000	0.3961660
4	P	0.9383000	0.6204040
5	P	0.2733000	1.0000000
6	D	1.34	1.0

Hartree Fock Total Energy = -99.394288

MQM Basis Name: F1 and F2D

Table 2. Results from Highly Correlated Wavefunction on the Barrier Height in the HF + H Exchange Reaction.

Authors	Basis[a]	Level[b]	R (Å)	E_a (kcal)
Wadt and Winter[d]	[4, 3, 1/2, 1]	GVB(3/6) + SD CI	1.17[e]	50.0
Wadt and Winter	[4, 3, 1/2, 1]	GVB(3/6) + SD CI	1.14	48.1
Wadt and Winter	[4, 3, 1/2, 1]	POL(3) CI	1.14	47.6
Bender et al.[e]	[5, 3, 1/3, 1]	HF + SD CI	1.14[c]	49.0
Dunning[f]	[3, 2, 1/2, 1]	SOGVB(3/6) + SD CI	1.18[c]	48.81
Botschwina and Meyer[e]	[8, 4, 2/4, 2]	PNO-CEPA	1.143[c]	45.0
Botschwina and Meyer	[9, 6, 3, 1/4, 2]	PNO-CEPA	1.143	44.9
This Work	[3, 2, 1/3, 1]	σ-full CI	1.176[c]	48.6
Bartoszek et al.[g]	--- experiment ---			42-53

[a] [4, 3, 1/2, 1] ≡ 4s, 3p, 1d on F, 2s, 1p on H.

[b] Abbreviations are defined in text.

[c] Optimized geometry.

[d] Reference 4.

[e] Reference 6.

[f] Reference 8.

[g] Reference 3.

Table 3. Results from Conceptually Simple Wavefunctions on the Barrier Height in the HF + H Exchange Reaction.

Level	E(HF)[a]	E(HFH)[b]	S_{AB}[d]	Barrier (kcal)[c]
HF	-0.046859	-0.438709		67.8
GVB(1/2)	-0.070146	-0.459273		69.5
GVB(1/5)	-0.077287	-0.464658		70.6
σ-SOGI(3)	-0.070146	-0.478162		57.7[e]
σ-R-GVB(1/2)	-0.070146	-0.46418	0.9437	66.5
σ-R-GVB(1/2)(pr)	-0.070146	-0.46422	0.9436	66.4
R-GVB(1/5)	-0.077287	-0.467857		68.6
R-GVB(1/5)(pr)	-0.077287	-0.467879		68.6
σ-GRHF	-0.046859	-0.4632	-0.590	52.5[e]
σ-GRVB(1/2)	-0.070146	0.4929	0.501	48.4[e]
GRVB(1/2)	-0.070146	-0.4940	0.405	47.7
GRVB(1/5)	-0.077287	-0.50023		48.3
σ-full CI	-0.093466	-0.515924		48.6[e]

[a] Energy relative to -100.0 hartrees at R = 0.9176 Å.

[b] Energy relative to -100.0 hartrees at $R_1 = R_2 = 1.17$ Å.

[c] E(H) = -0.499940 in this basis.

[d] S_{AB} = overlap of ψ_A with reflected ψ_A = $\langle \psi_A | \psi_B \rangle$; only listed for wavefunctions that are actually resonated.

[e] These wavefunctions use only the sigma space as described in the text and should be compared with the σ-full CI barrier of 48.6 kcal.

Table 4. Geometry of Saddle Point in HF + H Exchange Reaction for Various Levels of Wavefunction.[a]

Level	R(Å)	k(r/Å^2)	Barrier Height (kcal)
Hartree-Fock	1.10	1.089	66.3
σ-GRVB(1/2)	1.178	0.994	48.4
σ-full CI	1.176	1.062	48.6

[a] obtained from a fit to three points: R_1=R_2=1.13, 1.17 and 1.21Å

Table 5. Results From Calculations Along a Model HF + H Reaction Coordinate. R_{HF} is Fixed at R = 1.17 Å. Total Energies are in Hartrees, Relative Energies are in Kcal.

R_{FD} =	1.17	1.27	1.37	1.47	1.57	1.77	10.0	HF + H
E(GVB(1/2))[a]	0.459273	0.470798	0.483878	0.495137	0.504175	0.516518	0.531591	
E(σ-full CI)[a]	0.515924	0.518099	0.523287	0.529375				
E(σ-GRVB(1/2))[a]	0.4930	0.4950	(0.5010)[c]	(0.510)[c]	(0.517)[c]			
E_{REL}(GVB(1/2))[b]	69.5	62.3	54.1	47.0	41.4	33.6	24.4	24.4
E_{REL}(σ-full CI)[b]	48.6	47.3		40.2				24.1
E_{REL}(σ-GRVB(1/2))[b]	48.4	47.1	(43.3)[c]	(37.8)[c]	(33.5)[c]			
E (σ-GRVB)	96.3	71.7	(63.9)[c]	(85.6)[c]	(68.0)[c]			
E_B (σ-GRVB)	96.3	123.3	(135.5)[c]	(105.4)[c]	(110.6)[c]			
S_{AB}	0.4539	0.4628	(0.4975)[c]	(0.6909)[c]	(0.7580)[c]			
C_A	0.5863	0.7354	(0.7687)	(0.5904)	(0.6375)			
C_B	0.5863	0.4180	(0.36 8)	(0.4965)	(0.4262)			
exc. state (σ-GRVB(1/2))[b]	136.3							
exc. state (σ-full CI)[b]	133.3							

[a]Total energy - subtract value shown from -100.0 hartrees.

[b]Kcal relative to E(HF) + E(H) at consistent level of calculation.

[c]These GRVB wfns converged to a non-meaningful form - see text.

Table 6. Results for Bent HFH Transition State Geometries

Reference[a]	Level	Basis[b]	R_{HF}(Å)	θ(deg)	E(h)	Barrier(kcal)
WW	GVB(3/6)	WW-I	1.03	109	-0.4523	81.8
WW	GVB(3.6)	WW-II	1.03	109	-0.4841	63.4[c]
WW	POL(2)CI	WW-I	1.08	106	-0.5710	59.6
WW	POL(2)CI	WW-II	1.08	106	-0.5944[d]	47.2
WW	POL(3)CI	WW-II	1.08	106	-0.5942[d]	47.6
This work	σ-GRVB(1/2)	WW-II	1.08	106	-0.4971	46.9
This work	σ-GRVB(1/2)	V	1.08	106	-0.4912	49.5

[a]WW ≡ reference 4.

[b]WW-I is valence double zeta plus polarization; WW-II is the same as WW-I plus s and p Rydberg functions on F; V is the basis described in Section II-B of this chapter.

[c]Geometry optimized at this level.

[d]There appears to be a discrepancy, since the POL(3) CI should give a lower energy than the POL(2) CI. This is as printed in reference 4.

Table 7. Contracted Gaussian Basis Used for HCl + H Calculations.

Hydrogen Basis (4s, 1p/2s, 1p) "DZ + pol"

Function	Type	Exponent	Coefficient
1	S	19.2405660	0.0190600
1	S	2.8991520	0.1342400
1	S	0.6534101	0.4744900
2	S	0.1775765	0.5090700
3	P	1.0	1.0

Hartree-Fock Total Energy = 0.499277 (when unscaled)

MQM Basis Name: HS2Z4 and HS1P

Chlorine Basis (14s, 9p/4s, 3p) "VDZ + pol"

Function	Type	Exponent	Coefficient
1	S	40850.0000000	0.0010043
1	S	6179.0000000	0.0076146
1	S	1425.0000000	0.0377671
1	S	409.2000000	0.1370181
1	S	135.5000000	0.3395575
1	S	50.1300000	0.4383927
1	S	20.2100000	0.1862295
2	S	55.9124593	-0.0888737
2	S	17.4882249	-0.0323297
2	S	6.2830000	0.5374505
2	S	2.4600000	0.5542866
3	S	2.8413781	-0.2598590
3	S	0.5271000	1.1399213
4	S	0.1884000	1.0000000
5	P	240.8000000	0.0132703
5	P	56.5600000	0.0896296
5	P	17.8500000	0.2990394
5	P	6.3500000	0.4923323
5	P	2.4030000	0.3022806
6	P	6.2162548	-0.0484020
6	P	2.4092929	0.0903526
6	P	0.6410000	0.9573171
7	P	0.1838000	1.0000000
8	D	0.60	1.00

MQM Basis Name: CL1 and Cl1D

Table 8. Barrier Heights for the HCl + H Exchange Reaction.

Level	E(HCl)[a]	E(HClH)[b]	S_{AB}	Barrier (kcal)[c]
Hartree-Fock	-0.04777	-0.477081	--	43.9
GVB(1/2)	-0.06384	-0.48518		48.9
GVB(1/5)	-0.7340	-0.490989		51.3
R-GVB(1/2)	-0.06384	-0.493486	0.944	43.7
R-GVB(1/2)(pr)	-0.06384	-0.49522	0.939	42.6
R-GVB(1/5)	-0.073403	-0.501281	0.937	44.8
R-GVB(1/5)(pr)	-0.073403	-0.503366	0.932	43.5
σ-GRVB(1/2)	-0.06384	-0.5228	0.533	25.3
GRVB(1/2)	-0.6384	-0.5231		25.1
σ-full CI	-0.082604	-0.541169		25.5
	Other Workers			
Pol CI	Dunning[d]			25.3
PNO-CEPA	Botschwina and Meyer[e]			23.9
PNO-CEPA	Botschwina and Meyer[f]			22.1

[a] Energy relative to -460 hartrees at R_e = 1.27455 Å.

[b] Energy relative to -460 hartrees at $R_1 = R_2$ = 1.502 Å.

[c] E(H) = -0.499277 in this basis.

[d] Reference 42.

[e] 11s, 7p, 2d/5s, 2p basis; reference 43.

[f] 13s, 10p, 3d, 1f/6s, 2p basis; reference 43.

Table 9. Energy Quantities for the $H_2 + F \rightarrow H + HF$ Reaction. All Energies Except E_s are in Kcal as Defined in Figure 12.

Level	BDE(H_2)	BDE(HF)	ΔH	Geometry[a]	E_s(h)[b]	E_{a_1}	E_{a_2}
Hartree-Fock	83.1	95.8	-12.7	0.79, 1.413	0.49832	17.7	30.4
GVB(1/2)	94.9	110.4	-15.5	0.79, 1.413	0.51386	19.8	35.3
σ-GRVB(1/2)	94.9	110.4	-15.5	0.79, 1.413	0.52833	10.7	26.2
GVB(1/5)	102.4	114.9	-12.5	0.79, 1.413	0.52329	21.3	33.8
σ-full CI	100.0	113.0	-12.9	0.79, 1.413	0.55525	11.0	23.9
full CI	103.5	--	--	0.79, 1.413	--	--	--
Experiment	109.4	140.2	-30.80[f]			1.7	32.5
Other Workers							
SOGVB[c]	94.71	110.77	-16.06				
GVB CI[c]	94.71	111.36	-16.65				
POL CI[c]	94.71	128.36	-33.65	0.779, 1.595[d]			36.53
GVB+SDCI[c]	105, 36	129.31	-23.95	0.790, 1.413[d]			31.42
INO CI[e]				0.836, 1.18			

[a]Geometries are collinear R_{HH}, R_{HF} for saddle point calculation.

[b]To obtain the total energy, add value to -100.0 h.

[c]Dunning, ref. 8.

[d]Geometry optimized.

[e]Iterative Natural Orbital first order CI, Bender et al., ref. 7.

[f]Corrected to eliminate relativistic effects - ref. 8.

Table 10. ΔE_a for various values of E_a, ΔH, and λ. All values are in kcal.

		E_a						
	ΔH	Ø	1	2	5	1Ø	25	5Ø
$\lambda = 1$	Ø.Ø	-	Ø.6	Ø.5	Ø.5	Ø.5	Ø.5	Ø.5
	-5.Ø	Ø.1	Ø.3	Ø.4	Ø.4	Ø.5	Ø.5	Ø.5
	-1Ø.Ø	Ø.Ø	Ø.2	Ø.3	Ø.4	Ø.4	Ø.5	Ø.5
	-2Ø.Ø	Ø.Ø	Ø.2	Ø.2	Ø.3	Ø.4	Ø.4	Ø.5
	-3Ø.Ø	Ø.Ø	Ø.2	Ø.2	Ø.3	Ø.3	Ø.4	Ø.4
$\lambda = 2$	Ø.Ø	-	1.3	1.1	1.Ø	1.Ø	1.Ø	1.Ø
	-5.Ø	Ø.2	Ø.7	Ø.8	Ø.9	Ø.9	1.Ø	1.Ø
	-1Ø.Ø	Ø.1	Ø.5	Ø.6	Ø.8	Ø.8	Ø.9	1.Ø
	-2Ø.Ø	Ø.1	Ø.4	Ø.5	Ø.6	Ø.7	Ø.9	Ø.9
	-3Ø.Ø	Ø.Ø	Ø.3	Ø.4	Ø.6	Ø.7	Ø.8	Ø.9
$\lambda = 10$	Ø.Ø	-	11.3	8.1	6.3	5.6	5.3	5.1
	-5.Ø	5.Ø	5.Ø	5.Ø	5.Ø	5.Ø	5.Ø	5.Ø
	-1Ø.Ø	2.5	3.7	3.9	4.3	4.6	4.8	4.9
	-2Ø.Ø	1.3	2.6	3.Ø	3.6	4.Ø	4.5	4.7
	-3Ø.Ø	Ø.8	2.1	2.5	3.1	3.6	4.2	4.5
$\lambda = 20$	Ø.Ø	-	35.Ø	22.5	15.Ø	12.5	11.Ø	1Ø.5
	-5.Ø	2Ø.Ø	14.2	13.Ø	11.7	11.Ø	1Ø.5	1Ø.2
	-1Ø.Ø	1Ø.Ø	1Ø.Ø	1Ø.Ø	1Ø.Ø	1Ø.Ø	1Ø.Ø	1Ø.Ø
	-2Ø.Ø	5.Ø	6.8	7.3	8.1	8.7	9.3	9.6
	-3Ø.Ø	3.3	5.4	6.Ø	7.Ø	7.8	8.7	9.2

Table 11. Energy Quantities for Square and Rectangular H_4.

R_1(Å)	R_2(Å)	R-GVB(h)	E_{TOT}[a] (kcal)	E_{exec}[a]	E_A[a] (kcal)	E_B-E_A (kcal)	S_{AB}	E_{RES}[b] (kcal)
0.9	0.9	-1.995482	192.3	243.7	215.0	0	0.11642	22.7
1.0	1.0	-2.039433	164.8	219.7	188.3	0	0.14276	23.6
1.1	1.1	-2.062527	150.3	207.9	174.1	0	0.17100	23.9
1.2	1.2	-2.072393	144.1	203.2	167.7	0	0.20080	23.6
1.3	1.3	-2.073942	143.1	202.6	165.9	0	0.23166	22.9
1.4	1.4	-2.070397	145.3	203.8	166.9	0	0.29922	21.6
5.0	5.0	-1.999764	189.8	189.8	189.8	0	0.49999	0.0
1.28	1.28	-2.074125[c]	143.0	202.5	166.0	0	0.22543	23.1
1.26	1.30	-2.075956	141.8	203.8	157.8	16.5	0.22546	16.0
1.24	1.32	-2.081026	138.7	207.5	149.8	33.1	0.22550	11.1
1.22	1.34	-2.088437	134.0	213.0	141.9	49.6	0.22556	7.9
1.20	1.36	-2.097335	128.4	219.7	134.1	66.2	0.22556	5.7
1.18	1.38	-2.107112	122.3	227.3	126.4	82.8	0.22576	4.2
1.16	1.40	-2.117381	115.8	235.6	118.9	99.4	0.22589	3.1
1.14	1.42	-2.112243	109.2	244.4	111.6	116.1	0.22605	2.4
1.12	1.44	-2.138502	102.6	253.7	104.4	132.7	0.22630	1.8
0.734	∞	-2.301983	0	0				0.0

[a] Relative to $2H_2$ at GVB(1/2) level.

[b] E_{RES} = lower of E_A or E_B minus E_{TOT}.

[c] By comparison, a σ-full CI leads to E_{TOT} = -2.093055, a barrier of 141.6 kcal.

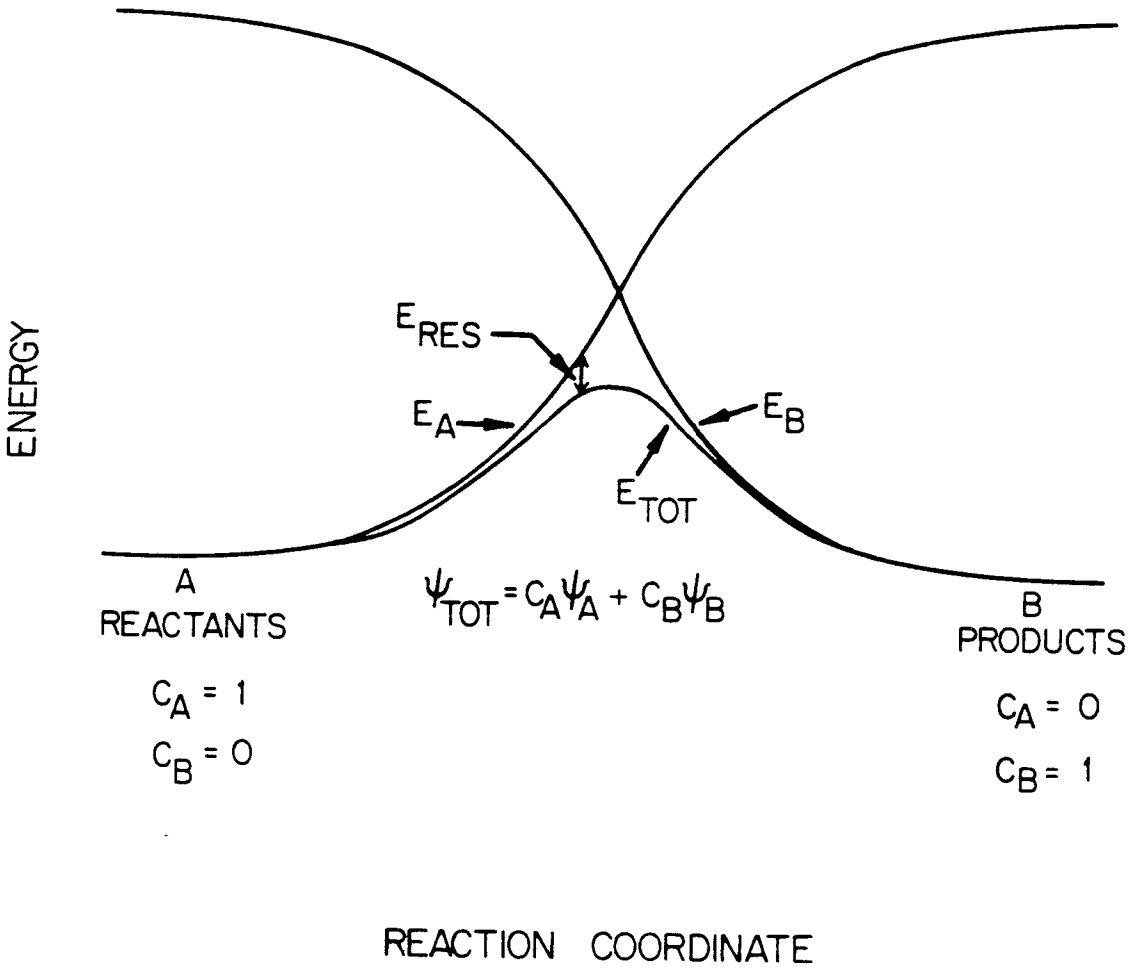

Figure 1. Hypothetical energy diagram for a reaction such as HCl + D -> H + ClD

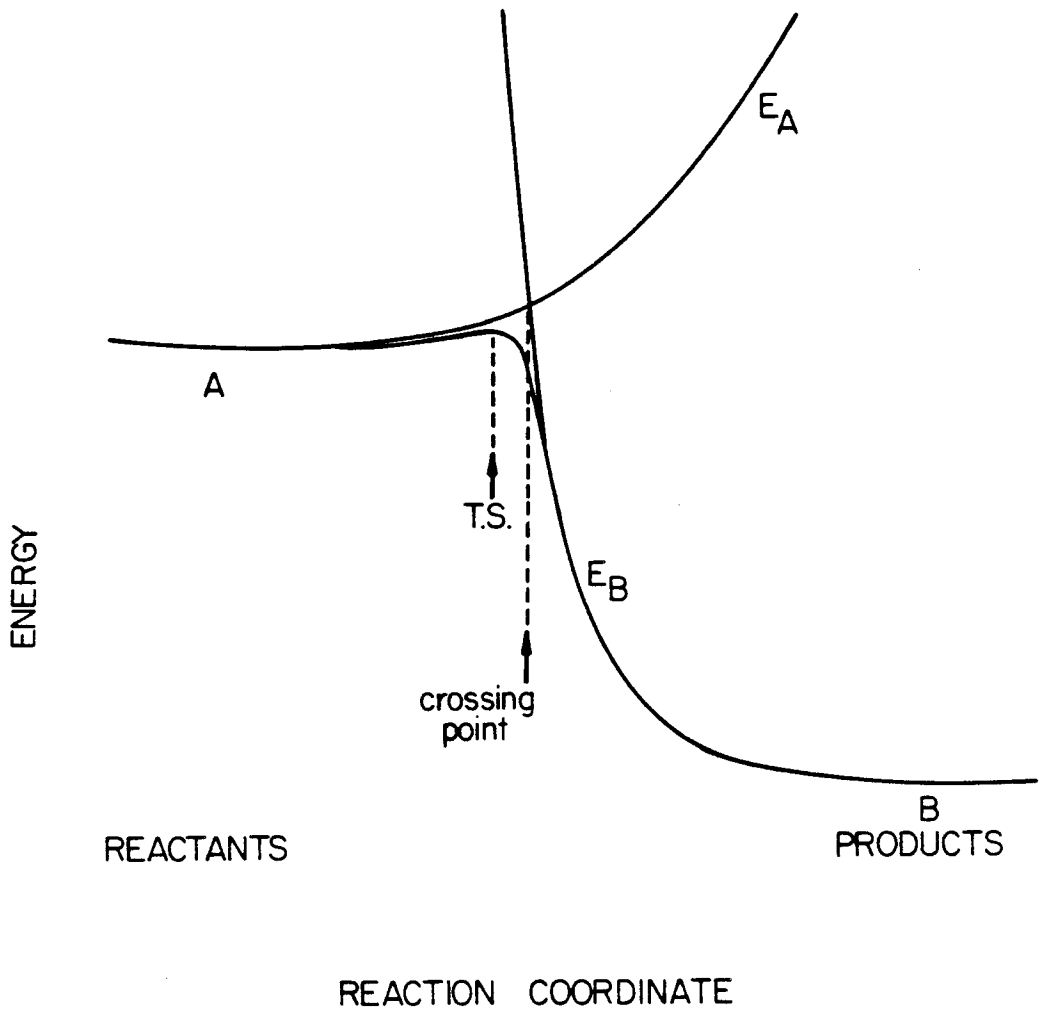

Figure 2. Energy diagram for an asymmetric reaction. The transition state (T.S.) is shifted from the diabatic crossing towards the less steep slope.

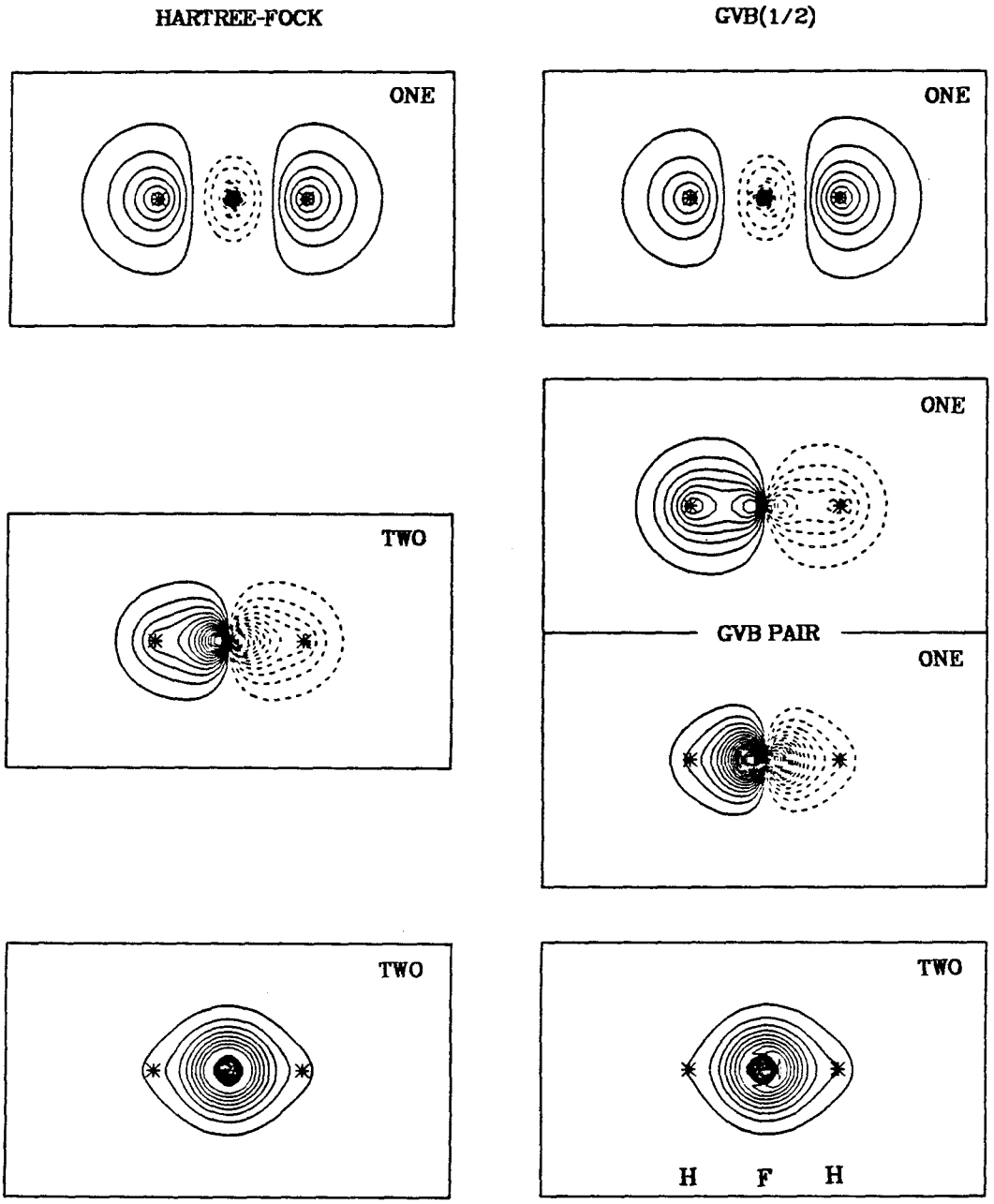

Figure 3. The Hartree-Fock (left) and GVB (right) orbitals for the symmetric HFH transition state. Notice that the GVB orbitals are only slightly asymmetric.

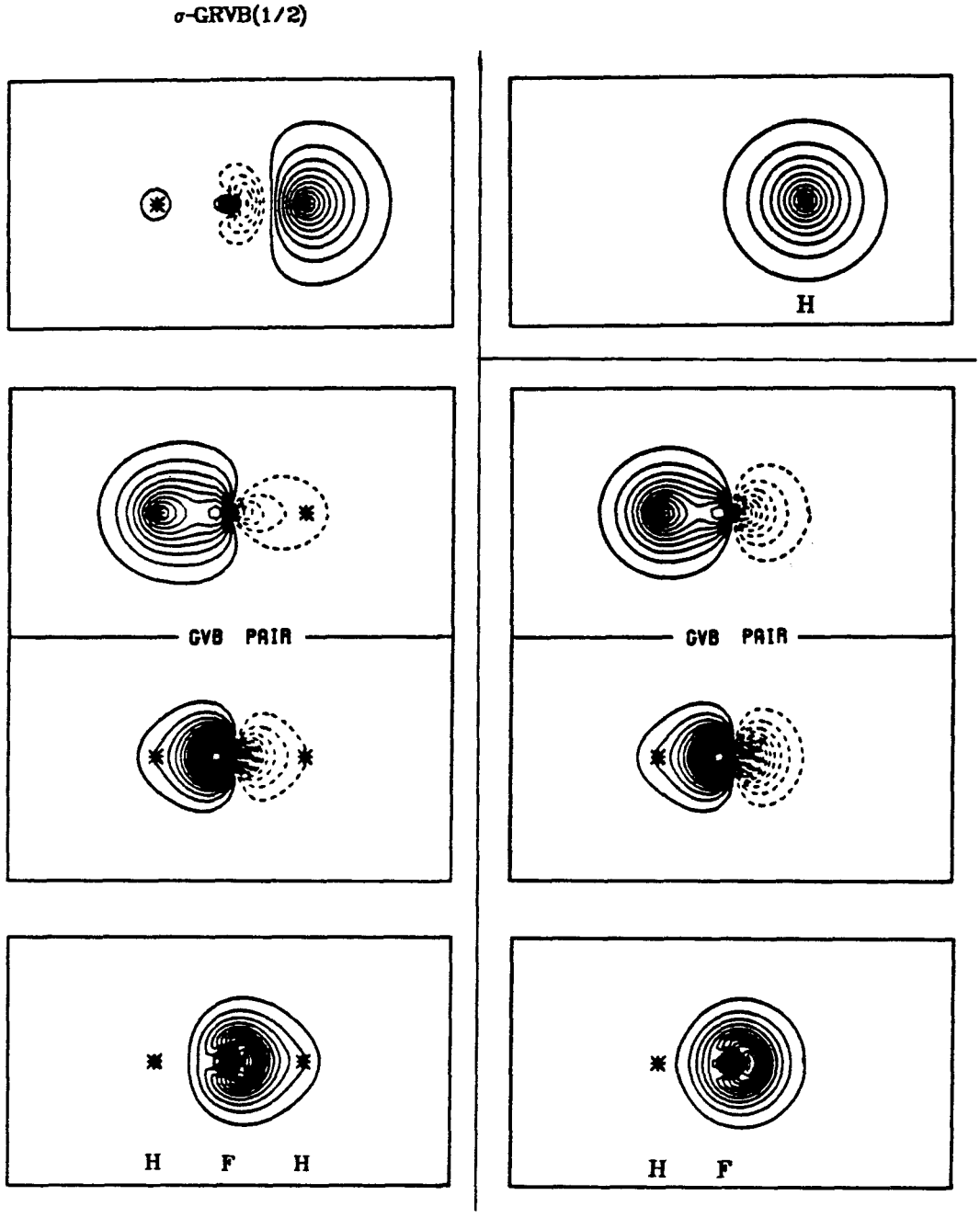

Figure 4. The orbitals from one subwavefunction of the σ-GRVB(1/2) wavefunction at the symmetric HFH saddle point. Juxtaposed on the right side are the orbitals from free HF (GVB(1/2)), and free H atom (Hartree-Fock), which show a striking similarity to the GRVB orbitals.

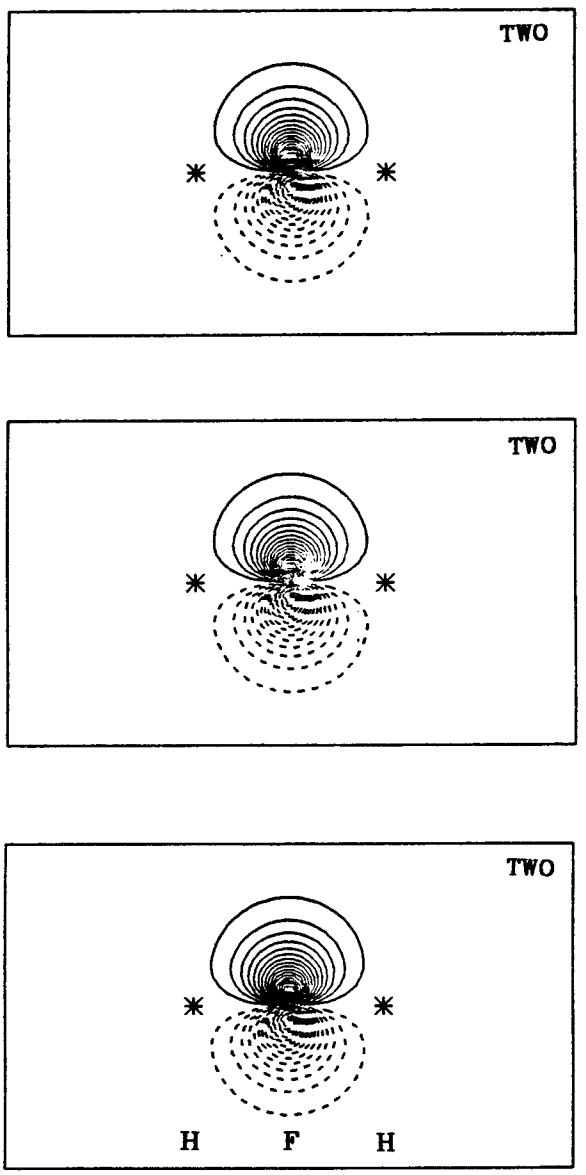

Figure 5. $2p\ \pi$ orbitals at symmetric HFH saddle point. Top: symmetric Hartree-Fock; Middle: GVB(1/2); Bottom: (GRVB(1/2)

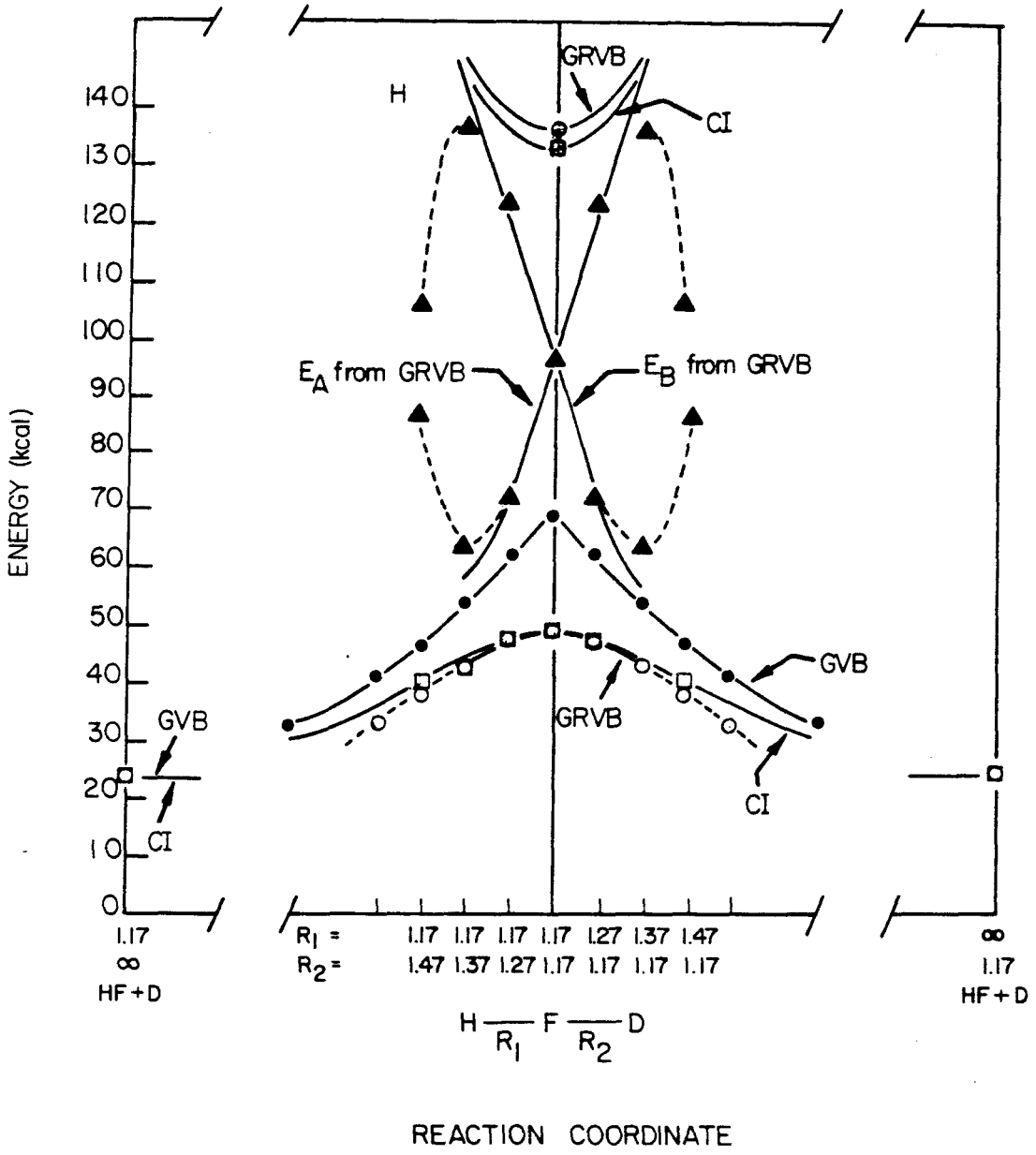

Figure 6. σ-GRVB(1/2), GVB(1/2) and σ-full CI energies along the HFH reaction coordinate. See discussion in text.

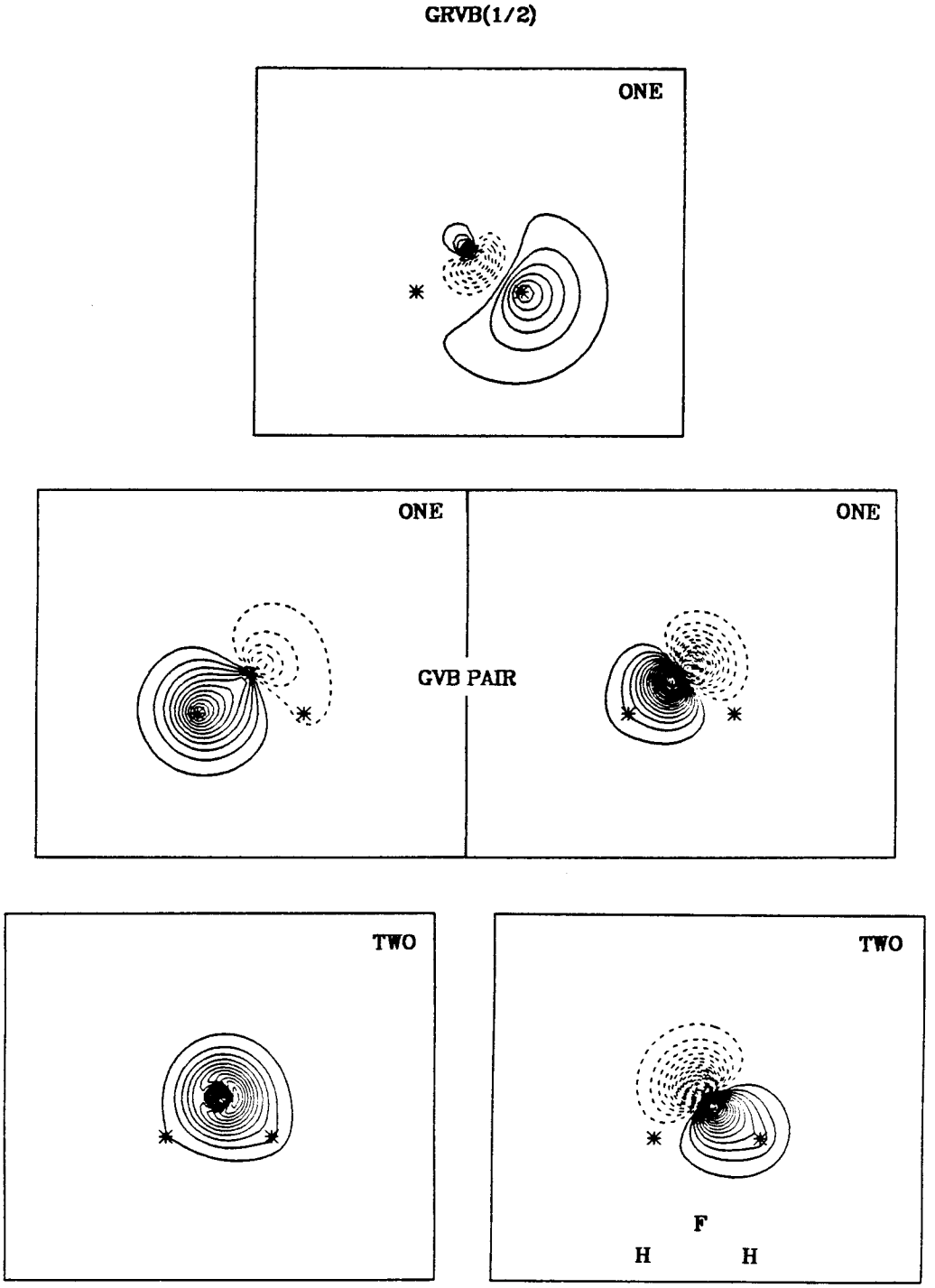

Figure 7. σ-GRVB(1/2) orbitals for the bent HFH transition state. Notice the Rydberg character in the singly-occupied orbital.

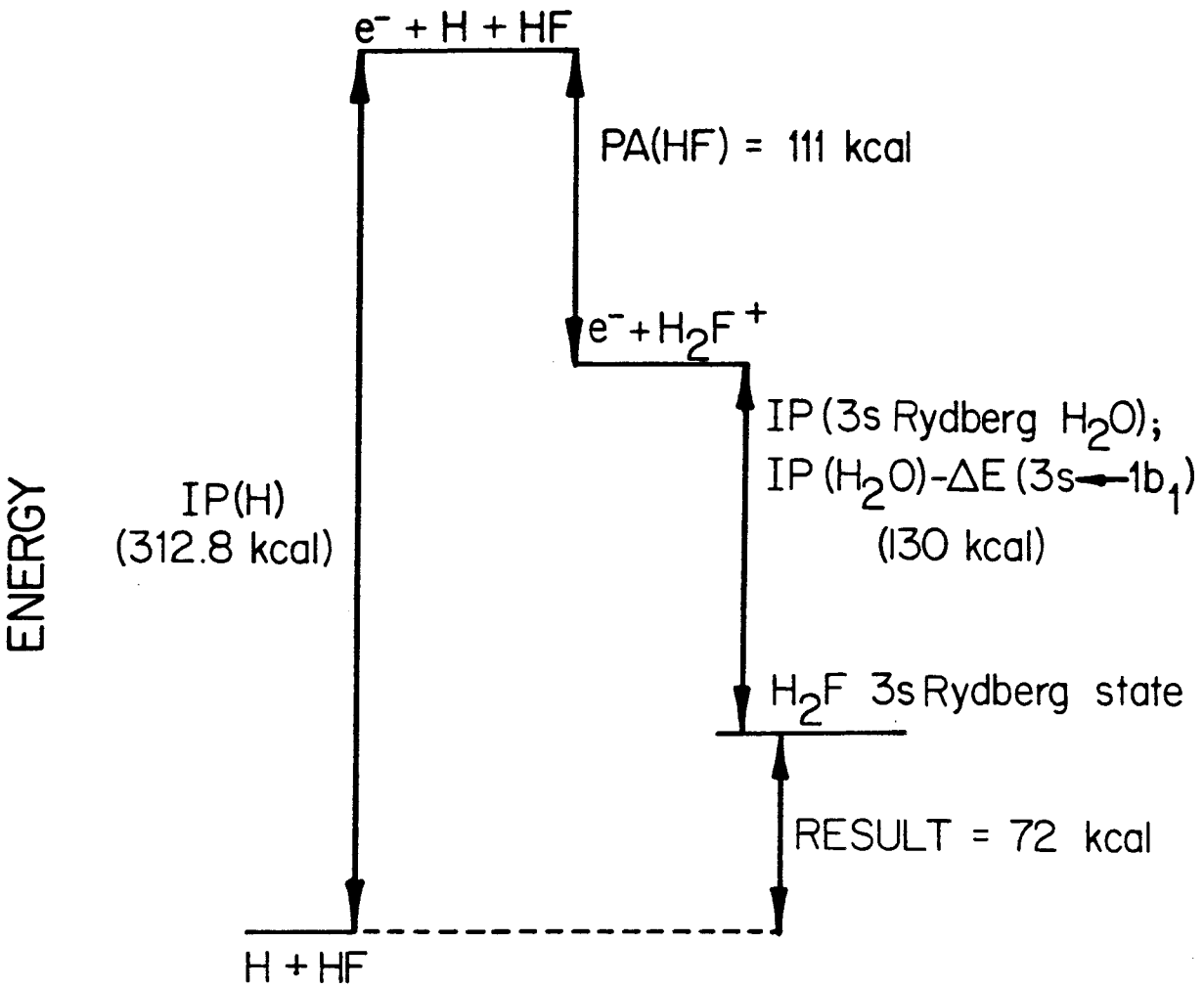

Figure 8. Thermochemical estimate of the energy of the HFH 3s Rydberg species.

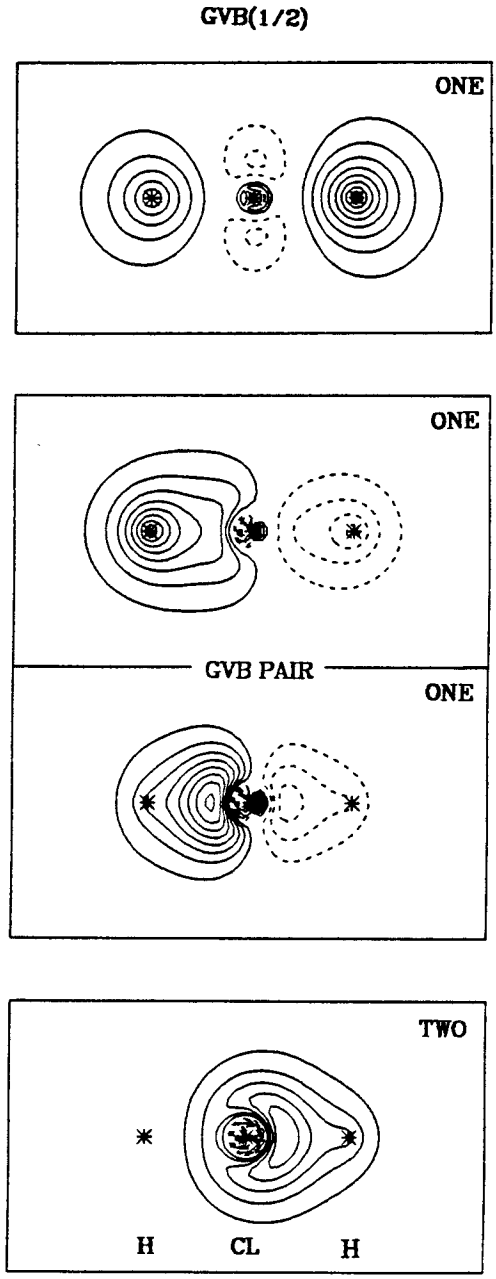

Figure 9. GVB(1/2) orbitals for the HClH transition state.

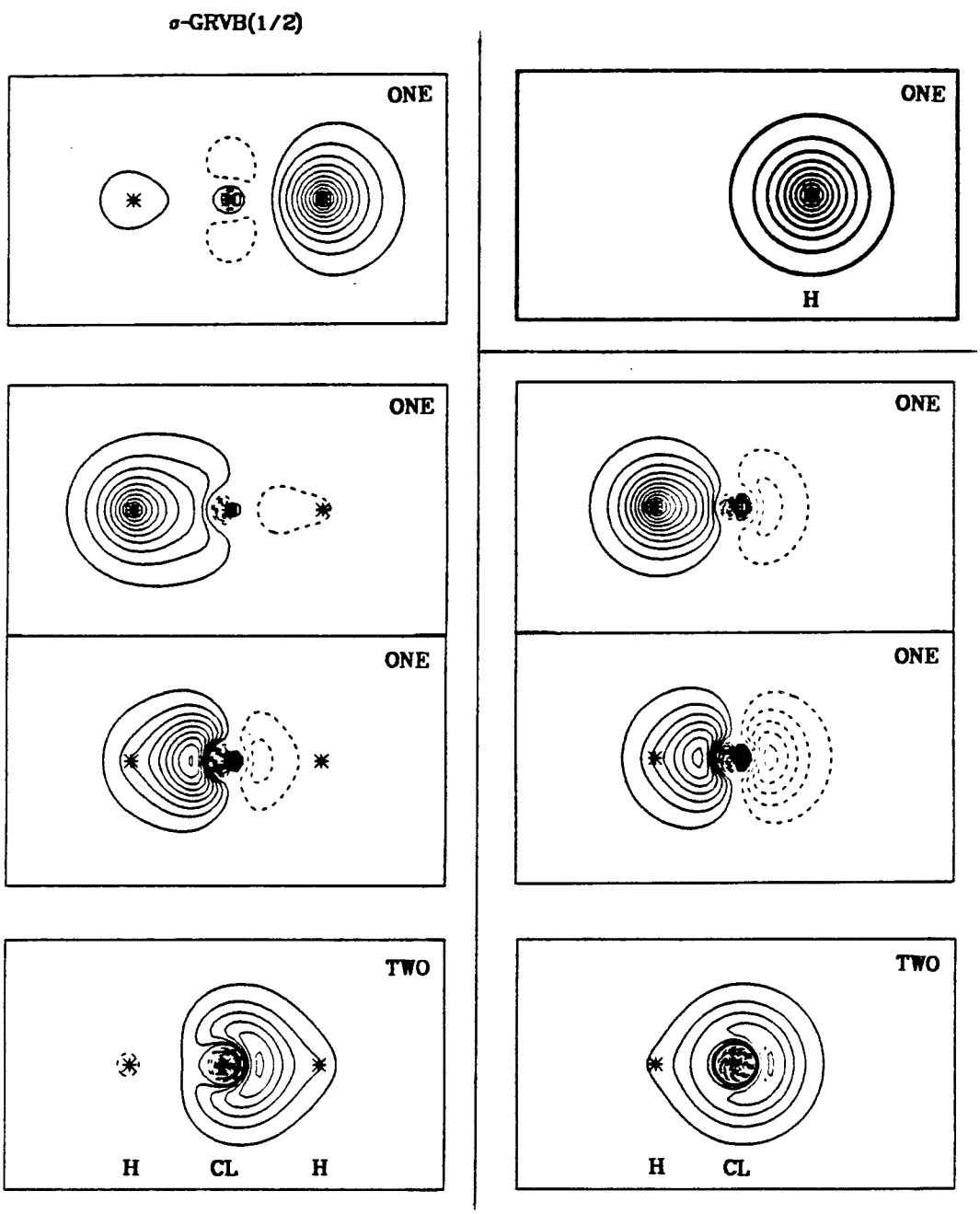

Figure 10. The orbitals from one subwavefunction of the σ-GRVB(1/2) wavefunction at the symmetric state. Juxtaposed on the right are the orbitals from free HF (GVB(1/2)) and free H atom, which show a strong similarity to the GRVB orbitals.

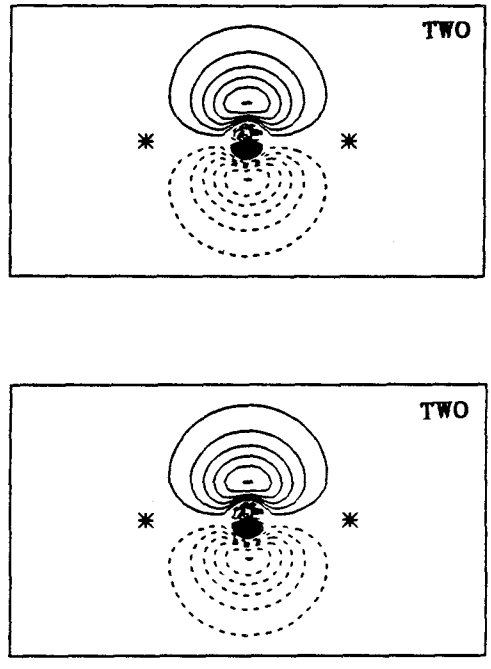

Figure 11. $3p\,\pi$ orbitals at symmetric HClH transition state. Top: GVB(1/2); Bottom: GRVB(1/2).

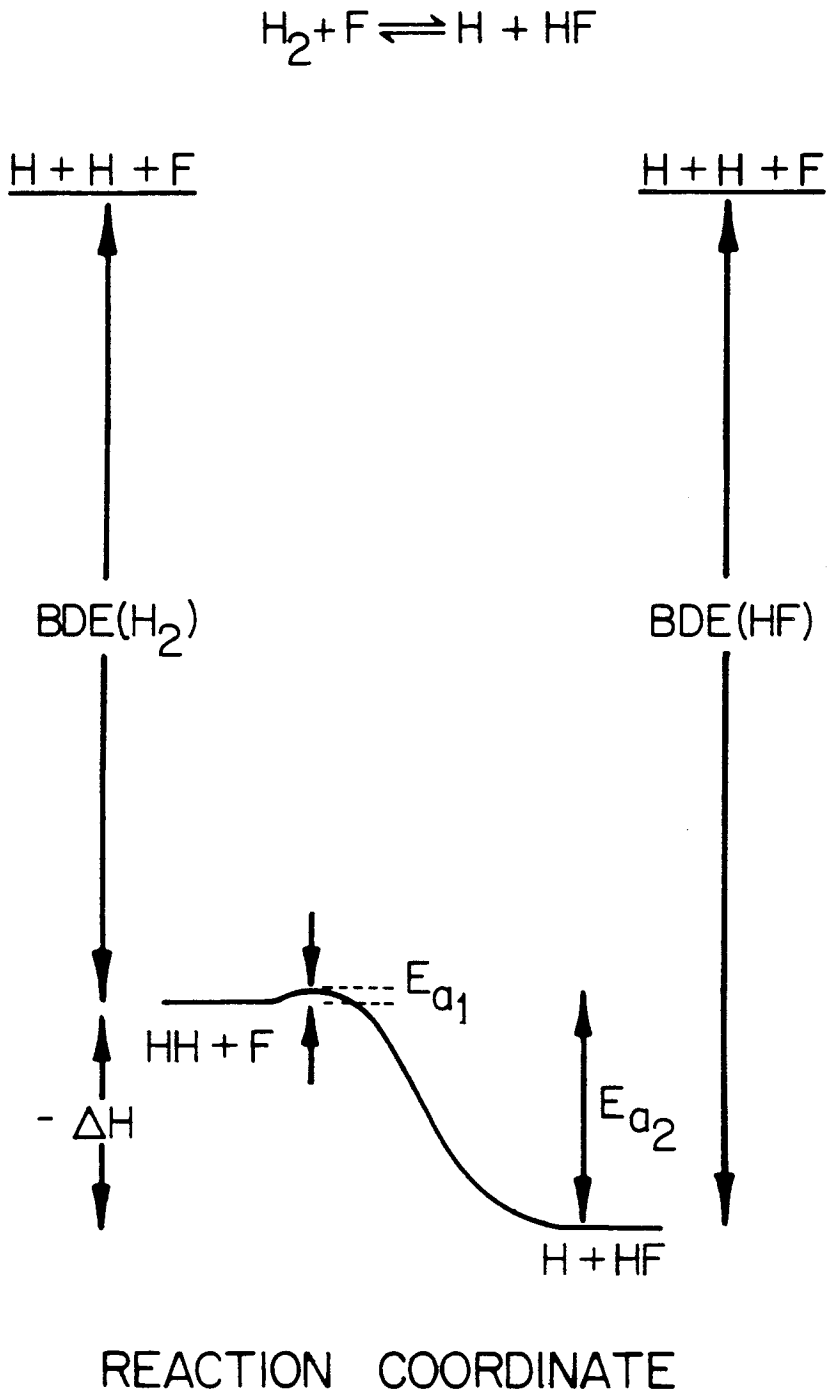

Figure 12. Energy diagram for the H_2 + F abstraction reaction.

GVB(1/2)

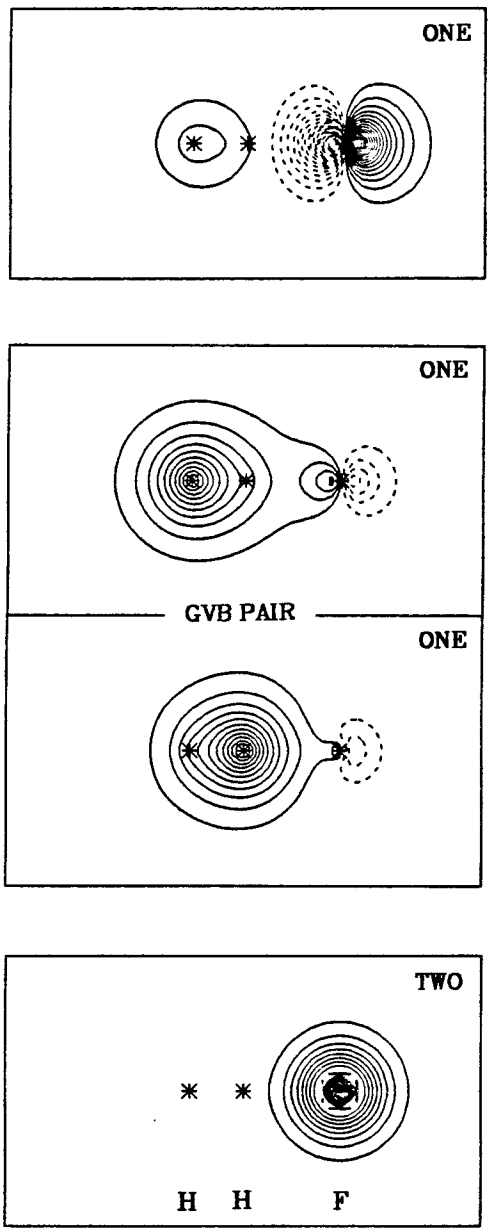

Figure 13. GVB(1/2) orbitals for HHF transition state

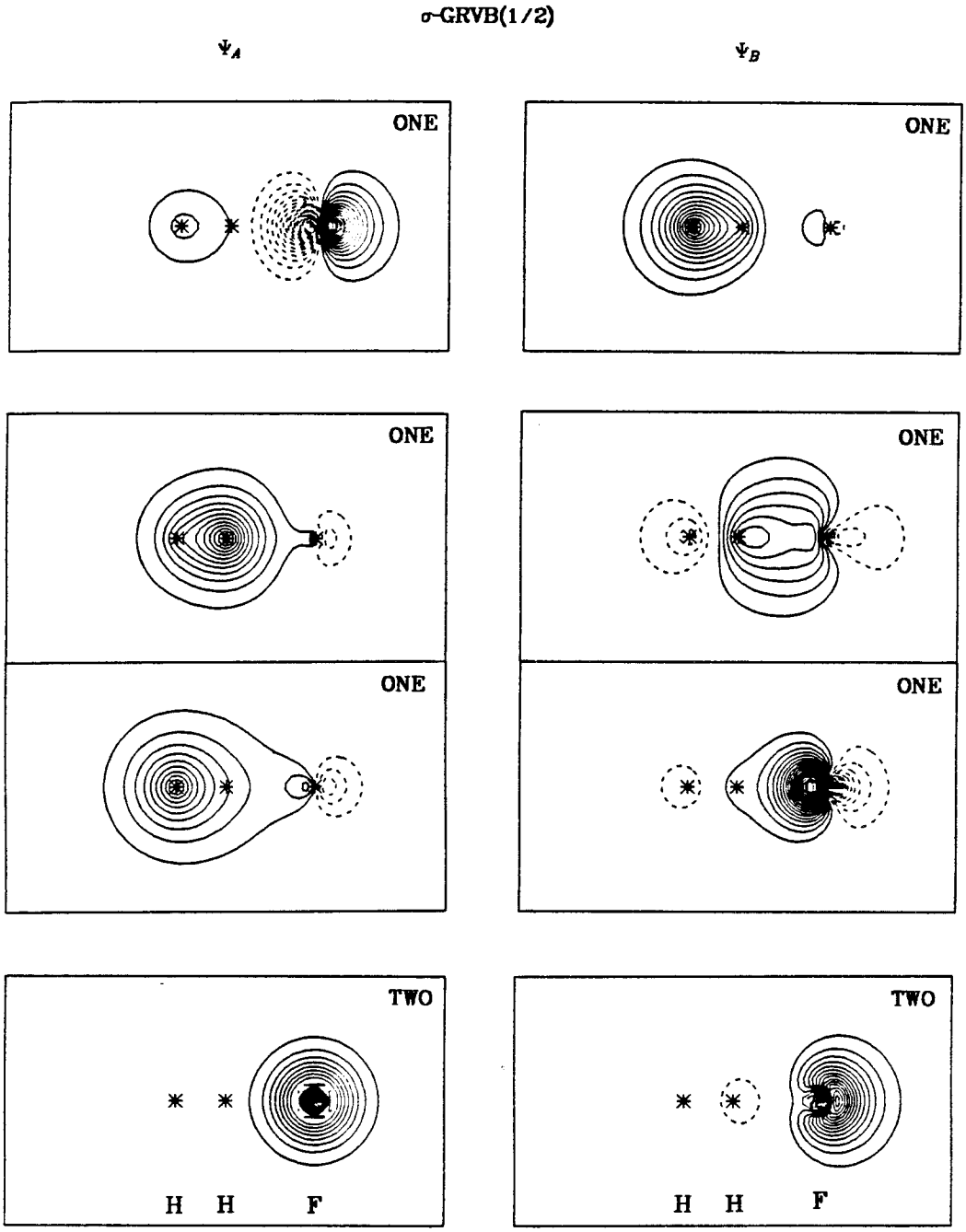

Figure 14. σ-GRVB(1/2) orbitals for HHF transition state. Both Ψ_A and Ψ_B are shown.

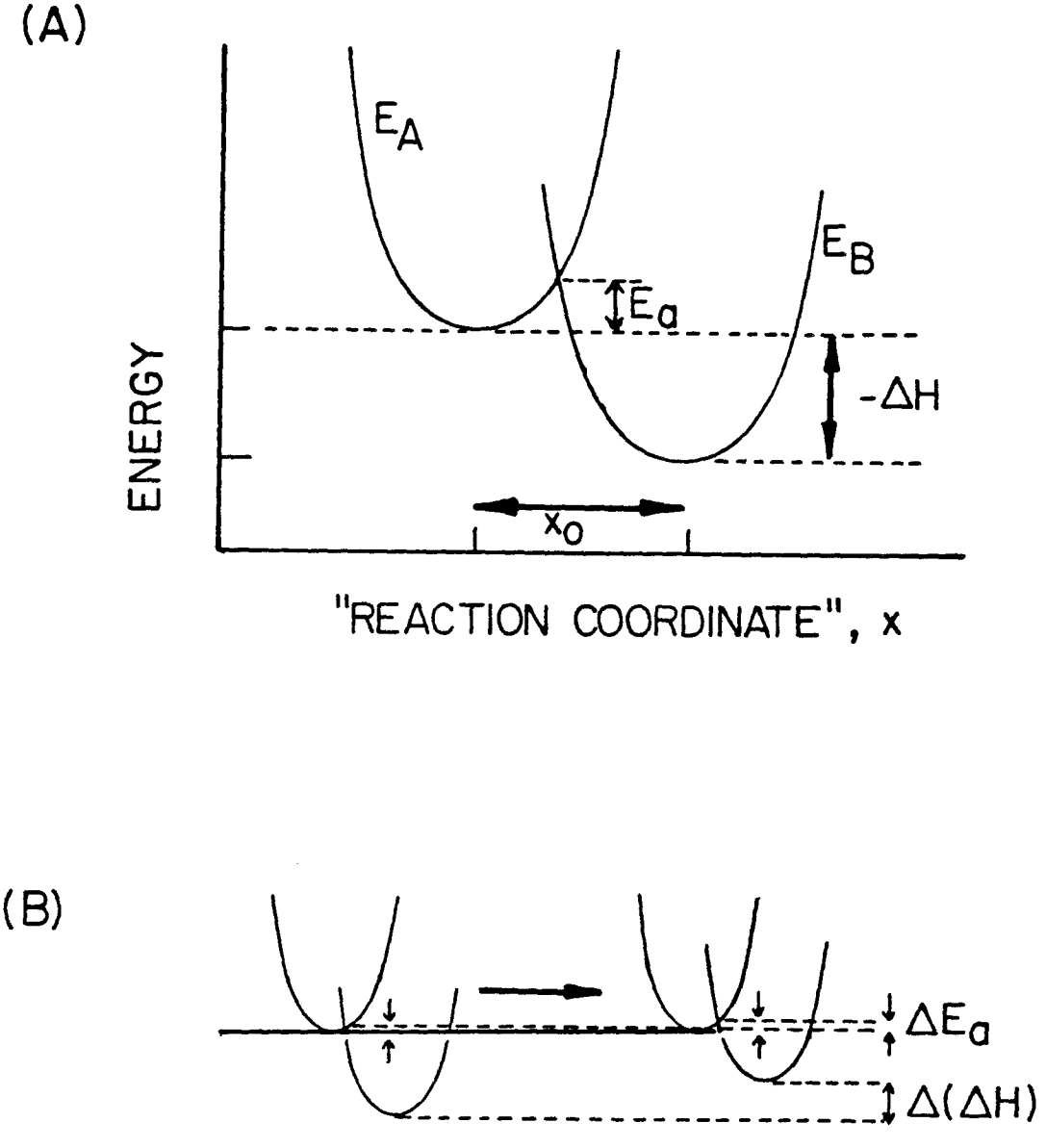

Figure 15. (a) Energy diagram for model reaction coordinate. The diabatic curves are taken as parabolas, and the resonance effects are neglected. (b) Diagrammatic demonstration of stability of calculated E_a with respect to errors in calculated ΔH, for very early transition states.

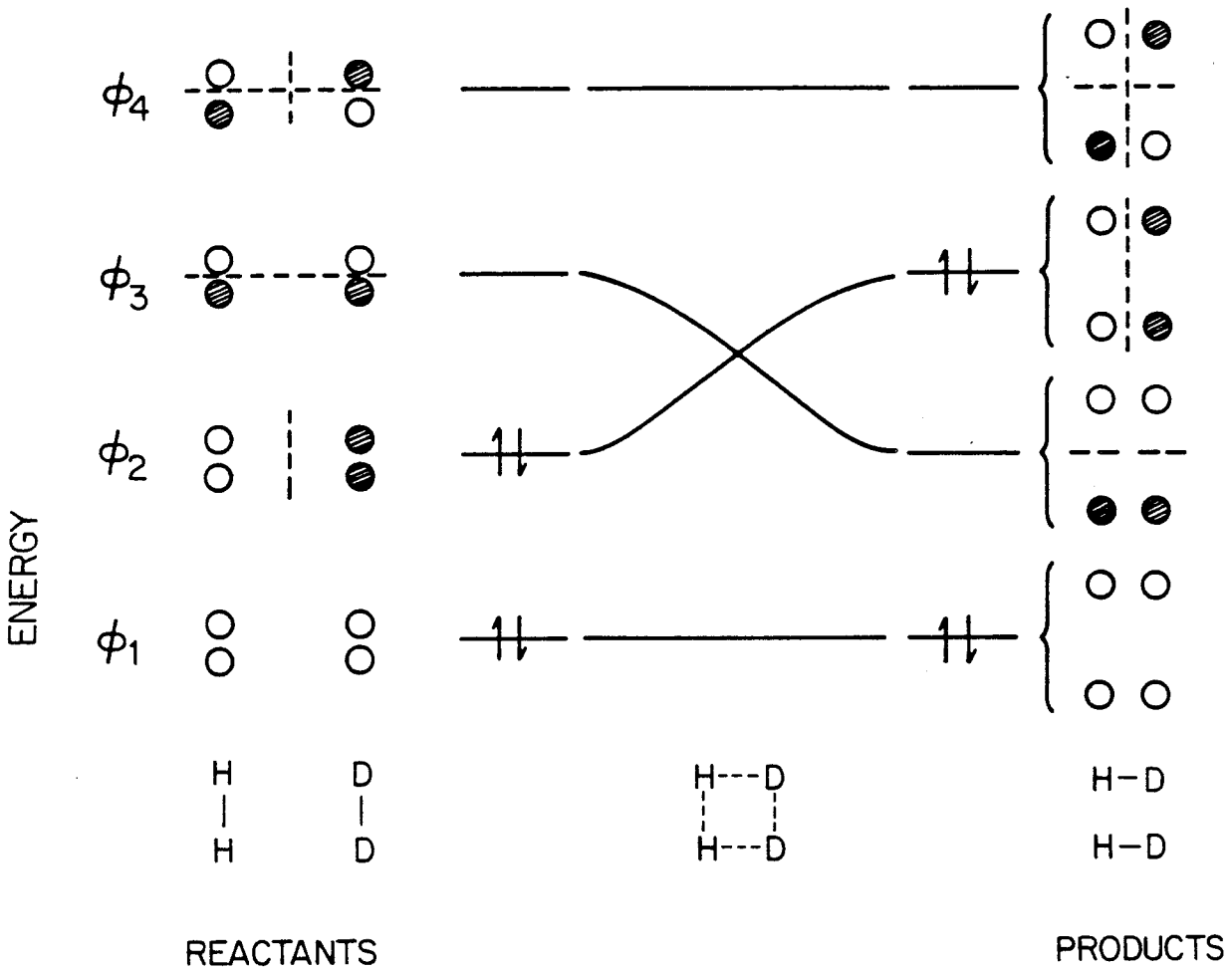

Figure 16. Correlation diagram demonstrating forbidden nature of the H_2 + D_2 --> 2 HD reaction. The lowest MO state at the reactants correlates with an excited state of the products due to the mapping of the nodal structures between reactants and products

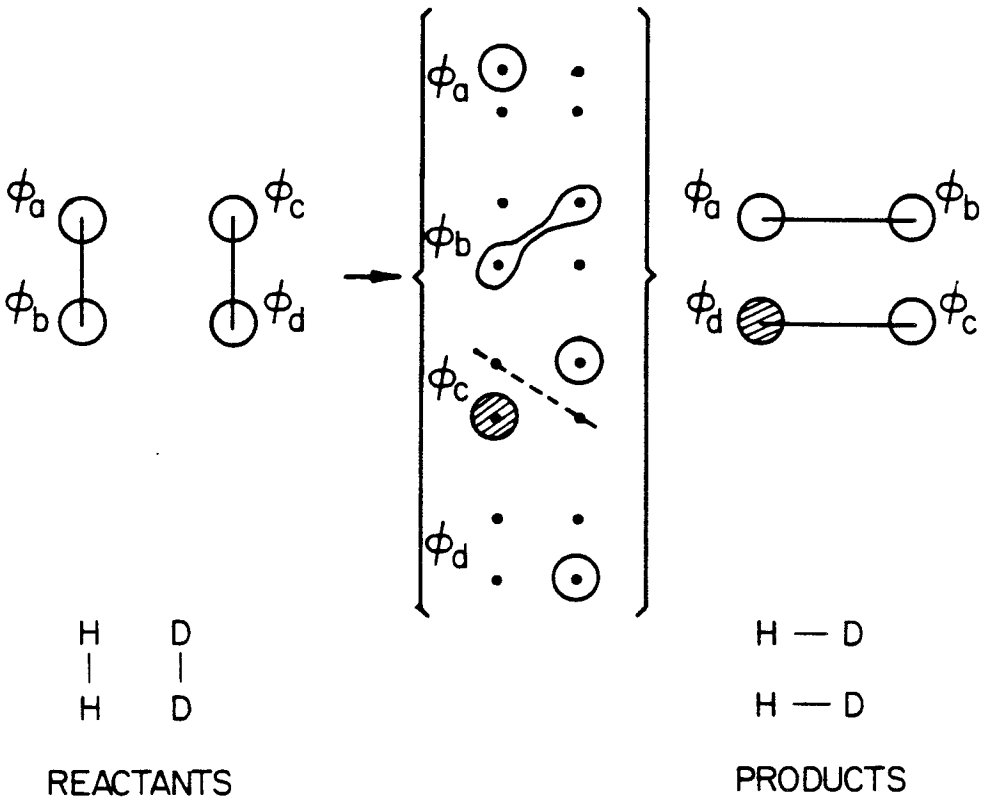

$$\psi = \mathcal{A}\left\{(\phi_a\ \phi_b + \phi_b\phi_a)(\phi_c\ \phi_d + \phi_d\ \phi_c)\ \alpha\beta\alpha\beta\right\}$$

Figure 17. OPCP analysis of the forbidden H_2 + D_2 --> 2 HD reaction. As φ_b and φ_c change centers to move the bonds, φ_c must build in a node to maintain orthogonality to φ_b. This causes φ_c to change phase as it grows into its new position, so that the overlap between φ_c and φ_d changes from positive in the reactants to negative in the products. Thus, the bond between φ_c and φ_d must be broken during the reaction, because the bonding overlap $\langle\varphi_c|\varphi_d\rangle$ passes through zero.

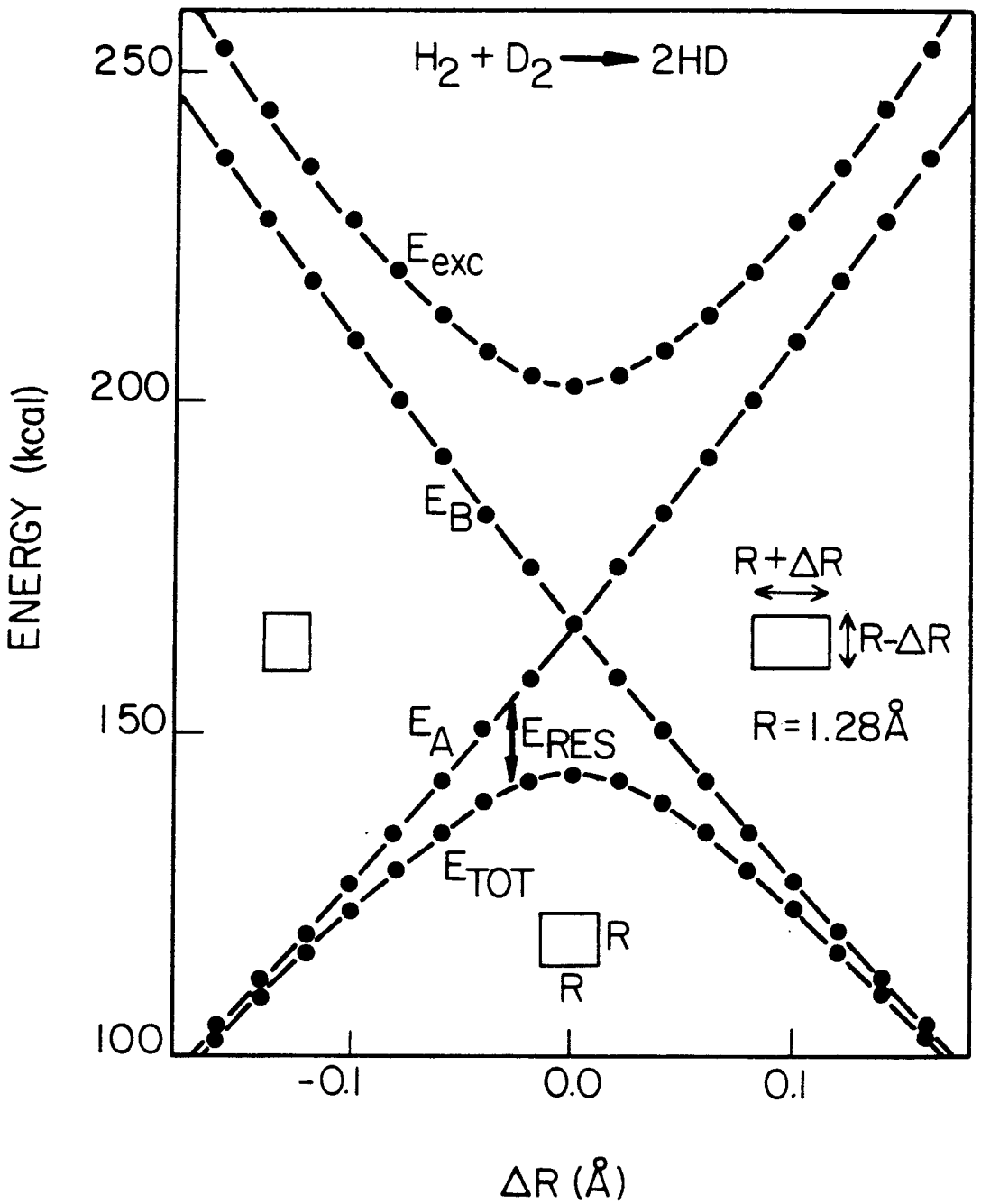

Figure 18. R-GVB energy quantities for the rectangle-square-rectangle reaction coordinate of the H_2 + D_2 --> 2 HD reaction. E_{TOT} is the resonant state, E_A and E_B are the diabatic states, and E_{exc} is the antiresonant state.

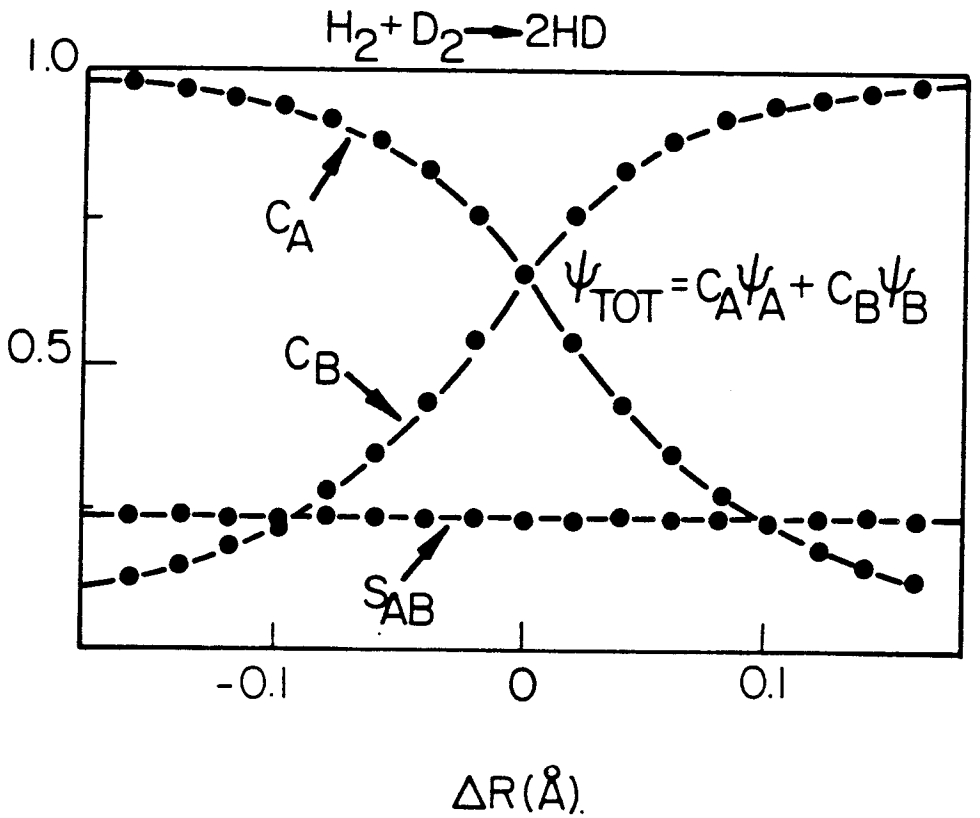

Figure 19. Dependence of C_A, C_B and S_{AB} from an R-GVB wavefunction along the H_2 + D_2 --> 2 HD reaction coordinate. The coordinate is defined as in Figure 18.

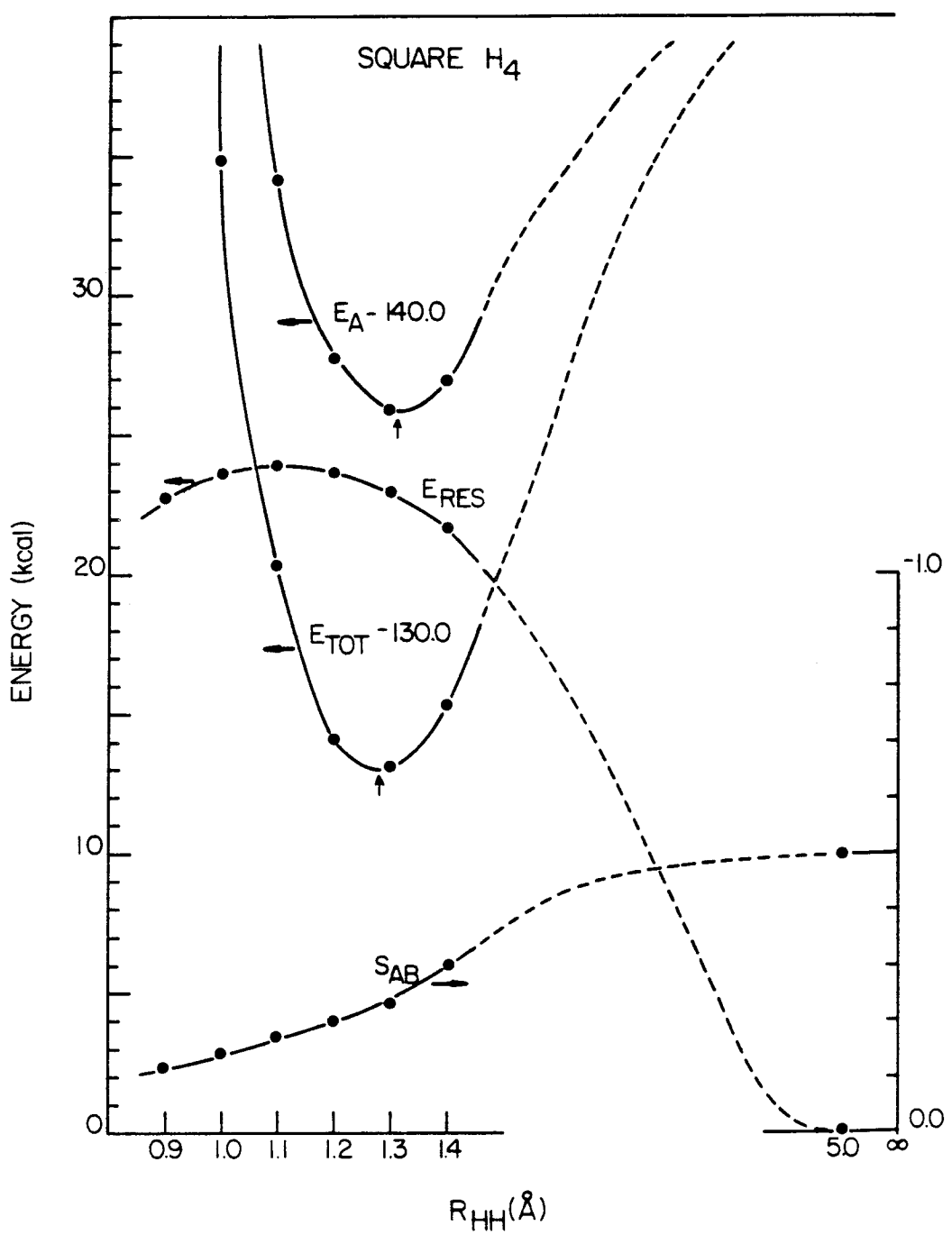

Figure 20. E_A, E_{TOT}, S_{AB} and E_{RES} as a function of symmetric stretch for square H_4.

CHAPTER 6

Core Ionized N_2^+ and Allyl Radical

Preface

The following is a paper which presents the R-GVB method and two applications, the localized core hole states of N_2^+ and the resonance in allyl radical. The description of the method is redundant, since it is presented also as part of Chapter 3 of this thesis.

Chemical Physics 57 (1981) 253–259
North-Holland Publishing Company

A METHOD FOR DESCRIBING RESONANCE BETWEEN GENERALIZED VALENCE BOND WAVEFUNCTIONS

Arthur F. VOTER and William A. GODDARD III
Arthur Amos Noyes Laboratory of Chemical Physics, California Institute of Technology, Pasadena, California 91125, USA*

Received 8 December 1980

In a valence bond (VB) description of wavefunctions there may be several distinct but energetically similar bonding structures. Examples include aromatic molecules (e.g. benzene) and excited states of molecules with equivalent chromophores (e.g. glyoxal). The variational generalization of VB theory, the generalized valence bond (GVB) method, has limitations for such systems since it can only describe one of the bonding structures, allowing no explicit mixing or "resonance" with the other structures. We present herein a method for evaluating the matrix elements necessary to optimize the mixing between the various distinct bonding structures. Evaluation of such matrix elements has heretofore been computationally difficult since the wavefunctions in general have nonzero overlap. Applications of the method are presented for the resonance in allyl radical and the splitting of the localized core hole states of N_2^+.

1. Introduction

For many molecules the natural approach to studying the electronic wavefunction is to superimpose the wavefunctions for various bonding structures. For example,


(1)

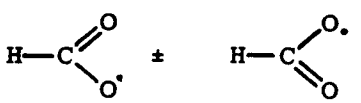
(2)

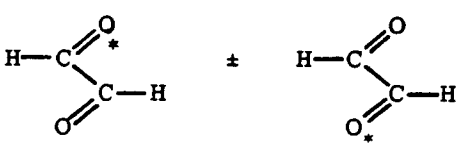
(3)

Unfortunately the wavefunctions for different bonding structures are generally nonorthogonal, leading to severe difficulties in evaluating the energy and in optimizing the orbitals. These difficulties become even more severe when electron correlation effects are included.

In this paper we describe an approach for calculating the interaction of nonorthogonal correlated wavefunctions that does not suffer from the usual computational dependence. In addition, we report applications of this approach to two typical problems:

(a) The resonance of the two equivalent configurations of allyl (1) where each π bond is correlated (GVB level).

(b) The resonance of the 1s core ionization states of N_2

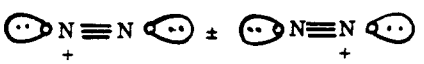

where the core hole is allowed to be localized on one N atom, and the remainder of the molecule is fully correlated (GVB level).

2. The method

Consider a state Ψ involving the superposition of two wavefunctions Ψ^A and Ψ^B,

$$\Psi = C_A\Psi^A + C_B\Psi^B, \tag{4}$$

* Contribution No. 6355.

where Ψ^A and Ψ^B are correlated (multi-configurational) wavefunctions for two possible bonding structures. [For simplicity we consider only two configurations in (4); the generalization to multiple terms is trivial.] Each correlated wavefunction Ψ^A and Ψ^B can be expanded in terms of determinantal wavefunctions $\{\psi_i^A\}$ as

$$\Psi^A = \sum_i C_i^A \psi_i^A, \tag{5}$$

where

$$\psi_i^A = \mathscr{A}\left[\left(\prod_j \phi_j^{iA}\right)\chi_i^A\right]. \tag{6}$$

Assuming that Ψ^A and Ψ^B are normalized, the energy of the wavefunction Ψ is

$$E = \frac{C_A^2 E_A + C_B^2 E_B + 2C_A C_B H_{AB}}{C_A^2 + C_B^2 + 2C_A C_B S_{AB}}, \tag{7}$$

where E_A and E_B are the energies of Ψ^A and Ψ^B, respectively, and

$$S_{AB} = \langle \Psi^A | \Psi^B \rangle = \sum_i \sum_j C_i^A C_j^B \langle \psi_i^A | \psi_j^B \rangle, \tag{8}$$

$$H_{AB} = \langle \Psi^A | \mathscr{H} | \Psi^B \rangle = \sum_i \sum_j C_i^A C_j^B \langle \psi_i^A | \mathscr{H} | \psi_j^B \rangle. \tag{9}$$

Because of the nonorthogonality of the orbitals

$$\{\phi_k^{iA} : k = 1, ..., M\} \tag{10}$$

with

$$\{\phi_k^{jB} : k = 1, ..., M\} \tag{11}$$

the evaluation of terms like $\langle \psi_i^A | \psi_j^B \rangle$ and $\langle \psi_i^A | \mathscr{H} | \psi_j^B \rangle$ would normally involve tedious computation of numerous minors and subminors of the determinant of the overlaps between the A and B sets of orbitals.

The determinantal wavefunctions ψ_i^A and ψ_j^B are invariant (to within a phase) under unitary transformations $\hat{U}^{iA}$ and $\hat{U}^{jB}$ of the orbitals

$$\bar{\phi}_l^{iA} = \sum_k \phi_k^{iA} U_{kl}^{iA}, \quad \bar{\phi}_l^{jB} = \sum_k \phi_k^{jB} U_{kl}^{jB}. \tag{12}$$

Thus, by choosing these transformations so that the new orbitals are biorthogonal [1]

$$\langle \bar{\phi}_k^{iA} | \bar{\phi}_l^{jB} \rangle = \lambda_k \delta_{kl}, \tag{13}$$

we can greatly simplify evaluation of matrix elements such as $\langle \psi_i^A | \mathscr{H} | \psi_j^B \rangle$ and $\langle \psi_i^A | \psi_j^B \rangle$. For a closed-shell configuration (only doubly-occupied orbitals) the same transformations are applied to the α-spin and β-spin orbitals, leading to

$$\langle \psi_i^A | \psi_j^B \rangle = \lambda_1^2 \lambda_2^2, ..., \lambda_n^2, \tag{14}$$

$$\langle \psi_i^A | \mathscr{H} | \psi_j^B \rangle = 2 \sum_k \eta_k \langle \bar{\phi}_k^A | h | \bar{\phi}_k^B \rangle + \sum_{k,l} \eta_{kl} [2(\bar{\phi}_k^A \bar{\phi}_k^B | \bar{\phi}_l^A \bar{\phi}_l^B) - (\bar{\phi}_k^A \bar{\phi}_l^B | \bar{\phi}_l^A \bar{\phi}_k^B)] \tag{15}$$

(where $\bar{\phi}^{iA}$ and $\bar{\phi}^{jB}$ have been denoted simply as $\bar{\phi}^A$ and $\bar{\phi}^B$) and

$$(\phi_i \phi_j | \phi_k \phi_l) \equiv \int d^3 r_1 \int d^3 r_2 \, \phi_i^*(1) \phi_j(1) \phi_k^*(2) \phi_l(2) \tag{16}$$

and

$$\eta_k = (\lambda_1^2 \lambda_2^2 ... \lambda_n^2)/\lambda_k, \quad \eta_{kl} = (\lambda_1^2 \lambda_2^2 ... \lambda_n^2)/\lambda_k \lambda_l. \tag{17}$$

For a more general wavefunction in which the determinants are not closed-shell, the transformations factor into a transformation among α spin orbitals and a different transformation among β spin orbitals (taking care that the transformation does not change the phase). The result in this case is

$$\langle \psi_i^A | \psi_j^B \rangle = \lambda_{1a} \lambda_{2a} ... \lambda_{na} \lambda_{1b} \lambda_{2b} ... \lambda_{mb}, \tag{18}$$

$$\langle \psi_i^A | \mathscr{H} | \psi_j^B \rangle = \sum_{ka} \eta_{ka} \langle \bar{\phi}_{ka}^A | h | \bar{\phi}_{ka}^B \rangle + \sum_{kb} \eta_{kb} \langle \bar{\phi}_{kb}^A | h | \bar{\phi}_{kb}^B \rangle + \sum_{ka>la} \eta_{ka,la} [(\bar{\phi}_{ka}^A \bar{\phi}_{ka}^B | \bar{\phi}_{la}^A \bar{\phi}_{la}^B) - (\bar{\phi}_{ka}^A \bar{\phi}_{la}^B | \bar{\phi}_{la}^A \bar{\phi}_{ka}^B)] + \sum_{kb>lb} \eta_{kb,lb} [(\bar{\phi}_{kb}^A \bar{\phi}_{kb}^B | \bar{\phi}_{lb}^A \bar{\phi}_{lb}^B) - (\bar{\phi}_{kb}^A \bar{\phi}_{lb}^B | \bar{\phi}_{lb}^A \bar{\phi}_{kb}^B)] + \sum_{ka,lb} \eta_{ka,lb} (\bar{\phi}_{ka}^{iA} \bar{\phi}_{ka}^{jB} | \bar{\phi}_{lb}^{iA} \bar{\phi}_{lb}^{jB}), \tag{19}$$

where ka, la indicate orbitals corresponding to α spin, kb, lb indicate orbitals corresponding to β spin

$$\eta_{ka} = \langle \psi_i^A | \psi_j^B \rangle / \lambda_{ka} \tag{20a}$$

and

$$\eta_{ka,lb} = \langle \psi_i^A | \psi_j^B \rangle / \lambda_{ka} \lambda_{lb}. \tag{20b}$$

Thus the S_{AB} and H_{AB} of eqs. (8) and (9) can be evaluated by applying the above formulae to each pair of determinants (for an open-shell system, this requires four separate transformations to biorthogonal orbitals). For a GVB wavefunction in which each of n bonds is correlated with two natural orbitals, the resulting GVB($n/2n$)-PP wavefunction can be written as

$$\mathscr{A}\{[\text{core}][C_{a1}\phi_{a1}^2 + C_{b1}\phi_{b1}^2][C_{a2}\phi_{a2}^2 + C_{b2}\phi_{b2}^2]\ldots$$
$$\ldots [C_{an}\phi_{an}^2 + C_{bn}\phi_{bn}^2]\}, \qquad (21)$$

leading to 2^n determinants. [This leads to the evaluation of 2^{2n} terms of the form (8) and (9).] The approach can, of course, be applied to find H_{AB} between any two multiconfigurational wavefunctions.

Wavefunctions obtained by this procedure are referred to as resonating generalized valence bond or R-GVB.

The computational time required for the allyl case (13 orbitals per wavefunctions, four determinant pairs) was 105 s of CPU on a VAX 11/780, to be compared with 1300 s required to calculate the integrals over 37 gaussian basis functions and 936 s to converge the GVB 1/2 wavefunction (19 iterations).

3. Allyl radical

There are two bonding structures for allyl radical (H_2C—CH—CH_2), namely,

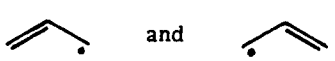

(22)

That is, the π bond can be on the left or right, and the π radical orbital is on the opposite center. These wavefunctions can be combined into a resonance (stabilized) form

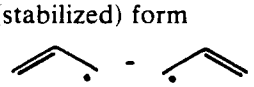

(23)

and an antiresonance (destabilized) form

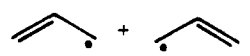

(24)

The experimental consequence of this resonance stabilization is that the CH bond energy of propene

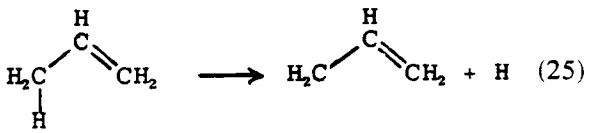

(25)

is 87 kcal [2], whereas a terminal CH bond for an alkane would normally be 98 kcal [2]. This difference, 11 kcal, is generally referred to as the resonance energy. It need not be identical to the resonance stabilization of (23) for reasons discussed later in this section.

The wavefunctions for the bonding structures in (22) are

$$\psi_\ell = \mathscr{A}\{[\sigma_1](\phi_\ell\phi_c + \phi_c\phi_\ell)\phi_r\alpha\beta\alpha\}$$

and (26)

$$\psi_r = \mathscr{A}\{[\sigma_r](\phi_r\phi_c + \phi_c\phi_r)\phi_\ell\alpha\beta\alpha\}$$

(where only the π electrons are written explicitly), each containing a two-electron π bond to the central atom. Optimizing the orbitals of ψ_ℓ and ψ_r leads to π orbitals ϕ_ℓ, ϕ_c, and ϕ_r that are different between ψ_ℓ and ψ_r. Fig. 1 shows the π orbitals for ψ_ℓ. The energies for the resonant and antiresonant states are given by

$$E_{res} = (H_{\ell\ell} - H_{\ell r})/(1 - S_{\ell r}) = H_{\ell\ell} - \epsilon_r,$$
$$E_{anti} = (H_{\ell\ell} + H_{\ell r})/(1 + S_{\ell r}) = H_{\ell\ell} + \epsilon_a, \qquad (27)$$

where

$$H_{\ell\ell} = H_{rr} = \langle\psi_\ell|\mathscr{H}|\psi_\ell\rangle, \quad S_{\ell r} = \langle\psi_\ell|\psi_r\rangle,$$
$$H_{\ell r} = \langle\psi_\ell|\mathscr{H}|\psi_r\rangle \qquad (28)$$

and the resonance energy ϵ_r and antiresonant energy ϵ_a are defined. Note that the σ orbitals of ψ_ℓ and ψ_r are also slightly different, an effect that *is* included in these calculations.

The results are in table 1. Mixing the GVB wavefunctions ψ_ℓ and ψ_r yields $S_{\ell r} = -0.754$ and $H_{\ell r} = 87.763$ hartree, leading to a resonance energy $\epsilon_r = 9.8$ kcal. This resonance energy does not correspond exactly to the experimental value for three reasons. First, the experimental resonance energy is obtained by comparing two bonds with different steric interactions. Second, the experimental resonance energy includes the energy required to change the geometry from one long carbon–carbon single bond and one

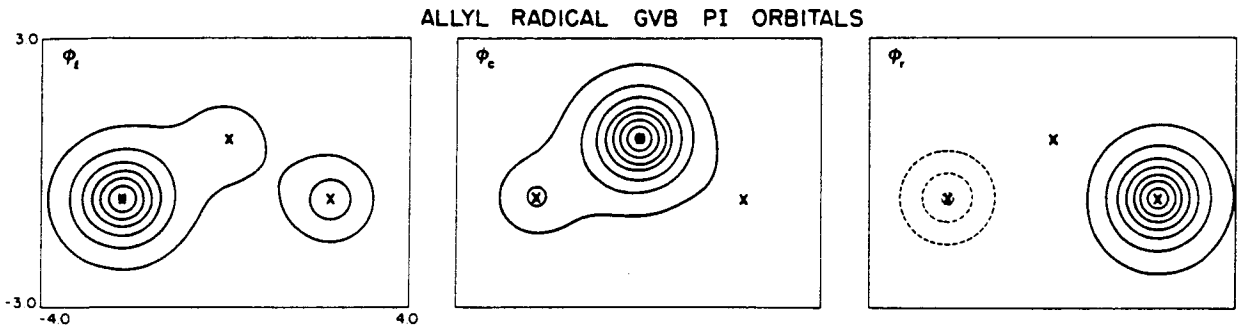

Fig. 1. GVB π orbitals for the localized wavefunction of allyl radical ψ_ℓ (26). The overlap between the paired orbitals ϕ_ℓ and ϕ_c is 0.719. The plotting plane is 0.5 bohr above the molecular plane with projected carbon atom positions indicated for clarity. The amplitude increment is 0.05 au.

short double bond to a symmetric geometry that can maximize electronic resonance. This acts to decrease the perceived resonance energy. Third, the ϵ_r we define compares the energy of the optimized GVB wavefunction ψ_ℓ with the wavefunction Ψ_{res} in which the orbitals have not been reoptimized in the presence of the resonance. Including this reoptimization would increase ϵ_r. The close agreement between ϵ_r (9.8 kcal) and experiment (11 kcal) implies that these effects roughly balance. Work directed at quantifying these effects is currently in progress. Previous studies of the resonance in allyl using the full GVB method [3] (including optimization of spin coupling) yielded a resonance energy of 11.4 kcal. Use of a spatially projected GVB [4] wavefunction gave a value of 14.3 kcal. Each of those calculations used a frozen symmetric σ core taken from a Hartree–Fock (HF) calculation, as optimization of the σ orbitals was not feasible at that level of calculation.

The antiresonance energy ϵ_a is found to be 69.9 kcal, and decreases to 65.6 kcal if the GVB natural orbital coefficients are allowed to readjust in the presence of the resonance. This leads to a $^2A_2 \rightarrow {}^2B_1$ excitation energy of 75.6 kcal, which compares very well with the full π configuration interaction (CI) result of 75.4 kcal, indicating that the resonant–antiresonant description of these states is valid.

Table 1
Energies for allyl wavefunctions [a,b]

Calculation	Single bonding structure ($H_{\ell\ell}$) (hartree)	Resonance state ($^2A_2$) (hartree)	Resonance energy (ϵ_r) (kcal)	Antiresonance energy (ϵ_a) (kcal)	Excitation energy $^2B_1 \leftarrow {}^2A_2$ (kcal)
HF	−116.4130	−116.4129 [f]	–		114.1
R-GVB [c]	−116.4296	−116.4452	9.8	69.9	79.7
R-GVB(r) [d]		−116.4454	10.0	65.6	75.6
full π CI [e]		−116.4596	–	–	75.4

[a] All calculations use the symmetric geometry R(CC) = 1.40 Å, R(C—H) = 1.08 Å, all angles 120°.
[b] All calculations use the Dunning–Huzinaga valence double zeta basis (9s/5p) contracted to (3s/2p) for C and the scaled basis for H 4s to 2s (scaled by 1.2).
[c] One π bond was correlated, as indicated in (26).
[d] The CI coefficients for the natural orbital expression of the GVB wavefunction [see (21)] were allowed to reoptimize after including resonance. This is still rigorously a GVB wavefunction.
[e] The σ core was taken from the HF wavefunction of the $^2A_2$ state.
[f] Note that the symmetry-restricted HF solution has an energy 0.0001 hartree higher than the best HF wavefunction.

While a CI calculation can produce the most accurate results for a given basis set, it cannot yield conceptually important quantities like ϵ_a and ϵ_r.

4. Core ionization of N_2

Molecular orbitals of symmetric molecules are generally taken as symmetry functions for the symmetry group of the molecule. While this is appropriate for closed-shell molecules, some spectacular failures are known for open-shell molecules, where imposing symmetry upon the molecular orbitals leads to a much higher energy than if symmetry is relaxed. Well known examples include the lowest ionization of pyrazine [5],

(29)

and the singlet state of trimethylene methane [6],

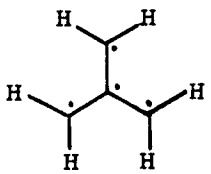

(30)

A similar difficulty occurs upon ionizing electrons from core orbitals. Thus, for N_2 the ionization potential out of the 1s orbital is predicted to be almost 10 eV higher when symmetry orbitals are used to describe the ion state than when localized orbitals are used [7].

This indicates that the nature of the core ionized state is really that of a localized hole, which we can understand in the following way. The contribution each valence electron makes to the total energy goes roughly as the square of the effective nuclear charge (Z_{eff}) the electron "sees" (assuming hydrogenic behavior). For the case of the delocalized hole, each valence electron sees a new effective charge of $Z_{eff}+0.5$, while for the localized case half the valence electrons see $Z_{eff}+1.0$, while the other half see Z_{eff}. Since $(Z_{eff}+1.0)^2-Z_{eff}^2$ is always greater than $2[(Z_{eff}+\frac{1}{2})^2-Z_{eff}^2]$, more energy is gained by the localized hole. This is borne out by the fact that the relaxation energy for the localized ion is 16.5 eV (Koopmans' IP versus direct HF), which is very close to the 15.3 eV relaxation energy of the 1s ionized nitrogen atom, while the delocalized relaxation energy for N_2 is only 7.3 eV. While the core ion state has the nature of a localized hole, the total wavefunction should still retain the full molecular symmetry, and does if we take the linear combinations

$$\psi_g = \psi_\ell + \psi_r \tag{31a}$$

and

$$\psi_u = \psi_\ell - \psi_r, \tag{31b}$$

where ψ_ℓ and ψ_r are the overlapping localized core hole wavefunctions.

The results of various calculations are shown in table 2. Calculations were carried out treating the neutral and ion states both at the HF level and with all valence electrons correlated, GVB(5/10). For the neutral the latter calculation leads to three bond pairs (σ, π_x, π_y) and two lone pairs ("2s") localized one on each N,

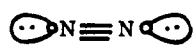

(32)

The delocalized HF calculations not only lead to an ionization potential 9.2 eV too large but they also lead to a g–u splitting energy 50% too large (0.126 versus 0.082 eV). Correlating the valence electrons leads to a slight decrease (0.32 eV) in the ionization potential and a slight increase in the splitting energy (0.082–0.093 eV). The final calculated ionization potential is 409.84 eV, in good agreement with the experimental value of 409.9 eV [8]. Such close agreement is fortuitous since correlation of the electron pair in the 1s orbital being ionized was not included (this would increase the ionization potential by $\approx$1 eV). Probably this error is balanced by some inadequacy in the basis set for describing the shape readjustment in the ion.

The very small resonant splittings are due to the very small overlap ($S_{\ell r}=0.0023$) of the localized wavefunctions in (32).

Table 2
Ionization potentials for N_2 [a]

	Level	Neutral ground state total energy (hartree)	Ionization potential (eV)			Splitting energy (eV)
			localized	$^2\Sigma_u^-$	$^2\Sigma_g^+$	
Basis I [b]						
	Koopmans' IP		427.59 [f]	427.54	427.64	0.096
	delocalized HF	−108.9059	–	420.28	420.41	0.124
	localized HF		411.05	411.01 [e]	411.09 [e]	0.082
	GVB 5/10	−109.0049	410.65	410.63 [e]	410.72 [e]	0.090
Basis II [c]						
	Koopmans' IP		426.81 [f]	426.76	426.86	0.095
	delocalized HF	−108.9808	–	419.41	419.53	0.126
	localized HF		410.16	410.12 [e]	410.20 [e]	0.082
	GVB 5/10	−109.0731	409.84	409.79 [e]	409.88 [e]	0.093
	experiment [d]			409.9		

[a] All calculations performed at experimental ground state geometry ($R_e = 1.09768$ Å) [12].
[b] Basis I is Huzinaga's (11s/7p) primitive gaussian basis contracted to (7s/4p), allowing four functions to describe the 1s orbital.
[c] Basis II is Huzinaga's (11s/7p) primitive gaussian basis contracted to (7s/5p) plus an optimized d exponent of 0.9 (further decontraction of the s and p was found unnecessary).
[d] Ref. [9]. [e] These numbers result from the resonance of two overlapping wavefunctions.
[f] Localized Koopmans' IP values were obtained by forming a localized $\phi_{1s} = 2^{-1/2}(1\sigma_g + 1\sigma_u)$ and evaluating the ion energy with frozen orbitals.

Many previous calculations on core hole states of first-row diatomics have been performed [7–10] and the need for a localized description has been well established. The calculations presented here are the first to restore full symmetry to the ionic states while retaining a localized description.

Müller et al. [7] have studied the effect of core hole localization on the predicted lineshape of the photoelectron peak. They found that while a delocalized hole predicts a linewidth too large by ≈80%, a localized hole description predicts a linewidth of 0.32 eV, in reasonable agreement with the experimental value of 0.42 eV. This agreement becomes even closer if one includes the peak broadening due to the 0.093 eV state splitting we calculate.

5. Discussion

One of the first studies of the importance of symmetry lowering in HF wavefunctions was the work by Wadt and Goddard [5] on the n ion and $n\pi^*$ excitation states of pyrazine. They showed that the optimized wavefunction is localized but did not calculate the resonance energy by the R-GVB procedure. Instead, they converted the localized orbitals into a double set of symmetry orbitals and designed a CI calculation to mimic a resonating wavefunction. Recently Martin [11] tested these results for the positive ion by calculating the resonance energy of the localized HF wavefunction in the same fashion described in section 2. He found resonance energies essentially identical to those of Wadt and Goddard.

We have generalized this treatment to allow calculation of resonance interactions for correlated multiconfigurational wavefunctions. This is important since many electronic states are not adequately described at the HF level. This method is not limited to resonance of equivalent configurations, allowing treatment of resonance as a function of geometry, as in rectangular cyclobutadiene,

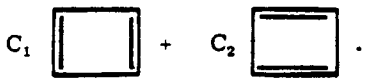

The remaining flaw in the resonating GVB approach is that the orbitals are calculated before resonating. As a result, the orbitals tend to delocalize in order to incorporate part of the resonance effect. We are currently developing an approach in which the orbitals are optimized in the presence of resonance, thus allowing each orbital to have the optimum shape for a particular localized form. This approach is more difficult than the usual self-consistent field methods because of the overlapping orbitals. It will be especially useful for cases where the delocalization tendency is so strong that the conventional wavefunction is totally delocalized.

We believe that the resonating GVB method will be useful both for quantitative and conceptual progress in analyzing wavefunctions. With this method, many complicated electronic states that previously required extensive CI calculations may be adequately described in terms of a small number of meaningful resonance contributors, a picture that is conceptually simple and chemically appealing.

Acknowledgement

The work was partially supported by a contract from the US Department of Energy (Contract No. DE-AC03-76SF00767, Project Agreement No. DE-AT03-80ER10608). The research reported in this paper made use of the Dreyfus-NSF Theoretical Chemistry Computer which was funded through grants from the Camille and Henry Dreyfus Foundation, the National Science Foundation (Grant No. CHE78-20235), and the Sloan Fund of the California Institute of Technology.

References

[1] W.A. Goddard III, J. Chem. Phys. 48 (1968) 450, and references therein.
[2] S.W. Benson, Thermochemical kinetics, 2 Ed. (Wiley, New York, 1976) p. 309.
[3] G. Levin and W.A. Goddard III, J. Am. Chem. Soc. 97 (1975) 1649.
[4] G. Levin and W.A. Goddard III, Theoret. Chim. Acta (Berl.) 37 (1975) 253.
[5] W.R. Wadt and W.A. Goddard III, J. Am. Chem. Soc. 97 (1975) 2034.
[6] D.R. Yarkony and H.F. Schaefer III, J. Am. Chem. Soc. 96 (1974) 3754.
[7] J. Müller, H. Agren and O. Goscinski, Chem. Phys. 38 (1979) 349.
[8] K. Siegbahn, C. Nordling, G. Johansson, J. Hedman, P.F. Hedén, K. Hamrin, U. Gelius, T. Bergmark, L.O. Werme, R. Manne and Y. Baer, eds., ESCA applied to free molecules (North-Holland, Amsterdam, 1969).
[9] P.S. Bagus and H.F. Schaefer III, J. Chem. Phys. 56 (1972) 224.
[10] H. Agren, L. Selander, J. Nordgren, C. Nordling, K. Siegbahn and J. Müller, Chem. Phys. 37 (1979) 161, and references therein.
[11] R.L. Martin, W.R. Wadt and D.A. Kleier, Abstract of Talks Presented at the Second Annual West Coast Theoretical Chemistry Conference, California Institute of Technology, Pasadena, California, 9–11 April 1980.
[12] K.P. Huber and G. Herzberg, Molecular spectra and molecular structure: Constants of diatomic molecules (Van Nostrand, Princeton, 1979).

CHAPTER 7

The Resonating Valence Bond Description of Three-Electron Bonds

I. Introduction

Three-electron bonds are quite common in chemical systems,[1] and are often quite strong. Examples include the π system in O_2, the noble gas dimer ions, and sulfur radical cations.[2] It was proposed by Pauling over 50 years ago that the strength of such bonds lies in the ability of the system to resonate between two forms,

$$\ddot{A}\dot{B} \leftrightarrow \dot{A}\ddot{B} \qquad (1)$$

This resonance will be largest if the two forms are equivalent in energy, as is evident from the bond energies shown in Table 1. The homonuclear ions Ne_2^+, F_2^-, Ar_2^+, and Cl_2^-, in which the two forms in (1) are isoenergetic, each have a bond of $\approx$30 kcal, while the mixed species NeF and ArCl have almost no bond, due to the instability of the resonance structure

$$Ne^- F^+.$$

This resonance is also important in the O_2 π system, causing a discrepancy between the O-H bond energy in OOH and HOOH. The first hydrogen approaching O_2 must disrupt the resonance to form a bond,

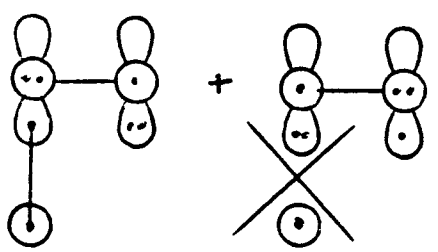

while the second bond to a hydrogen causes no loss in resonance (assum-

ing the $H-\overset{+}{O}-\overset{-}{O}$ structure is unimportant). The first bond is worth 45.6 kcal, while the second is 88.7 kcal, consistent with a resonance energy of 43.1 kcal.[4] Thus, the evidence seems consistent with a resonating valence bond model of three-electron bonds. In this chapter we examine two prototype three-electron bond systems, He_2^+ and Ne_2^+, using the resonating generalized valence bond (R-GVB) and generalized resonating valence bond (GRVB) methods. These *ab initio* approaches allow us to describe the resonance in a conceptually straight-forward fashion.

II. Calculational Details

The He_2^+ calculations were performed using Huzinaga's 7*s* gaussian basis[5] contracted to 4*s*,[6] augmented by a *p* polarization function with exponent 1.0. This basis gives a Hartree-Fock(HF) total energy of −1.999741 hartree for He^+, and −2.861491 hartree for He. The Ne_2^+ calculations employed the Huzinaga 9*s*5*p* basis[5] contracted to valence double zeta (3*s*.2*p*) by Dunning.[7] This basis yields an energy of −127.79338 hartree for Ne_2^+ (HF), and −128.52235 hartree for Ne atom (HF). The programs used to perform the various calculations are described elsewhere.[8] The GRVB calculations on Ne_2^+ employed a frozen 1*s* orbital on each Ne atom, taken from the symmetric HF wavefunction at the same geometry, but all other orbitals were optimized. This restriction was found to have an effect of less than 10^{-6} hartree on the energy of a localized HF wavefunction at $R = 100.0$ Å (the most critical test).

The "Valence Bond" (VB) wavefunction listed in Table 2 consists of the properly antisymmetrized product of orbitals taken from separate HF calculations on He and He^+. Thus,

$$\Psi^{VB} = A[\varphi_{He}^2 \varphi_{He^+} \alpha\beta\alpha] \ , \qquad (2)$$

where φ_{He^+} has been Schmidt-orthogonalized to φ_{He}. The R-VB calculation is simply the resonance of Ψ_{VB} with its spatially reflected form (i.e. corresponding to (1)). The gR-VB wavefunction is the R-VB wavefunction which has orbitals optimized in two-dimensional space composed of φ_{He} and φ_{He^+}. This optimization is performed via a parameter, λ, which mixes φ_{He} and φ_{He^+},

$$\varphi'_{He} = \varphi_{He} + \lambda\varphi_{He^+} \tag{3a}$$

$$\varphi'_{He^+} = \varphi_{He^+} - \lambda\varphi_{He} \quad . \tag{3b}$$

(ignoring normalization), and we find that the optimum value for λ is -1.1, corresponding to a node in the doubly-occupied orbital, as observed in the GRHF wavefunction.

III. Results and Discussion - He_2^+

Because the He_2^+ system has so few electrons, the best ab initio results are in excellent agreement with experiment. The extended-basis full CI calculations of Liu[9] yield a bond energy (D_e) of 56.4 kcal, while the experimental value is 56.9 kcal.[10] Because we will be comparing various conceptually simple wavefunctions which have only sigma orbitals occupied, we will take the "correct" bond energy to be 54.1 kcal, the result of a full CI in the sigma space of our basis set. The very good agreement with the near-exact result of Liu implies that we are not excluding any conceptually important portion of the wavefunction. In the simplest ab initio description of the bonding process, we allow one orbital for the two He electrons and one orbital for the one electron on He^+, and let these orbitals take any shape as R is varied. This is simply the Hartree-Fock (HF) wavefunction,

$$\Psi^{HF} = A[\varphi_1^2\varphi_2\alpha\beta\alpha], \tag{4}$$

and leads to a bond energy of 37.7 kcal, as shown in Table 2. The optimum orbitals in this wavefunction are symmetric (i.e. φ_1 is φ_g and φ_2 is φ_u), just as in Molecular Orbital Theory.

We wish to describe resonance in this system, and the simplest resonating wavefunction consists of allowing the optimum shape for φ_1 and φ_2, while simultaneously mixing in the other resonance structure. We call this a generalized resonating HF (GRHF) wavefunction, written as

$$\Psi^{GRHF} = A[\varphi_1^2\varphi_2\alpha\beta\alpha] - A[\varphi_1^2\varphi_2\alpha\beta\alpha] \tag{5}$$

where φ_1 and φ_2 are generated from φ_1 and φ_2 via the spatial reflecton operator which is perpendicular to the bond axis,

$$\varphi_1 = \hat{R}\,\varphi_1 \tag{6a}$$

$$\varphi_2 = \hat{R}\,\varphi_2 \tag{6b}$$

While the HF wavefunction included a certain amount of resonance through orbital delocalization, the GRHF wavefunction includes resonance explicitly, allowing the orbitals to localize, as shown in Fig. 1. Notice that the doubly occupied φ_1 has a node while φ_2 does not. This is contrary to the usual behavior of SCF wavefunctions. This may indicate that the GRHF wavefunction is including some extra correlation energy beyond that expected from the form in (5). Further evidence for this is the fact that Ψ_{GRHF} remains partially delocalized at infinite R, leading to a total energy 1.6 kcal lower than Ψ^{HF}. This is surprising, since infinitely separated He and He^+ would not be expected to interact, so that the "resonance energy" should be zero. Thus, this extra 1.6 kcal is presumably describing some atomic correlation. If we assume that this atomic correlation energy is independent of R, then we can obtain a valid GRHF

bond energy by comparing the short-R GRHF energy to the long-R GRHF energy, thus cancelling out the extra correlation effect. This leads to a bond energy of 55.5 kcal, 1.4 kcal greater than the σ - full CI bond. Since bond energies are usually low when the correlation is not complete, we can infer that the GRHF wavefunction still contains more correlation at the molecular geometry than at long R. If instead of resonating two HF wavefunctions, we resonate two correlated wavefunctions, this effect should diminish. The dominant correlation in He atom is in-out, describable with a GVB(1/2) wavefunction, and the orbitally optimized resonance of two GVB(1/2) wavefunctions is a GRVB(1/2) wavefunction. The GRVB(1/2) wavefunction leads to a bond energy of 53.8 kcal, and gives the same energy at large R as a GVB(1/2) wavefunction. Thus the delocalization at large R is no longer necessary once the dominant in-out correlation is explicitly included in the wavefunction.

We can get another estimate of the magnitude of the extra correlation in the short-R GRHF wavefunction by using a VB wavefunction. The VB wavefunction is restricted to have the orbital shapes from atomic He and He^+ wavefunctions. The VB wavefunction leads to a bond energy of -40.8 kcal, while the R-VB bond is 38.4 kcal. Clearly, resonance is important in this wavefunction. Since the R-VB wavefunction has frozen orbital shapes, it cannot contain any of the extra correlation that the GRHF wavefunction apparently has. Letting the two VB orbitals mix with each other (gR-VB, see calc. details section) leads to a node in φ_1, just as in the GRHF wavefunction, so we can infer that this gR-VB wavefunction is including the same type of atomic correlation as GRHF. The difference in energy between R-VB and gR-VB is only 1.0 kcal, so the magnitude of this effect is small.

IV. Results and Discussion - Ne_2^+

The results for Ne_2^+ are similar to those of He_2^+, as shown in Table 3. One difference is that the short-R HF wavefunction for Ne_2^+ chooses to be localized, leading to an energy 6.2 kcal lower than the symmetry restricted HF wavefunction.[11] The localization force is stronger in Ne_2^+ because there are more electrons in the system which can relax in response to the localized hole. For systems such as core ionized N_2^+, this relaxation energy is 10 eV, as discussed in Chapter 6, Section 4. Because the HF wavefunction is localized, we can test the effect of resonance without reoptimizing the orbitals, by using an R-HF wavefunction. This leads to a bond energy of 11.6 kcal, a resonance lowering of 10.2 kcal. Optimizing the orbitals in a GRHF calculation leads to a bond energy of 30.1 kcal, in good agreement with the CI results of Cohen and Schneider[12] (27.7 kcal), and the experimental value of 31.2 kcal.[13] Because of the size of the Ne_2^+ system, we cannot perform a full CI in our basis to use as a reference energy. Figure 2 shows the R dependence of the various wavefunctions, and as expected, the GRHF wavefunction leads to a shorter bond than HF, because the resonance is stronger at shorter R.

As in He_2^+, the GRHF wavefunction dissociates to a wavefunction which is lower in energy than HF, and the effect is larger for Ne_2^+ due to the extra electrons. Thus, for both of these cases, we needed to correct for this extra correlation energy by using the GRHF wavefunction at all bond distances. In the GRVB description of reactions,[14] we did not encounter this problem, so that the GRVB wavefunction near the transition state was appropriate for comparison to a GVB wavefunction at the separated limits. The GRVB wavefunction is equivalent to GVB at the reaction limits because only one subwavefunction is dominant, while the other

subwavefunction corresponds to a "bad" bonding structure at higher energy,

Also, the anomalous nodal structure found in He_2^+ and Ne_2^+ was not observed in the transition state wavefunctions.

V. Conclusions

We have examined the prototype three-electron bond systems He_2^+ and Ne_2^+, using the resonating valence bond model,

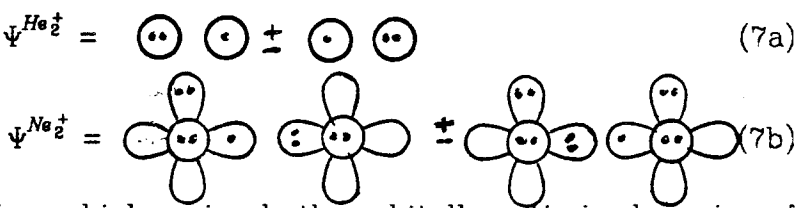

The GRHF wavefunction, which is simply the orbitally-optimized version of (7a) or (7b), leads to quantitative accuracy for the total bond energy in each system, indicating the validity of this model. In the Ne_2^+ system, the resonance is responsible for almost all the bonding, while the He_2^+ wavefunction is harder to dissect due to the unknown amount of resonance present in the delocalized Hartree-Fock wavefunction. Thus, we understand why the mixed-atom systems in Table 1 have essentially no bond - they have no resonance.

The GRHF wavefunction is found to include some extra correlation energy beyond the "resonance energy", but this effect can be cancelled by using the GRHF wavefunction at all bond distances.

References

1) N.C. Baird, J. Chem. Ed. **54,** 291 (1977)

2) M. Bonifacic and K.-D. Asmus, J. Chem. Soc. Perkins Trans. II, 758 (1980)

3) K.P. Huber and G. Herzberg, *Molecular Spectra and Molecular Structure, Vol. 4, Constants of Diatomic Molecules*, (Van Nostrand Reinhold Co., New York 1979)

4) D.D. Wagman, W.H. Evans, V.B. Parker, I. Halow, S.M. Bailey and R.H. Schumm, N.B.S. Tech. Note 270-3 (Inst. for Basic Standards, Nat. Bur. Stand. (U.S.) 1968)

5) S. Huzinaga, J. Chem. Phys. **42,** 1293 (1965)

6) We employed a 3111 contraction.

7) T.H. Dunning, Jr. and P.J. Hay, in: *Modern Theoretical Chemistry, Vol. 3, Methods of Electronic Structure Theory*, edited by H.F. Schaeffer III (Plenum, New York 1977), Chap. 1

8) See Chapter 5, Section II-B of this thesis.

9) B. Liu, Phys. Rev. Lett. **27,** 1251 (1971)

10) For interpretation of and references to the experimental results, see Reference 9.

11) It is interesting to note that symmetric Hartree-Fock gives a very accurate representation of the potential curve if it is shifted downward by the amount that HF misdescribes the separated limit.

12) J.S. Cohen and B. Schneider, J. Chem. Phys. **61,** 3230 (1974)

13) H.-U. Mittman and H.-P. Wise, Z. Naturforsch. **29a,** 400 (1974); L. Frommhold and M.A. Biondi, Phys. Rev. **185,** 244 (1969)

14) See Chapter 5 of this thesis.

Table 1: Some Three-Electron Bond Energies (kcal).

Molecule	D_0[a]
He_2^+	54.6
H_2^-	20-40
Ne_2^+	30.0
F_2^-	29.5
Ar_2^+	30.7
Cl_2^-	29.1
HeH	<0.1
NeF	not observed
ArCl	very weak

[a] Reference 3.

Table 2. He_2^+ Bond Energies.

Wavefunctions				
He_2^+	He	He^+	$E(He_2^+)$[a]	D_e (kcal)
Hartree-Fock	HF	HF	-4.92128	37.7
GRHF	HF	HF	-4.95222	(57.1)
GRHF	GRHF		-4.95222	55.5
GRVB(1/2)	GVB(1/2)	HF	-4.9631	53.8
GRVB(1/2)	GRVB(1/2)		-4.9631	53.8
VB[b]	HF	HF	-4.79621	-40.8
R-VB[c]	HF	HF	-4.92249	38.4
gR-VB[d]	HF	HF	-4.92399	39.4
σ-full CI	σ-full CI		4.970055	54.1
full CI[e]	full CI		-4.99389	56.4
experiment[f]				56.9

[a] At R = 1.09 Å.

[b] The VB wavefunction is defined as an atomic He^+ orbital orthogonalized to an atomic He orbital.

[c] R-VB is the resonance mixing of the VB wavefunction.

[d] gR-VB is an "optimized" version of R-VB, in which the two VB atomic orbitals (after orthogonalization) are rotated with each other. The optimum rotation angle is $\lambda = -0.124$.

[e] B. Liu (Ref. 1) 4s, 3p, 2d, 1f basis at 1.08 Å.

[f] Reference 10.

Table 3. Ne_2^+ Bond Energies.

Wavefunctions						
Ne_2^+	Ne	Ne^+	Basis	$E(Ne_2^+)$[a]	R (Å)	D_e (kcal)
HF (sym.)[b]	HF	HF	DZ	0.30663	1.75[d]	-5.8
HF (loc.)[c]	HF	HF	DZ	0.31801	2.12	1.4
R-HF	HF	HF	DZ	0.33311	1.75	11.6
GRHF	HF	HF	DZ	0.38026	1.77[d]	(40.5)
GRHF	GRHF		DZ	0.38026	1.77	30.1
CI[e]					1.75	27.7
Experiment						31.2

[a] To obtain total energy in hartrees, subtract these values from -256.0.

[b] Hartree-Fock with full symmetry imposed on orbitals.

[c] Hartree-Fock with broken symmetry.

[d] Optimized geometry.

[e] Cohen and Schneider, Ref. 13.

HARTREE-FOCK

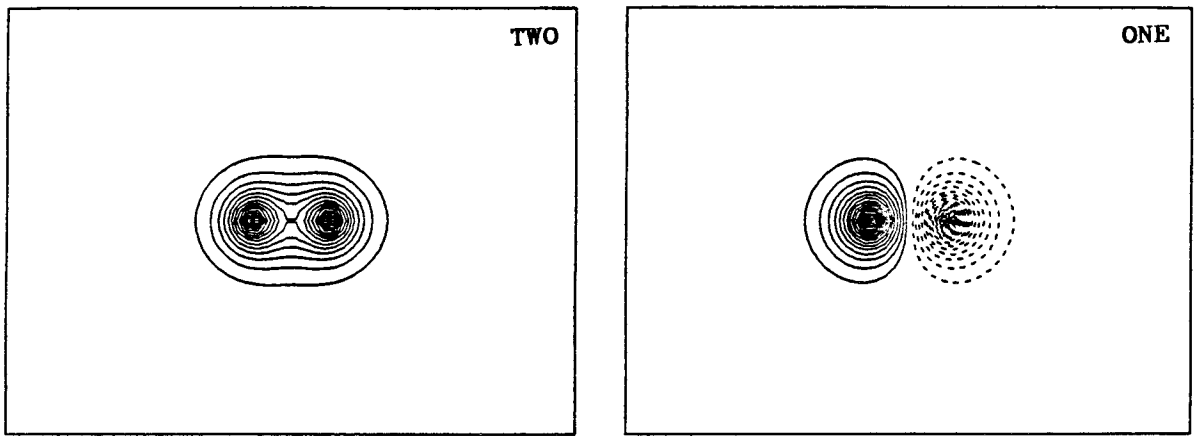

GRFH

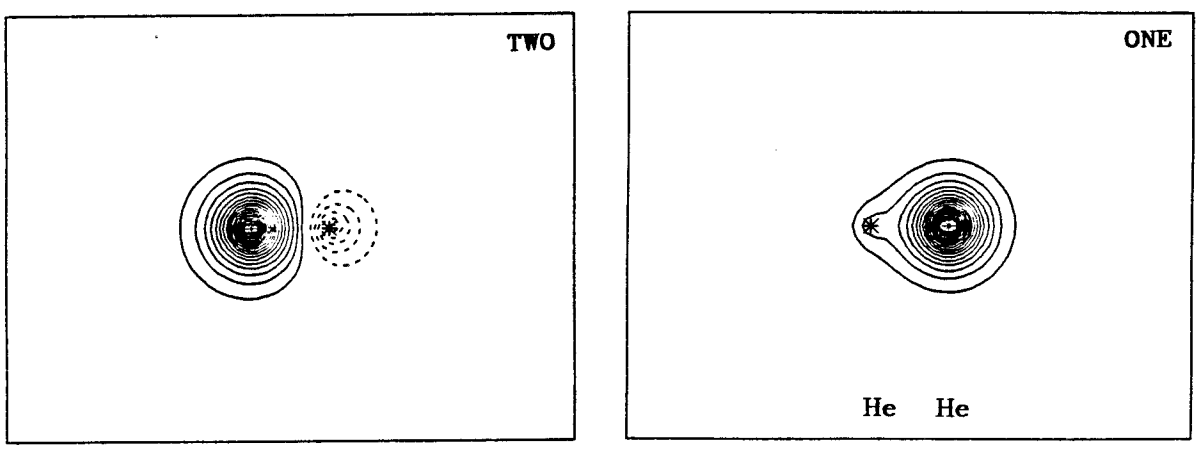

Figure 1. The HF (top) and GRHF (bottom) orbitals for He_2^+. The orbitals in the other GRHF subwavefunction are not shown.

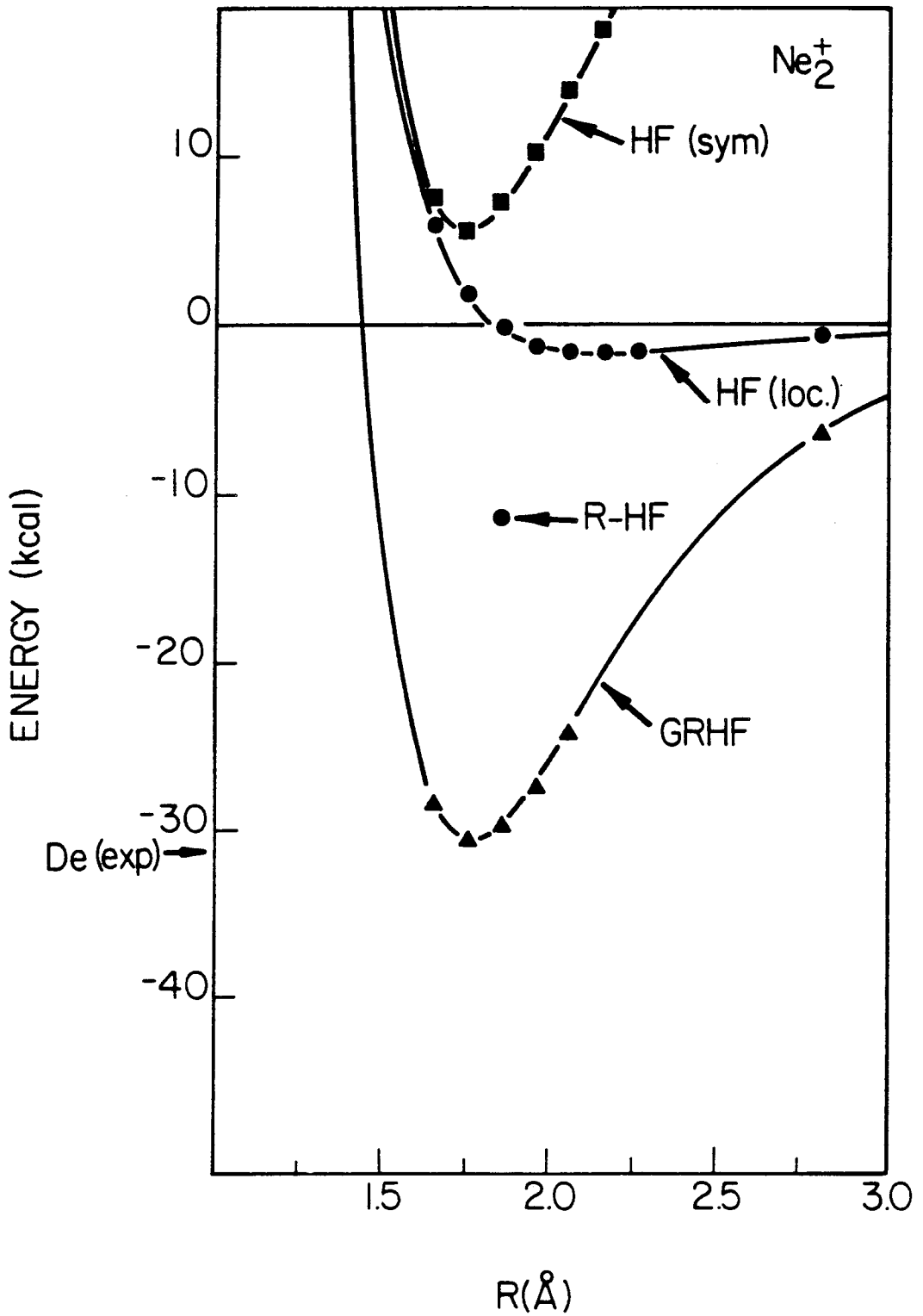

Figure 2. Energies of various Ne_2^+ wavefunctions.

Thesis Conclusions

We are encouraged by the results presented in the preceding chapters, and feel that the R-GVB and GRVB approaches will lead to quantitative and conceptual progress in understanding a variety of chemical systems. The accuracy of GRVB in describing reaction transition states and three-electron bonds is strong testimony to the validity of the resonating VB model.

The GRVB method increases by one the number of classes of systems which can be accurately represented with a conceptually simple wavefunction. For atoms, the Hartree-Fock (HF) wavefunction is generally an appropriate description; it is not unreasonable to envision two electrons in each atomic orbital. In describing a covalent bond, the HF wavefunction is inadequate, because the wavefunction dissociates improperly. The two-configuration GVB wavefunction avoids this problem, describing the salient features of the bonding process with a VB model. For the class of systems which involve resonance, the GVB wavefunction is inadequate, as it only describes one resonance structure. Thus, for example, the GVB description of a three-electron bond leads to a bond energy many kcal too low. The GRVB approach handles this type of bond easily, because it includes the resonance explicitly. Similarly, the GVB description of a reaction transition state will lead to activation energies 10 to 20 kcal too high while the GRVB wavefunction yields quantitative results. It is interesting to note that the GRVB method often leads to more accurate results for the systems to which it is suited than the GVB method does in describing covalent bonds. For a covalent bond, the VB model is qualitatively appropriate, but an accurate bond energy

calculation requires the inclusion of many instantaneous correlations, because the bonding process takes two non-interacting electrons and places them into intimate proximity as a bond pair. In contrast, no covalent bond is formed in the three-electron bonding process. Thus, while there is considerable correlation error in a HF description of the active electron pair (e.g. the He 1*s* pair in He_2^+), the *differential* correlation effects are small, because the correlations are atomic in nature, and do not change significantly in the bonding process. The dominant correlation effect is that of resonance, which is included in the GRVB wavefunction. The errors involved in the GRVB description of a reaction process cancel in a similar way. Each subwavefunction retains the same number of bonds throughout the reaction, so that the dominant feature is the change in resonance energy as the reaction coordinate is traversed.

We have presented in depth only a few of the possible applications of R-GVB and GRVB. Other problems suited to a resonating VB treatment include the calculation of electron transfer rates,[1] separation of the covalent and ionic character in a partial ionic bond such as HF or BeO, and description of the bonding in hypervalent complexessuch as ClF_3. Another application is the calculation of photoelectron (PE) cross sections for core-ionized states. Daasch *et al.*[2] have recently found that a localized hole description of the CO_2^+ ion leads to a qualitatively different PE spectrum than a delocalized hole. However, they did not allow the hole state to relax (which is worth ~10 eV), and this should lead to an even larger change in the PE spectrum. The proper treatment of such a problem would require the R-GVB mixing of the two localized-hole states to restore the full molecular symmetry.

Finally, we note that the most important future use for GRVB is prob-

ably in the description of chemical reactions. While the current version of the GRVB program is very CPU intensive, an analytical optimization procedure would make GRVB competitive with (if not significantly faster than) the current CI approaches. The fourth proposition attached to this thesis discusses such a procedure.

In his classic text, *The Nature of the Chemical Bond*, Pauling's concluding remarks include a prediction (in 1960) of the future course of the theory of chemical reactions,[3] in which he states, "It is hoped that the quantitative treatments can be made more precise and more reliable; but before this can be done effectively, an extensive development of the qualitative theory of chemical reactions must take place, probably in terms of resonance." We hope that the work presented here represents a step in that direction.

References

1) M.D. Newton, Int. J. Quantum Chem. Symp. **14,** 363 (1980)

2) W.R. Daasch, E.R. Davidson and A.U. Hazi, J. Chem. Phys. **76,** 6031 (1982)

3) L. Pauling, *The Nature of the Chemical Bond*, 3rd *ed.* (Cornell University Press, Ithaca, New York, 1960) p. 570

PROPOSITIONS

Proposition I

ABSTRACT

A method is presented which should allow the rigorous inclusion of the Pauli Principle in the Quantum Monte Carlo (QMC) method. With this modification, QMC can be used to find exact many-electron solutions to the Schrodinger equation to within a statistical uncertainty. Since this uncertainty can be made arbitrarily small, chemically "exact" calculations on real molecules should be possible.

I. Introduction

One of the ultimate goals of quantum chemistry is the ability to calculate molecular properties to arbitrary accuracy. The majority of work in this field has employed self consistent field (SCF), multiconfiguration SCF (MCSCF), and configuration interaction (CI) approaches,[1] in which the molecular wavefunction is taken as a linear combination of slater determinants and the orbital shapes and or expansion coefficients are optimized to give the lowest energy. Because of the Variational Principle, the energy of this optimized wavefunction will be above the exact energy unless the size of the basis set and the number of determinants is made infinitely large. In practice it has been found that many molecular properties can be accurately calculated with wavefunctions which fall short of the exact energy by many percent.[2] This is accomplished by including in the calculation all electron correlation effects which are differential for the process of interest.

An alternative approach which has received attention recently is the Quantum Monte Carlo (QMC)[3,4,5,11] or Random Walk[6,7,8,9] method. In this approach the Schrodinger equation is solved stochastically by taking advantage of its similarity to the diffusion equation. By allowing "particles" to diffuse in imaginary time, a solution is obtained which is the exact many-electron Schrodinger solution to within a statistical uncertainty. In principle this uncertainty may be made arbitrarily small by following the evolution of a large enough number of particles over a long enough time. This is quite appealing since unlike the variational

approaches in which one never knows for sure how much correlation error remains in the best attainable wavefunctions, in the QMC approach the uncertainty is known, and can be reduced to an acceptable value.

There remains a problem with the QMC method however, since simulating the diffusion equation leads to the solution appropriate for a set of bosons rather than fermions. This is because the Schrodinger equation does not explicitly include the Pauli Principle. For systems with two singlet coupled electrons (e.g. H_2, He, H_3^+) in which the boson and fermion solutions are identical, the QMC approach has been employed with excellent results.[8,9] For more than two electrons the Pauli Principle may be included by imposing nodal surfaces on the many electron space through which the particles are not allowed to diffuse. However, as will be shown in section III, there is no way to know *a priori* where the nodal surfaces should be located. Placing them approximately (as from a trial wavefunction which is properly antisymmetrized) yields a solution which is a variational upper bound to the exact energy,[10] in addition to the statistical uncertainty. While the energies thus obtained are better than with any other variational approach,[11] the QMC method will be of limited chemical utility until the problem of exact nodal placement is solved. The reason for this is as follows. The most common applications of molecular quantum mechanical calculations (e.g. bond energies, excitation energies, activation energies) involve a comparison of two energies. The current variational approaches have achieved considerable success in this area because much effort has gone into learning how to eliminate the

differential error for a particular type of chemical process. Thus for example, the triplet to singlet excitation energy in methylene may be calculated to an accuracy of 1 kcal, even though the correlation error remaining in the calculation is many times that.[12] Presumably it would take many years to develop an analogous methodology for QMC methods, and until then the results would not be as reliable as the current variational approaches. However, if an approach can be developed which allows the exact nodal shapes to be found, the QMC method should lead to significant advances in quantum chemistry. While one procedure for allowing node readjustment has been proposed by Ceperly,[5] it is in general unstable, collapsing to the boson solution. The next section contains a closer look at how QMC is actually implemented for the spinless Schrodinger equation. In Section III the current methods of imposing the Pauli Principle are discussed, and in Section IV a new procedure is proposed which should allow the exact nodal structure to be found.

II. The Quantum Monte Carlo Method

The purpose of this section is to give the spirit of the QMC method and present enough information about the calculational procedure to lay a foundation for the proposal in Section IV. A detailed description of the method may be found elsewhere.[13]

The time dependent Schrodinger equation for a single particle in one dimension,

$$i\bar{h}\frac{\partial\Psi}{\partial t} = -\frac{\bar{h}^2}{2\mu}\frac{\partial^2\Psi}{\partial x^2} + V\Psi \quad , \tag{1}$$

where μ is the particle's reduced mass, and $V = V(x)$ is the potential energy, is similar in form to the diffusion equation

$$\frac{\partial C}{\partial t} = D\frac{\partial^2 C}{\partial x^2} , \tag{2}$$

where $C = C(x,t)$ is the concentration of, say, dye molecules and D is the diffusion coefficient. If we rewrite the Schrodinger equation as

$$\frac{\partial \Psi}{\partial \tau} = \left(\frac{\hbar^2}{2\mu}\right)\frac{\partial^2 \Psi}{\partial x^2} - V\Psi , \tag{3}$$

where

$$\tau = \frac{it}{\hbar} , \tag{4}$$

and momentarily ignore the $-V\Psi$ term, we see that the Schrodinger equation can be thought of as describing the diffusion in imaginary time of particles with distribution $\Psi(x,t)$ and diffusion coefficient $D = \frac{\hbar^2}{2\mu}$. These "particles" are not physical particles, but rather points in configuration space, and we will henceforth call these "psi particles" or "psips". Since diffusion can be described by a collection of particles undergoing independent random walks, equation (3) (still ignoring the $-V\Psi$ term) can be simulated by following a collection of psips performing random walks with diffusion coefficient $\frac{\hbar^2}{2\mu}$. To include the $V\Psi$ term in our simulation, we note the similarity to the equation describing a first order rate process

$$\frac{\partial C}{\partial t} = -kC , \tag{5}$$

so that

$$\frac{\partial \Psi}{\partial t} = -V\Psi \tag{6}$$

can be modeled by allowing our psips to radioactively decay with rate constant $k = V$, or if V is negative, to give birth. The actual calculational procedure is as follows:

1) Start with N psips (e.g. $N = 1000$) distributed over configuration space (each psip specifies a position for every electron in the system.) This is our starting guess for Ψ.

2) Increment the (imaginary) time coordinate τ by $\Delta\tau$. During this time, each psip will have walked a distance dependent on the diffusion coefficient D. Since the probability of finding the particle at some new position is a gaussian distribution with standard deviation $\sigma = \sqrt{2D\Delta\tau}$ the new position for each psip is chosen by picking a random number weighted by that gaussian.

3) Calculate the potential energy V for each psip. This is simply the sum of all coulombic interactions with all the other electrons and nuclei in the system. Note that we never have to worry about the kinetic energy, since that is accounted for by allowing the psips to diffuse.

4) For each psip, decide whether there is decay or birth based on the probability

$$P_{decay} = (V - V_{ref})\Delta\tau \ . \tag{7}$$

If the psip decays, delete it from the list of active psips. If it gives birth, add a new psip to the list with identical coordinates. The constant term V_{ref} is included to keep the total number of decays and births roughly equal, so that the total psip population N is fairly constant. V_{ref} has no other effect on the solution.

5) The energy of the wavefunction at this point is $\bar{V}$, the potential energy averaged over all the psips. Store this energy, readjust V_{ref} and go to 2).

As steps 2-5 are repeated, the energy will approach the exact energy and then fluctuate about it with an amplitude dependent on the time step $\Delta\tau$ and the psip population N. The statistical uncertainty is reduced by using large N, following the propagation over a long time τ, and extrapolating the results of multiple runs to $\Delta\tau = 0$. The wavefunction amplitude at any point in configuration space is given by the concentration of psips in that region (for higher accuracy this may be averaged over many time steps). The overall precision and speed of convergence may be increased by a procedure called importance sampling,[9,13] in which a trial wavefunction guides the motion of the psips, but the fundamental idea remains that the psips wander about in configuration space with a probability of decaying or multiplying proportional to the potential they sense.

III. Inclusion of the Pauli Principle

The method described thus far will give the correct ground state only for systems with up to two electrons. For more than two electrons (or for a two electron triplet), the effects of the Pauli Principle must be included. This is accomplished by imposing nodes on the wavefunction which separate regions of positive and negative amplitude. If a psip tries to wander through the node, it vanishes. While we know something about the node location based on the antisymmetry of the wavefunction, we can not specify its shape completely. The easiest way to demonstrate this is by considering a two electron triplet system where each electron may move in two dimensions, leading to a four dimensional configuration space. From the antisymmetry of the wavefunction we know that

$$\Psi(x_1,y_1,x_2,y_2) = -\Psi(x_2,y_2,x_1,y_1) \ , \tag{8}$$

which specifies a plane ($x_1=x_2$, $y_1=y_2$) where $\Psi=0$. However, a plane is not sufficient to define a boundary in four dimensional space, just as a line is not sufficient to subdivide three dimensional space. Thus, the node we need is a three dimensional solid,[14] but we do not know the shape of the third dimension.

The current approach to this problem has been to use the nodal shapes obtained from a properly antisymmetrized trial wavefunction (e.g. an MCSCF wavefunction). Using the procedure described in Section II with the additional constraint that a psip vanishes if it passes through a node leads to a very accurate wavefunction. However, as pointed out in

the introduction, since the nodes are not necessarily correctly placed, the energy is a variational upper bound to the exact energy.

IV. Proposed Method for Nodal Relaxation

Just as allowing the psips to diffuse in configuration space automatically finds the optimal shape for Ψ, the same principle can be applied to find the optimal nodal structure. By letting each node move in response to the pressure of the diffusing particles, an equilibrium position will be reached which has minimal energy. That is, simply let the node move around until in any given region the number of psips that run into it and vanish is the same on each side of the node. While it seems intuitive that this would yield the lowest Pauli-allowed energy state, a more rigorous proof may be given. Consider a QMC simulation using an infinite number of psips, so that at any point in configuration space the wavefunction amplitude is given accurately by the density of psips at that point. In the region near one side of a nodal surface, the wavefunction amplitude will die off smoothly and vanish at the node. This is because the nearer a psip is to the node, the greater chance it has of straying across the node in the next time step, so that the population in that area is continually depleted. Hence, assuming the potential is not singular, and by considering a small enough region of space, we can say that the psip density increases monotonically with the distance from the node. The slope of this psip density is a monotonic function of the number of psips destroyed by the node per unit time. If we consider an infinitessimally

short time step, so that any psip which could bump into the node comes from a position so close to the node that the potential energy can be considered constant, then if the number of psips destroyed on each side of the node is equal, the psip density slopes are also equal. Since the psip densities on opposite sides of the node represent wavefunction amplitudes of opposite phase, then only if the psip density slopes are equal will the first derivative of the wavefunction amplitude be continuous. Since we require any valid wavefunction to have a continuous first derivative (for a nonsingular potential), the node is thus correctly placed.

Implementation of this procedure for a noninfinite number of psips could be accomplished in various ways. One approach would be to count the number of psips which are destroyed on each side of a given section of a nodal surface in a certain time period, and then readjust the nodal shape towards equilibrium. The disadvantage of this approach is that it requires the storage and continual updating of all nodal surfaces, and decisions must be made about the most appropriate functional form to describe the node.

An alternative to actually storing information about nodal surfaces would be to keep track of the phase of each psip, and then simply delete any pair of psips with opposite phase which approach closer than a threshhold distance. The positive and negative psips would be initially distributed based on a trial wavefunction, and the integrity of the positive and negative zoning would be maintained during the diffusion process by keeping the threshhold distance large enough (or the average psip den-

sity large enough) so that psips of one phase could not sneak between psips of the other phase. The diffusing psips would define their own phase boundaries similar to the boundary between two immiscible liquids. This procedure may require an unfeasibly large number of psips, and has the additional disadvantage that the situation where two psips are very close but on opposite sides of a node would be unallowed, leading to a bias in the statistical simulation.

An improvement could be made in the following manner. Rather than using a fixed cutoff distance, assign a probability for annihilation of a pair of psips which goes as the overlap of two gaussians centered on each psip. This has physical meaning since the probability distribution for the location of a psip after a time step $\Delta\tau$ is the gaussian

$$W(\Delta x) = \frac{1}{\sqrt{2\pi\sigma}} \exp\left[\frac{(\Delta x)^2}{2\sigma^2}\right] , \tag{9}$$

where

$$\sigma = \sqrt{2D\Delta\tau} , \tag{10}$$

and hence the overlap of two of these gaussians can be thought of as how much the psips "touch". Replacing the simple gaussian by the approximate Green's function for the system,

$$G(\Delta x) = \frac{1}{\sqrt{2\pi\sigma}} \exp\left[\frac{(\Delta x)^2}{2\sigma^2}\right] \exp\left[-(V - V_{ref})\Delta\tau\right] , \tag{11}$$

takes into account the probability that the psip will decay (or multiply) as it diffuses.

One other possible procedure will be described here and this is probably the best one. After moving a particular psip and allowing it to decay or give birth, decide whether it is destroyed by a node according to the following test. Call the location of this i^{th} psip R_i. Sum up the Green's function value at R_i for every positive and negative psip in the system except the i^{th} one. If the i^{th} psip has a phase opposite to that of the sum, delete it, since it has moved into a region dominated by psips of opposite phase. If the sum and the i^{th} psip have the same phase, the psip survives.

V. Conclusions

Implementation of the procedure described in section IV could lead to a QMC approach which yields exact wavefunctions and energies while rigorously including the Pauli Principle. Since in principle the statistical uncertainty may be made arbitrarily small, chemical properties could be calculated to any desired accuracy. While in variational approaches the choice of basis set and the number and type of configurations employed is critical, such considerations are completely eliminated with QMC. Another appealing aspect of QMC is that there is no need for the Born-Oppenheimer approximation. By simply allowing the nuclei to diffuse along with the electrons (the diffusion coefficient for the nuclei would be smaller) the fully-coupled nuclear-electronic wavefunction can be found (such a calculation has not yet been attempted). The one remaining unknown is the effect of relativity, since the nonrelativistic hamiltonian is

used, but for many systems of chemical interest these effects are known to be small. Work is currently in progress to incorporate relativistic effects into the QMC method.[10]

References

1) *Methods of Electronic Structure Theory*, edited by H.F. Schaefer III (Plenum, New York 1977)

2) see, for example, J.A. Pople, in: *Modern Theoretical Chemistry, Vol. 4, Methods of Electronic Structure Theory*, edited by H.F. Schaeffer III (Plenum, New York 1977), Chap. 1; P.W. Paine and L.C. Allen, ***ibid***, Chap. 2; W.J. Hehre, ***ibid***, Chap. 7; S.R. Langhoff and C.W.Kern, ***ibid***, Chap. 10.

3) M.H. Kalos, D. Levesque, L. Verlet, Phys. Rev. A **9,** 2178 (1974)

4) D.M. Ceperly and M.H. Kalos, in *Monte Carlo Methods in Statistical Physics*, K. Binder, ed. (Springer-Verlag, Berlin, 1979)

5) D.M. Ceperly and B.J. Alder, Phys. Rev. Lett. **45,** 566 (1980)

6) J.B. Anderson, J. Chem. Phys. **63,** 1499 (1975)

7) J.B. Anderson, J. Chem. Phys. **65,** 4121 (1976)

8) J.B. Anderson, J. Chem. Phys. **73,** 3897 (1980)

9) F. Mentch and J.B. Anderson, J. Chem. Phys. **74,** 6307 (1981)

10) P.J. Reynolds, D.M. Ceperly, B.J. Alder, and W.J. Lester, to be published

11) Any energy from a standard variational wavefunction can be made lower by using QMC to optimize the wavefunction within the fixed nodal structure.

12) C.E. Dykstra, J. Chem. Phys. **68,** 1829 (1978); L.B. Harding and W.A. Goddard III, Chem. Phys. Lett. **55,** 217 (1978).

13) For a lucid and basic description see reference 6. Finer details may be found in refs. 7-9.

14) For the general case of Ne electrons in three dimensional space, each nodal surface will be a 3Ne-1 dimensional surface.

15) J.W. Moskowitz, K.E. Schmidt, M.A. Lee, and M.H. Kalos, J. Chem. Phys. **77,** 349 (1982)

Proposition II

ABSTRACT

It is proposed that a modification of the Quantum Monte Carlo method may be used to directly calculate key features of potential energy surfaces to very high accuracy, by allowing the nuclei to "diffuse" in imaginary time along with the electrons. We discuss application of the method to finding the barrier height in the vinylidene-acetylene rearrangement, a task which is beyond the capabilities of the current theoretical methods.

I. Introduction

One of the challenges currently facing quantum chemists is the accurate calculation of molecular potential energy surfaces. This is important for obtaining equilibrium geometries and vibrational force constants, and also for the accurate estimation of activation barriers to obtain reaction rates and mechanisms. The difficulty lies in the fact that there are $3N-6$ coupled coordinates which need to be searched for either the saddle point or the minimum, leading to large amounts of computational work.

One way of reducing this work is through the use of gradient approaches. Methods have been developed which yield the energy gradient as a function of nuclear displacement for Hartree Fock[1] and certain configuration interaction (CI)[2] wavefunctions at roughly three times the computational cost of obtaining the wavefunction with no gradient. By accumulating the gradient information at a number of geometries, a curvature matrix may be constructed, which both speeds convergence to the minimum (or saddle point), and yields the desired force constant information.

Conventional self-consistent field (SCF) and CI approaches, in conjunction with gradient methods, have been successful in many applications for finding equilibrium geometries[3] and transition state saddle points.[4] However, cases are known which tax the limits of the current methods.[5] One example is the rearrangement of vinylidene to acetylene,

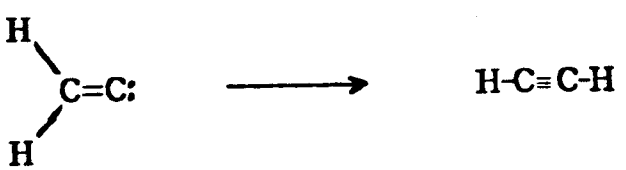

(1)

The reaction is known to be downhill by roughly 42 kcal,[6] but high quality calculations disagree on the barrier height, i.e. the depth of the local minimum in the potential energy surface corresponding to the vinylidene structure. Calculations by Dykstra and Schaeffer[7] using the self-consistent electron pairs (SEPA) method (roughly equivalent to all singles and doubles CI) in a double zeta plus polarization basis yielded a barrier of 8.6 kcal. Pople et al[8] obtained a barrier of 8.1 kcal using fourth-order Moller-Plesset perturbation theory (MP4) in a similar basis set. Later calculations by Krishnan, Frisch, Pople and von Rague Schleyer[6] using a more extended basis (6-311G^{**} - triple zeta plus polarization) lowered this barrier to 2.2 kcal, and recent calculations by Osamura, Schaeffer, Gray and Miller[9] yielded 5.4 kcal. Inclusion of the zero point energies for all modes other than the isomerization coordinate lowers these barriers by 1-2 kcal. The question arises whether the vinylidene structure represents a minimum at all -- Krishnan et al[6] speculate that further increasing the basis set quality and correlation level could eliminate the activation barrier completely. If indeed the true surface has no barrier, then state-of-the-art calculations are giving a qualitatively incorrect description of the surface. While Skell et al[10] predicted a lifetime of slightly less than 10^{-10}s based on trapping experiments, which is in accord with a barrier of 2-5 kcal,[9] the possibility that triplet vinylidene (which should have a substantial barrier to rearrangement[11]) was being formed in the trapping reaction means the lifetime of singlet vinylidene could be much shorter. Reiser and Steinfeld[12] have reported that multi-

ple infra-red photon excitation of vinyl chloride ($H_2C=CHCl$) to eliminate HCl yields only acetylene. However, due to the vibrationally excited nature of the initially formed vinylidene, this experiment also could not distinguish a barrier of zero kcal from a barrier of 5 kcal. Hence, accurate determination of the kinetic stability of vinylidene appears to be beyond the reach of both theory and experiment at the present time. In the next section we outline a new method for calculating potential energy surfaces which should be accurate enough to settle the vinylidene issue.

II. Description of the Method

It is proposed that the key features of a potential surface may be obtained directly from a single calculation, using a modification of the Quantum Monte Carlo (QMC) method. The QMC method has been described in detail elsewhere,[13,14] and an overview is presented in Proposition I. Using QMC, the full Schrodinger equation is solved directly using a random walk process which yields the wavefunction and energy to within a statistical uncertainty which can (in principle) be made arbitrarily small. In this approach there is no need for the Born-Oppenheimer approximation, so that the full electronic-nuclear wavefunction may be found (though QMC has not been used in this way before). This would be accomplished by simply allowing the "psips" (psi particles -- see Proposition I) to move not only along the electronic coordinates, but along the nuclear coordinates as well. The diffusion coefficient in the nuclear directions is much smaller, but the procedure

is otherwise unchanged. In this application of QMC, the nodal relaxation outlined in Proposition I would be important. The resulting wavefunction, $\Psi(\mathbf{R})$, would be a distribution of psips in the full N dimensional space where

$$N = N_e + N_n \tag{2}$$

with

N_e = number of electrons
N_n = number of nuclei

and $\mathbf{R}$ is the coordinate in N-space. Projecting $\Psi(\mathbf{R})$ onto the N_n dimensional nuclear space (by simply ignoring the other N_e coordinates for each psip) yields a distribution of psips representing a nuclear wavefunction $\Psi(\mathbf{R}_n)$. By inverting the Schrodinger equation for the motion of the nuclei,

$$V(\mathbf{R}_n) = \frac{1}{\Psi(\mathbf{R}_n)} \sum_i \frac{\bar{h}^2}{2\mu_i} \nabla_i^2 \Psi(\mathbf{R}_n) \ , \tag{3}$$

a potential energy surface $V(\mathbf{R}_n)$ could be obtained from $\Psi(\mathbf{R}_n)$. The summation in (3) is over a complete set of orthonormal vibrational coordinates, each with reduced mass μ_i. While $V(\mathbf{R}_n)$ corresponds roughly to the energy surface which would result from solving for a highly correlated electronic wavefunction at many nuclear geometries, it is not the same, since $V(\mathbf{R}_n)$ includes the effects of electronic-nuclear coupling. The inversion of $\Psi(\mathbf{R}_n)$ to give $V(\mathbf{R}_n)$ may prove tedious for the general case, but certain features would be easily obtained. For example, the equilibrium geometry, $\mathbf{R}_n^{eq}$, corresponds to the maximum in $\Psi(\mathbf{R}_n)$. Harmonic force

constants could also be extracted by solving (3) for various slices through a set of trial normal coordinates, and then applying the F-G matrix method of Wilson.[15] The location and properties of saddle points for intramolecular rearrangement could even be computed, provided the barriers are low enough that $\Psi(\mathbf{R}_n)$ is not vanishingly small in the saddle point region.

It is interesting to note that it is generally thought that calculation of potential energy surfaces would prove the downfall of the QMC method, since the statistical uncertainty in the energy at a given geometry would lead to very large uncertainties in numerical derivatives calculated using adjacent points. However, in this proposed method, the surface is found from only one calculation, so that this problem is eliminated. There may be a problem, however, in inverting a wavefunction which is described by a distribution of particles (psips), rather than as a linear combination of analytical functions. This could be handled by accumulating the psip distribution over many time steps, until the density of psips in all regions of interest is high enough to allow an accurate fit to some analytical function.

A more serious objection is that using QMC in this way may be prohibitively expensive, since the nuclei diffuse thousands of times slower than the electrons. The development of QMC is still young, and considerable improvements in speed and size scaling have been made in just a few years.[13] There is thus no reason to believe that QMC applied to potential surfaces might not rapidly become competitive with current methods for

computing potential surfaces, especially given that QMC scales better than conventional approaches (n^2 versus n^4 -- where n is the number of electrons)[16]. In addition, the fact that QMC leads to a chemically "exact" result (since the uncertainty can be made arbitrarily small), makes it especially powerful, so that it should be useful in cases where standard methods fail, even if it is expensive. The vinylidene rearrangement may be such a case, and we outline below how QMC would be applied to solve this problem. We then propose using this approach to find the transition state and barrier height in the rearrangement of the negative ion of vinylidene, a task which would be essentially impossible using current methods.

III. Application of Relaxed-Nucleui QMC to Vinylidene

Finding the barrier height for the vinylidene rearrangement could be accomplished with the following procedure:

(1) Given a suitable starting guess for the vinylidene geometry and the nodal structure of the electronic wavefunction, solve for the QMC wavefunction at this fixed geometry.

(2) Starting from this wavefunction, partially relax the frozen nuclei restriction by allowing the nuclei to diffuse along the three nuclear coordinates corresponding to the totally symmetric A_1 representation in C_{2v}, as shown below.

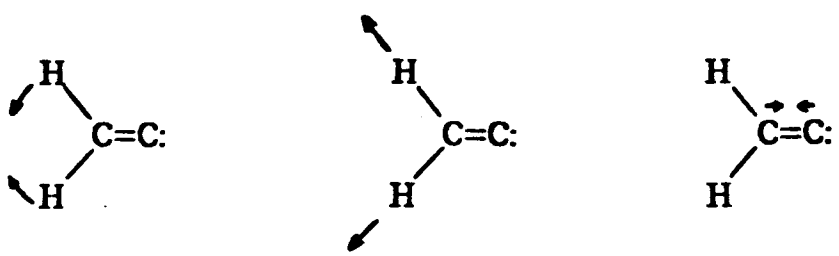

This yields the best possible description of the vinylidene species (assuming it is planar).

(3) Starting with the partially relaxed distribution of psips from step (2), allow the nuclei to diffuse along any direction in the plane of the molecule. If there is no barrier to rearrangement, the wave packet will steadily diffuse along the reaction coordinate, leaving no maximum in the psip distribution in the region of the vinylidene geometry, and form a pool in the region of the acetylene geometry, mapping out the ground vibrational wavefunction of acetylene. If there is a barrier to rearrangement, there will still be significant diffusion along the reaction coordinate (since the barrier is known to be low), but there will remain a maximum in the psip distribution at the vinylidene geometry. These two cases are sketched in Fig. 1.

(4) For the no-barrier case, the calculation is done at this point. If there is a barrier, we wish to know how high it is. To get an accurate representation of the wavefunction, the psips must be allowed to diffuse for a long (imaginary) time. A psip which drifts past the barrier has only a very small probability of returning to the high-energy vinylidene region, so ultimately the majority of psips will be in the acetylene pool. Since we are not interested in an accurate representation of $\Psi(\mathbf{R}_n)$ for acetylene, we continually remove psips from that region, and periodically double the psip population (by adding a new psip everywhere one exists currently) to maintain a roughly constant number of psips. This should have a negligable effect on the random walk statistics, since the reaction is so exo-

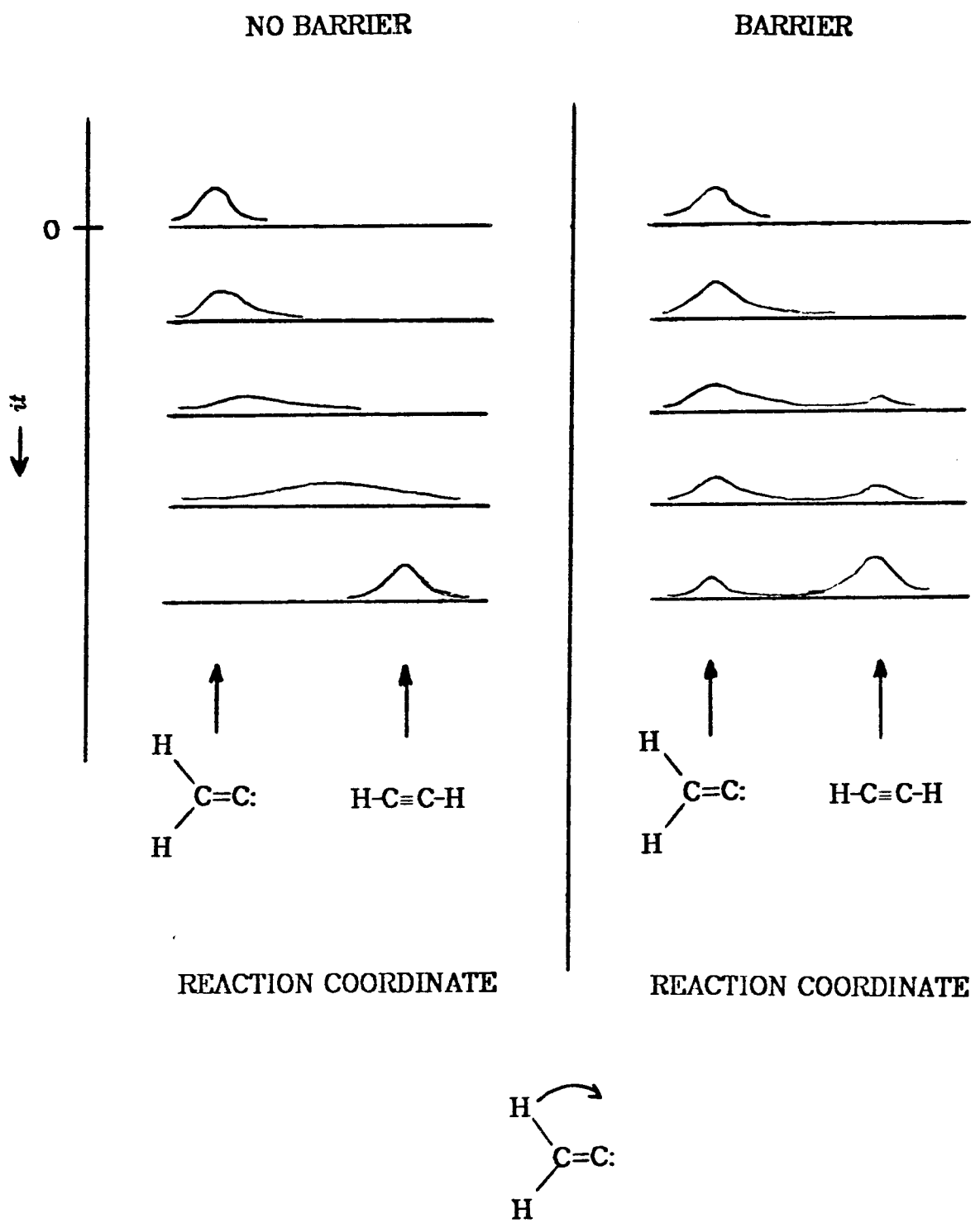

Figure 1. Imaginary time evolution of psip distribution for the vinylidene - acetylene rearrangement potential surface.

thermic, and keeps a high enough density of psips in the region of interest (the vinylidene pool and the saddle point region) so that the desired features of $V(\mathbf{R}_n)$ can be extracted.

(5) To calculate the barrier height once $\Psi(\mathbf{R}_n)$ has stabilized, two geometries must be located, the vinylidene equilibrium geometry, $\mathbf{R}_n^{eq}$, and the saddle point geometry, $\mathbf{R}_n^{eq}$. $\mathbf{R}_n^{eq}$ corresponds to the local maximum in $\Psi(\mathbf{R}_n)$, and $\mathbf{R}_n^{eq}$ is at the stationary point in $\Psi(\mathbf{R}_n)$ that has exactly one positive curvature (the direction of this positive curvature is the reaction coordinate). The barrier could then be calculated by solving (3) for $V(\mathbf{R}_n^{eq}) - V(\mathbf{R}_n^{eq})$,[17] but a better approach would be to evaluate $E(\mathbf{R}_n sp)$ and $E(\mathbf{R}_n^{eq})$ by using clamped-nuclei QMC at these two geometries. This would give the Born-Oppenheimer adiabatic barrier height without zero point correction. The statistical error bars on this barrier height would be $\sqrt{2}$ times the error in a single fixed-nucleus QMC calculation, and this should be well under one kcal.

IV. Application to Vinylidene Negative Ion

A radical anion with the composition $C_2H_2^-$ has been observed in the gas phase as a product of the reaction of O^- with ethylene.[18] The question of whether this is the negative ion of vinylidene or acetylene has been addressed recently by Chandrasekhar et al.[19] Using double zeta plus polarization basis sets at the MP2 level, they found a negative electron affinity of −1.7 eV for acetylene (vertical electron transmission spectroscopy has obtained −2.6 eV[20]), and a positive electron affinity of 0.21 eV for

vinylidene. The energy of the vinylidene anion is 43 kcal above neutral acetylene, so that $C_2H_2^-$ is thermodynamically unstable with respect to ejection of an electron and isomerization to acetylene. It would be interesting to know what the barrier to this rearrangement is, and what the transition state looks like, since it involves the simultaneous breaking of a C-H bond, the formation of a new C-H bond, and the ejection of an electron. Accurate calculation of this potential surface in the transition state region would be extremely difficult using current CI methods, because the wavefunction would require a high level of correlation to describe the two valence bond structures, and many very diffuse basis functions to describe the escaping electron. Thus the $C_2H_2^-$ system is ideally suited to the relaxed-nuclei QMC method, since the QMC wavefunction is completely correlated, and an electron is free to wander off to infinity if necessary. The procedure outlined in Section III would work for this case, though since the barrier is higher, the imaginary-time evolution of the psip distribution would have to be run longer to accumulate a reasonable description of $\Psi(\mathbf{R}_n)$ in the saddle point region.

IV. Conclusions

We have proposed a method for elucidating molecular potential surfaces which consists of extending Quantum Monte Carlo to allow the nuclei to diffuse in imaginary time simultaneously with the electrons. Such a procedure leads to the exact, fully-coupled solution to the Schrodinger equation, to within a statistical uncertainty which can be made

arbitrarily small given enough computer time. The resulting wavefunction, $\Psi(\mathbf{R})$, can be projected onto the nuclear geometry space to give $\Psi(\mathbf{R}_n)$, and $\Psi(\mathbf{R}_n)$ can be inverted to yield a potential surface $V(\mathbf{R}_n)$.

We have proposed applying this approach to accurately determine the kinetic stability of the elusive vinylidene species, and to describing the electron ejection process in the rearrangement of vinylidene anion. Each of these applications is beyond the capabilities of the current theoretical methods.

References

1) P. Pulay, in: *Modern Theoretical Chemistry, Vol. 4, Methods of Electronic Structure Theory*, edited by H.F. Schaeffer III (Plenum, New York 1977), Chap. 4

2) Y. Osamura, Y. Yamaguchi, H.F. Schaefer, J. Chem. Phys. **75,** 2919 (1981)

3) See, for example, ref. 1, p. 167.

4) Y. Osamura, H.F. Schaefer III, M. Dupuis, W.A. Lester, Jr., J. Chem. Phys **75,** 5828 (1981)

5) See, for example, ref. 1, p. 169.

6) R. Krishnan, M.J. Frisch, J.A. Pople, and P. von R. Schleyer, Chem. Phys. Lett. **79,** 408 (1981)

7) C.E. Dykstra and H.F. Schaeffer III, J. Am. Chem. Soc. **100,** 1378 (1978)

8) J.A. Pople, R. Krishnan, H.B. Schlegel, and J.S. Binkley, Int. J. Quantum Chem. **14,** 545 (1978)

9) Y.O. Osamura, H.F. Schaeffer III, S.K. Gray, and W.H. Miller, J. Am. Chem. Soc. **103,** 1904 (1981)

10) P.S. Skell, F.A. Fagone, and K.J. Kablunde, J. Am. Chem. Soc. **94,** 7862 (1972)

11) Y. Osamura and H.F. Schaeffer III, Chem. Phys. Lett. **79,** 412 (1981)

12) C. Reiser and J.I. Steinfeld, J. Phys. Chem. **84,** 680 (1980)

13) M.H. Kalos, D. Levesque, L. Verlet, Phys. Rev. A **9,** 2178 (1974)

14) J.B. Anderson, J. Chem. Phys. **63,** 1499 (1975); J.B. Anderson, J. Chem. Phys. **65,** 4121 (1976); J.B. Anderson, J. Chem. Phys. **73,** 3897 (1980); F. Mentch and J.B. Anderson, J. Chem. Phys. **74,** 6307 (1981)

15) E.B. Wilson, Jr., J.C. Decius, and P.C. Cross, *Molecular Vibrations* (McGraw-Hill, 1955)

16) P.J. Reynolds, D.M. Ceperly, B.J. Alder, and W.J. Lester, to be published

17) This requires evaluating $\nabla^2\Psi(\mathbf{R}_n)$ for each of a complete set of orthogonal vibrational coordinates at both $\mathbf{R}_n^{sp}$ and $\mathbf{R}_n^{eq}$ and then using equation (3).

18) J.H.J. Kawson and N.M.M. Nibbering, J. Am. Chem. Soc. **100,** 1928 (1978); I. Dotan, W. Lindinger, and D.L. Albritton, J. Chem. Phys. **64,** 4544 (1976); E.E. Ferguson, J. Chem. Phys. **63,** 3238 (1975)

19) J. Chandrasekhar, R.A. Kahn, and P. von R. Schleyer, Chem. Phys. Lett. **85,** 493 (1982)

20) K.D. Jordan and P.D. Burrow, Acc. Chem. Res. **11,** 341 (1978)

Proposition III

ABSTRACT

A formalism is presented for generating configuration interaction (CI) wavefunctions appropriate for describing localized hole states within a symmetry adapted molecular orbital basis. The prescription can be applied to find a consistent level of description for states arising from an excitation, or ionization out of a localized orbital. The use of a symmetry adapted basis results in computational savings, and only standard self-consistent field (SCF) and CI programs are required.

The deficiency of symmetry constrained SCF solutions in describing states with localized excitations or ionizations is well known.[1] The removal of the symmetry restrictions can lead to SCF solutions as much as 10 eV lower in energy,[2] clearly indicating the importance of the localized character. Including this localized character in the wavefunction is thus crucial for accurate predictions of transition energies and other properties.

One approach to describing such states is to recombine the symmetry-broken SCF solutions to form wavefunctions with the full molecular symmetry which explicitly contain the localized hole character. This approach has been described extensively elsewhere in this dissertation,[3] and will not be elaborated on here.

The alternative approach is to start from the symmetry constrained SCF solution and restore the localized character to the wavefunction through a CI calculation. The advantage of this procedure is that standard SCF and CI programs may be used (the above approach requires the use of a special program such as R-GVB), and retaining symmetry in the orbitals results in significant computational savings in the SCF step.[4] However, the set of CI configurations necessary to restore localized character to the wavefunction is not well defined. Performing all possible excitations (a full CI) is clearly sufficient, though probably not necessary, and such a calculation is unfeasible for systems with more than 4 or 5 electrons. Restricting the CI to all single and double excitations, a standard level of correlation whose properties are well characterized,[5] can

still lead to unacceptably long CI lists,[6,7] especially when these excitations are done from multiple reference configurations, as is appropriate in this application. For example, Butscher et al[6] achieved accurate results for the core ionized shakeup states of N_2^+ using an all singles and doubles approach, but performed CI calculations which selected from more than 200,000 configurations. Hence, the search is still active for a CI expansion of manageable size which can include the effects of localization using delocalized orbitals.

Very recently, Benard presented a procedure for generating a very short CI list which he felt achieved this goal.[7] Using the $3d_\sigma$ hole states of Cu_2^+ as a test case, he applied his prescription to generate two CI wavefunctions: one using the delocalized, symmetry adapted SCF orbitals as the CI basis, and the other using the localized ("symmetry-broken") SCF orbitals. Because the symmetry adapted CI yielded a lower energy than the symmetry-broken CI, he concluded that the localization energy had been recovered in the symmetry adapted CI. This is a reasonable way to test the method; however, for reasons given later, we feel that Benard's CI is too restrictive to pass the same test on a state which requires more substantial electron readjustment in response to moving the hole from one site to another (symmetry equivalent) site. For example, more readjustment would be expected to occur in more deeply ionized states such as 3s ionized Cu_2^+. We present here a method which should overcome this defficiency while maintaining an acceptably short configuration list.

Consider a molecule with n centers equivalent by symmetry. For each core atomic function of type χ_α ($\alpha = 1s, 2s, 2p_x \cdots$), there are n occupied MO's in the symmetry constrained SCF wavefunction corresponding to linear combinations of χ_α on each equivalent center. We are interested in describing an ionization, or excitation, of an electron out of a particular core function χ_{α_0}. Denote the set of n symmetry adapted occupied orbitals corresponding to χ_{α_0} as $i_1, i_2, \cdots i_n$, and denote the product of occupied spin orbitals other than the set $\{i\}$ as Φ_0. The ground state wavefunction becomes

$$\Psi_0 = A[\Phi_0(i_1^2 i_2^2 \cdots i_n^2)] \ ,$$

where A is the antisymmetrizer. There are n energetically similar SCF wavefunctions that can be optimized for the excited case, which can be written as

$$\Psi_1 = A[\Phi_0'(i_1^2 i_2^2 \cdots i_{n-1}^2 i_n^1)] \ ,$$
$$\Psi_2 = A[\Phi_0'(i_1^2 i_2^2 \cdots i_{n-1}^1 i_n^2)] \ ,$$
$$\vdots$$
$$\Psi_n = A[\Phi_0'(i_1^1 i_2^2 \cdots i_{n-1}^2 i_n^2)] \ ,$$

where Φ_0' replaces Φ_0 because an electron has been excited, though $\Phi_0' = \Phi_0$ if the electron has been ionized out of the molecule (ignoring the fact that the shapes of the orbitals in Φ_0 will have changed in response to the ionization). Ψ_1 through Ψ_n possess the correct symmetries for the states arising from this excitation, but they do not contain the localized character. To obtain a balanced set of orbitals for the CI, an SCF is performed

with an orbital occupation that is the average of Ψ_1 to Ψ_n,

$$\Psi_A = A[\Phi_0'(i_1^{\bar{x}} i_2^{\bar{x}} \cdots i_n^{\bar{x}})] \quad ; \quad x = \frac{2n-1}{n} \quad .$$

This is easily accomplished with an SCF program which allows user-input Hamiltonians. Using the orbitals from Ψ_A as the CI basis, consider the wavefunction resulting from moving the electron hole into each of the n positions in the set $\{i\}$ (i.e. the orbital occupations in Ψ_1 through Ψ_n), and denote this Ψ_{CI}^1. This corresponds to a full CI within the orbital space $\{i\}$, and thus Ψ_{CI}^1 is invariant under any unitary transformation of these orbitals. Since we could choose this (hypothetical) transformation to be the one which converts $\{i\}$ into the set of n localized functions, $\{\chi_{a_0}\}$, we see that Ψ_{CI}^1 is equivalent to mixing n localized hole states. However, the shapes of these localized holes, and (more importantly) the shapes of the other occupied orbitals, are not the same as would result from a symmetry-broken SCF. This shape readjustment can be included through first order by using single excitations. Thus, we propose the following procedure, and call the resulting CI wavefunction Ψ_{CI}^2. Using the occupied plus virtuals from Ψ_A as the CI basis, generate all single excitations from each of the n configurations in Ψ_{CI}^1, with the restriction that the total occupation of the $\{i\}$ set of orbitals is less than or equal to $2n-1$ electrons. This restriction prevents the character of the ground and low-lying states from mixing into the excited state. (Such a restriction is not necessary if the CI program is capable of solving for the correct highly excited root of the secular equation,[6] but this requires much extra work for most CI programs.) Excluding these configurations should have a

slight effect on the first order shape readjustments. For a system such as Cu_2^+, Ψ_{CI}^2 would consist of less than 100 configurations per state.[7]

It is now easy to describe Benard's CI, Ψ_{CI}^B. Using the orbitals from Ψ_{CI}^1 as the CI basis he performed single excitations from all configurations in Ψ_{CI}^1 *except* the one with occupation corresponding to Ψ_{CI}^1. Since Ψ_{CI}^B does not include all the occupations in Ψ_{CI}^1, it allows the hole to localize, but does not include the necessary shape readjustment in a balanced way. If this relaxation is substantial, Ψ_{CI}^B may be inadequate, especially in describing the splittings between the n states resulting from one hole type. Ψ_{CI}^2 should give a reasonably balanced description of these states, since no bias is built in at either the SCF of CI step, and should also be superior to Ψ_{CI}^B in describing the relative energies of states arising from different hole types.

Since the shape relaxation is only included to first order, Ψ_{CI}^2 may be insufficient for deeply ionized states. A test to determine the limitations of the method would be to compute the energy for the states of Cu_2^+ resulting from ionization out of the $1s, 2s, 2p_\sigma, 2p_\pi, 3s, 3p_\sigma, 3p_\pi, 3d_\sigma, 3d_\pi$, and $3d_\delta$ orbitals using three different wavefunctions: Ψ_{CI}^2, Ψ_{CI}^B, and R-HF (the resonance of two symmetry-broken HF solutions[8]). The R-HF wavefunction is used as a reference, since it is exactly what these CI wavefunctions are designed to mimic. The total energies of Ψ_{CI}^2 and Ψ_{CI}^B will probably be lower than the corresponding R-HF states, because they include some extra correlation energy in addition to the localization energy, but the appropriate test is how well the

state splittings match. It is anticipated that Ψ^2_{CI} will be superior to Ψ^B_{CI} in all comparisons, though it may fail to reproduce the R-HF results for the $\Delta E[Cu_2^+(3d_\sigma) - Cu_2^+(1s)]$ energy difference. Testing the ability of Ψ^2_{CI} to match R-HF for transitions between various core to valence excitations (e.g. oxygen $^{1,3}\Pi_{g,u}(pi^* \leftarrow 3s)$) would also be useful.

In conclusion, we have presented a generalizable CI procedure, which should be capable of mimicking a resonating, symmetry-broken SCF for localized hole states of symmetric molecules. The number of configurations generated is small, e.g. less than 100 for the hole states of Cu_2^+. The molecular symmetry can be retained throughout the calculations, which saves time in both the SCF and CI, and leads to states of pure symmetry. The generalization to handle correlated wavefunctions such as GVB is trivial, consisting of simply multiplying the CI list times the various GVB occupations of the natural orbitals.

References

1) See Chap. 2 of this thesis.

2) A.F. Voter and W.A. Goddard III, J. Chem. Phys. **75,** 3638 (1981)

3) See Chap. 3 of this thesis.

4) Typically a factor of two is gained in the SCF time.

5) I. Shavitt, in: *Modern Theoretical Chemistry, Vol. 3, Methods of Electronic Structure Theory*, edited by H.F. Schaeffer III (Plenum, New York 1977), Chap. 6.

6) W. Butscher, R.J. Buenker and S.D. Peyerimhoff, Chem. Phys. Lett. **52,** 449 (1977)

7) M. Bénard, Theor. Chim. Acta, **61,** 379 (1982)

8) Using the R-GVB procedure described in Chap. 3 of this thesis.

Proposition IV

ABSTRACT

A pseudo Generalized Resonating Valence Bond (p-GRVB) method is proposed, in which the localized character which appears naturally in a true GRVB wavefunction is artificially induced by a modified self-consistent field (SCF) procedure which optimizes only one subwavefunction. The "localization force" is simulated by optimizing an SCF wavefunction with the constraint that it have a specified overlap with its mirror image wavefunction, and multiple SCF runs allow the p-GRVB energy to be minimized as a function of this overlap. Since the p-GRVB energy is an upper bound on the true GRVB energy, the p-GRVB method would be useful for systems too large to handle with GRVB. The necessary SCF equations are derived by expanding the overlap term through second order in the orbital mixing coefficient δ. We discuss the implications of using a similar expansion to find the analytical derivatives necessary to optimize a true GRVB wavefunction.

I. INTRODUCTION

In the Generalized Resonating Valence Bond (GRVB) method, a wavefunction of the form

$$\Psi_{TOT} = c_A\Psi_A + c_B\Psi_B \tag{1}$$

is optimized, where Ψ_A and Ψ_B are subwavefunctions which may overlap. GRVB has been demonstrated to yield quantitative results from this conceptually simple wavefunction,[1] but due to the overlap of orbitals in Ψ_A with orbitals in Ψ_B, the orbital optimization requires far more computer time than a standard SCF calculation.

For many resonating systems, an adequate description is obtained using the resonating Generalized Valence Bond (R-GVB) wavefunction,[2] which has the form in (1) but with the orbitals in Ψ_A and Ψ_B optimized in separate SCF calculations, without resonance. R-GVB has the advantage of being much less expensive than GRVB, and works well in cases where the orbitals in Ψ_A and Ψ_B have a natural tendency to localize. This occurs for transition states of reactions which are forbidden by orbital symmetry, such as $H_2 + D_2 \rightarrow 2HD$, in systems whose electronic structure is isomorphic with a forbidden reaction, such as the π space of cyclobutadiene, and in localized core hole states, such as 1s ionized N_2^+. In each of these cases, the orbitals in one subwavefunction localized strongly at the GVB level, and the orbitals change only slightly if they are reoptimized using GRVB. For example, in cyclobutadiene, optimizing a GVB wavefunction leads to two localized π bonds,

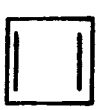

Mixing this with the other localized form using R-GVB,

Ψ^{R-GVB} =  , (2)

leads to a resonance energy of 20.7 kcal, while the GRVB energy is only 1 kcal lower than R-GVB and the change in orbital shapes is imperceptible.

R-GVB is inadequate, however, if the orbitals tend to delocalize to include the resonance at the SCF level, so that Ψ_A and Ψ_B are very similar. In these cases, mixing Ψ_A and Ψ_B does not gain very much energy. This occurs in the transition states of "allowed" reactions, such as $HF + D \rightarrow H + FD$, or in states which are isomorphic with an allowed reaction, such as the π space of allyl radical or benzene. For example, at the symmetric saddle point in the HF+D exchange reaction, $\langle \Psi_A^{GVB} | \Psi_B^{GVB} \rangle = 0.95$, with a resonance energy of only 3.0 kcal, while $\langle \Psi_A^{GRVB} | \Psi_B^{GRVB} \rangle = 0.45$, and the GRVB energy is 19 kcal below R-GVB. For the $H_2 + D \rightarrow H + HD$ transition state the GVB wavefunction will not localize at all, ($\langle \Psi_A^{GVB} | \Psi_B^{GVB} \rangle = 1$), so that R-GVB is inapplicable.

R-GVB can also be difficult to apply if Ψ_A and Ψ_B are not isoenergetic, since sometimes the higher energy subwavefunction cannot be "trapped", and instead converges to the lower energy result. This occurs for the H-H-F transition state of the $H + HF \rightarrow H_2 + F$ reaction, where the GVB wavefunction with a bond between the two hydrogens can be optimized, but the H-F bonded form cannot.

For these cases where R-GVB will not suffice, the GRVB method is

appropriate, but many systems are too large for GRVB treatment. As an alternative, we have been interested in developing an approximate GRVB method with the computational dependence of a standard SCF. In such an approach, GRVB would be simulated by artificially inducing in each subwavefunction the orbital localization which is characteristic of a true GRVB wavefunction, and then mixing these subwavefunctions (using R-GVB) to obtain a total energy. This pseudo GRVB (p-GRVB) wavefunction would be useful as a starting guess for GRVB in cases that will not localize at the GVB level. In addition, for molecules that are too large for GRVB, the p-GRVB method could be used instead to yield an upper bound to the true GRVB energy. That the p-GRVB energy is an upper bound to GRVB is easy to show, as follows. The form of the p-GRVB wavefunction is as in (1), where Ψ_A and Ψ_B are each normalized, antisymmetric wavefunctions, but the orbitals shapes are found by some special (as yet unspecified) SCF scheme designed to give localized orbitals. The energy of Ψ_{TOT} evaluated with these special subwavefunctions is E(p-GRVB), and E(GRVB) is the energy obtained if Ψ_{TOT} is variationally optimized. Since the p-GRVB orbital shapes can at *best* be exactly the same as the GRVB orbitals, we can state that E(p-GRVB) is an upper bound to E(GRVB),

$$\mathrm{E(p-GRVB)} \geq \mathrm{E(GRVB)} \quad . \tag{3}$$

We have tried various approaches to obtain reasonable p-GRVB subwavefunctions, but have been unsuccessful in obtaining an energy even as low as R-GVB. In one approach, appropriate for transition states, the wavefunctions from the isolated reactant fragments were suitably

orthogonalized at the transition state geometry and used as Ψ_A, while Ψ_B was obtained analogously from product fragments. This approach did give localized structures, but E(p-GRVB) was far above E(R-GVB), since the juxtaposed subwavefunctions were not allowed to relax in response to each other. This, and other tests, led to the (not surprising) conclusion that the energy is very sensitive to minor shape readjustments. Thus, any successful p-GRVB method will have to impose the localized character on Ψ_A and Ψ_B in a *gentle* fashion, i.e. the energy of the localized wavefunctions must not be disregarded.

II. THE PROPOSED METHOD

We wish to find localized wavefunctions Ψ_A and Ψ_B which are as distinct as possible, so that mixing them maximizes the amount of configuration space contained in the total wavefunction. Since a good indicator of the extent Ψ_A and Ψ_B sample different regions of configuration space is the wavefunction overlap,

$$S_{AB} = \langle \Psi_A | \Psi_B \rangle \quad , \tag{4}$$

a reasonable p-GRVB subwavefunction might result from optimizing Ψ_A while minimizing S_{AB}. Since we do not know in advance how small S_{AB} should be, a more general approach would be to optimize Ψ_A with the constraint that S_{AB} be fixed at some value. By optimizing Ψ_A and Ψ_B in this way for a few values of S_{AB}, the p-GRVB energy can be minimized as a parametric function of S_{AB}. This method has the feature that the orbi-

tals are localized in the least brutal way possible. In the following, we derive the equations necessary to optimize such a wavefunction for the case in which Ψ_A and Ψ_B are related by a symmetry operation, and show that the computational dependence of p-GRVB is comparable to a standard SCF.

III. DESCRIPTION OF THE METHOD

We wish to mimimize the functional

$$F = E_A + W(S_0 - S_{AB})^2 \ , \tag{5}$$

where E_A is the energy of Ψ_A,

$$E_A = \langle \Psi_A | H | \Psi_A \rangle \ , \tag{6}$$

S_0 is the value to which S_{AB} will be constrained, and W is a fixed weighting factor. The derivation will be valid for any multiconfigurational wavefunction expressed as a linear combination of determinants,

$$\Psi_A = \sum_I c_I \Psi_A^I \ , \tag{7}$$

in which the other resonance structure, Ψ_B, is related to Ψ_A by the symmetry operator **R**,

$$\Psi_B = \mathbf{R}(\Psi_A) \ . \tag{8}$$

Because of this symmetry property, we can express the orbitals in both Ψ_A and Ψ_B in terms of one orthonormal set of orbitals, $\{\varphi_i\}$, some of which appear in some (or all) determinants in Ψ_A (these are called occu-

pied orbitals), and some of which do not appear in any determinants in Ψ_A (virtual orbitals). Thus

$$\varphi_i^A = \varphi_i \ , \tag{9a}$$

$$\varphi_i^B = \mathbf{R}(\varphi_i) \ . \tag{9b}$$

Our approach will be to find the change in F resulting from an incremental rotation (δ_{kl}) of two orbitals in Ψ_A, φ_k and φ_l,

$$\varphi_k^{(\delta_{kl})} = \frac{1}{1+\delta_{kl}^2}(\varphi_k + \delta_{kl}\varphi_l) \tag{10a}$$

$$\varphi_l^{(\delta_{kl})} = \frac{1}{1+\delta_{kl}^2}(\varphi_l - \delta_{kl}\varphi_k) \ . \tag{10b}$$

Thus we seek $\frac{\partial F}{\partial \delta_{kl}}$ and $\frac{\partial^2 F}{\partial \delta_{kl}^2}$, and from (5) we have

$$\frac{\partial F}{\partial \delta_{kl}} = \frac{\partial E_A}{\partial \delta_{kl}} + 2W(S_0 - S_{AB})\frac{\partial S_{AB}}{\partial \delta_{kl}} \tag{11}$$

and

$$\frac{\partial^2 F}{\partial \delta_{kl}^2} = \frac{\partial^2 E_A}{\partial \delta_{kl}^2} + 2W(S_0 - S_{AB})\frac{\partial^2 S_{AB}}{\partial \delta_{kl}^2} - 2W\left[\frac{\partial S_{AB}}{\partial \delta_{kl}}\right]^2 \ . \tag{12}$$

The derivatives $\frac{\partial E_A}{\partial \delta_{kl}}$ and $\frac{\partial^2 E_A}{\partial \delta_{kl}^2}$ are well known,[3] and are used in the standard optimizion of an MCSCF wavefunction. The derivatives $\frac{\partial S_{AB}}{\partial \delta_{kl}}$ and $\frac{\partial^2 S_{AB}}{\partial \delta_{kl}^2}$ are nonstandard, and we derive them here. We will restrict our consideration to a single orbital rotation, dropping the kl subscript from δ, and will make no explicit distinction between occupied and virtual orbitals, though clearly the derivatives are zero if both φ_k and φ_l are

virtual orbitals. The capital roman subscripts I and J will always refer to determinants, k and l will *always* refer to the orbitals being rotated, and i, j, p, and q will be used as general orbital indices. The total number of orbitals (occupied plus virtual) is N, and the number of electrons is n. Often the orbitals will be notated simply be their index, so that for example, $<i\,|\,j> \equiv <\varphi_i\,|\,\varphi_j>$.

From (7) and (4) we have

$$S_{AB} = \sum_{I,J} c_I c_J S_{AB}^{IJ} \quad , \tag{13}$$

where

$$S_{AB}^{IJ} = <\Psi_A^I\,|\,\Psi_B^J> \quad , \tag{14}$$

so that

$$\frac{\partial S_{AB}}{\partial \delta} = \sum_{I,J}^{NDET} c_I c_J \frac{\partial S_{AB}^{IJ}}{\partial \delta} \tag{15a}$$

and

$$\frac{\partial^2 S_{AB}}{\partial \delta^2} = \sum_{I,J}^{NDET} c_I c_J \frac{\partial^2 S_{AB}^{IJ}}{\partial \delta^2} \quad . \tag{15b}$$

We will now restrict our discussion to only one pair of determinants (I,J), and take Ψ_A^I and Ψ_B^J to be simple high spin determinants (we will consider the more general case later),

$$\Psi_A^I = A\{(\cdots \varphi_i^A \cdots \varphi_j^A \cdots)\alpha\alpha\cdots\alpha\} \tag{16a}$$

and

$$\Psi_B^J = A\{(\cdots \varphi_i^B \cdots \varphi_j^B \cdots)\beta\beta\cdots\beta\} \quad , \tag{16b}$$

so that there are n orbitals in each determinant, and (16) is intentionally vague about exactly which of the N orbitals appear in Ψ_A^I and Ψ_B^J. Alternatively, we could write

$$\Psi_A^I = A\{\prod_{i\varepsilon I}^{N}(\varphi_i\alpha)\} \tag{17a}$$

and

$$\Psi_B^J = A\{\prod_{i\varepsilon J}^{N}(\mathrm{R}\varphi_i\alpha)\} \ , \tag{17b}$$

where $i\varepsilon I$ means i is summed only over occupieds in determinant I, and we have made use of the symmetry relations in (9). Note that because of (8), the n occupieds appearing in determinant Ψ_A^I are the same as those in Ψ_B^J (so that "occupieds in determinant I" is unambiguous), except that they have been reflected. Since we will be considering S_{AB}^{IJ}, where I does not necessarily equal J, we do not know whether the reflection of a certain orbital appearing in Ψ_A^I appears in Ψ_B^J. We now apply the biorthogonalization procedure[4] to the orbitals in (17a) and (17b) to yield a new set of orbitals for Ψ_A^I and Ψ_B^J,

$$\bar{\varphi}_i^A = \sum_{j\varepsilon I}^{N} \varphi_j \, U_{ji}^A \tag{18a}$$

and

$$\bar{\varphi}_i^B = \sum_{j\varepsilon J}^{N} \mathrm{R}(\varphi_j) \, U_{ji}^B \ , \tag{18b}$$

such that

$$\langle \bar{\varphi}_i^A | \bar{\varphi}_j^B \rangle = \lambda_i \delta_{ij} \ , \tag{19}$$

where δ_{ij} is the kronicker-delta function (*not* a rotation between orbitals i and j), and U^A and U^B are the unitary matrices which perform the biorthogonalization. We can now rewrite Ψ_A^I and Ψ_B^J as

$$\Psi_A^I = \bar{\Psi}_A^I = A\{(\bar{\varphi}_1^A\bar{\varphi}_2^A \cdots \bar{\varphi}_n^A)\alpha\alpha \cdots \alpha\} \tag{20a}$$

$$\Psi_B^J = \bar{\Psi}_B^J = A\{(\bar{\varphi}_1^B\bar{\varphi}_2^B \cdots \bar{\varphi}_n^B)\beta\beta \cdots \beta\} \tag{20b}$$

where the $\bar{\varphi}^A$ and $\bar{\varphi}^B$ orbitals are uniquely numbered from 1 to n. It is important to note that U^A, U^B, $\{\lambda_i\}$, and of course $\{\bar{\varphi}_i^A\}$ and $\{\bar{\varphi}_i^B\}$ are unique to this particular determinant pair (I,J), but to avoid clutter, no IJ index will be tagged on. Using the new orbital sets $\{\bar{\varphi}^A\}$ and $\{\bar{\varphi}^B\}$, S_{AB}^{IJ} becomes simply the product of the diagonal overlaps,

$$S_{AB}^{IJ} = \lambda_1\lambda_2 \cdots \lambda_n \ , \tag{21}$$

because all other terms generated by the antisymmetrizer vanish due to the biorthogonality condition (19). Because the biorthogonalization mixes up the orbitals in Ψ_A^I and Ψ_B^J, the orbital rotation δ_{kl} affects every orbital in the biorthogonalized sets $\{\bar{\varphi}_i^A\}$ and $\{\bar{\varphi}_i^B\}$. From (10) and (18), $\bar{\varphi}_i^{A(\delta)}$ and $\bar{\varphi}_i^{B(\delta)}$ can be expressed as

$$\bar{\varphi}_i^{A(\delta)} = \sum_{j\varepsilon I}\varphi_j U_{ji}^A + \delta\varphi_l U_{ki}^A - \delta\varphi_k U_{li}^A \tag{22a}$$

and

$$\bar{\varphi}_i^{B(\delta)} = \sum_{j\varepsilon J}\mathrm{R}(\varphi_j) U_{ji}^B + \delta\,\mathrm{R}(\varphi_l) U_{ki}^B - \delta\,\mathrm{R}(\varphi_k) U_{li}^B \ , \tag{22b}$$

where we have dropped the $\frac{1}{1+\delta^2}$ renormalization term (we will pick it up later), or more simply

$$\Delta\bar{\varphi}_i^A = \bar{\varphi}_i^{A(\delta)} - \bar{\varphi}_i^A = \delta(\varphi_l U_{ki}^A - \varphi_k U_{li}^A) \tag{23a}$$

$$\Delta\bar{\varphi}_i^B = \bar{\varphi}_i^{B(\delta)} - \bar{\varphi}_i^B = \delta(\mathbf{R}(\varphi_l) U_{ki}^B - \mathbf{R}(\varphi_k) U_{li}^B) \ . \tag{23b}$$

Rather than worrying explicitly about whether φ_k and φ_l appear in the determinants, we simply define

$$U_{ji}^A = 0 \quad \text{if } \varphi_j \text{ is not in } \Psi_A^I$$

$$U_{ji}^B = 0 \quad \text{if } \mathbf{R}(\varphi_j) \text{ is not in } \Psi_B^J \tag{24}$$

which results because the summation in (18) is only over orbitals that appear in the determinant. We wish to expand $S_{AB}^{IJ(\delta)}$ through second order in δ,

$$S_{AB}^{IJ(\delta)} = S_{AB}^{IJ} + \delta(\Delta_1 S_{AB}^{IJ}) + \delta^2(\Delta_2 S_{AB}^{IJ}) + \text{higher order terms} \ , \tag{25}$$

so that the desired derivatives may be found (equation (15)).

First Order Terms

Substituting the rotated orbitals into (21) yields

$$S_{AB}^{IJ(\delta)} = \prod_i^n <\bar{\varphi}_i^A + \Delta\bar{\varphi}_i^A | \bar{\varphi}_i^B + \Delta\bar{\varphi}_i^B> \ , \tag{26}$$

and retaining only the terms through first order gives

$$S_{AB}^{IJ(\delta)} = S_{AB}^{IJ} + \delta \sum_i^n \frac{S_{AB}^{IJ}}{\lambda_i} (\Delta)_{ii}^{AB} \ , \tag{27}$$

where we have defined

$$(\Delta)_{ij}^{AB} = \frac{1}{\delta}[<\bar{\varphi}_i^A | \Delta\bar{\varphi}_j^B> + <\Delta\bar{\varphi}_i^A | \bar{\varphi}_j^B>] \ . \tag{28}$$

Thus the first order correction term in (25) is

$$\Delta_1 S_{AB}^{IJ} = \sum_i^n \frac{S_{AB}^{IJ}}{\lambda_i} (\Delta)_{ii}^{AB} \quad . \tag{29}$$

Note that $\frac{S_{AB}^{IJ}}{\lambda_i}$ does not present a problem when $\lambda_i = 0$, because this term is actually computed by omitting λ_i from the product in (21).

Second Order Terms

Second order terms arise both from the diagonal overlap in (26), and from the single transpositions generated by the antisymmetrizer. We consider the diagonal overlap terms first. Extracting terms in δ^2 from (26) yields

$$\Delta_2 S_{AB}^{IJ}(26) = \sum_i^n \frac{S_{AB}^{IJ}}{\lambda_i} <\Delta\bar{\varphi}_i^A | \Delta\bar{\varphi}_i^B>$$
$$+ \sum_{i>j} \left[\frac{S_{AB}^{IJ}}{\lambda_i \lambda_j} \left(<\bar{\varphi}_i^A | \Delta\bar{\varphi}_i^B> + <\Delta\bar{\varphi}_i^A | \bar{\varphi}_i^B> \right) \left(<\bar{\varphi}_j^A | \Delta\bar{\varphi}_j^B> + <\Delta\bar{\varphi}_j^A | \bar{\varphi}_j^B> \right) \right] \quad , \tag{30}$$

and introducing the notation

$$(\Delta\Delta)_{ij}^{AB} = \frac{1}{\delta^2} <\Delta\bar{\varphi}_i^A | \Delta\bar{\varphi}_j^B> \tag{31}$$

simplifies (30) to

$$\Delta_2 S_{AB}^{IJ}(26) = \sum_i^n \frac{S_{AB}^{IJ}}{\lambda_i} (\Delta\Delta)_{ii}^{AB} + \sum_{i>j}^n \frac{S_{AB}^{IJ}}{\lambda_i \lambda_j} (\Delta)_{ii}^{AB} (\Delta)_{jj}^{AB} \quad . \tag{32}$$

The other second order terms arise by considering single transpositions generated by the antisymmetrizer,

$$S_{AB}^{IJ} = \lambda_1 \lambda_2 \cdots \lambda_n - \sum_{i>j} <\bar{\Psi}_A^I | \tau_{ij} \bar{\Psi}_B^J> \quad , \tag{33}$$

$$<\bar{\Psi}_A^I|\tau_{ij}\bar{\Psi}_B^J> =$$
$$\lambda_1\lambda_2\cdots<\bar{\varphi}_i^A+\Delta\bar{\varphi}_i^A|\bar{\varphi}_j^B+\Delta\bar{\varphi}_j^B><\bar{\varphi}_j^A+\Delta\bar{\varphi}_j^A|\bar{\varphi}_i^B+\Delta\bar{\varphi}_i^B>\cdots\lambda_n \quad . \tag{34}$$

Bearing in mind that $<\bar{\varphi}_i^A|\bar{\varphi}_j^B>=0$ for $i\neq j$, we obtain the following second order terms from (33):

$$\Delta_2 S_{AB}^{IJ}(33) = -\sum_{i>j}\frac{S_{AB}^{IJ}}{\lambda_i\lambda_j}(\Delta)_{ij}^{AB}(\Delta)_{ji}^{AB} \quad . \tag{35}$$

Collecting the terms from (32) and (35) we obtain the full second order correction,

$$\Delta_2 S_{AB}^{IJ} =$$
$$\sum_i^n\frac{S_{AB}^{IJ}}{\lambda_i}(\Delta\Delta)_{ii}^{AB} + \sum_{i>j}^n\frac{S_{AB}^{IJ}}{\lambda_i\lambda_j}\left[(\Delta)_{ii}^{AB}(\Delta)_{jj}^{AB} - (\Delta)_{ij}^{AB}(\Delta)_{ji}^{AB}\right] \quad . \tag{36}$$

To actually evaluate $\Delta_1 S_{AB}^{IJ}$ and $\Delta_2 S_{AB}^{IJ}$, we need to expand $(\Delta)_{ij}^{AB}$ and $(\Delta\Delta)_{ii}^{AB}$ (off diagonal $(\Delta\Delta)_{ij}^{AB}$ terms are not needed) in terms of the original orbitals $\{\varphi_i\}$. Using (28), (23), and (10), we obtain

$$\begin{aligned}(\Delta)_{ij}^{AB} &= \frac{1}{\delta}\left[<\bar{\varphi}_i^A|\Delta\bar{\varphi}_j^B> + <\Delta\bar{\varphi}_i^A|\bar{\varphi}_j^B>\right] \\ &= <\bar{\varphi}_i^A|\,U_{kj}^B\mathrm{R}\varphi_l - U_{lj}^B\mathrm{R}\varphi_k> + <U_{ki}^A\varphi_l - U_{li}^A\varphi_k\,|\bar{\varphi}_j^B> \\ &= \sum_q^n\left[(U_{qi}^A U_{kj}^B + U_{ki}^A U_{qj}^B)<q\,|\mathrm{R}|\,l> - (U_{qi}^A U_{lj}^B + U_{li}^A U_{qj}^B)<q\,|\mathrm{R}|\,k>\right] ,\end{aligned} \tag{37}$$

and from (31) and (23),

$$\begin{aligned}(\Delta\Delta)_{ii}^{AB} &= \frac{1}{\delta^2}<\Delta\bar{\varphi}_i^A|\,\Delta\varphi^B> \\ &= <U_{ki}^A\varphi_l - U_{li}^A\varphi_k\,|\,\mathbf{R}|\,U_{ki}^B\varphi_l - U_{li}^B\varphi_k> \\ &= U_{ki}^A U_{ki}^B<l\,|\mathbf{R}|\,l> + U_{li}^A U_{li}^B<k\,|\mathbf{R}|\,k> - (U_{ki}^A U_{li}^B + U_{li}^A U_{ki}^B)<l\,|\mathbf{R}|\,k> ,\end{aligned} \tag{38}$$

where we have made use of*

$$\langle \varphi_i | R\varphi_j \rangle = \langle i | R | j \rangle = \langle j | R | i \rangle \ .$$

The Denominator

Until now, we have neglected the $\frac{1}{1+\delta^2}$ factor which appears for every occurrence of $\varphi_k^{(\delta)}$ or $\varphi_l^{(\delta)}$. Let m equal the number of occurrences of either $\varphi_k^{(\delta)}$ or $\varphi_l^{(\delta)}$ in Ψ_A^I or $R\Psi_B^J$. Thus m can range from 0 to 4, and for $m = 0$, S_{AB}^{IJ} is left unchanged by δ_{kl}. We can express S_{AB}^{IJ} as

$$S_{AB}^{IJ(\delta)} = \frac{1}{(1+\delta^2)^m}\left[S_{AB}^{IJ} + \delta(\Delta_1 S_{AB}^{IJ}) + \delta^2(\Delta_2 S_{AB}^{IJ})\right] \qquad (39a)$$

(so that (25) is actually incorrect), or expanding the denominator through second order in δ

$$S_{AB}^{IJ(\delta)} = \frac{1}{1+m\delta^2}\left[S_{AB}^{IJ} + \delta(\Delta_1 S_{AB}^{IJ}) + \delta^2(\Delta_2 S_{AB}^{IJ})\right] \ . \qquad (39b)$$

Differentiating yields

$$\left[\frac{\partial S_{AB}^{IJ}}{\partial \delta}\right]_{\delta=0} = (\Delta_1 S_{AB}^{IJ}) \qquad (40)$$

and

$$\left[\frac{\partial^2 S_{AB}^{IJ}}{\partial \delta^2}\right]_{\delta=0} = -2mS_{AB}^{IJ} + 2(\Delta_2 S_{AB}^{IJ}) \ . \qquad (41)$$

Equations (40) and (41) thus give the derivatives ready to contract over determinant pairs by (15) and plug into (11) and (12) to obtain $\frac{\partial F}{\partial \delta}$ and

* This is true because the orbitals are real.

$\frac{\partial^2 F}{\partial \delta^2}$ for this orbital rotation.

Computational Dependence

To decide whether this method is feasible, we need to know the computational dependence of evaluating $\frac{\partial S_{AB}}{\partial \delta}$ and $\frac{\partial^2 S_{AB}}{\partial \delta^2}$. Because each determinant pair requires a unique biorthogonalization, the dependence on $NDET$ will be $(NDET)^2$. Examination of (29) and (38) shows that for a given rotation kl the evaluation of $\frac{\partial S_{AB}^{IJ}}{\partial \delta}$ requires work which scales as n^2 (note that we ignore any constant pre-multiplier) and since there are nN (number of occupieds times total number of orbitals), possible kl rotations which will lead to a change in S_{AB}*, the total work involved in obtaining $\frac{\partial S_{AB}}{\partial \delta}$ scales as

$$\text{work}\left(\frac{\partial S_{AB}}{\partial \delta}\right) \approx NDET^2 N n^3 \quad . \tag{42}$$

Analogously, from inspection of (36) and (37), $\frac{\partial^2 S_{AB}}{\partial \delta^2}$ appears to require $n + n^3 \approx n^3$ work per kl (assuming the $\langle q | \mathbf{R} | l \rangle$ terms are precalculated) for a total dependence of $(NDET)^2 N n^4$. However, by precalculating the terms

$$\chi_{il}^{A} = \sum_{q}^{n} U_{qi}^{A} \langle q | \mathbf{R} | l \rangle \tag{43a}$$

* Rotations between occupied orbitals with the same Hamiltonian may also be excluded, so that Nn is an upper bound.

and

$$\chi_{il}^{B} = \sum_{q}^{n} U_{qi}^{B} \langle q \,|\, \mathbf{R} \,|\, l \rangle \ , \tag{43b}$$

which only depend on i and l (Nn terms, n summation for each; total work = n^3), we can write

$$(\Delta)_{ij}^{AB} = \chi_{il}^{A} U_{kl}^{B} + U_{ki}^{A} \chi_{jl}^{B} - \chi_{ik}^{A} U_{lj}^{B} - U_{li}^{A} \chi_{jk}^{B} \ , \tag{43c}$$

so that the total dependence for $\dfrac{\partial^2 S_{AB}}{\partial \delta^2}$ is reduced to

$$\text{work}\left[\frac{\partial^2 S_{AB}}{\partial \delta^2}\right] \approx (NDET)^2 N n^3 \ . \tag{44}$$

In a normal SCF, the evaluation of $\dfrac{\partial E}{\partial \delta}$ and $\dfrac{\partial^2 E}{\partial \delta^2}$ scales as

$$\text{work}\left[\frac{\partial^2 E}{\partial \delta^2}\right) \approx (NHAM) n^4 \ , \tag{45}$$

where NHAM is the number of Hamiltonians in the wavefunction (roughly equal to NDET), so that the evaluation of the extra S_{AB} derivatives could add significant work to each iteration, but does not affect the overall scaling dependence on the number of basis functions or the number of electrons.

General Case - both α and β spin in determinants.

For the case in which Ψ_A^I and Ψ_B^J contain both α and β spin orbitals, two biorthogonalizations are performed, one for the α orbitals, and one for the β orbitals. The summations in (29), (36), and (37) are performed

twice, once for the n_α α orbitals and once for the n_β β orbitals. The terms which will differ between α and β are λ_i, $(\Delta)_{ij}^{AB}$, $(\Delta\Delta)_{ii}^{AB}$, and any U^A or U^B matrix element, while S_{AB}^{IJ}, and $<i|\mathbf{R}|j>$ will remain unchanged. For example,

$$S_{AB}^{IJ}=\lambda_1^{(\alpha)}\lambda_2^{(\alpha)}\cdots\lambda_{n_\alpha}^{(\alpha)}\lambda_1^{(\beta)}\lambda_2^{(\beta)}\cdots\lambda_{n_\beta}^{(\beta)} \tag{46}$$

and

$$\Delta_1 S_{AB}^{IJ} = \sum_i^{n_\alpha} \frac{S_{AB}^{IJ}}{\lambda_i^{(\alpha)}} (\Delta^{(\alpha)})_{ii}^{AB} + \sum_i^{n_\beta} \frac{S_{AB}^{IJ}}{\lambda_i^{(\beta)}} (\Delta^{(\beta)})_{ii}^{AB} , \tag{47}$$

and so forth. The computational dependence on n, N and $NDET$ is unchanged.

CI Coefficient Optimization

Until now, we have only considered the change in F due to orbital mixing. We must also consider the effect on F of varying the determinant coefficients $\{c_I\}$ in equation (7). In a general CI expansion over determinants as in (7), the coefficients which optimize the energy (for the current set of orbitals) are found by

$$E = \sum_{I,J}^{NDET} c_I c_J H_{IJ} \tag{48}$$

with the constraint

$$\sum_I^{NDET} c_I c_J = 1 , \tag{49}$$

where

$$H_{IJ} = \langle \Psi_A^I | H | \Psi_A^J \rangle \tag{50a}$$

$$S_{IJ} = \langle \Psi_A^I | \Psi_A^J \rangle = \delta_{IJ} \tag{50b}$$

(here δ_{IJ} is the kronicker-delta). This yields the secular equation

$$\mathbf{HC} = \mathbf{CE} \ , \tag{51}$$

where **H** is the matrix of H_{IJ} elements (**S** does not appear due to the orthonormality of the $\{\Psi_A^I\}$ determinants), **C** is the matrix of solution vectors, and **E** is the diagonal matrix of energies. If we instead differentiate (5),

$$\frac{\partial F}{\partial c_K} = \frac{\partial E_A}{\partial c_K} + 2W(S_0 - S_{AB}) \sum_I^{NDET} 2c_I S_{AB}^{IK} \ , \tag{52}$$

and apply the same constraint (49), we obtain the modified secular equation

$$\mathbf{GC} = \mathbf{CF} \ , \tag{53}$$

where

$$G_{IJ} = H_{IJ} + 2W(S_0 - S_{AB}) S_{AB}^{IK} \ , \tag{54}$$

which yields the solution (**C**), and the diagonal matrix of F values (**F**), for our special energy expression in (5). For a special MCSCF wavefunction such as GVB, we need to apply additional constraints to retain pairwise normalization of the GVB pairs, and we outline this in the next section.

GVB Coefficient Optimization

The GVB wavefunction with q pairs[3] can be written as*

$$\Psi_A^{GVB} = A\{[\text{core}](g_{1a}\varphi_{1a}^2 + g_{1b}\varphi_{1b}^2)(g_{2a}\varphi_{2a}^2 + g_{2b}\varphi_{2b}^2) \cdots (g_{qa}\varphi_{qa}^2 + g_{qb}\varphi_{qb}^2)\} \quad (55)$$

and we wish to optimize the GVB pair coefficients (g_{ia}, g_{ib}) while maintaining pairwise normalization

$$g_{ia}^2 + g_{ib}^2 = 1 \quad (56)$$

for each GVB pair. By re-expressing Ψ^{GVB} as

$$\Psi^{GVB} = g_{ia}\Psi_{ia} + g_{ib}\Psi_{ib} \quad , \quad (57)$$

where

$$\Psi_{ia} = A\{[core](g_{1a}\varphi_{1a}^2 + g_{1b}\varphi_{1b}^2) \cdots (\varphi_{ia}^2) \cdots (g_{qa}\varphi_{qa}^2 + g_{qb}\varphi_{qb}^2)\} \quad (58a)$$

and

$$\Psi_{ib} = A[core](g_{1a}\varphi_{1a}^2 + g_{1b}\varphi_{1b}^2) \cdots (\varphi_{ib}^2) \cdots (g_{qa}\varphi_{qa}^2 + g_{qb}\varphi_{qb}^2) \, , \quad (58b)$$

we can solve the two by two secular equation using the basis states Ψ_{ia} and Ψ_{ib}, to yield improved values for g_{ia} and g_{ib}. Repeatedly cycling through the q GVB pairs gives a converged set of coefficients for all pairs. To modify this approach for the special energy expression in (5), we replace

$$H_{ia,ib} = \langle \Psi_{ia} | H | \Psi_{ib} \rangle \quad (59)$$

Here we are treating the case with two Natural Orbitals per GVB pair; the generalization to multiple Natural Orbitals per pair is trivial.

with

$$G_{ia,ib} = \langle \Psi_{ia}^{A} | H + 2W(S_0 - S_{AB})\mathbf{R} | \Psi_{ib}^{A} \rangle$$

$$= H_{ia,ib} + 2W(S_0 - S_{AB}) S_{AB}^{ia,ib} \quad , \tag{60}$$

where $S_{AB}^{ia,ib}$ is obtained by

$$S_{AB}^{ia,ib} = \sum_{I \varepsilon ia,\, J \varepsilon ib} c_I c_J S_{AB}^{IJ} \quad . \tag{61}$$

The meaning of $I \varepsilon ia, J \varepsilon ib$ is that the summation only allows those values of I and J for which φ_{ia} appears in Ψ_{ia}^{A} and φ_{ib} appears in Ψ_{ib}^{A}.

IV. IMPLICATIONS FOR ANALYTICALLY-OPTIMIZED GRVB

We have shown that the change in $\langle \Psi_A | \mathbf{R}(\Psi_A) \rangle$ resulting from an orbital rotation δ can be found through second order in δ with a computational dependence of $(NDET)^2 N n^3$. If a similar approach could be used to find the derivatives of $\langle \Psi_A | H | \mathbf{R}(\Psi_A) \rangle$, a rigourous GRVB wavefunction could be optimized analytically, leading to vast computational savings over the current numerical optimization. Writing the Hamiltonian matrix element between two determinants in the biorthogonalized orbitals gives

$$H_{AB}^{IJ} = \sum_{i}^{n} \frac{S_{AB}^{IJ}}{\lambda_i} \langle \bar{\varphi}_i^{A} | h | \bar{\varphi}_i^{B} \rangle$$

$$+ \sum_{i,j} \frac{S_{AB}^{IJ}}{\lambda_i \lambda_j} \langle \bar{\varphi}_i^{A} \bar{\varphi}_j^{A} | \frac{1}{r_{12}} | \bar{\varphi}_i^{B} \bar{\varphi}_j^{B} \rangle - \langle \bar{\varphi}_i^{A} \bar{\varphi}_j^{A} | \frac{1}{r_{12}} | \bar{\varphi}_j^{A} \bar{\varphi}_i^{B} \rangle \quad , \tag{62}$$

where again we are treating the simple high-spin determinant case. Considering first order changes in δ, the worst computational dependence

lies in the terms arising from transposing orbital i or j with orbital q in the two-electron sum over i and j, and this gives rise to

$$\Delta_1 H_{AB}^{IJ}(\text{worst}) = -\sum_{q,i,j}^{n} \frac{S_{AB}^{IJ}}{\lambda_i \lambda_j \lambda_q} \left[(\Delta)_{qi}^{AB} \langle \bar{\varphi}_i^A \bar{\varphi}_j^A | \frac{1}{r_{12}} | \bar{\varphi}_q^B \bar{\varphi}_j^B \rangle + \text{three similar terms} \right], \quad (63)$$

which would have a total computational dependence of $(NDET)^2(Nn)(n^3) = NDET^2Nn^4$, assuming the two-electron integrals of the type $\langle \bar{\varphi}_i^A \bar{\varphi}_j^A | \frac{1}{r_{12}} | \bar{\varphi}_q^B \bar{\varphi}_j^B \rangle$ are precalculated (this can be accomplished with n^5 work if the integrals of the form $\langle ij | \frac{1}{r_{12}} | pq \rangle$ have been precalculated at the beginning of the iteration at a cost of N^4n). For large N, the N^4n integral transformation (once per iteration) would dominate the scaling dependence. Thus an analytical GRVB program with first-order convergence could be written, and should run much faster than the current numerical version,[1] which has a computational dependence of $\approx NDET^2N^5n^2$. For comparison, this approach would scale roughly the same as (or faster than) the modern MCSCF procedures[5] which also require an integral transformation each iteration, though the number of iterations required would be much greater for the first-order GRVB. The convergence could be improved beyond first order by accumulating approximate diagonal second derivatives for each orbital rotation. This can be accomplished knowing the gradient of a given orbital rotation and its value from the previous iteration, along with the component of the solution vector along this rotation.

References

1) A.F. Voter and W.A. Goddard III, J. Chem Phys. **75,** 3638 (1981); also, see this Thesis.

2) A.F. Voter and W.A. Goddard III, Chem. Phys. **57,** 253 (1981)

3) See, for example, F.W. Bobrowicz, and W.A. Goddard III, in: *Modern Theoretical Chemistry: Methods of Electronic Structure Theory*, edited by H.F. Schaefer III (Plenum Press, New York, 1977), Vol. 4, Chap. 4 - pp. 79-127.

4) P.-O. Löwdin, Rev. Mod. Phys. **35,** 496 (1963)

5) L.G. Yaffe and W.A. Goddard III, Phys. Rev. A **13,** 1682 (1976).

Proposition V

ABSTRACT

It is shown that for separated-pair wavefunctions, such as Hartree Fock or generalized valence bond (GVB), the total energy of a homonuclear diatomic molecule can be expressed as a sum of contributions from each occupied orbital, thus allowing the unique partitioning of the bond energy into σ and π components. The key to such an analysis is correctly dividing the nuclear repulsion into orbital contributions. Unlike analyses based on orbital energies, the method presented here yields a meaningful dependence of each orbital contribution on the internuclear distance, R. Thus this method can be used to isolate the various bonding, antibonding and nonbonding interactions which act together to yield observed bond strengths, leading to a deeper understanding of molecular bonding.

Introduction

A tantalizing unsolved problem is the separation of the bond energy of a molecule such as O_2, N_2, or F_2 into its σ and π components. One reason this would be useful is that the bonding in these simple molecules is unperturbed by steric repulsions or ring strain, so that the N_2 σ bond, for example, would be close to the "intrinsic bond energy" for an N-N sigma bond. The concept of an intrinsic bond strength implies that the cohesive energy of a molecule is the sum of the intrinsic bond energies for all the bonds in the molecule, corrected for any steric repulsions, lone pair repulsions, ring strain, etc., peculiar to the molecule. That such a concept is valid is supported by the fact that Benson group additivity calculations[1] can predict heats of formation to kcal accuracy for a large number of molecules using only a small number of group values. Intrinsic bond strengths, as opposed to total bond strengths, would be expected to follow very simple trends. For example, the observed bond strengths of the dihalogens are[2]

F_2	36.9 kcal
Cl_2	57.2 kcal
Br_2	45.4 kcal
I_2	35.6 kcal .

There is a clear trend towards increasing bond strength as we move up the column from I_2 to Cl_2, as expected from contragradience arguments,[3] but F_2 does not fit this trend. This is probably due to the increased magnitude of the pπ interactions in the $n=2$ row compared to the $n\geq3$ rows.

If this pπ repulsion could be separated out, the intrinsic bond strengths obtained would be expected to increase monotonically from I_2 to F_2. In fact, the F-F intrinsic σ bond may be the strongest homonuclear σ bond in the periodic table, even though the observed F_2 bond is one of the weakest.

While quantum chemical methods can be used to compute highly accurate total bond energies,[4] the division into separate interactions has not been performed. Using bond energies (experimental or calculated) from various molecules can yield useful transferrable bond energies, but these are always masked by some extra interactions. For example, the strength of a C-C π bond can be roughly calculated as the rotational barrier height in ethylene (65 kcal[5]), but this also contains a change in the steric interactions between the C-H bonds. In the following we present an approach for partitioning the total energy of a Hartree Fock or generalized valence bond (GVB) description of a diatomic molecule into contributions from each occupied orbital. While these wavefunctions do not yield highly accurate bond energies, the ability to dismantle the bond into its various components should lead to valuable insight, and take us a step closer to the direct evaluation of intrinsic bond eneries.

Description of the Method

We wish to express the total energy of a wavefunction as a sum over orbital contributions. Consider a closed shell Hartree Fock wavefunction with n doubly-occupied spatial orbitals,

$$\Psi^{HF} = A[\varphi_1^2\varphi_2^2 \cdots \varphi_n^2] \ . \tag{1}$$

Given the full Hamiltonian for an N electron system

$$\hat{H} = \sum_{p}^{N}\hat{h}(p) + \sum_{p,q}^{N}\frac{1}{r_{pq}} + \Omega \ , \tag{2}$$

where $h(p)$ contains the electron-nuclear attraction and kinetic energy terms for electron p, $\frac{1}{r_{pq}}$ is the coulomb repulsion between electrons p and q, and Ω is the nuclear repulsion energy, we can write the energy of (1) as

$$E^{HF} = <\Psi^{HF}|\hat{H}|\Psi^{HF}> \tag{3}$$

$$= \sum_{i}2h_{ii} + \sum_{i,j}2J_{ij} - K_{ij} + \Omega \ ,$$

where h_{ii} is the expectation value of φ for the one-electron operator h

$$h_{ii} = <\varphi_i|\hat{h}|\varphi_i> = <\varphi_i|\sum_{p}\hat{h}(p)|\varphi_i> \tag{4}$$

and

$$J_{ij} = <\varphi_i\varphi_j|\frac{1}{r_{12}}|\varphi_i\varphi_j> \tag{5a}$$

$$K_{ij} = <\varphi_i\varphi_j|\frac{1}{r_{12}}|\varphi_j\varphi_i> \ . \tag{5b}$$

Defining the Fock operator H^{HF} as

$$\hat{H}^{HF} = \hat{h} + \sum_{j}(2\hat{J}_{\varphi_j} - \hat{K}_{\varphi_j}) \tag{6}$$

where J_j and K_j are defined by

$$\langle \varphi_i | \hat{J}_{\varphi_j} | \varphi_i \rangle = J_{ij} \tag{7a}$$

$$\langle \varphi_i | \hat{K}_{\varphi_j} | \varphi_i \rangle = K_{ij} \quad , \tag{7b}$$

we can write (3) as

$$E^{HF} = \sum_i (h_i + \varepsilon_{ii}) + \Omega \tag{8}$$

where

$$\varepsilon_{ij} = \langle \varphi_i | \hat{H}^{HF} | \varphi_j \rangle \quad . \tag{9}$$

Equation (8) represents the total energy as the desired sum, *except* for the nuclear repulsion Ω. We now propose a method for partitioning Ω into orbital contributions for a diatomic moleulule AB. For this case, we have simply

$$\Omega = \frac{Z_A Z_B}{R_{AB}} \quad , \tag{10}$$

where Z_A and Z_B are the nuclear charges, and we seek the set of values $\{f_i\}$ such that

$$E^{HF} = \sum_i E_i = \sum_i (h_{ii} + \varepsilon_{ii} + f_i \Omega) \quad , \tag{11}$$

where

$$\sum_i f_i = 1 \quad . \tag{12}$$

Consider an electron pair localized in φ_k on atom A, (e.g. a 1s pair) which does not participate in the bonding process. If f_k is chosen correctly, E_k for this pair will not depend on R_{AB}. Taking R_{AB} to be very large, so that

there is no significant overlap between the orbitals on A with those on B, the two electron integrals between φ_k on center A and φ_j on center B simplify to

$$2J_{kj} - K_{kj} \approx 2J_{kj} \approx \frac{2}{R} . \tag{14}$$

Thus, E_k becomes

$$E_k = 2\langle\varphi_k | \frac{-Z_A}{r_A} + \frac{-Z_B}{r_B} - \frac{1}{2}\nabla^2 | \varphi_k\rangle + \sum_j (2J_{kj} - K_{kj}) \tag{15}$$

$$+ \frac{Z_B}{R} + \frac{f_k Z_A Z_B}{R}$$

where the $\frac{Z_B}{R}$ term arises from summing (14) over the $\frac{Z_B}{2}$ MOs on B. Defining E_k^∞ as the part of E_k which is independent of R (at long R), we have

$$E_k = E_k^\infty + 2\langle\varphi_k | \frac{-Z_B}{R} | \varphi_k\rangle + \frac{Z_B}{R} + \frac{f_k Z_A Z_B}{R} \tag{16a}$$

$$= E_k^\infty - \frac{Z_B}{R} + \frac{f_k Z_A Z_B}{R} . \tag{16b}$$

Thus, the value for f_k which makes E_k independent of R is

$$f_k = \frac{Z_B}{Z_A Z_B} = \frac{1}{Z_A} . \tag{18}$$

We can understand this result as follows. Ignoring bonding effects, two atoms at large distance have no net attraction or repulsion because the nuclear repulsion ($\frac{Z_A Z_B}{R}$) and the electron-electron repulsion ($\frac{Z_A Z_B}{R}$)

are exactly balanced by the attraction of the electrons on A(B) to the nuclei on B(A) ($2\frac{-Z_A Z_B}{R}$). In equation (16a), the $2\langle\varphi_k|\frac{-Z_B}{R}|\varphi_k\rangle = \frac{-2Z_B}{R}$ term arises from the attraction of the electron pair in φ_k for the nuclei on center B, while the $\frac{+Z_B}{R}$ term is half of the repulsion of this pair with each pair on B. (The other half of this repulsion is contained in the E_i terms for each of the orbitals on B.) Thus, an additional $\frac{+Z_B}{R}$ is required to make these balance, and we take that from the nuclear repulsion energy. To verify that the sum of these contributions over all occupied orbitals adds up to the total nuclear repulsion energy, we note that the number of doubly occupied orbitals on center A is $\frac{Z_A}{2}$ and on B is $\frac{Z_B}{2}$ (assuming neutral atoms), so that (12) becomes

$$\sum_i f_i = \frac{Z_A}{2}\left(\frac{1}{Z_A}\right) + \frac{Z_B}{2}\left(\frac{1}{Z_B}\right) \qquad (19)$$

$$= 1 \ .$$

So, assuming each orbital can be assigned to either atom A or B, the contributions to Ω add up to the total Ω correctly. However, there is a dilemma if φ_k has character on both A and B (as a bond would). A population analysis could be used to modify f_k according to how much of φ_k is on A and how much is on B, so that

$$f_k = p_{A_k}\left(\frac{1}{Z_A}\right) + p_{B_k}\left(\frac{1}{Z_B}\right) \ , \qquad (20)$$

where p_{A_k} and p_{B_k} are the populations of φ_k on A and B, respectively, and

$$p_{A_k} + p_{B_k} = 1 \ , \tag{21}$$

but it is not obvious which (if any) method of population analysis would be appropriate, and there are many to choose from.[6] Rather than deal with this issue, we instead restrict ourselves to homonuclear diatomic molecules, where

$$Z_A = Z_B = Z \ , \tag{22}$$

and it is easily verified from equation (20) that f_k is independent of p_{A_k} and p_{B_k},

$$\begin{aligned} f_k &= p_{A_k}\left(\frac{1}{Z}\right) + p_{B_k}\left(\frac{1}{Z}\right) \\ &= \left(p_{A_k} + p_{B_k}\right)\frac{1}{Z} \\ &= \frac{1}{Z} \ . \end{aligned} \tag{23}$$

We now consider more complex wavefunctions, such as open shell Hartree-Fock (as would be required for a description of ground state O_2) or GVB. We restrict ourselves to separated-pair wavefunctions[7] whose energy can be written as[8]

$$E = \sum_i g_i h_{ii} + \sum_i \varepsilon_{ii} \tag{24}$$

where g_i is an occupation parameter ($g_i = 1$ for a doubly-occupied orbital), and

$$\varepsilon_{ii} = \langle \varphi_i | F_i | \varphi_i \rangle \tag{25}$$

where F_i is the generalized Fock operator,

$$F_i = g_i h + \sum_j (a_{ij} J_j + b_{ij} K_j) \ , \tag{26}$$

and the a_{ij} and b_{ij} coefficients correctly describe the coupling between orbitals. For example, $g_i = 1$, $a_{ij} = 2$, and $b_{ij} = -1$, if φ_i and φ_j are doubly-occupied orbitals, as in (6). The reader should see reference 13 for a more detailed discussion of these wavefunctions; (note that g_i here corresponds to f_i in that paper). For such wavefunctions, it is still easy to partition the energy by orbital, and it can be shown that the appropriate value of f_k for this case is

$$f_k = \frac{g_k}{Z} \ , \tag{27}$$

that is, f_k is simply weighted by the occupation of φ_k. We demonstrate here that this is true for the case of a Hartree-Fock wavefunction with high-spin open shells (singly-occupied orbitals). For a singly-occupied orbital φ_k on center A ($g_k = \frac{1}{2}$) we have

$$E_k^{open} = g_k h_{kk} + \varepsilon_{kk} + \frac{g_k}{Z}\Omega$$

$$= h_{kk} + \tfrac{1}{2}\sum_j (2J_{kj} - K_{kj}) + \tfrac{1}{2}\sum_j (J_{kj} - K_{kj}) + \tfrac{1}{2}\frac{\Omega}{Z} \ , \tag{28}$$

which at long R (assuming no bonding) reduces to

$$E_k^{open} = E_k^{\infty} + \langle \varphi_k | \frac{-Z_A}{r_B} | \varphi_k \rangle + \tfrac{1}{2} \sum_{closed} \frac{2}{R} + \tfrac{1}{2} \sum_{open} \frac{1}{R} + \tfrac{1}{2}\frac{\Omega}{Z} \tag{29}$$

$$= E_k^{\infty} - \frac{Z_B}{R} + \tfrac{1}{2}\left(\frac{Z_B}{R}\right) + \tfrac{1}{2}\frac{\Omega}{Z}$$

$$= E_k^{\infty} \ , \qquad (29)$$

where we have made use of the fact that the total number of electrons on center B is Z_B, and we are only distinguishing Z_A and Z_B to make clear which interactions are being discussed. As before, we see that E_k^{open} does not depend on R since f_k has been chosen properly. We can thus make the following postulate:

For a neutral, homonuclear diatomic molecule with charge Z on each nucleus, the contribution to the total energy of a separated-pair wavefunction (such as Hartree-Fock or GVB) from a given occupied orbital φ_k is

$$E_k = g_k h_{kk} + \varepsilon_{kk} + g_k \frac{Z}{R} \ , \qquad (30)$$

and the behavior of E_k as a function of R will correctly reflect the bonding, antibonding, or nonbonding character of φ_k.

We note at this point that the most general separated pair wavefunction[7] is the highest level wavefunction for which a decomposition such as (30) is possible, since in more complicated wavefunctions there is no longer a one-to-one correspondence between a pair of electrons and an orbital (or set of orbitals for a GVB pair). A separated-pair wavefunction is written as an antisymmetrized product of normalized two-electron subwavefunctions (or one-electron subwavefunctions, for open shell orbi-

tals). An example of this type of wavefunction is

$$\Psi = A[\varphi_1^2\varphi_2^2 \cdots \varphi_{ncore}^2(c_{1a}\varphi_{1a}^2 + c_{1b}\varphi_{1b}^2)(c_{2a}\varphi_{2a}^2 + c_{2b}\varphi_{2b}^2) \quad (31)$$

$$\cdots (\varphi_m\varphi_{m+1}\cdots\varphi_n)] \quad (31)$$

where φ_1 through φ_{ncore} are doubly-occupied Hartree-Fock orbitals, φ_{1a} and φ_{1b} make up the first GVB pair, with

$$c_{1a}^2 + c_{1b}^2 = 1 \ , \quad (32)$$

and φ_m through φ_n are high-spin orbitals, with all orbitals mutually orthogonal.

Applications of the Method

One interesting study would be the decomposition of the dihalide bond energies into σ and π components, as mentioned in the Introduction. This would be accomplished by summing the E_k values from the four π orbitals to obtain the π contribution, and summing E_k over the σ space to obtain the σ contribution, and subtracting from each of these the corresponding sums for the two independent halide atoms. While Hartree-Fock predicts a *negative* bond energy for F_2,[9] correlating the σ bond pair with two natural orbitals $(c_g\sigma_g^2 + c_2\sigma_u^2)$ in a GVB(1/2) wavefunction[10] leads to a more reasonable value of 12.5 kcal. Increasing the correlation to GVB(1/5) (5 natural orbitals*) should lead to a good, if not quantitative, description of the total bond, suitable for this study. The trend in intrinsic bond energies calculated in this manner should be

* Note that in a GVB(1/5) wavefunction, E_σ would contain some contributions from orbitals of π symmetry which are used in correlating the σ bond.

monotonic, leading to a very strong F_2 σ bond. Correspondingly, the antibonding nature of the π space should show a marked increase for F_2 as compared to Cl_2, Br_2, and I_2.

Another quantity that could be extracted using this approach is the ideal bond length for an N-N σ bond or an N-N π bond. It is well known that $p\pi$ bonds tend to be shorter than $p\sigma$ bonds of the same principle quantum number and this method could show for the first time the R dependence of these separate bonding interactions. It would be interesting to know, for example, how much bonding energy is lost due to the compromise in bond length.

Many other applications are possible, and we mention just one more. The exceptionally weak bond in the Li_2 molecule (D_0 = 24.1 kcal[2]) is thought to be due to the Pauli repulsion of the two 1s core orbitals. The approach presented here could be used to determine how short and strong the Li-Li bond would be if this repulsion were eliminated. A GVB(1/5) wavefunction would be an appropriate level for this study.

Conclusions

Chemists have for years used orbital energies (ε_{ii}) as a way of analyzing the energy properties of the orbitals in a wavefunction.[11] Since the negative orbital energy corresponds to the ionization potential in the frozen-orbital approximation,[12] such an analysis has physical meaning. However, the orbital energies do not sum to the total electronic energy and do not contain any nuclear repulsion energy, and as a result, some

models have led to erroneous predictions.[13] Similarly, for analyzing the R dependence of bonding interactions in a diatomic molecule, orbital energies are inadequate. The E_i quantities we define here do sum to the total energy, and should have meaningful behavior as a function of R, though they have no correspondence to the ionization potential. The E_i approach should lead to valuable insight into the components of bonding interactions which lead to observed bond strengths and bond strength trends.

References

1) S.W. Benson, *Thermochemical Kinetics*, (John Wiley and Sons, N.Y., N.Y. 1968)

2) K.P. Huber and G. Herzberg, *Molecular Spectra and Molecular Structure, Vol. 4, Constants of Diatomic Molecules*, (Van Nostrand Reinhold Co., New York 1979)

3) C.W. Wilson, Jr. and W.A. Goddard III, Chem. Phys. Lett. **5,** 45 (1970)

4) H.F. Schaefer III, *The Electronic Structure of Atoms and Molecules. A Survey of Rigorous Quantum Mechanical Results* (Addison-Wesley, London, 1972)

5) J.E. Douglas, B.S. Rabinovich and F.S. Looney, J. Chem. Phys. **23,** 315 (1955)

6) A. Streitweiser, Jr., J.B. Collins, J.M. McKelvey, D. Grier, J. Sender and A.G. Toczko, Proc. Natl. Acad. Sci. **76,** 2499 (1979), and references therein.

7) See, for example, W. Kutzelnigg, in: *Modern Theoretical Chemistry, Vol. 3, Methods of Electronic Structure Theory*, edited by H.F. Schaeffer III (Plenum, New York 1977), Chap. 5; E.L. Mehler, K. Ruedenberg and D.M. Silver, J. Chem. Phys. **52,** 1181 (1970); D.M. Silver, K.

Ruedenberg and E.L. Mehler, J. Chem. Phys. **52,** 1206 (1970)

8) F.W. Bobrowicz and W.A. Goddard III, in: *Modern Theoretical Chemistry, Vol. 3, Methods of Electronic Structure Theory*, edited by H.F. Schaeffer III (Plenum, New York 1977), Chap. 4

9) A.C. Wahl, J. Chem. Phys. **41,** 2600 (1964)

10) G. Das and A. C. Wahl, J. Chem. Phys. **44,** 876 (1966)

11) J.P. Lowe, *Quantum Chemistry* (Academic Press, N.Y., N.Y., 1978), p. 437.

12) T. Koopmans, Physica **1,** 104 (1933)

13) For a discussion, see P.W. Paine and L.C. Allen, in: *Modern Theoretical Chemistry, Vol. 4, Methods of Electronic Structure Theory*, edited by H.F. Schaeffer III (Plenum, New York 1977), Chap. 2.